High throughput assessment of platelet signaling, function and inhibition

HIGH THROUGHPUT ASSESSMENT OF PLATELET SIGNALING, FUNCTION AND INHIBITION

DELIA IRENE FERNÁNDEZ DE LA FUENTE

High throughput assessment of platelet signaling, function and inhibition

Delia Irene Fernández de la Fuente

High throughput assessment of platelet signaling, function and inhibition

High throughput assessment of platelet signaling, function and inhibition

DISSERTATION

To obtain the degree of Doctor at Maastricht University and Doctor
at Universidade de Santiago de Compostela, on the authority
of the Rector Magnificus, Prof. Dr. Pamela Habibović,
in accordance with the decision of the Board of Deans,
to be defended in public on

19 June 2023 at 16 hours

by

Delia Irene Fernández de la Fuente

Born 29th of April 1995 in Madrid, Spain

Promotor
Prof. Dr. Johan W. M. Heemskerk, Maastricht University

Co-promotors
Dr. Marijke J. E. Kuijpers, Maastricht University
Dr. Ángel García, Universidade Santiago de Compostela

Assessment Committee
Prof. Dr. Guido Haenen, Maastricht University (chair)
Prof. Dr. María Isabel Loza, Universidade Santiago de Compostela
Dr. Floor C. Heubel-Moenen, Maastricht University
Dr. Manuel Campos, Universidade Santiago de Compostela
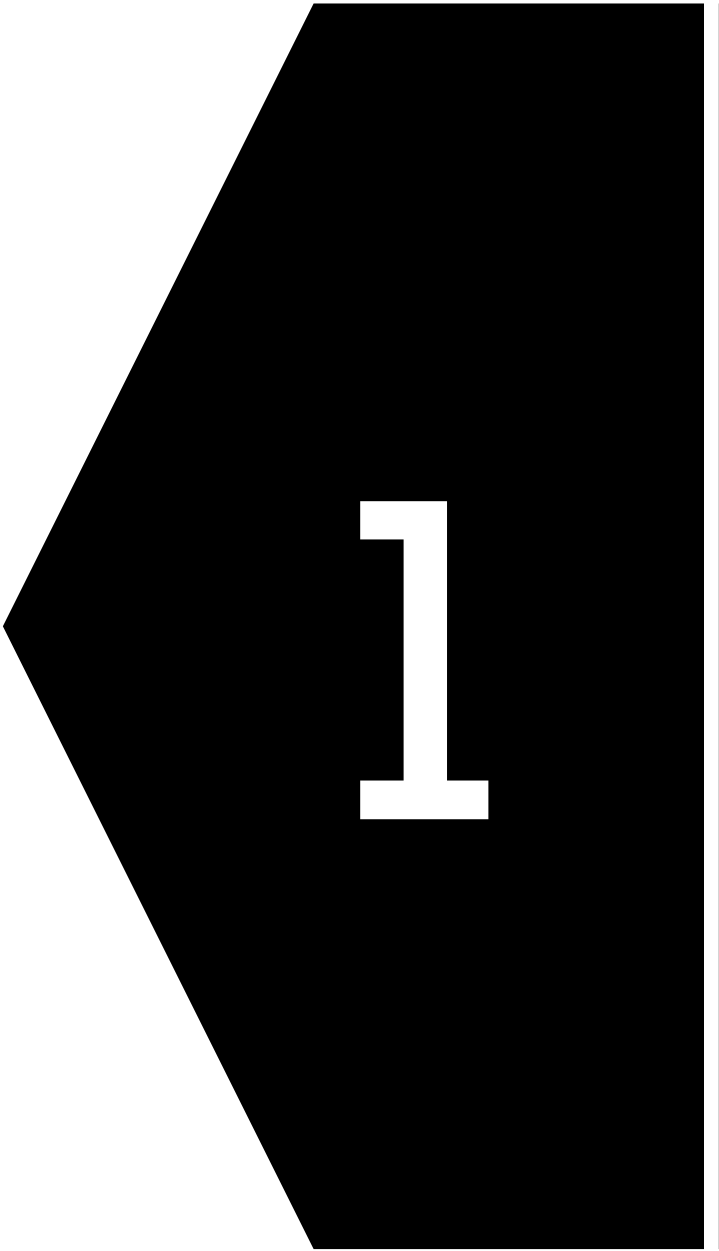Prof. Dr. Hans Deckmyn, Katholieke Universiteit Leuven
Prof. Dr. Helen Philippou, University of Leeds

Contents

1

Chapter 1

General introduction

Cardiovascular disease is still a leading cause of morbidity and disability, accounting for approximately 32% of all deaths worldwide, and causing a high economic burden [1,2]. Blood platelets contribute to the pathophysiological manifestations of major cardiovascular diseases, *i.e.,* ischemic heart disease and stroke, in which vaso-occlusive arterial thrombus formation precedes the organ damage [3]. Platelets are small, anucleate blood cells (2-5 µm in diameter), which protrude from megakaryocytes in the bone marrow in a process called thrombopoiesis [4]. Once formed, platelets circulate in the blood of a healthy individual at numbers ranging from 150 to 450 x 10^9/L, where they have a short lifespan (7-10 days). In addition to major roles in thrombosis and hemostasis, platelets have other (patho)physiological functions, such as in development, tissue repair, host immune defense, inflammation, and cancer [5]. Their clinical relevance is also highlighted by the insight that quantitative or qualitative platelet disorders are associated with a dysregulated hemostasis.

Through this chapter, a general background is provided of the different platelet receptors and signaling pathways that are studied in this thesis. Furthermore, a brief overview is given on recent drug developments and high throughput screening assays, which are available for the search of new anti-platelet agents and for the assessment of platelet function disorders.

Platelet receptors and signaling in hemostasis and thrombosis

Platelet functions are determined by a repertoire of unique surface receptors able to detect physiologic and pathologic stimuli. Upon vascular injury, platelets aggregate to form a plug to seal the injury and initially stop the bleeding [4,6,7]. During platelet activation, many of the receptor-induced signaling pathways converge into the release of Ca^{2+} ions from intracellular stores in the endoplasmic reticulum. The elevated cytosolic Ca^{2+} supports the platelet shape change with pseudopod formation, and also granule secretion, procoagulant activity, and the formation of platelet aggregates [8]. The regulation of this Ca^{2+} signaling and the application of this platelet response for drug discovery is a major theme of this thesis. A prominent role in the maintenance of hemostasis, and also relevant for this thesis, are in platelets glycoprotein (GP)Ib-IX-V, G-protein coupled receptors (GPCR) for soluble agonists, receptors with an immunoreceptor tyrosine-based activation motif (ITAM) as well as integrins [4] (Figure 1).

The initial tethering of circulating platelets to an injured vessel wall occurs at arterial shear rates through interaction between von Willebrand factor (VWF) and glycoprotein Ibα (GPIbα), which is part of the GPIb-IX-V complex [6,9]. The VWF is abundantly present in the circulation, being released by endothelial cells, and it binds to collagen fibers present in the subendothelial matrix exposed upon injury. Unfolding of VWF as a result of shear and collagen binding exposes its A1 domain, which provides the binding site to GPIbα [10]. Platelets become only limitedly activated via GPIbα, for instance by showing transient cytosolic Ca^{2+} oscillations via Src family kinases (SFK), the tyrosine kinase Syk and the effector protein phospholipase Cγ2 (PLCγ2) [11]. Because the VWF-GPIbα

interaction is particularly important under high shear conditions, it is considered that drug interference with this interaction does not result in major bleeding problems [10]. In this thesis, we explored novel ways to block this interaction based on custom-designed cyclic peptides.

Stable platelet adhesion to vascular collagen occurs through the ITAM-containing collagen receptor complex of glycoprotein VI (GPVI) and the Fc receptor γ-chain (FcRγ), with a supporting role of the adhesive collagen receptor, integrin α2β1 (GPIb/IIa), which maintains and stabilizes platelet adhesion [12-16]. The major signaling receptor for collagen is GPVI, which is exclusively expressed in megakaryocytes and platelets, and becomes activated by GPO (glycine-proline-hydroxyproline) motifs in the collagen fibers [16,17]. Adhesion to collagen induces GPVI dimerization and tyrosine phosphorylation of the ITAM motif of FcRγ by Src-family kinases (SFK). This phosphorylation constitutes a docking site for the Src homology 2 (SH2) domain-containing protein tyrosine kinase Syk [18]. The activation of Syk triggers a tyrosine kinase cascade that culminates in PLCγ2 activation, and a prominent increase in cytosolic Ca^{2+} [6,19] (Figure 1).

Studies using GPVI-deficient mice have pointed to a major role of platelet GPVI in vascular integrity, thrombo-inflammation, arterial thrombosis, and thrombus stabilization, but only a minor role in hemostasis [20-22]. Along the same line, platelets from humans with a loss of GPVI show impairments in collagen-induced thrombus formation *in vitro*, while bleeding symptoms are only mild [23]. Besides collagen, also other ligands for GPVI have been discovered, such as fibrin(ogen), laminin, and fibronectin [13,24]. Different agonist-dependent roles of GPVI are known, such as a fibrin-dependent mechanism in the regulation of thrombus stability [24].

Antagonism of GPVI has been suggested as a target for the prevention of arterial thrombosis and thrombo-inflammation [4,13]. It is speculated that also agonist-specific GPVI targeting provides a way of therapeutic interventions [25]. A phase II clinical trial with the GPVI antagonist Glenzocimab in patients with acute ischemic stroke has already provided the first promising results [26].

During collagen-induced platelet activation, autocrine mediators are released from α-granules (containing VWF, fibrinogen, and inflammatory proteins) and dense (δ)-granules (with ADP, ATP, and polyphosphates). In addition, thromboxane A_2 (TxA_2) is released from the platelets through a Ca^{2+}, phospholipase A_2, and cyclooxygenase-1 (COX-1) dependent arachidonic acid metabolism [4]. These released soluble agonists augment the platelet activation process through several GPCRs, including the thromboxane-prostanoid receptor (TP), the purinergic ADP receptors $P2Y_1$ and $P2Y_{12}$, and the ATP receptor channel $P2X_1$ [7]. Further signaling related mechanisms of GPCR in platelets is provided in Chapter 2. The importance of these secondary mediators appears from the knowledge that platelet granule deficiencies (α- and/or δ-granules) are often associated with bleeding symptoms of various severity [27,28].

Another soluble agonist is thrombin, which is generated during the coagulation

process, in particular, triggered by vascular tissue factor. Thrombin stimulates human platelets via the cleavage and tethered-ligand binding of the protease-activated receptors (PAR) 1 and 4. The GPCRs for ADP ($P2Y_1$), TxA_2 (TP), and thrombin (PAR1, PAR4) activate human platelets through PLCβ-dependent cytosolic Ca^{2+} release. Kinetic differences exist in the Ca^{2+} release between ITAM-linked receptors (via PLCγ2) and GPCR (via PLCβ) and subsequent Ca^{2+} entry pathways, which are detailed in the review of Chapter 2. The combined stimulation by collagen (ITAM-linked receptor) and thrombin (GPCR receptor) leads to a high and prolonged Ca^{2+} signal, that is required for the exposure of phosphatidylserine, inducing the so-called procoagulant platelet phenotype, which further stimulates the coagulation process by coagulation factor assembly and activation [4].

After the collagen-induced platelet adhesion and activation, additional platelets are recruited under flow to start the processes of platelet aggregation and thrombus growth [7]. Platelet aggregate formation involves the binding of fibrinogen to integrin αIIbβ3, which is the most abundant integrin on platelets [29]. On resting platelets, the αIIbβ3 is present at low ligand affinity. The activation of platelets through most activating receptors induces the so-called inside-out integrin activation, which converts the αIIbβ3 from resting to an activated conformation [7,30]. The inside-out signaling can occur via a Ca^{2+}-dependent activation of protein kinase C (PKC) or the small GTPase regulator CalDAG-GEFI. This pathway culminates in Rap1b activation, which bridges the actin-binding proteins talin-1 and kindlin-3 to the cytoplasmic αIIbβ3 domains [7,30,31]. This integrin conformational change is reversible and increases its affinity for fibrin, fibrinogen, VWF, and fibronectin [32]. Ligand binding furthermore induces outside-in integrin signaling which via activation of the pathway of SFK Src, Lyn, and/or Fyn, culminates in PLCγ2 and phosphatidylinositol 3-kinase (PI3K) activation [7,33]. The outside-in signaling leads to the cytoskeletal changes required for platelet spreading, and for clot and thrombus contraction.

Extending current antiplatelet treatment

Antiplatelet drugs are important for the prevention and treatment of cardiovascular diseases, such as those induced by atherothrombotic thrombus formation [4]. Common drugs are aspirin, which irreversibly inhibits cyclooxygenase 1 (COX-1), thereby abolishing TxA_2 formation. Low-dose aspirin is widely used as a prophylactic approach in individuals at increased risk of cardiovascular disease, at the expense of an increased risk of bleeding [34,35]. Antagonists of $P2Y_{12}$, such as thienopyridines that irreversibly block the receptor (prodrugs clopidogrel and prasugrel) or reversible $P2Y_{12}$ antagonists (ticagrelor and cangrelor), when used in combination with aspirin, constitute the so-called dual antiplatelet therapy (DAPT, Figure 1). DAPT is recommended as secondary prevention of atherothrombotic events in patients with acute coronary syndrome and after stent implantation for 1 year, while major reductions in events are already seen in the first 3 months [36,37]. The duration of DAPT is recommended to be modified depending on the patient's characteristics, such as a bleeding risk [37,38]. The use of DAPT in comparison to aspirin monotherapy is also recommended for the prevention of recurrent ischemic stroke or transient ischemic attacks, but again taking into account a

bleeding risk [39]. In this respect, recent guidelines suggest a new approach to identify individuals who will most benefit from aspirin use [40].

In use are also intravenous antiplatelet agents blocking integrin αIIbβ3 (abciximab, eptifibatide, or tirofiban), which are mostly restricted to patients undergoing a percutaneous coronary intervention after acute coronary syndrome [34,35]. Less frequent is the use of PAR1 antagonist vorapaxar after an isolated ischemic event. Increased risk of bleeding exists with all these drugs [1,34,41]. Consequently, there is an unmet clinical need for antiplatelet agents that effectively prevent arterial thrombosis, but with no or minimal risk of bleeding.

Over the past years, several new molecular targets for platelet inhibition have been identified. Some novel compounds with good efficacy and safety profile have gone through several phases of drug development and (pre)clinical approval [35]. Biologic inhibitors of GPVI are currently being evaluated as novel antiplatelet drugs, while no reports of bleeding have been reported until now [26,42,43]. Although the biologic anti-GPVI agents (peptide- or antibody-based) show promising results, there is still high interest in finding and clinically testing GPVI-directed small molecules that can be taken by oral administration [44]. Recently, also tyrosine kinase inhibitors, currently applied for some cancer treatments, have shown promising antiplatelet effects, for instance by inhibiting the signaling downstream of GPVI. However, further research is needed for a successful repurpose as antithrombotic drugs [45]. Some time ago, also class I PI3K isoforms, also acting downstream of GPVI, were proposed as platelet-directed antithrombotic targets [46]. Nevertheless, there is still a need to find oral agents interfering at the receptor level of GPVI or proteins downstream. Given that the majority of the current anti-platelet drugs (in)directly target GPCRs, for this thesis I was particularly interested in finding inhibitors with differential effects.

Negative regulators of platelet activation

Several inhibiting agents are known to be critical to maintain platelets in a quiescent, non-adhesive state. These agents also limit the duration and intensity of the activation process in thrombus growth upon injury. Important negative regulation is exerted by molecules released from the endothelium, in particular prostacyclin, acting via the platelet IP receptor, and nitric oxide (NO) diffusing through the platelet membrane (Figure 1) [7]. Prostacyclin and NO increase cyclic AMP and cyclic GMP, respectively, both of which second messengers inhibit platelet functions [41,47]. Other platelet inhibitors include the ecto-nucleotidases CD39 and CD73, present on the surface of endothelial cells, which convert the platelet agonists ATP and ADP into AMP and adenosine. In the blood, thrombin is quickly antagonized by antithrombin, secreted by the liver [6,48].
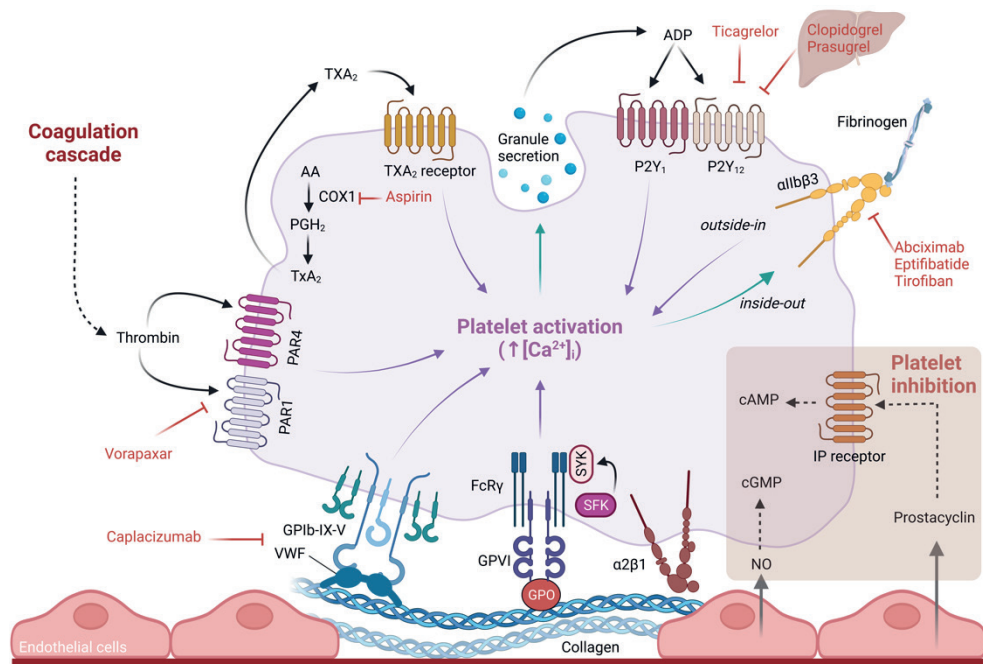
Figure 1. **Model of key receptors in platelet activation and targets of current antiplatelet drugs.** Current models indicate consecutive steps of platelet activation in thrombus formation. (**1**) Upon vessel wall damage, flow-dependent platelets adhere to extracellular matrix components, in particular, collagen and VWF via their receptors, GPVI and GPIb-IX-V, respectively. The GPVI-induced platelet activation requires docking of Syk to a phosphorylated ITAM motif of the co-receptor FcRγ, which leads to signaling responses including a cytosolic $[Ca^{2+}]_i$ rise and integrin αIIbβ3 activation to induce platelet aggregates. (**2**) Granule secretion of ADP and release of the secondary mediator thromboxane A_2 (TxA$_2$), enforces the activation and aggregation of platelets. TxA$_2$ is generated from arachidonic acid (AA) via prostaglandin H$_2$ (PGH$_2$) by cyclooxygenase 1 (COX-1). (**3**) Stimulation of the coagulation cascade generates thrombin, which activates the GPCRs PAR1 and PAR4, implicated among others in cytosolic $[Ca^{2+}]_i$ rises. (**4**) Fibrinogen binding to integrin αIIbβ3 induces thrombus contraction to stabilize the platelet plug. (**5**) The endothelial release of nitric oxide (NO) and prostacyclin (PGI$_2$), which by transmembrane diffusion or IP receptor generate the second messengers, cyclic guanosine monophosphate (cGMP) and cyclic adenosine monophosphate (cAMP), respectively, which play a role in platelet inhibition. For further explanation of the illustrated receptors, see text. Depicted in red are antiplatelets agents approved for clinical use [49,50]. Figure created with BioRender.com.

In recent years, several reports have also indicated a contribution of immunoreceptor tyrosine-based inhibition motif (ITIM)-bearing receptors and their associated tyrosine phosphatases [49]. ITIM-bearing receptors include PECAM1, G6b-B, TREM-like transcript-1 (TLT-1), carcinoembryonic antigen-related cell adhesion molecule 1 and 2 (CEACAM1, 2), and PIR-B [49]. Such receptors have appeared to partly counteract the signaling by the ITAM-linked receptors, GPVI and CLEC-2. The hemi-ITAM-linked CLEC-2 (C-type lectin-like receptor 2) shares its signaling pathway via Syk with GPVI [50]. It likely plays a role in thrombo-inflammation and deep vein thrombosis [13] and has a variety of ligands including podoplanin [51,52]. Another ITAM-linked receptor is the IgG receptor FcγRIIa, the relevance of which in pathological conditions is described in the review of Chapter 2.

In platelets, eight non-receptor protein phosphatases are expressed with either positive or negative modulatory roles, depending on the agonist type [55,56]. The two best-studied Src homology-2 containing protein tyrosine phosphatases (SHP) isoforms, namely SHP1 and SHP2, are encoded by the genes *PTPN6* and *PTPN11*, respectively. Both structurally related proteins can bind to phosphorylated residues of the ITIM-bearing receptors and may thus restrain the ITAM signaling [49,57-59]. The ubiquitously expressed SHP2 is generally regarded as a positive regulator of growth factor and cytokine receptor signaling [60]. Yet, in platelets, SHP2 has been shown to negatively regulate collagen-induced thrombus formation, such as concluded from murine studies with conditional knockouts and mice with a loss-of-function mutation in *Ptpn11* [61,62].

In humans, gain-of-function mutations in SHP2 link to the so-called Noonan syndrome. Somatic mutations have also been observed in some types of cancers, including leukemias, neuroblastomas, and lung and breast cancers [63]. In agreement with a negative regulatory role of human platelet SHP2, bleeding symptoms are observed in about half of the Noonan patients [64]. Blood from these patients often shows a reduced platelet aggregation in response to low collagen, and a low thrombus build-up under flow conditions [61]. The idea of targeting SHP2 in cancers led to the discovery of the compound SHP099 as a first-in-class selective, potent, and orally available allosteric inhibitor of SHP2 [65,66]. The drug SHP099 acts by stabilizing the phosphatase SHP2 in an auto-inhibited conformation. Clinical trials with derivatives of this compound are ongoing for the treatment of solid cancers [60]. In platelet research, in the context of the mild bleeding defect in Noonan syndrome, the effects of SHP099 have not yet been examined.

Assessment of platelet-based bleeding disorders: potential of microfluidic flow chambers

Genetic-based platelet function disorders form a heterogeneous group of diseases caused by mutations in genes that are relevant for platelet formation or platelet functions [67,68]. Such disorders present with variable bleeding complications that can be low or even life-threatening. The platelet disorders can present as thrombocytopenia or as defects in platelet responses with a normal platelet count. In a recent genome database, the prevalence of loss-of-function variants in platelet-regulating genes, excluding von Willebrand disease and coagulation factors, was estimated at 0.33% of the general population [69]. However, in patients presenting with bleeding problems, the prevalence of platelet dysfunctions, including platelet secretion defects and menorrhagia, ranges from 19% up to 40% [68,70-74]. This suggests that abnormalities of platelet responses are common, but also heterogeneous with genetic and non-genetic causes of bleeding.

Over the past decades, the diagnostics of platelet disorders have been improved with a growing list of mutated genes, so-called pathogenic or likely pathogenic mutations, which are known to associate with quantitative or qualitative platelet defects [75,76]. While the use of genetic testing has helped in the identification of molecular links and diagnosis, in many

cases the cause of a platelet disorder remains unclear [77-79]. This is exemplified by the UK GAPP and Bloodomics studies, where in the different cohorts, the genetic cause of 11 to 78.9% of patients, with platelet function defects and /or bleeding symptoms could not be identified [28,79,80]. Therefore, this topic requires further attention.

The current standard diagnosis of aberrant platelet function is based on the use of light transmission aggregation (LTA) with a panel of platelet agonists (ADP, epinephrine, collagen, arachidonic acid, ristocetin), in combination with blood cell counts, and a detailed assessment of the personal and family medical history [68,81]. In the initial stage, exclusion of a coagulopathy or von Willebrand disease is needed, which is done by plasma measurements of the prothrombin time, activated partial thromboplastin time, and VWF activity and antigen [68]. While LTA primarily informs on a platelet aggregation defect, it can also provide information on the secretion of ATP. However, LTA measurements are time-consuming and require blood centrifugation, while the outcome may depend on pre-analytical variables [82,83].

Specialized clinical laboratories perform additional platelet tests. Flow cytometry is used for the characterization of platelet receptor defects and to assess for granule secretion (markers P-selectin and CD63) or phosphatidylserine exposure (marker annexin A5). An alternative is the measurement of platelet uptake and secretion of mepacrine [68,81]. The only test used in most laboratories that measures platelet activation under (patho)physiological shear stress is the platelet function analyzer (PFA-100), although because of limited sensitivity, it is not recommended as a screening test for mild platelet disorders [68,83]. Other point-of-care instruments using whole blood - used in some hospitals -, are VerifyNow, PlateletWorks, T-TAS, and thrombo-elastography, but also here the sensitivity to detect a bleeding disorder is limited [84]. Therefore, more sensitive diagnostic assays are needed that detect platelet hemostatic abnormalities preferably using whole-blood samples.

Multiple laboratories have been using microfluidic whole-blood flow assays to study platelet thrombus formation *in vitro* using human blood [85,86]. By including a number of platelet-adhesive surfaces*, e.g.* collagen, VWF, fibrinogen, and laminin, detailed information can be obtained on the function of distinct adhesive receptors for a certain blood sample. Microfluidic assays can thus report on the effects of genetic variation of the collagen receptor GPVI [23,87], and on platelet dysfunction in inherited bleeding disorders such as gray platelet syndrome (defect in α-granule secretion), storage pool disease (defect in δ-granule secretion), Bernard-Soulier syndrome (defect in GPIb-V-IX), Glanzmann's thrombasthenia (defect in integrin αIIbβ3), and von Willebrand disease [88-90].

Recently, microfluidic testing has been proposed as an additive platelet function test in patients with prolonged PFA-100 closure times and bleeding of unknown cause [91]. It might also be useful to phenotype the platelets from patients with other pathogenic variants. In addition, this testing can be used to quantify the effect of anti-platelet medication in patients at risk [92,93]. In this thesis, we investigated whether current clinical approaches may benefit from the use of microfluidics to characterize patients with hemostatic abnormalities.

Discovery approaches for the development of anti-platelet drugs: *in silico* and phenotypic screening methods

The field of drug discovery and development uses complex, expensive, time-consuming, and multi-stage procedures with high attrition rates [94,95]. Starting with a target discovery stage, extensive validation procedures, hit identification, and lead discovery phases are required for obtaining a candidate drug (Figure 2). During the hit identification phase, small molecules, biologics, peptides, or peptidomimetics can be tested by way of functional screening assays or by *in silico* methods [94,96]. The lead discovery phase aims to find and select a drug-like small molecule or biological, that may progress into preclinical testing models. If successful, the candidate drug passes to clinical development and ultimately can become a marketable medicine.

A variety of screening methodologies exist to identify hit molecules. In this thesis, the focus is on high throughput screening (HTS) of small molecules and also on the *in silico* structure-based molecular design of receptor-interfering peptides. HTS refers to integrated protocols that allow the rapid evaluation of high numbers of molecules using a standardized bioassay [94,97]. It involves robust laboratory automation and assay miniaturization techniques in order to save time and reduce costs. Additionally, HTS involves automated data processing tools to aid in the analysis of many biological data and to predict the efficacy and side effects of lead compounds in animals and humans [96,98]. The output of a small-molecule screen is termed a hit molecule [94], which needs to have a selective activity towards the target protein (biochemical HTS) or for the cellular response (phenotypic HTS) (Figure 2). A strong phenotypic HTS provides new biological information, preferably in combination with drug toxicity information [97].

In the last decades, a few HTS assays have been carried out to find new molecules that can modulate platelet functions, as a novel approach in platelet pharmacological research. These were directed at phosphodiesterase inhibitors [99], 1,3-diamino benzenes [100], platelet Ca^{2+} flux assays [101], and PAR4 antagonists [102]. In the present thesis, I have extended the earlier work to obtain an ultra-HTS assay based on 1536-well plates for the assessment of agonist-induced cytosolic $[Ca^{2+}]_i$ rises in platelets. The assay needs to assess the effects of a high number of compounds on platelets at the same time.

In general, nine out of ten drug candidates fail between the clinical trial and the regulatory approval [94], revealing a need for alternative strategies to reduce the time frame and the costs of drug discovery. In this respect, *in silico* drug discovery can be a valuable tool to predict the optimal characteristics of a first hit and to develop this into a viable clinical candidate drug [96,98]. For this purpose, computer-aided molecular design methods can be used in the development of new chemical entities for testing in phase I clinical trials [103].
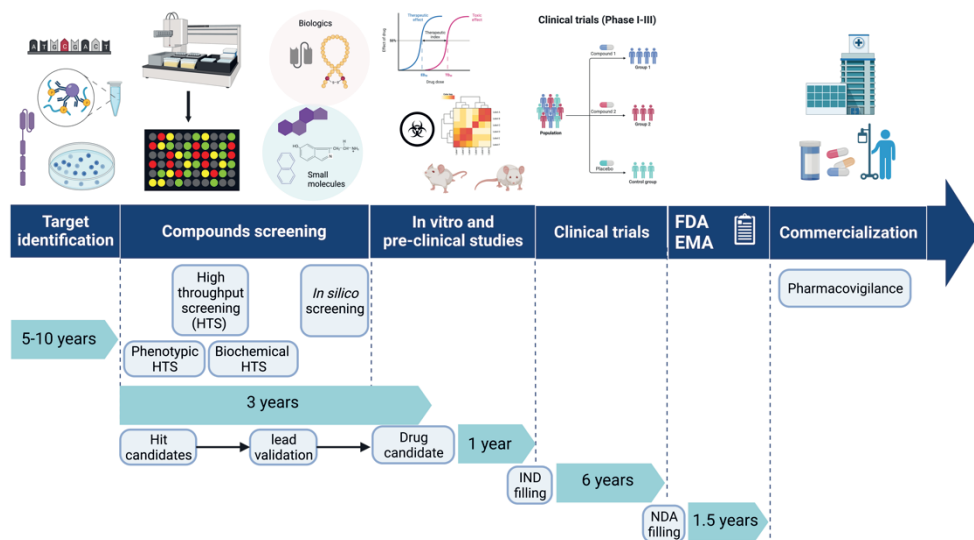
Figure 2. Overview of a typical drug discovery and clinical development program. Shown is a drug discovery process from the target identification until the commercialization, with an approximate time scale for each step. The druggable protein under study will determine the selection of appropriate compound data for screening (*i.e.* drug-like small molecules, natural compounds, or peptide libraries). Once a hit has been identified, secondary assays are needed to confirm its efficacy and selectivity, and to establish the pharmacological properties. The compound then undergoes a hit-to-lead optimization to improve the affinity and bioavailability. This finally results in a drug candidate that can be assessed *in vivo* and may further be studied in clinical trials. *Abbreviations*: FDA, Food and Drug Administration; EMA, European Medication Agency; IND, Investigational New Drug, NDA, New Drug Application. Adapted from Refs. [90,101,102]. Figure created with BioRender.com

As examined in this thesis, *in silico* methods can also be used for the design of peptides able to interfere in defined protein-protein interactions. Software packages generating structure-based protein conformations exploit the three-dimensional structure of a target protein-protein complex to rationally design modulatory compounds (inhibitors or stabilizers). Molecular dynamic simulations and minimal binding free energy calculations are often used to predict native-like docking conformations [96,104]. These *in silico* methods are highly cost-effective, which can accelerate the discovery process and optimal drug design. However, the results of *in silico* methods are only predictive and may not correlate with biological affinities. Accordingly, this approach needs biological validation.

Screening approaches usually focus on small compounds or biologics. Small molecules are suitable for oral intake but may be less suited to interfere in complex and extended protein-protein interactions [94,96,107]. In this thesis, we performed an *in silico* screening for peptides aimed to interfere in the complex, shear-dependent interaction of VWF with platelet GPIbα. Herein, we made use of developments in the peptide field for obtaining chemical modifications to improve the stability, affinity, and specificity [108]. Accordingly, we synthesized a series of cyclic peptides, as these have small molecule drug-like properties and still show antibody-like high binding affinities with minimal toxicity.

Aims and outline of this thesis

This thesis aims to develop and use high-throughput assays to better evaluate the functions and signaling pathways of platelets, and to find novel ways of inhibition of platelet functions in disease. The focus is on platelet Ca^{2+} signaling and multiparameter microfluidic thrombus formation. The general introduction of this **Chapter 1** provides background information on the signaling pathways controlling platelet activation, as well as information on platelet-based bleeding disorders, compound screening methods, and drug development procedures. **Chapter 2** reviews the main platelet cytosolic Ca^{2+} signaling pathways such as those induced by GPCRs, acting via PLCβ isoforms; and induced by ITAM-linked receptors, acting via PLCγ isoforms. The chapter highlights both the differences and the synergy between the two Ca^{2+} signaling pathways. Jointly these routes evoke the Ca^{2+}-dependent activation of the channel protein, anoctamin-6, which accomplishes the formation of a population of coagulation-active platelets, *i.e.* procoagulant platelets expressed phosphatidylserine. In addition, Chapter 2 raises the question of whether the pathway-dependent Ca^{2+} flux measurements in platelets can be used to find new antiplatelet compounds. In **Chapter 3**, we examine the role of the protein tyrosine kinase Syk in platelet activation via the ITAM-linked GPVI receptor in response to multiple ligands, such as collagen types and collagen-related peptides. Investigated is to which extent these ligands can induce Syk-dependent cytosolic Ca^{2+} rises in platelets, and how these trigger thrombus formation via GPVI and Syk pathway in whole blood microfluidic experiments. **Chapter 4** describes the development of an ultra-high throughput assay for the kinetic measurements of platelet cytosolic Ca^{2+} rises in 96-well, 384-well, and 1536-well plates. The obtained method provides a means to differentiate between the Ca^{2+} signal induced by either GPVI or GPCR. A new multiparameter way of Ca^{2+} curve analysis is introduced to fully describe the platelet Ca^{2+} responses. Verification of the assay is done with a robustness compound library and with a panel of clinically relevant platelet inhibitors. In **Chapter 5**, the assay method of chapter 4 is further employed to conduct a screening to find novel antiplatelet hits using a chemical library of 16,640 small molecules. After a stringent selection process, small molecules are further evaluated using platelet function tests in comparison to a panel of established platelet inhibitors. Thereby, we want to understand the mechanism of action and the suitability of the new compounds. **Chapter 6** concentrates on the supposed inhibitory pathway of GPVI via the protein tyrosine phosphatase SHP2. In this chapter, using the allosteric SHP2 inhibitor, SHP099, the conditions at which the phosphatase pathway can restrain the platelet-activating effect of GPVI are determined. The drug-like compound SHP099 is tested on blood from Noonan patients with a gain-of-function mutation in the *PTPN11* gene coding for SHP2, often combined with a bleeding phenotype. The question is whether this drug can improve the hemostatic profile of the patients, as assessed by microfluidic whole blood tests *in vitro*. Plasma-derived VWF binds to collagen and allows shear-dependent platelet aggregation and thrombus formation via the GPIb-V-IX complex. In **Chapter 7**, we investigate the possibility to interfere in the shear-dependent VWF interaction with GPIbα, using a set of *in silico*

designed and chemically synthesized cyclic peptides. Structural peptide templates are designed in two rounds, and, after synthesis, tested for their effects on platelet adhesion and aggregation in shear-dependent thrombus formation. In **Chapter 8**, the high-throughput microfluidic method of whole blood thrombus formation on a series of microspotted surfaces is used to phenotype the platelets from multiple patients with a familial history of bleeding and extensive genotyping. The suitability of the multiparameter procedures for distinguishing genetic-related phenotypes is evaluated. In the last chapter of this thesis, **Chapter 9**, the most important findings of this thesis are highlighted and discussed in relation to the current literature.

References

1. Baqi Y, Muller CE. Antithrombotic P2Y$_{12}$ receptor antagonists: recent developments in drug discovery. *Drug Discov Today.* 2019;24:325-333.
2. World Health Organisation. Cardiovascular disease (CVDs). https://www.who.int/en/news-room/fact-sheets/detail/cardiovascular-diseases-(cvds). Published 11 June, 2021. Accessed 10 November, 2022.
3. Koupenova M, Kehrel BE, Corkrey HA, Freedman JE. Thrombosis and platelets: an update. *Eur Heart J.* 2017;38:785-791.
4. Van der Meijden PE, Heemskerk JW. Platelet biology and functions: new concepts and clinical perspectives. *Nat Rev Cardiol.* 2019;16:166-179.
5. Tyagi T, Jain K, Gu SX, et al. A guide to molecular and functional investigations of platelets to bridge basic and clinical sciences. *Nat Cardiovasc Res.* 2022;1:223-237.
6. Versteeg HH, Heemskerk JW, Levi M, Reitsma PH. New fundamentals in hemostasis. *Physiol Rev.* 2013;93:327-358.
7. Estevez B, Du X. New concepts and mechanisms of platelet activation signaling. *Physiology (Bethesda).* 2017;32:162-177.
8. Varga-Szabo D, Braun A, Nieswandt B. Calcium signaling in platelets. *J Thromb Haemost.* 2009;7:1057-1066.
9. Clemetson KJ. Platelets and primary haemostasis. *Thromb Res.* 2012;129:220-224.
10. Vanhoorelbeke K, Ulrichts H, Van de Walle G, Fontayne A, Deckmyn H. Inhibition of platelet glycoprotein Ib and its antithrombotic potential. *Curr Pharm Des.* 2007;13:2684-2697.
11. Ruggeri ZM, Mendolicchio GL. Interaction of von Willebrand factor with platelets and the vessel wall. *Hamostaseologie.* 2015;35:211-224.
12. Depraetere H, Wille C, Gansemans Y, et al. The integrin $\alpha2\beta1$ (GPIa/IIa)-I-domain inhibits platelet-collagen interaction. *Thromb Haemost.* 1997;77:981-985.
13. Rayes J, Watson SP, Nieswandt B. Functional significance of the platelet immune receptors GPVI and CLEC-2. *J Clin Invest.* 2019;129:12-23.
14. Nieswandt B, Brakebusch C, Bergmeier W, et al. Glycoprotein VI but not $\alpha2\beta1$ integrin is essential for platelet interaction with collagen. *EMBO J.* 2001;20:2120-2130.
15. Kuijpers MJ, Schulte V, Bergmeier W, et al. Complementary roles of glycoprotein VI and $\alpha2\beta1$ integrin in collagen-induced thrombus formation in flowing whole blood ex vivo. *FASEB J.* 2003;17:685-687.
16. Nieswandt B, Watson SP. Platelet-collagen interaction: is GPVI the central receptor? *Blood.* 2003;102:449-461.
17. Feitsma LJ, Brondijk HC, Jarvis GE, et al. Structural insights into collagen binding by platelet receptor glycoprotein VI. *Blood.* 2022;139:3087-3098.
18. Poulter NS, Pollitt AY, Owen DM, et al. Clustering of glycoprotein VI (GPVI) dimers upon adhesion to collagen as a mechanism to regulate GPVI signaling in platelets. *J Thromb Haemost.* 2017;15:549-564.

19. Mammadova-Bach E, Nagy M, Heemskerk JW, Nieswandt B, Braun A. Store-operated calcium entry in thrombosis and thrombo-inflammation. *Cell Calcium.* 2019;77:39-48.

20. Jandrot-Perrus M, Busfield S, Lagrue AH, et al. Cloning, characterization, and functional studies of human and mouse glycoprotein VI: a platelet-specific collagen receptor from the immunoglobulin superfamily. *Blood.* 2000;96:1798-1807.

21. Dumont B, Lasne D, Rothschild C, et al. Absence of collagen-induced platelet activation caused by compound heterozygous GPVI mutations. *Blood.* 2009;114:1900-1903.

22. Bender M, May F, Lorenz V, et al. Combined in vivo depletion of glycoprotein VI and C-type lectin-like receptor 2 severely compromises hemostasis and abrogates arterial thrombosis in mice. *Arterioscler Thromb Vasc Biol.* 2013;33:926-934.

23. Nagy M, Perrella G, Dalby A, et al. Flow studies on human GPVI-deficient blood under coagulating and noncoagulating conditions. *Blood Adv.* 2020;4(13):2953-2961.

24. Perrella G, Nagy M, Watson SP, Heemskerk JW. Platelet GPVI (glycoprotein VI) and thrombotic complications in the venous system. *Arterioscler Thromb Vasc Biol.* 2021;41:2681-2692.

25. Montague SJ, Hicks SM, Lee CS, et al. Fibrin exposure triggers αIIbβ3-independent platelet aggregate formation, ADAM10 activity and glycoprotein VI shedding in a charge-dependent manner. *J Thromb Haemost.* 2020;18:1447-1458.

26. Wichaiyo S, Parichatikanond W, Rattanavipanon W. Glenzocimab: a GPVI (glycoprotein VI)-targeted potential antiplatelet agent for the treatment of acute ischemic stroke. *Stroke.* 2022;53:3506-3513.

27. Nurden A, Nurden P. Advances in our understanding of the molecular basis of disorders of platelet function. *J Thromb Haemost.* 2011;9 Suppl 1:76-91.

28. Watson SP, Lowe GC, Lordkipanidze M, Morgan NV, GAPP_Consortium. Genotyping and phenotyping of platelet function disorders. *J Thromb Haemost.* 2013;11 Suppl. 1:351-363.

29. Burkhart JM, Vaudel M, Gambaryan S, et al. The first comprehensive and quantitative analysis of human platelet protein composition allows the comparative analysis of structural and functional pathways. *Blood.* 2012;120:e73-82.

30. Stefanini L, Bergmeier W. RAP GTPases and platelet integrin signaling. *Platelets.* 2019;30:41-47.

31. Nieswandt B, Varga-Szabo D, Elvers M. Integrins in platelet activation. *J Thromb Haemost.* 2009;7 Suppl. 1:206-209.

32. Zou J, Swieringa F, de Laat B, de Groot PG, Roest M, Heemskerk JW. Reversible platelet integrin αIIbβ3 activation and thrombus instability. *Int J Mol Sci.* 2022;23:12512.

33. Durrant TN, van den Bosch MT, Hers I. Integrin αIIbβ3 outside-in signaling. *Blood.* 2017;130:1607-1619.

34. Grove EL, Wurtz M, Thomas MR, Kristensen SD. Antiplatelet therapy in acute coronary syndromes. *Expert Opin Pharmacother.* 2015;16:2133-2147.

35. Tscharre M, Michelson AD, Gremmel T. Novel antiplatelet agents in cardiovascular disease. *J Cardiovasc Pharmacol Ther.* 2020;25:191-200.

36. Wilson SJ, Newby DE, Dawson D, Irving J, Berry C. Duration of dual antiplatelet therapy in acute coronary syndrome. *Heart.* 2017;103:573-580.

37. Sidhu MS, Lyubarova R, Bangalore S, Bonaca MP. Challenges of long-term dual antiplatelet therapy use following acute coronary syndromes. *Am Heart J.* 2022;246:44-64.

38. Levine GN, Bates ER, Bittl JA, et al. 2016 ACC/AHA guideline focused update on duration of dual antiplatelet therapy in patients with coronary artery disease: a report of the American College of Cardiology/American Heart Association Task Force on Clinical Practice Guidelines. *J Am Coll Cardiol.* 2016;68:1082-1115.

39. Bhatia K, Jain V, Aggarwal D, et al. Dual antiplatelet therapy versus aspirin in patients with stroke or transient ischemic attack: meta-analysis of randomized controlled trials. *Stroke.* 2021;52:e217-223.

40.   Cofer LB, Barrett TJ, Berger JS. Aspirin for the primary prevention of cardiovascular disease: time for a platelet-guided approach. *Arterioscler Thromb Vasc Biol.* 2022;42:1207-1216.

41.   Mega JL, Simon T. Pharmacology of antithrombotic drugs: an assessment of oral antiplatelet and anticoagulant treatments. *Lancet.* 2015;386:281-291.

42.   Groschel K, Uphaus T, Loftus I, et al. Revacept, an inhibitor of platelet adhesion in Symptomatic carotid artery stenosis: design and rationale of a randomized phase II clinical trial. *TH Open.* 2020;4:e393-399.

43.   Mayer K, Hein-Rothweiler R, Schupke S, et al. Efficacy and safety of Revacept, a novel lesion-directed competitive antagonist to platelet glycoprotein VI, in patients undergoing elective percutaneous coronary intervention for stable ischemic heart disease: the randomized, double-blind, placebo-controlled ISAR-PLASTER phase 2 trial. *JAMA Cardiol.* 2021;6:753-761.

44.   Foster H, Wilson C, Philippou H, Foster R. Progress toward a glycoprotein VI modulator for the treatment of thrombosis. *J Med Chem.* 2020;63:12213-12242.

45.   Tullemans BM, Heemskerk JW, Kuijpers MJ. Acquired platelet antagonism: off-target antiplatelet effects of malignancy treatment with tyrosine kinase inhibitors. *J Thromb Haemost.* 2018;16:1686-1699.

46.   Jackson SF, Schoenwaelder SM. Type I phosphoinositide 3-kinases: potential antithrombotic targets? *Cell Mol Life Sci.* 2006;63:1085-1090.

47.   Kherallah RY, Khawaja M, Olson M, Angiolillo D, Birnbaum Y. Cilostazol: a review of basic mechanisms and clinical uses. *Cardiovasc Drugs Ther.* 2022;36:777-792.

48.   Deaglio S, Robson SC. Ectonucleotidases as regulators of purinergic signaling in thrombosis, inflammation, and immunity. *Adv Pharmacol.* 2011;61:301-332.

49.   Coxon CH, Geer MJ, Senis YA. ITIM receptors: more than just inhibitors of platelet activation. *Blood.* 2017;129:3407-3418.

50.   Izquierdo I, Barrachina MN, Hermida-Nogueira L, et al. A comprehensive tyrosine phosphoproteomic analysis reveals novel components of the platelet CLEC-2 signaling cascade. *Thromb Haemost.* 2020;120:262-276.

51.   Bourne JH, Colicchia M, Di Y, et al. Heme induces human and mouse platelet activation through C-type-lectin-like receptor-2. *Haematologica.* 2021;106:626-629.

52.   Moran LA, Di Y, Sowa MA, et al. Katacine is a new ligand of CLEC-2 that acts as a platelet agonist. *Thromb Haemost.* 2022;122:1361-1368.

53.   Franchi F, Angiolillo DJ. Novel antiplatelet agents in acute coronary syndrome. *Nat Rev Cardiol.* 2015;12:30-47.

54.   Angiolillo DJ, Galli M, Collet JP, Kastrati A, O'Donoghue ML. Antiplatelet therapy after percutaneous coronary intervention. *EuroIntervention.* 2022;17:e1371-1396.

55.   Faria AV, Andrade SS, Peppelenbosch MP, Ferreira-Halder CV, Fuhler GM. The role of phospho-tyrosine signaling in platelet biology and hemostasis. *Biochim Biophys Acta.* 2021;1868:118927.

56.   Heemskerk JW. More than reverting tyrosine kinases. *Blood.* 2022;140:939-941.

57.   Barrow AD, Astoul E, Floto A, et al. Cutting edge: TREM-like transcript-1, a platelet immunoreceptor tyrosine-based inhibition motif encoding costimulatory immunoreceptor that enhances, rather than inhibits, calcium signaling via SHP-2. *J Immunol.* 2004;172:5838-5842.

58.   Mazharian A, Mori J, Wang YJ, et al. Megakaryocyte-specific deletion of the protein-tyrosine phosphatases Shp1 and Shp2 causes abnormal megakaryocyte development, platelet production, and function. *Blood.* 2013;121:4205-4220.

59.   Geer MJ, van Geffen JP, Gopalasingam P, et al. Uncoupling ITIM receptor G6b-B from tyrosine phosphatases Shp1 and Shp2 disrupts murine platelet homeostasis. *Blood.* 2018;132:1413-1425.

60.   Song Z, Wang M, Ge Y, et al. Tyrosine phosphatase SHP2 inhibitors in tumor-targeted therapies. *Acta Pharm Sin B.* 2021;11:13-29.

61.   Bellio M, Garcia C, Edouard T, et al. Catalytic dysregulation of SHP2 leading to Noonan syndromes affects platelet signaling and functions. *Blood.* 2019;134:2304-2317.

62.   Hu M, Liu P, Liu Y, et al. Platelet Shp2 negatively regulates thrombus stability under high shear stress. *J Thromb Haemost.* 2019;17:220-231.

63.   Bentires-Alj M, Paez JG, David FS, et al. Activating mutations of the Noonan syndrome-associated SHP2/PTPN11 gene in human solid tumors and adult acute myelogenous leukemia. *Cancer Res.* 2004;64:8816-8820.

64.   Artoni A, Selicorni A, Passamonti SM, et al. Hemostatic abnormalities in Noonan syndrome. *Pediatrics.* 2014;133:e1299-e1304.

65.   Chen YN, LaMarche MJ, Chan HM, et al. Allosteric inhibition of SHP2 phosphatase inhibits cancers driven by receptor tyrosine kinases. *Nature.* 2016;535:148-152.

66.   Garcia Fortanet J, Chen CH, Chen YN, et al. Allosteric inhibition of SHP2: identification of a potent, selective, and orally efficacious phosphatase inhibitor. *J Med Chem.* 2016;59:7773-7782.

67.   Palma-Barqueros V, Revilla N, Sanchez A, et al. Inherited platelet disorders: an updated overview. *Int J Mol Sci.* 2021;22:4521.

68.   Bourguignon A, Tasneem S, Hayward CP. Screening and diagnosis of inherited platelet disorders. *Crit Rev Clin Lab Sci.* 2022;59:1-40.

69.   Oved JH, Lambert MP, Kowalska MA, Poncz M, Karczewski KJ. Population based frequency of naturally occurring loss-of-function variants in genes associated with platelet disorders. *J Thromb Haemost.* 2021;19:248-254.

70.   Philipp CS, Dilley A, Miller CH, et al. Platelet functional defects in women with unexplained menorrhagia. *J Thromb Haemost.* 2003;1:477-484.

71.   Quiroga T, Goycoolea M, Panes O, et al. High prevalence of bleeders of unknown cause among patients with inherited mucocutaneous bleeding. A prospective study of 280 patients and 299 controls. *Haematologica.* 2007;92:357-365.

72.   Lotta LA, Maino A, Tuana G, et al. Prevalence of disease and relationships between laboratory phenotype and bleeding severity in platelet primary secretion defects. *PLoS One.* 2013;8:e60396.

73.   Seravalli V, Linari S, Peruzzi E, Dei M, Paladino E, Bruni V. Prevalence of hemostatic disorders in adolescents with abnormal uterine bleeding. *J Pediatr Adolesc Gynecol.* 2013;26:285-289.

74.   Vo KT, Grooms L, Klima J, Holland-Hall C, O'Brien SH. Menstrual bleeding patterns and prevalence of bleeding disorders in a multidisciplinary adolescent haematology clinic. *Haemophilia.* 2013;19:71-75.

75.   Ver Donck F, Labarque V, Freson K. Hemostatic phenotypes and genetic disorders. *Res Pract Thromb Haemost.* 2021;5:e12637.

76.   Megy K, Downes K, Simeoni I, et al. Curated disease-causing genes for bleeding, thrombotic, and platelet disorders: communication from the SSC of the ISTH. *J Thromb Haemost.* 2019;17:1253-1260.

77.   Maclachlan A, Watson SP, Morgan NV. Inherited platelet disorders: Insight from platelet genomics using next-generation sequencing. *Platelets.* 2017;28:14-19.

78.   Bastida JM, Lozano ML, Benito R, et al. Introducing high-throughput sequencing into mainstream genetic diagnosis practice in inherited platelet disorders. *Haematologica.* 2018;103:148-162.

79.   Downes K, Megy K, Duarte D, et al. Diagnostic high-throughput sequencing of 2396 patients with bleeding, thrombotic, and platelet disorders. *Blood.* 2019;134:2082-2091.

80.   Khan AO, Stapley RJ, Pike JA, et al. Novel gene variants in patients with platelet-based bleeding using combined exome sequencing and RNAseq murine expression data. *J Thromb Haemost.* 2021;19:262-268.

81.   Gomez K, Anderson J, Baker P, et al. Clinical and laboratory diagnosis of heritable platelet disorders in adults and children: a British Society for Haematology Guideline. *Br J Haematol.* 2021;195:46-72.

82.   Cattaneo M. Light transmission aggregometry and ATP release for the diagnostic assessment of platelet function. *Semin Thromb Hemost.* 2009;35:158-167.

83. Moenen F, Vries MJA, Nelemans PJ, et al. Screening for platelet function disorders with multiplate and platelet function analyzer. *Platelets.* 2019;30:81-87.

84. Paniccia R, Priora R, Liotta AA, Abbate R. Platelet function tests: a comparative review. *Vasc Health Risk Manag.* 2015;11:133-148.

85. Schoeman RM, Lehmann M, Neeves KB. Flow chamber and microfluidic approaches for measuring thrombus formation in genetic bleeding disorders. *Platelets.* 2017;28:463-471.

86. Provenzale I, Brouns SLN, van der Meijden PE, Swieringa F, Heemskerk JW. Whole blood based multiparameter assessment of thrombus formation in standard microfluidic devices to proxy in vivo haemostasis and thrombosis. *Micromachines (Basel).* 2019;10:787.

87. Van Geffen JP, Brouns SL, Batista J, et al. High-throughput elucidation of thrombus formation reveals sources of platelet function variability. *Haematologica.* 2019;104:1256-1267.

88. De Witt SM, Swieringa F, Cavill R, et al. Identification of platelet function defects by multi-parameter assessment of thrombus formation. *Nat Commun.* 2014;5:4257.

89. Brouns SL, van Geffen JP, Heemskerk JW. High-throughput measurement of human platelet aggregation under flow: application in hemostasis and beyond. *Platelets.* 2018;29:662-669.

90. Lehmann M, Ashworth K, Manco-Johnson M, Di Paola J, Neeves KB, Ng CJ. Evaluation of a microfluidic flow assay to screen for von Willebrand disease and low von Willebrand factor levels. *J Thromb Haemost.* 2018;16:104-115.

91. Heubel-Moenen FC, Brouns SLN, Herfs L, et al. Multiparameter platelet function analysis of bleeding patients with a prolonged platelet function analyser closure time. *Br J Haematol.* 2022;196:1388-1400.

92. Al Ghaithi R, Mori J, Nagy Z, et al. Evaluation of the total thrombus-formation system (T-TAS): application to human and mouse blood analysis. *Platelets.* 2019;30:893-900.

93. Herfs L, Swieringa F, Jooss N, et al. Multiparameter microfluidics assay of thrombus formation reveals increased sensitivity to contraction and antiplatelet agents at physiological temperature. *Thromb Res.* 2021;203:46-56.

94. Hughes JP, Rees S, Kalindjian SB, Philpott KL. Principles of early drug discovery. *Br J Pharmacol.* 2011;162:1239-1249.

95. Waring MJ, Arrowsmith J, Leach AR, et al. An analysis of the attrition of drug candidates from four major pharmaceutical companies. *Nat Rev Drug Discov.* 2015;14:475-486.

96. Rognan D. The impact of in silico screening in the discovery of novel and safer drug candidates. *Pharmacol Ther.* 2017;175:47-66.

97. Etzion Y, Muslin AJ. The application of phenotypic high-throughput screening techniques to cardiovascular research. *Trends Cardiovasc Med.* 2009;19:207-212.

98. Fleming N. How artificial intelligence is changing drug discovery. *Nature.* 2018;557:s55-57.

99. Sim DS, Merrill-Skoloff G, Furie BC, Furie B, Flaumenhaft R. Initial accumulation of platelets during arterial thrombus formation in vivo is inhibited by elevation of basal cAMP levels. *Blood.* 2004;103:2127-2134.

100. Dockendorff C, Aisiku O, Verplank L, et al. Discovery of 1,3-diaminobenzenes as selective inhibitors of platelet activation at the PAR1 receptor. *ACS Med Chem Lett.* 2012;3:232-237.

101. Bye AP, Unsworth AJ, Gibbins JM. Screening and high-throughput platelet assays. *Methods Mol Biol.* 2018;1812:81-94.

102. Young SE, Duvernay MT, Schulte ML, Lindsley CW, Hamm HE. Synthesis of indole derived protease-activated receptor 4 antagonists and characterization in human platelets. *PLoS One.* 2013;8:e65528.

103. Hillisch A, Heinrich N, Wild H. Computational chemistry in the pharmaceutical industry: from childhood to adolescence. *ChemMedChem.* 2015;10:1958-1962.

104. Wichapong K, Poelman H, Ercig B, et al. Rational modulator design by exploitation of protein-protein complex structures. *Future Med Chem.* 2019;11:1015-1033.

105.   Roses AD. Pharmacogenetics in drug discovery and development: a translational perspective. *Nat Rev Drug Discov.* 2008;7:807-817.

106.   Daoud NE, Borah P, Deb PK, et al. ADMET profiling in drug discovery and development: perspectives of in silico, in vitro and integrated approaches. *Curr Drug Metab.* 2021;22:503-522.

107.   Damaskinaki FN, Moran LA, Garcia A, Kellam B, Watson SP. Overcoming challenges in developing small molecule inhibitors for GPVI and CLEC-2. *Platelets.* 2021;32:744-752.

108.   Lee AC, Harris JL, Khanna KK, Hong JH. A comprehensive review on current advances in peptide drug development and design. *Int J Mol Sci.* 2019;20:2383.

2

Chapter 2

Platelet calcium signaling by G-protein coupled and ITAM-linked receptors regulating anoctamin-6 and procoagulant activity

Fernández DI, Kuijpers MJE, Heemskerk JWM

Abstract

Most agonists stimulate platelet Ca^{2+} rises via G-protein coupled receptors (GPCRs) or ITAM-linked receptors (ILRs). Well studied are the GPCRs stimulated by the soluble agonists thrombin (PAR1, PAR4), ADP ($P2Y_1$, $P2Y_{12}$), and thromboxane A_2 (TP), signaling via phospholipase (PLC)β isoforms. The platelet ILRs glycoprotein VI (GPVI), C-type lectin-like receptor 2 (CLEC2), and FcγRIIa are stimulated by adhesive ligands or antibody complexes and signal via tyrosine protein kinases and PLCγ isoforms. Marked differences exist between the GPCR- and ILR-induced Ca^{2+} signaling in: *(i)* dependency of tyrosine phosphorylation; *(ii)* oscillatory versus continued Ca^{2+} rises by mobilization from the endoplasmic reticulum; and *(iii)* smaller or larger role of extracellular Ca^{2+} entry via STIM1/ORAI1. Co-stimulation of both types of receptors, especially by thrombin (PAR1/4) and collagen (GPVI) leads to a highly enforced Ca^{2+} rise, involving mitochondrial Ca^{2+} release, which activates the ion and phospholipid channel, anoctamin-6. This highly Ca^{2+}-dependent process causes swelling, ballooning, and phosphatidylserine expression, establishing a unique platelet population swinging between vital and necrotic (procoagulant 'zombie' platelets). Additionally, the high Ca^{2+} status of procoagulant platelets induces a set of additional events: *(i)* Ca^{2+}-dependent cleavage of signaling proteins and receptors via calpain and ADAM isoforms; *(ii)* microvesiculation; *(iii)* enhanced coagulation factor binding; and *(iv)* fibrin-coat formation involving transglutaminases. Given the additive roles of GPCR and ILR in Ca^{2+} signal generation, high-throughput screening of biomolecules or small molecules based on Ca^{2+} flux measurements provides a promising way to find new inhibitors interfering with prolonged high Ca^{2+}, phosphatidylserine expression, and hence platelet procoagulant activity.

Introduction

Blood platelets respond to and become activated by multiple (patho)physiological agonists and chemically synthesized drugs. The majority of these compounds act by one out of two types of signaling pathways, *i.e.* via G-protein coupled receptors (GPCRs) or ITAM-linked receptors (ILRs, immunoreceptor tyrosine-based activation motif-linked receptors) [1,2]. Typically, soluble agonists mostly trigger platelets via GPCRs, with as an example the coagulation product thrombin, acting on the protease-activated receptors (PAR)1 and PAR4. On the other hand, but not exclusively, vascular-bound agonists trigger platelets via ILRs, with as an example collagen, stimulating via the ILR glycoprotein VI (GPVI). Both thrombin and collagen are considered to be key agonists in (pathological) thrombus formation in man and rodents [3,4], and both trigger directly or indirectly a whole range of platelet responses [1]. Markedly, thrombin and collagen also directly steer the coagulation process [2]. Given this, it may not be surprising that also platelets have a potent regulatory role in blood clotting [5], a role that is concentrated in the population of 'procoagulant platelets' stimulated through the membrane channel protein anoctamin-6 (previously known as TMEM16F) [6].

In the present paper, we outline how platelet activation via GPCR and ILR signaling pathways, synergizing into cytosolic Ca^{2+} rises, induces anoctamin-6 activation and causes procoagulant platelet formation. This also leads to a whole range of downstream responses in thrombosis and hemostasis, which culminate in the formation of a fibrin clot. Finally, we stipulate that high-throughput screening for molecules affecting the agonist-induced Ca^{2+} rises can provide a promising way to interfere with platelet-mediated blood clotting.

Platelet activation via GPCRs

As in their name, GPCRs couple to heterotrimeric G-proteins, comprising of α, β and γ subunits, each of them presenting different isoforms. For all GPCRs, receptor binding causes a switch from the inactive (GDP binding) to the active (GTP binding) form of the Gα subunits. The most relevant Gα-subunits for platelet Ca^{2+} signaling and ensuing processes are: *(i)* Gαq (raising cytosolic Ca^{2+} via PLCβ isoforms) and *(ii)* Gαs (lowering cytosolic Ca^{2+} via cAMP production) (Figure 1). The other G-proteins, Gα12/13 (activating the monomeric GTPase, RhoA) and Gαi (suppressing cAMP production and activating phosphatidylinositol 3-kinases via βγ subunit), modulate the Ca^{2+} signal only indirectly, as detailed below [1,7]. Of the dozens of GPCRs expressed by platelets, the most well-studied in relation to Ca^{2+} signaling are the receptors for thrombin (PAR1, PAR4), ADP ($P2Y_1$, $P2Y_{12}$), and thromboxane A_2 (TP). Dysfunctional mutations of most of these receptors have been described [8,9], as detailed below.

Protease-activated receptors (PARs)

Handbook knowledge is that the central coagulation protease thrombin cleaves and activates two GPCRs of human platelets, PAR1 and PAR4, both of which are directly coupled to Gαq. The isoform PAR1 is known to be more sensitive for thrombin and to prime for activation

of PAR4 [7,10,11]. PAR1 induces an acute and rather short-lived rise in Ca^{2+} plus initial integrin activation, whereas PAR4 causes a steady and more sustained Ca^{2+} signal that also depends on autocrine $P2Y_{12}$-mediated events. Accordingly, in thrombin-stimulated platelets, the total amount of Ca^{2+} signal is the time-integrated sum of contributions of both receptors (Figure 2A) [12-14]. In mouse platelets, PAR3 as a non-cleaved receptor replaces PAR1 [7]. Regardless of the species, the more prolonged PAR4 signaling is considered to be needed for the platelet procoagulant response and thrombus stabilization [15,16]. Part of the PAR-dependent signaling can occur independently of Ca^{2+} mobilization via a $G\alpha12/13$ pathway, which contributes to the platelet shape-change response [17].
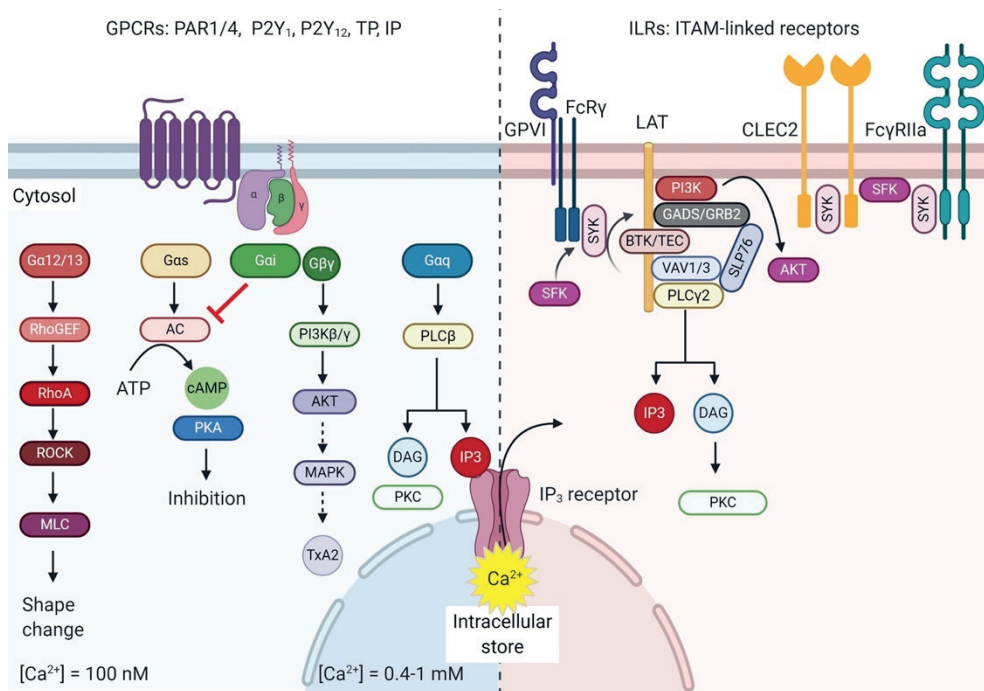
Figure 1. Schematic overview of the different signaling pathways in terms of calcium signaling. *Left part GPCRs:* G-protein coupled receptors bearing the $G\alpha q$ isoform activating subunit promote phospholipase C (PLC) β to generate phospholipase inositol-1,4,5-triphosphate (IP_3) and diacylglycerol (DAG). IP_3 triggers the release of Ca^{2+} from intracellular stores and DAG activates several proteins, such as different isoforms of protein kinase C (PKC). Other $G\alpha$ isoforms ($G\alpha12/13$, $G\alpha s$, $G\alpha i$) trigger signaling pathways that synergize or negatively regulate Ca^{2+} increase, and modulate integrin activation, thromboxane generation, and granule release. *Right part ILRs:* ITAM-linked-receptor activation results in the recruitment of several tyrosine kinase proteins to LAT. The formation of this signalosome results in the activation of $PLC\gamma2$, also eliciting IP_3 and DAG formation. Other abbreviations: AC: adenylyl cyclase, CLEC2: C-type lectin-like receptor 2, FcRγ: Fc receptor γ-chain, FcγRIIa: Fcγ receptor IIa, GPVI: glycoprotein VI, IP, prostaglandin I_2 receptor LAT: linker of activated T cells, MAPK: mitogen-activated protein kinase, PAR1/4: protease-activated receptor 1 and 4, PI3K: phosphatidylinositol 3-kinase, PKA: protein kinase A, PKC: protein kinase C, PLC: phospholipase C, $P2Y_1$ and $P2Y_{12}$: purinergic receptor 1 and 12, ROCK: Rho-associated protein kinase, SFK: Src family kinase, TP: thromboxane receptor, Syk: spleen tyrosine kinase, TxA_2: thromboxane A2. This figure was created using BioRender.com.

Several human PAR4 variants (gene *F2RL3*) are known to link to alterations in platelet responses [8,18]. Furthermore, blocking of PAR4 or its hyperreactive forms was found to provide an antithrombotic potential [19,20]. Regarding the other receptor PAR1 (gene *F2R*), antagonists like vorapaxar are being used in some countries for secondary prevention of atherothrombotic disease [21]. Current judgment is that a better understanding of the interindividual variation in the PARs' activities is needed to come to a better personalized medication [22].

Purinergic receptors P2Y$_1$ and P2Y$_{12}$

The two key purinergic GPCRs for ADP in platelets are P2Y$_1$ and P2Y$_{12}$ [23]. While ADP is considered to be a weak platelet agonist, it plays an important role in the amplification and stabilization of platelet responses to many other receptor agonists, including thrombin and thromboxane A$_2$ [24]. The low-level P2Y$_1$ receptors signal via Gαq- and PLCβ-mediated Ca^{2+} rises, whereas the more abundant P2Y$_{12}$ receptors are coupled to Gαi [23]. The relatively small Ca^{2+} signal evoked by P2Y$_1$ contributes to platelet shape change. On the other hand, the P2Y$_{12}$ pathway involves inhibition of adenylyl cyclase activity via the Gαi subunit and activation of phosphatidylinositol 3-kinases (PI3Ks) via the βγ subunits, the latter directing to integrin α$_{IIb}$β$_3$ activation [1]. Markedly, P2Y$_{12}$ was also found to contribute to the thrombin-induced exposure of phosphatidylserine (PS) in isolated platelets [25].

The literature provides also ample evidence for synergic action between the P2Y$_1$ and P2Y$_{12}$ receptors. Recent work shows that in rat megakaryocytes P2Y$_{12}$ signaling can enhance the P2Y$_1$-induced Ca^{2+} oscillations, which then stimulates integrin αIIbβ3 activation and fibrinogen binding [26]. This adds well to earlier evidence that P2Y$_{12}$ contributes to platelet activation by potentiation of the P2Y$_1$-induced Ca^{2+} responses both via inhibition of adenylate cyclase and activation of PI3Ks with a complex additional role of Src kinase [27]. Critical in this interplay of Ca^{2+}-dependent platelet activation via both P2Y receptors is also the guanine nucleotide exchange factor CalDAG-GEFI, which in a Ca^{2+}-dependent way regulates integrin activation through Rap1b [28].

Dysfunctional (gain- or loss-of-function) variants of the genes for both P2Y$_1$ and P2Y$_{12}$ (*P2RY1, P2RY12*) have been identified, which associate with a bleeding or a prothrombotic propensity [29,30]. As an illustration of the relevance of the P2Y$_{12}$-PI3K-αIIbβ3 activation pathway, (pro)drugs inhibiting this receptor are widely used for the secondary prevention of arterial thrombosis, even as monotherapy. Mostly prescribed drugs are thienopyridines that irreversibly block the receptor (prodrugs: clopidogrel and prasugrel), and the compounds ticagrelor and cangrelor that reversibly bind to P2Y$_{12}$ [31].

Thromboxane A$_2$ receptor (TP)

The TP receptor for thromboxane A$_2$ is expressed on platelets and vascular cells, and it couples to Gαq (regulating Ca^{2+} release) and Gα12 family proteins (regulating integrin activation) [7,32]. Aspirin, one of the hallmarks of current anti-platelet therapy, blocks the

formation of thromboxane A_2, thus preventing its interaction with the TP receptor. Without this drug, the autocrine platelet-released thromboxane A_2 greatly enhances the responses of other platelet agonists, in particular ADP and collagen [2]. Patients with a mutation in the *TBXA2R* gene develop bleeding symptoms, and their platelets react less to thromboxane A_2, ADP, and other agonists [33,34]. In the past, several efforts have been made to develop specific TP antagonists. The extra advantage of such antagonists was questioned, given the high clinical importance of aspirin as a 'gold-standard' anti-platelet drug for the prevention of cardiovascular events. However, it is well possible that receptor antagonists have fewer bleeding side effects.

Other GPCRs

In the context of Ca^{2+} signal generation, another relevant GPCR on platelets is the prostaglandin I_2 (IP) receptor for endothelial-derived prostacyclin. This receptor couples to $G\alpha s$ and raises the cAMP level, which downregulates Ca^{2+} rises via protein kinase A [35].

Platelet activation via ILRs

The most widely studied ILR in terms of signaling is GPVI, while less attention has been paid to the podoplanin receptor C-type lectin-like receptor 2 (CLEC2) and the IgG receptor FcγRIIa. In platelets, signaling via these ILRs relies on a tyrosine phosphorylation cascade starting at the (hemi-) ITAM motif YxxI/L [36]. Tyrosine phosphorylation of this domain creates a docking site for SH2-containing proteins of the Src kinase family, which mediate Syk phosphorylation ensuing activation of PLCγ and PI3K isoforms (Figure 1). Positive feedback loops mediated by crosstalk between the small GTPases Rap1b and Rac1 appear to be critical for a full ITAM-induced platelet activation [28].

As further detailed below, these ILRs, in particular the collagen/fibrin receptor GPVI, have a well-established enhancing effect on the GPCR-induced responses by thrombin, ADP, and thromboxane A_2 [1]. Exemplary is the platelet procoagulant response mediated by PS exposure, requiring the combined collagen and thrombin stimulation [5,37,38].

Glycoprotein VI (GPVI)

GPVI is uniquely expressed by megakaryocytes and platelets and requires co-expression with the ITAM-bearing co-receptor Fc receptor γ-chain (FcRγ) [39]. It is the central signaling receptor of collagen, collagen-related peptides (CRP), and the snake venom convulxin [40,41]. The strength of the GPVI signal in response to collagen ligands is regulated by receptor clustering [42]. Recent overviews of mouse studies indicate that GPVI is one of the few platelet signaling proteins that contributes to murine arterial thrombosis with only a minor role in hemostasis [43]. This feature makes GPVI an attractive target for the development of improved anti-platelet drugs to prevent thrombosis. Indeed, GPVI-deficient patients described so far present with no more than a minor bleeding tendency [40,44]. Interestingly, a genetic variant of *GP6* was found to associate with an increased risk of venous thrombosis [45].

Other (hem)-ITAM-linked receptors

The podoplanin receptor CLEC2 is highly expressed as a homodimer in platelets and megakaryocytes, and it is present at low levels in inflammatory dendritic cells and myeloid cells [36,46]. Mouse thrombosis studies suggest a blood-borne ligand, but this has not been identified yet [47]. In comparison to the GPVI-linked FcRγ chain, the CLEC2 receptor contains a hemi-ITAM domain with a single YxxL sequence [48], but its signaling pathway shows considerable overlap with that of GPVI. Besides a role in arterial thrombosis, CLEC2 is also involved in the maintenance of lymphatic vascular integrity and inflammation [36,46]. When stimulated by the snake venom rhodocytin, CLEC2 appeared to have no more than a limited role in the platelet procoagulant activity [49]. This is in agreement with the reported moderate Ca^{2+} rise induced by CLEC2 activation [50].

The FcγRIIa receptor (also named CD32a) acts as a low-affinity receptor for the constant fragment of immunoglobulin G [51]. Upon dimerization it allows platelets to bind to IgG immune complexes, resulting in platelet activation via a similar tyrosine kinase cascade as GPVI and ensuing Ca^{2+} mobilization [52]. The role of the platelet FcγRIIa is known for a range of pathologies, such as immune thrombocytopenia, heparin-induced thrombocytopenia, bacterial infections, and cancer [51].

Synergistic platelet calcium signaling via GPCRs and ILRs

Platelets respond in a context-dependent manner to the different stimuli to which they are exposed [2,53]. Accordingly, when these cells are stimulated through GPCRs (*e.g.*, with thrombin, autocrine ADP, thromboxane A_2) and ILRs (*e.g.*, with collagen) this results in additive responses because of the complementarity of both types of signaling pathways [1]. A key quantifiable and integratory signal of GPCR plus ILR stimulation is the rise in cytosolic Ca^{2+}, which then feeds forward to other responses such as pseudopod formation, integrin αIIbβ3 activation, granular secretion, procoagulant activity and formation of contracting aggregates [1].

A notable mechanism of Ca^{2+} signal integration is provided by the different PLC isoforms that become activated through GPCRs (PLCβ2/3) and ILRs (PLCγ2) [54,55]. Both PLC types hydrolyze phosphatidylinositol 4,5 biphosphate into diacylglycerol (DAG) and inositol 1,4,5-triphosphate (IP_3) [15,56]. The messenger IP_3 binds to its receptors in the endoplasmic reticulum and promotes the release of stored Ca^{2+} (Figure 1). Feedback is provided by concomitant signals, including protein kinase C isoforms and CalDAG-GEFI [28]. In a way not very well understood, the signaling route via PLCβ2/3 or PLCγ2 leads to a different shape of the IP_3-induced Ca^{2+} mobilization and the related entry of extracellular Ca^{2+}, which hence differ between GPCR and ILR agonists.

In single platelets, a marked difference between GPCR and ILR stimulation is the IP_3-induced oscillatory, spiking Ca^{2+} rises in response to thrombin or ADP [57], and the continued Ca^{2+} rises in response to collagen [58] (Figure 2A, B). The reason for this difference

is still not well understood, but it likely involves a higher activity of Ca^{2+}-ATPases (SERCAs), pumping back the released Ca^{2+} into the stores after each spike [59], in the case of GPCR-stimulated platelets.

The agonist-induced regulation of Ca^{2+} entry channels in platelets is reviewed in detail elsewhere [60]. In brief, following Ca^{2+} store depletion, the endoplasmic reticulum Ca^{2+} sensor STIM1 interacts with the store-operated Ca^{2+} entry (SOCE) channel Orai1, causing an influx of Ca^{2+} from the extracellular medium (Figure 3). Studies with genetically modified mice have shown that this SOCE pathway is more predominant upon ILR stimulation (collagen) than upon GPCR stimulation (thrombin) [60]. Yet, patients with mutations in *STIM1* or *ORAI1* were found to suffer from immune deficiency and bleeding symptoms, linked to defects in GPCR signals and thrombus formation [61]. An additional non-SOCE Ca^{2+} entry mechanism via the non-selective TRPC cation channels is stimulated by thrombin, with a significant role in PS exposure [62]. In particular, co-stimulation with collagen and thrombin activates these TRPC, allowing entry of Na^+ and Ca^{2+} [62].

Furthermore, mitochondrial stored Ca^{2+} can play a role upon dual platelet stimulation. The current understanding is that signals including elevated Ca^{2+} trigger the mitochondrial Ca^{2+} release via mitochondrial permeability transition pores, which results in the 'supramaximal Ca^{2+} signals' that are required for platelet PS exposure and procoagulant activity [63,64].

Another platelet ion channel highly selective for Ca^{2+} is provided by the $P2X_1$ receptor for ATP, which also plays a regulatory role in thrombus formation [65,66]. $P2X_1$ contributes to Ca^{2+} signaling and platelet function upon low-level stimulation by GPCRs and ILRs [67]. The contribution of the $P2X_1$ signal to PS exposure is less clear. Regarding secondary lowering of the Ca^{2+} signal, next to SERCA isoforms, also plasma membrane Ca^{2+}-ATPases and Na^+/Ca^{2+} exchangers play a role in this [60], although it is unclear if these roles differ between platelet agonists.

Overall, it appears that the magnitude and duration of the Ca^{2+} signal in platelets is a function of their exposure to agonists, in which GPCR and ILR agonists together evoke the platelet procoagulant response. A differential exposure to agonists can also explain, on top of differences between platelets, why the platelets in a thrombus are heterogeneous in activation stages [68,69]. Herein, the population of most strongly activated platelets is the one showing PS exposure [38,53]. Taken together, the physiological consequences of procoagulant platelet formation can be summarized as: *(i)* limiting the thrombus growth by reducing the adhesive function of platelets, *(ii)* enhancing the coagulation by thrombin and fibrin formation, and *(iii)* a thrombin-induced stabilization and contraction of the platelet plug.
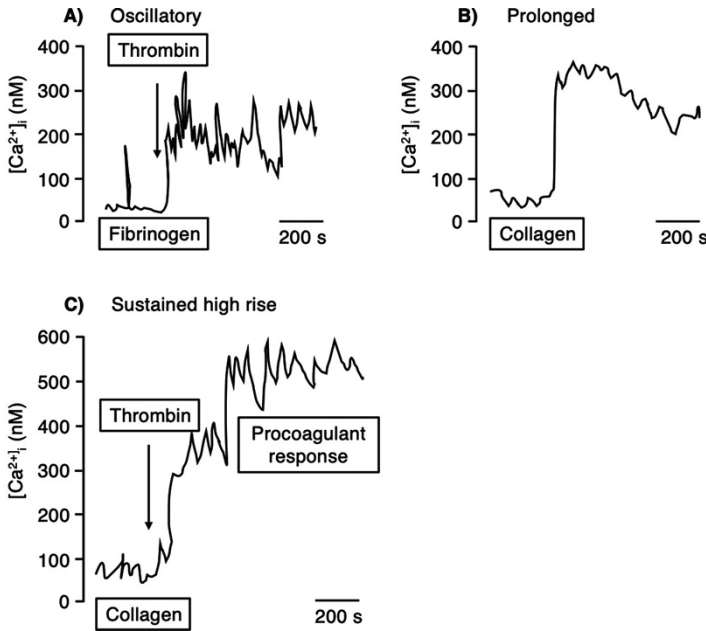
Figure 2. Schematic representation of the different patterns of calcium responses in a single platelet stimulated by GPCRs or ILRs agonists. Fura-2-labeled platelets were allowed to adhere to fibrinogen (**A**) or collagen (**B**, **C**) surfaces. Thrombin addition is indicated by an arrow. (**A**) The GPCR agonist, thrombin, promotes oscillatory calcium traces in single platelets Ca^{2+} signaling, while (**B**) collagen, as an agonist of ILRs, promotes a sustained calcium rise. (**C**) Procoagulant response, due to anoctamin-6 activation, was triggered by a continued high calcium rise after stimulation by collagen and thrombin. Schematic traces are based on published measurements in single platelets [12,57,80,103].

Anoctamin-6 and the platelet procoagulant response

The channel anoctamin-6 is a multi-spanning integral membrane protein, coded by the gene *ANO6* (*TMEM16F*). It is highly expressed in platelets and serves as a Ca^{2+}-dependent ion channel as well as a channel for negatively charged phospholipids like PS [6,70]. Whereas first papers considered anoctamin-6 as a channel permeable to both monovalent and divalent cations, including Cl^-, Na^+, and Ca^{2+} [71], later reports emphasized the high Ca^{2+}-dependent Cl^- conductance [6,72]. Interestingly, recent structural and inter-species analyses suggest that the ion permeation occurs independently of phospholipid scrambling, *i.e.* PS exposure [72,73]. However, the ion channel activity is required for the anoctamin-6-dependent ballooning of platelets that accompanies PS exposure [74].

Dysfunctional mutations in *ANO6* are causative for the Scott syndrome (Table 1), resulting in a mild bleeding phenotype in mice and men [75-77]. To date, only six Scott patients have been reported, who only bleed after major trauma (surgery) without easy bruising from superficial cuts [78].

Studies with human and mouse platelets have confirmed the role of anoctamin-6 in the procoagulant responses upon sustained intracellular Ca^{2+} rises, such as induced by the co-stimulation of collagen and thrombin (Figure 2C) or Ca^{2+} ionophores. Such platelets swell

due to an anoctamin-6-mediated influx of Cl⁻ and (in)directly Na⁺, forming balloon-like structures, and simultaneously expose procoagulant PS due to phospholipid scramblase activity. Both types of responses are annulled in platelets from Scott syndrome patients and whole-body or platelet-specific *Ano6⁻/⁻* mice [74,76,77].

In platelets from at least two Scott patients, a reduced collagen/thrombin-induced activity of the Ca^{2+}-dependent protease calpain was found, which can explain lower microvesicle formation and lower intracellular cleavage of integrin αIIbβ3 and talin in these platelets [76,79,80]. For the Scott_UK patient, this could be linked to a decreased expression of one of the calpain isoforms [81]. Of relevance, in platelet-specific *Ano6⁻/⁻* mice, the hemostatic and thrombotic reactions were reduced, thus confirming that platelet PS exposure is a regulatory factor in blood clotting *in vivo* [77].
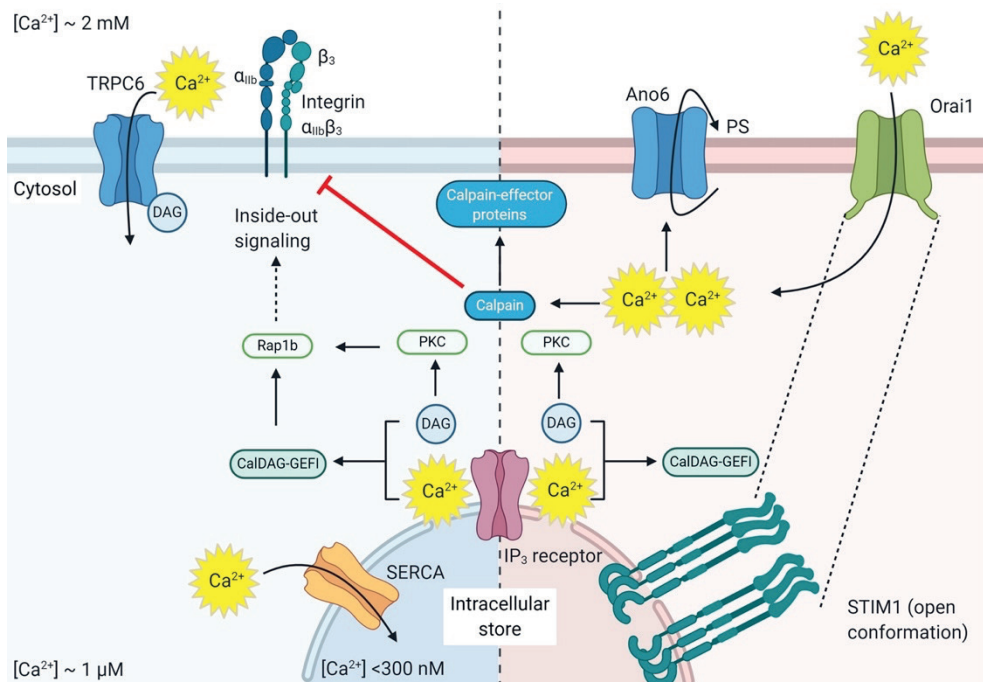
Figure 3. Schematic overview of the Ca^{2+} entry pathways and PS exposure. Left part GPCRs: Ca^{2+} depletion from the intracellular stores by GPCRs is mainly triggered through PLCβ-induced generation of IP_3. The DAG mediates transient receptor potential channel 6 (TRPC6) opening, allowing extracellular Ca^{2+} entry. The rise in cytosolic Ca^{2+} results in the activation of integrin αIIbβ3 via CalDAG-GEFI and Rap1b. **Right part ILRs:** ILR-induced Ca^{2+} depletion from the intracellular stores most strongly promotes STIM1-Orai1 channel coupling and activation by pumping Ca^{2+} ions inside the cytosol (store-operated calcium entry, SOCE). Mitochondrial depolarization and generation of mitochondrial permeability transition pore (MPTP) contribute to the increase of cytoplasmic Ca^{2+} levels. This high and sustained Ca^{2+} levels mediate anoctamin-6 (Ano6) scramblase activation and PS exposure, which also promotes ion channel opening and Na⁺, Cl⁻, and water entry. Among other processes, calpains are activated resulting in the cleavage of several proteins and receptors. In both pathways, high intracellular Ca^{2+} levels activate sarco/endoplasmic reticulum Ca^{2+} ATPases (SERCA), which pump Ca^{2+} back into the intracellular stores. Several channels in the plasma membrane such as plasma membrane Ca^{2+} ATPases (PMCA) and Na⁺/Ca^{2+} exchanger (NCX) also reduce the cytoplasmic Ca^{2+} levels (not shown). ROCK: Rho-associated protein kinase. For other abbreviations, see Figure 1. This figure was created using BioRender.com.

Table 1. Genetic pathologies altering platelet PS exposure. *Abbreviations*: ΔCRAC, combined immunodeficiency due to CRAC channel dysfunction; EV, extracellular vesicle; WAS, Wiskott-Aldrich syndrome.

Disorder	OMIM	Gene	Genetic transmission	Patient characteristics	Platelet defect	Ref.
Scott	262890	*ANO6*	autosomal recessive	mild bleeding	defected PS exposure and EV release	[78,96]
Stormorken	185070	*STIM1*	autosomal dominant (gain-of-function)	thrombocytopenia, asplenia, myopathy, mild bleeding	increased PS exposure, secondary loss of platelet function	[97]
WAS	301000	*WASP*	X-linked	infections, thrombocytopenia, bleeding	increased Ca^{2+} rise and PS exposure	[98]
ΔCRAC	612782	*ORAI1*	autosomal recessive	immune defect, myopathy	reduced Ca^{2+} rise and PS exposure	[61,99]
	612783	*STIM1*	autosomal recessive (loss-of-function)	immune defect, hypotonia	reduced Ca^{2+} rise and PS exposure	

As indicated before, a condition par excellence that induces anoctamin-6 mediated PS exposure and procoagulant activity is the activation of platelets by collagen plus thrombin (next to Ca^{2+} ionophore), resulting in 'supramaximal' high Ca^{2+} rises [5,82]. These high-Ca^{2+} PS-exposing platelets are furthermore characterized by a calpain-mediated cleavage and inactivation of integrin αIIbβ3 [83], the extracellular cleavage of GPVI and GPIbα [84], and a greatly enhanced binding ability of Gla-domain containing coagulation factors [15,85]. This assembly of coagulation factors causes a magnitude increase in the formation of factor Xa (tenase complex) and thrombin (prothrombinase complex) at the platelet surface, thereby strongly enhancing thrombin generation and the clotting process [1,49,86]. Since the ballooned PS-exposing platelets can collect a surrounding protein (fibrin) coat, they were also designated as COAT (COllagen And Thrombin) platelets [87,88]. Given the major morphological changes of the ballooned platelets, it is not a surprise that anoctamin-6 has a strong regulatory effect on the platelet neo-N-terminal and phospho-proteomes upon collagen/thrombin activation [81]. With the risk of popularizing, for these non-dead platelets, the term 'zombie' might be more appropriate than 'necrotic'.

On the other hand, PS exposure of platelets can also be induced by a different pathway, acting independently of anoctamin-6 and elevated Ca^{2+} [89,90]. The latter pathway is triggered by the apoptotic stimulus ABT-737, relies on caspase activation and is accompanied by a different set of intracellular proteolytic events [81]. The responsible PS-exposing enzyme most likely is the phospholipid scramblase XKR8 [91], the Ca^{2+} dependence of which is unclear.

As summarized elsewhere, mouse studies have shown that many other signaling proteins can modulate collagen/thrombin-induced PS exposure [92]. However, most of these are proteins that primarily alter the Ca^{2+} signal. As shown in Table 1, the clinical relevance of the altered PS exposure in patients with Stormorken, Wiskott-Aldrich, or Calcium Release-Activated Channel (CRAC) syndromes lies in bleeding symptoms and thrombocytopenia as a result of alterations in Ca^{2+} signaling proteins.

High-throughput screening to find new inhibitors affecting platelet calcium signaling and procoagulant activity

High-throughput screening (HTS) of small compounds or biomolecules is an established technique for the discovery of lead molecules to produce commercialized agents after several rounds of drug development [93]. So far, only a few high-throughput approaches have been used to search for platelet-related Ca^{2+} signal inhibitors (Table 2). A first example is a well-plate-based high-throughput approach employing *Drosophila* cell lines to identify novel inhibitors of the Orai1 CRAC channels [94]. Other examples are the use of HEK cells to identify the novel PAR4 antagonist BMS-986120 20 and search for a small molecule inhibitor of the non-selective Ca^{2+} influx channel TRPC6 [95]. In the platelet field, pharmaceutical screening approaches discriminating between GPCR- and ILR-induced Ca^{2+} signaling are still absent. In the reported studies in Table 2, platelets were used only after initial screening.

In this context, it is of interest to make use of the high and sustained Ca^{2+} rise that triggers PS exposure for a high-throughput screening setting of platelets to find novel molecules interfering with procoagulant activity. Finding inhibitors that block the appearance of procoagulant platelets may reduce the risk of thrombotic events, while preserving other populations of adhesive, secreting, and aggregating platelets, thereby limiting the risk of bleeding. However, fine-tuning inhibitory dosing would be needed to minimize the bleeding complications, such as those seen in Scott syndrome patients. Besides this, it will also be interesting to find new procoagulant molecules to strengthen hemostasis in conditions, where this is needed.

Table 2. Used approaches of high-throughput screening for platelet-related Ca^{2+} research. Abbreviations: HEK, human embryonic kidney; PP1ca, protein phosphatase 1catalytic subunit; TG, thrombin generation.

Target protein	Approach	Secondary assay	Ca^{2+}/PS	Outcome	Ref.
Orai1	Drosophila cell line	platelets	yes/no	CRAC channel	[94]
TRPC6	overexpressing HEK293 cells (hTRPC6-YPF)	platelets	yes/no	small molecule	[95]
PP1ca	yeast two-hybrid interactions (PP1ca vector)	platelets	no/no	Gβ1 subunit	[100]
PAR1	platelet secretion, luciferase-based assay	platelets	no/no	small molecule	[101]
PAR4	overexpressing HEK293 cells	platelets (TG)	yes/no	BMS-986120	[20]
Factor Xa	chromogenic substrate assay, prothrombin time (plasma)	platelets (plasma)	no/yes	Rivaroxaban	[102]

Conclusion

Several pathological conditions in the spectrum of cardiovascular disease present with hyperreactive platelets and increased levels of procoagulant platelets [38,53]. However, useful inhibitors - with a clinical potential - targeting the high Ca^{2+} levels and consequent PS exposure in platelets stimulated by GPCR plus ILR agonists have not yet been reported. Therefore, studies on the role of procoagulant platelets in pathological conditions are needed to find novel targets that help in the development of inhibitors that prevent procoagulant

platelet formation.

Funding

Disclosure of interest

The authors declare no conflicts of interest.

Supplementary data

Supplemental video 1. Video abstract (https://doi.org/10.6084/m9.figshare.16571086.v1)

References

1. Versteeg HH, Heemskerk JW, Levi M, Reitsma PS. New fundamentals in hemostasis. *Physiol Rev.* 2013;93:327-358.

2. Van der Meijden PE, Heemskerk JW. Platelet biology and functions: new concepts and future clinical perspectives *Nat Rev Cardiol.* 2019;16:166-179.

3. Kuijpers MJ, Munnix IC, Cosemans JM, et al. Key role of platelet procoagulant activity in tissue factor- and collagen-dependent thrombus formation in arterioles and venules in vivo. Differential sensitivity to thrombin inhibition. *Microcirculation.* 2008;15:269-282.

4. Kuijpers MJ, Gilio K, Reitsma S, et al. Complementary roles of platelets and coagulation in thrombus formation on plaques acutely ruptured by targeted ultrasound treatment: a novel intravital model. *J Thromb Haemost.* 2009;7:152-161.

5. Heemskerk JW, Cosemans JM, van der Meijden PE. Platelets and coagulation. *In: Platelets in Thrombotic and Non-Thrombotic Disorders (Eds. Gresele, P, Kleiman, N S, Lopez, J A, Page, C P).* 2017; pp. 447-462.

6. Kunzelmann K, Nilius B, Owsianik G, et al. Molecular functions of anoctamin 6 (TMEM16F): a chloride channel, cation channel, or phospholipid scramblase? *Pflügers Arch.* 2014;466:407-414.

7. Offermanns S. Activation of platelet function through G protein-coupled receptors. *Circ Res.* 2006;99:1293-1304.

8. Jones ML, Norman JE, Morgan NV, et al. Diversity and impact of rare variants in genes encoding the platelet G protein-coupled receptors. *Thromb Haemost.* 2015;113:826-837.

9. Stockley J, Nisar SP, Leo VC, et al. Identification and characterization of novel variations in platelet G-protein coupled receptor (GPCR) genes in patients historically diagnosed with type 1 von Willebrand disease. *Plos One.* 2015;10:e0143913.

10. Kahn ML, Zheng YW, Huang W, et al. A dual thrombin receptor system for platelet activation. *Nature.* 1998;6694:690-694.

11. Sambrano GR, Weiss EJ, Zheng YW, Huang W, Coughlin SR. Role of thrombin signalling in platelets in haemostasis and thrombosis. *Nature.* 2001;413:74-78.

12. Heemskerk JW, Feijge MA, Henneman L, Rosing J, Hemker HC. The Ca^{2+}-mobilizing potency of a-thrombin and thrombin-receptor-activating peptide on human platelets. Concentration and time effects of thrombin-induced Ca^{2+} signaling. *Eur J Biochem.* 1997;249:547-555.

13. Covic L, Gresser AL, Kuliopulos A. Biphasic kinetics of activation and signaling for PAR1 and PAR4 thrombin receptors in platelets. *Biochemistry.* 2000:5458-5467.

14. Shapiro MJ, Weiss EJ, Faruqi TR, Coughlin SR. Protease-activated receptors 1 and 4 are shut off with distinct kinetics after activation by thrombin. *J Biol Chem.* 2000;275:25216-25221.

15. Heemskerk JW, Mattheij N, Cosemans JM. Platelet-based coagulation: different populations, different functions. *J Thromb Haemost.* 2013;11:2-11.

16. French SL, Arthur JF, Lee H, et al. Inhibition of protease-activated receptor 4 impairs platelet procoagulant activity during thrombus formation in human blood. *J Thromb Haemost.* 2016;14:1642-1654.

17. Jin J, Mao Y, Thomas D, Kim S, Daniel JL, Kunapuli SP. RhoA downstream of G_q and $G_{12/13}$ pathways regulates protease-activated receptor-mediated dense granule release in platelets. *Biochem Pharmacol.* 2009;77:835-844.

18. Norman JE, Cunningham MR, Jones ML, et al. Protease-activated receptor 4 variant p.Tyr157Cys reduces platelet functional responses and alters receptor trafficking. *Arterioscler Thromb Vasc Biol.* 2016;36:952-960.

19. French SL, Thalmann C, Bray PF, et al. A function-blocking PAR4 antibody is markedly antithrombotic in the face of a hyperreactive PAR4 variant. *Blood Adv.* 2018;2:1283-1289.

20. Wong PC, Seiffert D, Bird JE, et al. Blockade of protease-activated receptor-4 (PAR4) provides robust antithrombotic activity with low bleeding. *Sci Transl Med.* 2017;9:371.

21. Gryka RJ, Buckley LF, Anderson SM. Vorapaxar: the current role and future directions of a novel protease-activated receptor antagonist for risk reduction in atherosclerotic disease. *Drugs.* 2017;65-72.

22. Tourdot BE, Stoveken H, Trumbo D, et al. Genetic variant in human PAR 4 enhances thrombus formation resulting in resistance to antiplatelet therapeutics. *Arterioscler Thromb Vasc Biol.* 2018;38:1632-1643.

23. Gachet C. Identification, characterization, and inhibition of the platelet ADP receptors. *Int J Hematol.* 2001;74:375-381.

24. Hechler B, Gachet C. P2 receptors and platelet function. *Purinergic Signal.* 2011;3:293-303.

25. Leon C, Ravanat C, Freund M, Cazenave JP, Gachet C. Differential involvement of the $P2Y_1$ and $P2Y_{12}$ receptor in platelet procoagulant activity. *Arterioscler Thromb Vasc Biol.* 2003;23:1941-1947.

26. Bye AP, Gibbins JM, Mahaut-Smith MP. Ca^{2+} waves coordinate purinergic receptor-evoked integrin activation and polarization. *Sci Signal.* 2020;13:e7354.

27. Hardy AR, Jones ML, Mundell SJ, Poole AW. Reciprocal cross-talk between $P2Y_1$ and $P2Y_{12}$ receptors at the level of calcium signaling in human platelets. *Blood.* 2004;104:1745-1752.

28. Stefanini L, Roden RC, Bergmeier W. CalDAG-GEFI is at the nexus of calcium-dependent platelet activation. *Blood.* 2009;114:2506-2514.

29. Mundell SJ, Rabbolini D, Gabrielli S, et al. Receptor homodimerization plays a critical role in a novel dominant negative *P2RY12* variant identified in a family with severe bleeding. *J Thromb Haemost.* 2018;16:44-53.

30. Janicki PK, Eyileten C, Ruiz-Velasco V, et al. Population-specific associations of deleterious rare variants in coding region of *P2RY1-P2RY12* purinergic receptor genes in large-vessel ischemic stroke patients. *Int J Mol Sci.* 2017;18:2678.

31. Khan SU, Singh M, Valavoor S, et al. Dual antiplatelet therapy after percutaneous coronary intervention and drug-eluting stents: a systematic review and network meta-analysis. *Circulation.* 2020;142:1425-1436.

32. Offermans S, Laugwitz KL, Spicher K, Schultz G. G proteins of the G_{12} family are activated via thromboxane A_2 and thrombin receptors in human platelets. *Proc Natl Acad Sci USA.* 1994;91:504-508.

33. Hirata T, Kakizuka A, Ushikubi F, Fuse I, Okuma M, Narumiya S. Arg60 to Leu mutation of the human thromboxane A2 receptor in a dominantly inherited bleeding disorder. *J Clin Invest.* 1994;94:1662-1667.

34. Mundell SJ, Mumford A. TBXA2R gene variants associated with bleeding. *Platelets.* 2018;29:739-742.

2

35. Swieringa F, Kuijpers MJ, Heemskerk JW, van der Meijden PE. Targeting platelet receptor function in thrombus formation: the risk of bleeding. *Blood Rev.* 2014;28:9-21.

36. Rayes J, Watson SP, Nieswandt B. Functional significance of the platelet immune receptors GPVI and CLEC-2. *J Clin Invest.* 2019;129:12-23.

37. Lecut C, Feijge MA, Cosemans JM, Jandrot-Perrus M, Heemskerk JW. Fibrillar type I collagens enhance platelet-dependent thrombin generation via glycoprotein VI with direct support of α2β1 but not αIIbβ3 integrin. *Thromb Haemost.* 2005;94:107-114.

38. Agbani EO, Poole AW. Procoagulant platelets: generation, function, and therapeutic targeting in thrombosis. *Blood.* 2017;130:2171-2179.

39. Stegner D, Haining E, Nieswandt B. Targeting glycoprotein VI and the immunoreceptor tyrosine-based activation motif signaling pathway. *Arterioscler Thromb Vasc Biol.* 2014;34:1615-1620.

40. Jandrot-Perrus M, Busfield S, Lagrue AH, et al. Cloning, characterization, and functional studies of human and mouse glycoprotein VI: a platelet-specific collagen receptor from the immunoglobulin superfamily. *Blood.* 2000;96:1798-1807.

41. Smethurst PA, Joutsi-Korhonen L, O'Connor MN, et al. Identification of the primary collagen-binding surface on human glycoprotein VI by site-directed mutagenesis and by a blocking phage antibody. *Blood.* 2004;103:903-911.

42. Poulter NS, Pollitt AY, Owen DM, et al. Clustering of glycoprotein VI (GPVI) dimers upon adhesion to collagen as a mechanism to regulate GPVI signaling in platelets. *J Thromb Haemost.* 2017;15:549-564.

43. Baaten CC, Meacham S, de Witt SM, et al. A synthesis approach of mouse studies to identify genes and proteins in arterial thrombosis and bleeding. *Blood.* 2018;132:e35-e46.

44. Nagy M, Perrella G, Dalby A, et al. Flow studies on human GPVI-deficient blood under coagulating and non-coagulating conditions. *Blood Adv.* 2020;4:2953-2961.

45. Morange PE, Suchon P, Trégouët DA. Genetics of venous thrombosis: update in 2015. *Thromb Haemost* 2015;114:910-919.

46. Suzuki-Inoue K, Inoue O, Ding G, et al. Essential in vivo roles of the C-type lectin receptor CLEC-2. Embryonic/neonatal lethality of CLEC-2-deficient mice by blood/lymphatic misconnections and impaired thrombus formation of CLEC-2-deficient platelets. *J Biol Chem.* 2010;285:24494-24507.

47. May F, Hagedorn I, Pleines I, et al. CLEC-2 is an essential platelet-activating receptor in hemostasis and thrombosis. *Blood.* 2009;114:3464-3472.

48. Hughes CE, Navarro-Nunez L, Finney BA, Mourao-Sa D, Pollitt AY, Watson SP. CLEC-2 is not required for platelet aggregation at arteriolar shear. *J Thromb Haemost.* 2010;8:2328-2332.

49. Brouns S, van Geffen JP, Campello E, et al. Platelet-primed interactions of coagulation and anticoagulation pathways in flow-dependent thrombus formation. *Sci Rep.* 2020; 10:11910.

50. Martyanov AA, Balabin FA, Dunster JL, Panteleev MA, Gibbins JM, Sveshnikova AN. Control of platelet CLEC-2-mediated activation by receptor clustering and tyrosine kinase signaling. *Biophys J.* 2020;118:2641-2655.

51. Qiao J, Al-Tamimi M, Baker RI, Andrews RK, Gardiner EE. The platelet Fc receptor, FcγRIIa. *Immunol Rev.* 2015;268:241-252.

52. Lee RH, Bergmeier W. Platelet immunoreceptor tyrosine-based activation motif (ITAM) and hemITAM signaling and vascular integrity in inflammation and development. *J Thromb Haemost.* 2016;14:645-654.

53. Baaten CC, ten Cate H, van der Meijden PE, Heemskerk JW. Platelet populations and priming in hematological diseases. *Blood Rev.* 2017;31:389-399.

54. Lian L, Wang Y, Draznin J, et al. The relative role of PLCβ and PI3Kγ in platelet activation. *Blood.* 2005;106:110-117.

55. Suzuki-Inoue K, Inoue O, Frampton J, Watson SP. Murine GPVI stimulates weak integrin activation in PLCγ2$^{-/-}$ platelets: involvement of PLCγ1 and PI-kinase. *Blood.* 2003;102:1367-1373.

56. Varga-Szabo D, Braun A, Nieswandt B. STIM1 and Orai1 in platelet function. *Cell Calcium.* 2011;50:70-278.

57. Heemskerk JW, Vis P, Feijge MA, Hoyland J, Mason WT, Sage SO. Roles of phospholipase C and Ca^{2+}-ATPase in calcium responses of single, fibrinogen-bound platelets. *J Biol Chem.* 1993;268:356-363.

58. Heemskerk JW, Siljander P, Vuist WM, et al. Function of glycoprotein VI and integrin $\alpha2\beta1$ in the procoagulant response of single, collagen-adherent platelets. *Thromb Haemost.* 1999;81:782-792.

59. Berridge MJ, Bootman MD, Roderick HL. Calcium signalling: dynamics, homeostasis and remodelling. *Nat Rev Mol Cell Biol.* 2003;4:517-529.

60. Mammadova-Bach E, Nagy M, Heemskerk JW, Nieswandt N, Braun A. Store-operated calcium entry in blood cells in thrombo-inflammation *Cell Calcium.* 2019;77:39-48.

61. Nagy M, Mastenbroek TG, Mattheij NJ, et al. Variable impairment of platelet functions in patients with severe, genetically linked immune deficiencies. *Haematologica.* 2018;103:540-549.

62. Harper MT, Camacho-Londono JE, Quick K, et al. Transient receptor potential channels function as a coincidence signal mediating phosphatidylserine exposure. *Sci Signal.* 2013;6:ra50.

63. Jobe SM, Wilson KM, Leo L, et al. Critical role for the mitochondrial permeability transition pore and cyclophilin D in platelet activation and thrombosis. *Blood.* 2008;111:1257-1265.

64. Abbasian N, Millington-Burgess SL, Chabra S, Malcor JD, Harper MT. Supramaximal calcium signaling triggers procoagulant platelet formation. *Blood Adv.* 2020;14:154-164.

65. Hechler B, Lenain N, Marchese P, et al. A role of the fast ATP-gated $P2X_1$ cation channel in thrombosis of small arteries in vivo. *J Exp Med.* 2003;198:661-667.

66. Oury C, Kuijpers MJ, Toth-Zsamboki E, et al. Overexpression of the platelet $P2X_1$ ion channel in transgenic mice generates a novel prothrombotic phenotype. *Blood.* 2003;101:3969-3976.

67. Fung CY, Cendana C, Farndale RW, Mahaut-Smith MP. Primary and secondary agonists can use P2X1 receptors as a major pathway to increase intracellular Ca^{2+} in the human platelet. *J Thromb Haemost.* 2007;5:910-917.

68. Munnix IC, Kuijpers MJ, Auger JM, et al. Segregation of platelet aggregatory and procoagulant microdomains in thrombus formation. Regulation by transient integrin activation. *Arterioscler Thromb Vasc Biol.* 2007;27:2484-2490.

69. Stalker TJ, Traxler EA, Wu J, et al. Hierarchical organization in the hemostatic response and its relationship to the platelet-signaling network. *Blood.* 2013;121:1875-1885.

70. Fujii T, Sakata A, Nishimura S, Eto K, Nagata S. TMEM16F is required for phosphatidylserine exposure and microparticle release in activated mouse platelets. *Proc Natl Acad Sci USA.* 2015;112:12800-12805.

71. Yang H, Kim A, David T, et al. TMEM16F forms a Ca^{2+}-activated cation channel required for lipid scrambling in platelets during blood coagulation. *Cell.* 2012;151:111-122.

72. Taylor KA, Mahaut-Smith MP. A major interspecies difference in the ionic selectivity of megakaryocyte Ca^{2+}-activated channels sensitive to the TMEM16F inhibitor CaCCinh-A01. *Platelets.* 2019;30:962-966.

73. Ye W, Han TW, He M, Jan YN, Jan LY. Dynamic change of electrostatic field in TMEM16F permeation pathway shifts its ion selectivity. *Elife.* 2019;8:e45187.

74. Agbani EO, van den Bosch MT, Brown E, et al. Coordinated membrane ballooning and procoagulant spreading in human platelets. *Circulation.* 2015;132:1414-1424.

75. Suzuki J, Umeda M, Sims PJ, Nagata S. Calcium-dependent phospholipid scrambling by TMEM16F. *Nature.* 2010;468:834-838.

76. Mattheij NJ, Braun A, van Kruchten R, et al. Survival protein anoctamin-6 controls multiple platelet responses including phospholipid scrambling, swelling and protein cleavage. *FASEB J.* 2016;30:727-737.

77. Baig AA, Haining EJ, Geuss E, et al. TMEM16F-mediated platelet membrane phospholipid scrambling is critical for hemostasis and thrombosis but not thromboinflammation in mice. *Arterioscler Thromb Vasc Biol.* 2016;36:2152-2157.

78. Millington-Burgess SL, Harper MT. Gene of the issue: ANO6 and Scott syndrome. *Platelets.* 2020;31:964-967.

79. Toti F, Satta N, Fressinaud E, Meyer D, Freyssinet JM. Scott syndrome, characterized by impaired transmembrane migration of procoagulant phosphatidylserine and hemorrhagic complications, is an inherited disorder. *Blood.* 1996;87:1409-1415.

80. Munnix IC, Harmsma M, Giddings JC, et al. Store-mediated calcium entry in the regulation of phosphatidylserine exposure in blood cells from Scott patients. *Thromb Haemost.* 2003;89:687-695.

81. Solari FA, Mattheij NJ, Burkhart JM, et al. Combined quantification of the global proteome, phosphoproteome and protein cleavage to characterize altered platelet functions in the human Scott syndrome. *Mol Cell Proteomics.* 2016;15:3154-3169.

82. Bevers EM, Comfurius P, van Rijn JL, Hemker HC, Zwaal RF. Generation of prothrombin-converting activity and the exposure of phosphatidylserine at the outer surface of platelets. *Eur J Biochem.* 1982;122:429-436.

83. Mattheij NJ, Gilio K, van Kruchten R, et al. Dual mechanism of integrin αIIbβ3 closure in procoagulant platelets. *J Biol Chem.* 2013;288:13325-13336.

84. Baaten CC, Swieringa F, Misztal T, et al. Platelet heterogeneity in activation-induced glycoprotein shedding: functional effects. *Blood Adv.* 2018;2:2320-2331.

85. Panteleev MA, Ananyeva NM, Greco NJ, Ataullakhanov FI. Two subpopulations of thrombin-activated platelets differ in their binding of the components of the intrinsic factor Xa-activating complex. *J Thromb Haemost.* 2005;3:2545-2553.

86. Reddy EC, Rand ML. Procoagulant phosphatidylserine-exposing platelets in vitro and in vivo. *Front Cardiovasc Med.* 2020;7:15.

87. Dale GL, Friese P, Batar P, et al. Stimulated platelets use serotonin to enhance their retention of procoagulant proteins on the cell surface. *Nature.* 2002;415:175-179.

88. Alberio L, Ravanat C, Hechler B, Mangin PH, Lanza F, Gachet C. Delayed-onset of procoagulant signalling revealed by kinetic analysis of COAT platelet formation. *Thromb Haemost.* 2017;117.

89. Schoenwaelder SM, Yuan Y, Josefsson EC, et al. Two distinct pathways regulate platelet phosphatidylserine exposure and procoagulant function. *Blood.* 2009;114:663-666.

90. Van Kruchten R, Mattheij NJ, Saunders C, et al. Both TMEM16F-dependent and TMEM16F-independent pathways contribute to phosphatidylserine exposure in platelet apoptosis and platelet activation. *Blood.* 2013;121:1850-1857.

91. Sakuragi T, Kosako H, Nagata S. Phosphorylation-mediated activation of mouse Xkr8 scramblase for phosphatidylserine exposure. *Proc Natl Acad Sci USA.* 2019;116:2907-2912.

92. De Witt S, Verdoold R, Cosemans JM, Heemskerk JW. Insights into platelet-based control of coagulation. *Thromb Res.* 2014;133:Suppl 2: S139-148.

93. Mayr LM, Bojanic D. Novel trends in high-throughput screening. *Curr Opin Pharmacol.* 2009;9:580-588.

94. Feske S, Gwack Y, Prakriya M, et al. A mutation in Orai1 causes immune deficiency by abrogating CRAC channel function. *Nature.* 2006;11:179-185.

95. Häfner S, Urban N, Schaefer M. Discovery and characterization of a positive allosteric modulator of transient receptor potential canonical 6 (TRPC6) channels. *Cell Calcium.* 2019;78:26-34.

96. Nurden AT, Nurden P. Inherited disorders of platelet function: selected updates. *J Thromb Haemost.* 2015;13:S2-S9.

97. Misceo D, Holmgren A, Louch WE, et al. A dominant STIM1 mutation causes Stormorken syndrome. *Hum Mutat.* 2014;35:556-564.

98. Lemahieu V, Gastier JM, Francke U. Novel mutations in the Wiskott-Aldrich syndrome protein gene and their effects on transcriptional, translational, and clinical phenotypes. *Hum Mutat.* 1999;14:54-66.

2

99.   Feske S. CRAC channels and disease: from human CRAC channelopathies and animal models to novel drugs. *Cell Calcium.* 2019;80:112-116.

100.   Pradhan S, Khatlani T, Nairn AC, Vijayan KV. The heterotrimeric G protein Gβ 1 interacts with the catalytic subunit of protein phosphatase 1 and modulates G protein-coupled receptor signaling in platelets. *J Biol Chem.* 2017;292:13133-13142.

101.   Dowal L, Sim DS, Dilks JR, et al. Identification of an antithrombotic allosteric modulator that acts through helix 8 of PAR1. *Proc Natl Acad Sci USA.* 2011;108:2951-2956.

102.   Gerotziafas GT, Elalamy I, Depasse F, Perzborn E, Samama MM. In vitro inhibition of thrombin generation, after tissue factor pathway activation, by the oral, direct factor Xa inhibitor rivaroxaban. *J Thromb Haemost.* 2007;5:886-888.

103.   Heemskerk JW, Vuist WM, Feijge MA, Reutelingsperger CP, Lindhout T. Collagen but not fibrinogen surfaces induce bleb formation, exposure of phosphatidylserine, and procoagulant activity of adherent platelets: evidence for regulation by protein tyrosine kinase-dependent Ca^{2+} responses. *Blood.* 1997;90:2615-2625

.

2

3

Chapter 3

Role of platelet glycoprotein VI and tyrosine kinase Syk in thrombus formation on collagen-like surfaces

Jooss NJ*, De Simone I*, Provenzale I*, **Fernández DI***, Brouns SLN, Farndale RW, Henskens YMC, Kuijpers MJE, ten Cate H, van der Meijden PEJ, Cavill R, Heemskerk JWM

Abstract

Platelet interaction with collagens, via von Willebrand factor, is a potent trigger of shear-dependent thrombus formation mediated by subsequent engagement of the signaling collagen receptor glycoprotein VI (GPVI), enforced by integrin α2β1. Protein tyrosine kinase Syk is central in the GPVI-induced signaling pathway, leading to elevated cytosolic Ca^{2+}. We aimed to determine the Syk-mediated thrombogenic activity of several collagen peptides and (fibrillar) type I and III collagens. High-shear perfusion of blood over microspots of these substances resulted in thrombus formation, which was assessed by eight parameters and was indicative of platelet adhesion, activation, aggregation, and contraction, which were affected by the Syk inhibitor PRT-060318. In platelet suspensions, only collagen peptides containing the consensus GPVI-activating sequence $(GPO)_n$ and Horm-type collagen evoked Syk-dependent Ca^{2+} rises. In whole blood under flow, Syk inhibition suppressed platelet activation and aggregation parameters for the collagen peptides with or without a $(GPO)_n$ sequence and for all of the collagens. Prediction models based on a regression analysis indicated a mixed role of GPVI in thrombus formation on fibrillar collagens, which was abolished by Syk inhibition. Together, these findings indicate that GPVI-dependent signaling through Syk supports platelet activation in thrombus formation on collagen-like structures regardless of the presence of a $(GPO)_n$ sequence.

Introduction

Platelet interaction with subendothelial collagen is a crucial step in hemostasis or arterial thrombosis after vascular injury or rupture of an atherosclerotic plaque, respectively [1,2]. In blood flowing with high shear rates, the initial capture of platelets is mediated by the von Willebrand factor (VWF), which avidly binds to collagens and is a ligand for the glycoprotein (GP) complex GPIb–V–IX [3]. The two platelet collagen receptors integrin α2β1 and GPVI ensure stable platelet adhesion and mediate platelet activation [4,5]. For over 20 years, GPVI has been recognized as the central signaling collagen receptor on platelets [6,7].

Studies using genetically modified mice have shown that the (patho)physiological process of arterial thrombus formation can be approximated using microfluidics devices, in which whole blood is perfused over a collagen surface [8]. The collagen fibers immobilized in such devices, for instance, those applied as microspots, also bind plasma VWF and thus promote shear-dependent adhesion, activation, and aggregation of platelets [3,9]. Previous results have revealed a strong interplay of GPIb-V-IX, GPVI, and integrin α2β1 in the formation of large and stable multilayered thrombi in a way where the two other receptors enforce the GPVI-induced activation of platelets [10,11]. Markedly, the thrombi that formed on collagen fibers appeared to be heterogeneous in structure, with on the one hand patches of aggregated platelets with activated integrin αIIbβ3 binding fibrinogen and CD62P expression via α-granule secretion and on the other hand single procoagulant platelets, exposing phosphatidylserine (PS), which is required for coagulation factor binding [12]. Particularly active in supporting thrombus formation is the standard collagen preparation "Horm" (collagen-H), which is a fibrillar type I collagen prepared in a proprietary process that is commonly used for diagnostics in the clinical laboratory. Still unexplained is why other fibril-forming type I and III collagen preparations, also binding with VWF, are less active in supporting thrombus formation under flow [9,13].

In previous years, a number of synthetic collagen-derived triple-helical peptides have been identified that, similarly to collagen-H, bind to GPVI and/or integrin α2β1 and thus induce platelet adhesion and activation *in vitro* [10]. Peptides containing the $(GPO)_n$ motif, in contrast to the supposedly inactive $(GPP)_n$ motif, bind to GPVI, while peptides with the GFOGER motif act as strong ligands for integrin α2β1 [14-16]. The prototypes of such triple-helical peptides are the cross-linked collagen-related peptide (CRP-XL) with a $(GPO)_{10}$ sequence, which hence acts as a potent GPVI agonist, and the combined GFOGER–$(GPO)_n$ sequence, which binds to platelets via both receptors. Subtle changes in the GFOGER sequence have been found to alter the affinity for α2β1. For instance, the substitution of phenylalanine in GFOGER by alanine in GAOGER resulted in lower-affinity α2β1 binding and diminished platelet adhesion under static conditions [17].

Platelet activation through GPVI [18-20], but not via GPIb-V-IX [21], relies on a potent protein tyrosine kinase cascade, culminating in the activation of the tyrosine kinase Syk. This GPVI signaling pathway involves phosphorylation of the Fc receptor γ-chain via Src-family

kinases and construction of a GPVI signalosome, in which Syk phosphorylates and activates phospholipase Cγ2 (PLCγ2), causing a rise in the central second messenger, Ca^{2+} [18,22-24]. However, the relative importance of this pathway has not been investigated thus far in platelets interacting under flow with surface-immobilized collagen peptides or fibrillar collagens.

In the present paper, we aimed to investigate the role of the GPVI-Syk pathway in thrombus formation on collagen-like surfaces at a high shear rate. In particular, we assessed the subprocesses of platelet adhesion, aggregation, and contraction as well as specific platelet activation responses. For this purpose, we used a panel of collagens, collagen peptides, and collagen-H (with established GPVI dependency) and the selective Syk inhibitor PRT-060318 (Syk-IN). The latter compound has recently been used to specify Syk-dependent pathways in mouse platelets [21,25] and human T cells [26]. As a direct readout of this signaling pathway, we also assessed Syk-dependent rises in cytosolic Ca^{2+}.

Materials and Methods

Materials

Collagen-related triple-helical peptides were synthesized as C-terminal amides and purified by reverse-phase high-performance liquid chromatography [44,45]: H-GPC(GPO)$_3$GFO GER(GPO)$_3$GPC-NH$_2$ (GFOGER-GPO), H-GPC(GPP)$_5$GFOGER(GPP)$_5$GPC-NH$_2$ (GFOGER-GPP), cross-linked collagen-related (GPO)$_n$ peptide (CRP-XL), GPC(GPO)$_3$-GAOGER(GPO)$_3$GPC-NH$_2$ (GAOGER-GPO), collagen type III-derived VWF-binding peptide VWF-III (VWF-BP), H-GPC(GPP)$_5$GPRGQOGVMGFO(GPP)$_5$GPC-NH$_2$ [46]. Collagen-I Horm derived from equine tendon (collagen-H) was obtained from Nycomed (Hoofddorp, The Netherlands). Human placenta-derived collagen-III (C4407), collagen-IV (C7521), and fibrillar collagen-I (C7774) came from Sigma-Aldrich (Zwijndrecht, The Netherlands). The latter was used to prepare monomeric collagen-I through pepsin treatment, as described in Ref. [47]. The selective spleen tyrosine kinase (Syk) inhibitor PRT-060318, 2-((1R,2S)-2-aminocyclohexylamino)-4-(m-tolylamino)pyrimidine-5-carboxamide (Syk-IN), came from Bio-Connect (Huissen, The Netherlands). Used for fluorescence staining were Alexa Fluor (AF)647-labeled antihuman CD62P mAb (304918, Biolegend, London, United Kingdom), FITC-labeled fibrinogen (F0111, Dako, Amstelveen, The Netherlands), and AF568-labeled annexin A5 (A13202, ThermoFisher, Eindhoven, The Netherlands). Fura-2 acetoxymethyl ester and Pluronic were from Invitrogen (Carlsbad, CA, USA). Human α-thrombin was from Kordia (Leiden, The Netherlands). Stable ADP (Me-S-ADP) and MRS-2179 were from Sigma-Aldrich. Other materials were from sources described before [31].

Blood isolation

Blood was obtained through venipuncture from healthy volunteers who had not received antiplatelet medication for at least two weeks. All subjects gave their full informed consent according to the Declaration of Helsinki. Studies were approved by the local Medical Ethics

Committee. Blood samples were collected into 3.2% trisodium citrate (Vacuette tubes, Greiner Bio-One, Alphen a/d Rijn, The Netherlands). All subjects had platelet counts within the reference range, as measured with a Sysmex XN-9000 analyzer (Sysmex, Cho-ku, Kobe, Japan).

Platelet isolation and loading with Fura-2

Platelet-rich plasma (PRP) was obtained from citrated blood through centrifugation at 870 g for 10 min. After the addition of 1:10 vol/vol acid citrate dextrose (ACD; 80 mM trisodium citrate, 183 mM glucose, 52 mM citric acid), the isolated PRP was centrifuged at 260 g for 2 min. Platelet pellets were resuspended into HEPES buffer, pH 6.6 (10 mM HEPES, 136 mM NaCl, 2.7 mM KCl, 2 mM $MgCl_2$, 5.5 mM glucose, and 0.1% bovine serum albumin). After the addition of apyrase (1 U/mL) and 1:15 *v/v* ACD, another centrifugation step was performed to obtain washed platelets [31]. The final pellet was resuspended in HEPES buffer, pH 7.45.

Light transmission aggregometry

The aggregation of washed platelets was measured by light transmission aggregometry, as described in Ref. [31], using an automated Chronolog aggregometer (Havertown, PA, USA). The platelet aggregation rate was determined from maximal curve slopes (% transmission change per min).

Whole-blood microfluidic perfusion over microspots

Selected collagen-like peptides and collagens were microspotted on glass coverslips, essentially as described before [9]. The coding of nine microspots (*M1–9*) is displayed in Table 1. In brief, washed coverslips were coated with three different microspots, each containing collagen (100 µg/mL) or a combination of a collagen-like peptide (250 µg/mL) and VWF-BP (100 µg/mL). Coating doses were chosen to obtain maximal platelet adhesion in flow assays [9]. The most active microspots were always located downstream, thus preventing the cross-activation of platelets between microspots [9]. The coated coverslips were incubated overnight in a humid chamber at 4 °C and then blocked with HEPES buffer (pH 7.45) containing 1% bovine serum albumin for 30 min before being mounted into Maastricht microfluidic chambers.

For flow perfusion, 500 µl of citrated whole blood was pre-incubated for 10 min with either vehicle (0.5% DMSO and 0.4 µg/mL Pluronic, f.c.) or inhibitor PRT-060318 (Syk-IN, 20 µM in vehicle solution, f.c.). After the addition of 40 µM PPACK and recalcification (3.75 mM $MgCl_2$ and 7.5 mM $CaCl_2$), blood samples were perfused through microspot-containing flow chambers for 3.5 min at a wall-shear rate of 1000 s^{-1}. After 2 min of staining for PS exposure (AF568-annexin A5), CD62P expression (AF647 anti-CD62P mAb), and integrin αIIbβ3 activation (FITC fibrinogen), the residual label was removed by postperfusion with HEPES buffer (pH 7.45) containing 2 mM $CaCl_2$ and 1 U/mL heparin. Vehicle controls were performed in duplicate, while samples containing Syk-IN were

repeated in triplicate using blood obtained from >5 different healthy donors.

Bright-field and fluorescence microscopy

From each microspot, two bright-field images (during labeling) and three 3-color fluorescence images (after removing the label) were taken using an EVOS-FL microscope (Life Technologies, Bleiswijk, The Netherlands) equipped with Cy5, RFP, and GFP LEDs; an Olympus UPLSAPO 60× oil immersion objective; and a sensitive 1360 × 1024 pixel CCD camera [32]. A standardized image analysis was performed using semiautomated scripts operated in Fiji (ImageJ), as described before [32]. Parameters extracted from bright-field images (*P1–5*), including thrombus signature scores (*P3–5*), and parameters from fluorescence images (*P6–8*) are specified in Table 1.

Cytosolic Ca^{2+} measurements

Washed human platelets (2×10^8/mL) were loaded with Fura-2 acetoxymethyl ester (3 μM) and pluronic (0.4 μg/mL) through a 40-min incubation at room temperature. After another wash step and resuspension of the platelets at the same concentration, changes in cytosolic $[Ca^{2+}]_i$ were measured in 96-well plates using a FlexStation 3 (Molecular Devices, San Jose, CA, USA). In brief, 200 μL of platelet suspension were pretreated with Syk-IN (5 μM) for 10 min or were left untreated. After the addition of 1 mM $CaCl_2$, the Fura-2-loaded cells were stimulated by automated pipetting with one of the following agonists (10 μg/mL) (for convenience, indicated as *M1–9* (see Table 1)): GFOGER-GPO (*M1*), CRP-XL (*M2*), GAOGER-GPO (*M3*), GFOGER-GPP (*M4*), VWF-BP (*M5*), collagen-H (*M6*), fibrillar collagen-I (*M7*), monomeric collagen-I (*M8*), or collagen-III (*M9*).

Changes in Fura-2 fluorescence were measured over time at 37 °C by ratiometric fluorometry at dual excitation wavelengths of 340 and 380 nm and an emission wavelength of 510 nm. The agonist injection speed was set at 125 μL/s, resulting in complete, diffusion-limited mixing. Separate wells contained Fura-2-loaded platelets that were lysed with 0.1% Triton-X-100 in the presence of either 1 mM $CaCl_2$ or 9 mM EGTA/Tris for a determination of the R_{max} and R_{min} values, respectively [33]. After correction for background fluorescence, $[Ca^{2+}]_i$ (as nM) was calculated from the ratio values [34]. Measurements were performed in duplicate wells and were completed within 2–3 h of preparation of the cells.

Data handling and statistics

GraphPad Prism 8 was employed for statistical analysis. Heatmaps were generated with the program R. For heatmap representation, all parameter values were univariate-normalized at a scale of 0–10 [46]. Thrombus values of duplicate or triplicate flow runs from the same blood donor were averaged to obtain one parameter set (vehicle or Syk-inhibited) per microspot and donor. Mean values of control and inhibitor runs were then compared per blood sample using paired Student's *t*-tests: *p*-values below 0.05 were considered to be significant. For subtraction heatmaps, a standard filter of *p*<0.05 was set to visualize relevant effects.

Modeling to predict GPVI activity

Complete datasets (8 parameters, 9 surfaces) for flow runs of ≥5 donors were used to construct a partial least square (PLS) model to predict GPVI dependency. First, range-scaled data for the collagen peptide surfaces (*M1–5*) with known GPVI dependency were used to generate a PLS model, after which collagen-H (*M6*) was then used to test the reliability of the model. A principal component analysis (PCA) in 1- and 2-component mode was then applied, the predictions of which were supported by cross-validated analysis of Q^2, defined as $1 - (PRESS/TSS)$ [35]. Subsequently, parameter sets of *M7–9* were predicted for GPVI-dependency from the PLS model, as were parameters of *M1–9* in the presence of Syk-IN. By default, prediction values >0.5 were considered to be positive for GPVI dependency.

Results

GPVI-dependent and Syk-dependent platelet activation by collagen peptides

As a first estimation of the potency of distinct collagen peptides to act as ligands for platelet GPVI, we examined their ability to stimulate PLCγ2-mediated rises in cytosolic Ca^{2+} using Fura-2-loaded platelets. For a selective inhibitor of the GPVI pathway, we used the compound PRT-060318 (Syk-IN), which was earlier used to identify Syk-dependent activation processes in platelets mediated by GPVI [21,25] or CLEC2 [36]. The Syk-IN compound was found to phenocopy the effects of Syk depletion on platelet responses in $Syk^{-/-}$ bone marrow chimeric mice [28]. Moreover, in human platelets, Syk-IN selectively blocked the GPVI/Syk-dependent tyrosine phosphorylation and aggregation responses induced by fibrin [37].

To confirm the selectivity of Syk-IN as an inhibitor of GPVI-induced responses of human platelets, we monitored its effect (using 5 μM throughout) on the aggregation of platelets induced by CRP-XL, thrombin, or stable ADP. This inhibitor caused the complete inhibition of aggregation only with the GPVI agonist CRP-XL, whereas with thrombin or ADP it was ineffective (Figure S1A). This was in agreement with earlier studies performed with mouse platelets [21,25]. Additional control experiments with Fura-2-loaded human platelets indicated that Syk-IN did not suppress thrombin- or ADP-induced Ca^{2+} rises (Figure S1B).

Using Syk-IN, we then evaluated the role of Syk in platelet Ca^{2+} fluxes, which were induced by several collagen peptides presumed to be GPVI-dependent or -independent. With three peptides containing the consensus GPVI-activating motif $(GPO)_n$, *i.e.*, GFOGER-GPO (for convenience designated as *M1*, see Table 1), CRP-XL (*M2*), and GAOGER-GPO (M3), we observed a potent rise in $[Ca^{2+}]_i$, which was fully abolished in the presence of Syk-IN (Figure 1). Close examination of the Ca^{2+} traces showed some differences between *M1-3* at onset and the maximum value. The reason for these differences was unclear, but they may have been linked to variations in the peptide conformation or GPVI clustering capacity of the triple-helical peptide in question. On the other hand, two other collagen peptides

containing a $(GPP)_n$ motif instead of $(GPO)_n$ were unable to induce $[Ca^{2+}]_i$ rises: these were GFOGER-GPP (M4) and the VWF-binding peptide (*M5*). The Ca^{2+} traces were not influenced by the presence of Syk-IN. Overall, these results indicated a high Syk dependency of the platelet $[Ca^{2+}]_i$ rises, which were induced by the $(GPO)_n$-containing collagen peptides containing an established GPVI-activating sequence.

GPVI- and Syk-dependent parameters of thrombus formation on collagen peptides

To assess how the five collagen peptides supported whole-blood thrombus formation, we applied these as microspots (*M1–5*) in a microfluidic device, as described before [9]. The microspots were supplemented with VWF-BP (peptide binding plasma VWF) to allow for GPIb-V-IX-mediated trapping of platelets. Whole-blood perfusion was performed at a wall-shear rate of 1000 s^{-1}. Through end-stage (3.5 min) multicolor microscopic imaging, it was possible to analyze up to eight thrombus and platelet characteristics: Overall platelet deposition (parameter *P1*, see Table 1); platelet aggregation (*P2*); thrombus signature, *i.e.*, morphology, multilayers, and contraction (*P3-5*); platelet procoagulant activity, measured as PS exposure (*P6*); platelet activation parameter CD62P expression (*P7*); and fibrinogen binding to activated integrin αIIbβ3 (*P8*).

Typically, the collagen peptides containing $(GPO)_n$ (*M1–3*) produced large thrombi with aggregated platelets with high levels of activation markers, *i.e.*, PS exposure, CD62P expression, and integrin activation (Figure 2). In contrast, the non-GPVI-stimulating $(GPP)_n$ peptide GFOGER-GPP (*M4*) caused the formation of smaller thrombi with residual CD62P expression and integrin activation, but essentially no PS exposure. Quantification of the raw image data confirmed high parameter values for all $(GPO)_n$ microspots from *M1–3*, indicating a strong ability to support thrombus formation (Figure S2). Interestingly, when comparing the two GFOGER peptides with or without the GPVI-binding motif (*M1* or *M4*), the latter still induced residual platelet activation, in spite of lower thrombus signature scores (*P4-5*) and limited PS exposure (*P6*). Furthermore, M1 (GFOGER), which had a supposedly higher-affinity α2β1 binding motif than *M3* (GAOGER), was less effective in promoting almost all thrombus parameters (*P1,2,3–5,7,8*). The differences between microspots were visualized in a univariate scaled heatmap of all parameters (Figure 3A). Together, the data suggested that the earlier distinction made between high- and low-affinity α2β1 binding sites (established under static conditions [11,15]) became confusing in part when immobilized collagen peptides were exposed to platelets in flowing whole blood. On the other hand, the apparent lack of both GPVI and α2β1 binding sites, as with *M5*, resulted in almost no stable platelet adhesion and activation.

Parallel flow runs on all microspots from *M1–5* were performed with blood samples pretreated with Syk-IN (maximum effective dose of 20 µM) or DMSO vehicle. This resulted in marked reductions in the majority of thrombus parameters (Figure 3A). A subtraction heatmap pinpointing only relevant changes ($p < 0.05$) indicated that for *M1–4*, essentially all parameters except for *P1* (platelet deposition) were reduced by Syk inhibition (Figure 3B). Most drastic complete reductions were seen with PS exposure (*P6*) on the "active" $(GPO)_n$

surfaces of *M1–3*. Surprisingly, Syk inhibition also affected platelet activation at the supposedly non-GPVI $(GPP)_n$ surface of *M4*. The other microspot, *M5*, was inactive in the absence of Syk-IN.

A summative plot was made indicating how individual (scaled) parameters were changed by Syk inhibition across all microspots (Figure 3C). This revealed a complete reduction in *P6* (PS exposure), along with strong reductions in *P2* (aggregate coverage), *P4* (thrombus multilayer), *P5* (thrombus contraction), and *P8* (fibrinogen binding). Less affected were *P3* (thrombus morphology) and *P7* (CD62P expression).

3

Table 1. Overview of the composition of microspots (*M1–9*), platelet receptors implicated in thrombus formation. Also indicated are the analyzed thrombus parameters (*P1–8*) from bright-field and fluorescence microscopic images. Measured ranges and scaling for heatmap analysis were as indicated. GP: glycoprotein; PS: phosphatidylserine; VWF-BP: von Willebrand factor binding peptide, SAC: surface area coverage; n.a.: not assessed.

	Microspot	Platelet Receptors		
		GPVI	*α2β1*	*GPIb*
M1	GFOGER-GPO + VWF-BP	++	++	++
M2	CRP-XL + VWF-BP	++	o	++
M3	GAOGER-GPO + VWF-BP	++	+	++
M4	GFOGER-GPP + VWF-BP	(o)*	++	++
M5	VWF-BP	o	o	++
M6	collagen-H (Horm type)	++	++	++
M7	collagen-I (human)	n.a.	n.a.	++
M8	monomeric collagen-I (human)	n.a.	n.a.	++
M9	collagen-III (human)	n.a.	n.a.	++

	Parameter	range	scaling
	Brightfield Images		
P1	platelet deposition (% SAC)	0–51.52	0–10
P2	platelet aggregate coverage (% SAC)	0–21.09	0–10
P3	thrombus morphological score	0–4.10	0–10
P4	thrombus multilayer score	0–2.60	0–10
P5	thrombus contraction score	0–2.94	0–10
	Fluorescence images		
P6	PS exposure (% SAC)	0–13.91	0–10
P7	CD62P expression (% SAC)	0–46.71	0–10
P8	fibrinogen binding (% SAC)	0–28.33	0–10

* No GPVI-activating $(GPP)_n$ motif
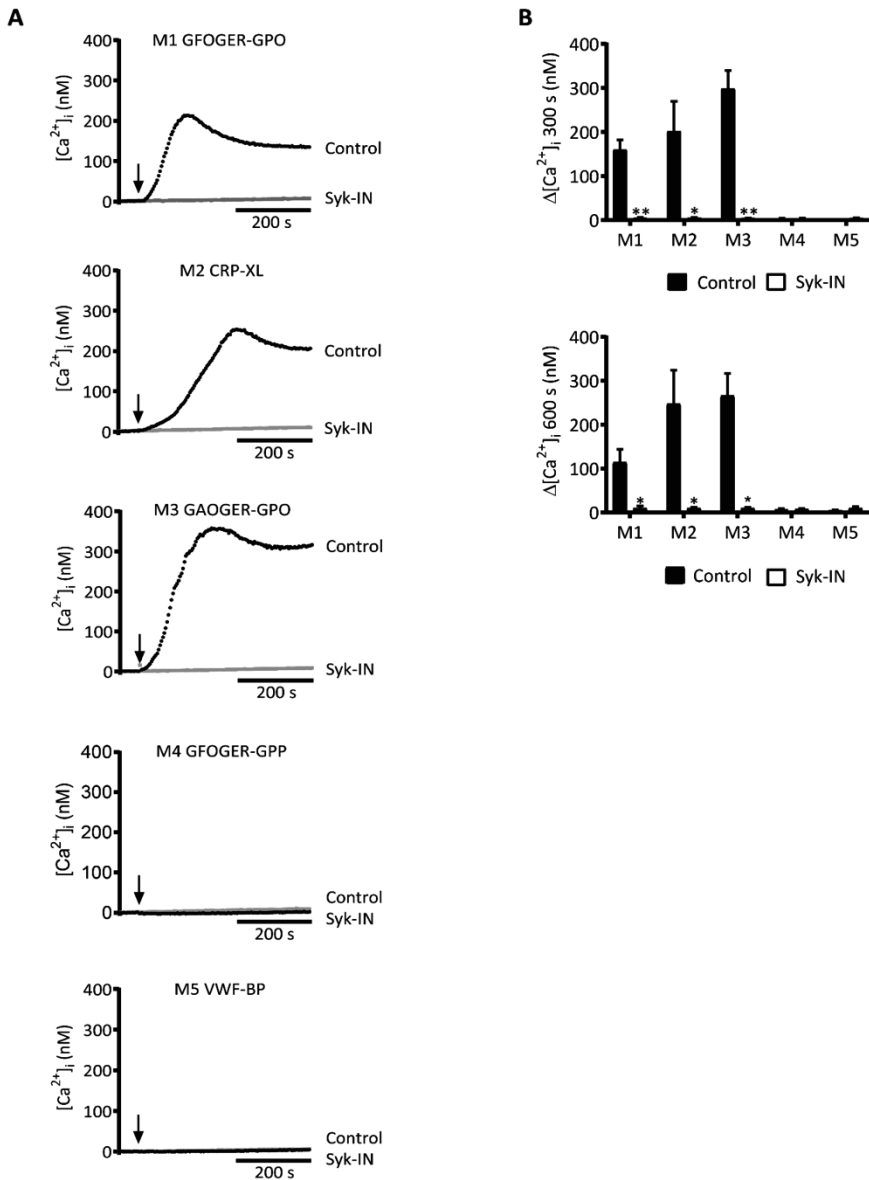
Figure 1. Syk inhibition affecting platelet Ca^{2+} rises by collagen peptides with (GPO)$_n$ motif. Fura-2-loaded platelets in 96-well plates were pre-incubated with Syk-IN (5 µM) or left untreated before stimulation with collagen peptide (*M1-5*, 10 µg/mL). Changes in [Ca^{2+}]$_i$ were recorded over time per well-plate row by ratio fluorometry using a FlexStation 3. Peptides were injected into wells at 60 s (arrow) and reached platelets in a diffusion-limited way. (**A**) Calibrated [Ca^{2+}]$_i$ traces recorded over 600 s in the absence (black, control) or presence (grey) of a Syk inhibitor. Traces are representative of three experiments. (**B**) Quantification for *M1-5* of increased [Ca^{2+}]$_i$ at 300 s (top graph) or 600 s (bottom graph). Means ± SEM (n=3). Paired Student's *t*-tests; * *p<0.05*, ** *p<0.01*.
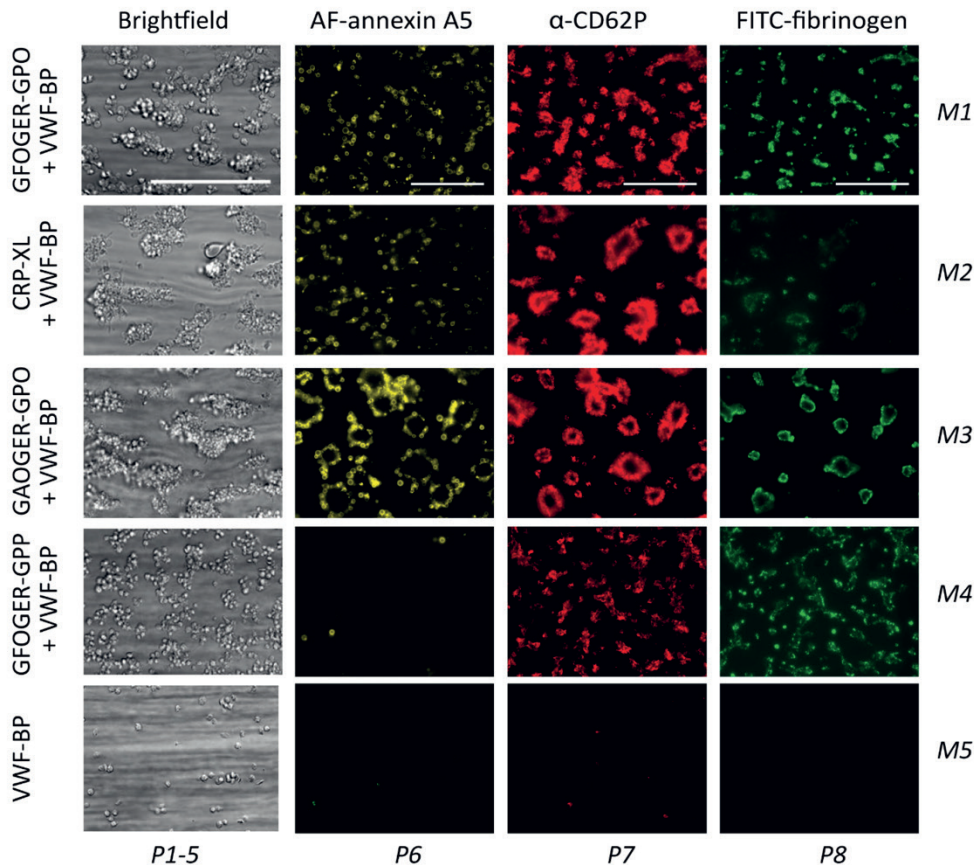
Figure 2. Thrombus formation on immobilized collagen peptides with or without a (GPO)ₙ motif. Whole blood was perfused over microspots *M1* (GFOGER-GPO + VWF-BP), *M2* (CRP-XL + VWF-BP), *M3* (GAOGER-GPO + VWF-BP), *M4* (GFOGER-GPP + VWF-BP), and *M5* (VWF-BP), with assumed platelet adhesion via GPIb, GPVI, and/or integrin α2β1, as in Table 1. The wall-shear rate was 1000 s⁻¹, with a perfusion time of 3.5 min. Representative bright-field microscopic images at the end stage are shown for analysis of platelet deposition (parameter *P1*) and thrombus characteristics (*P2–5*). In addition, end-stage three-color fluorescence images for analysis of PS exposure (AF568 annexin A5, *P6*), CD62P expression (AF647 α-CD62P, *P7*), and fibrinogen binding (FITC, *P8*) are shown. Scale bars represent 50 μm.

Figure 3. Effect of Syk inhibition on parameters of thrombus formation on immobilized collagen peptides. Blood samples pre-incubated with vehicle (Ctrl) or Syk-IN (20 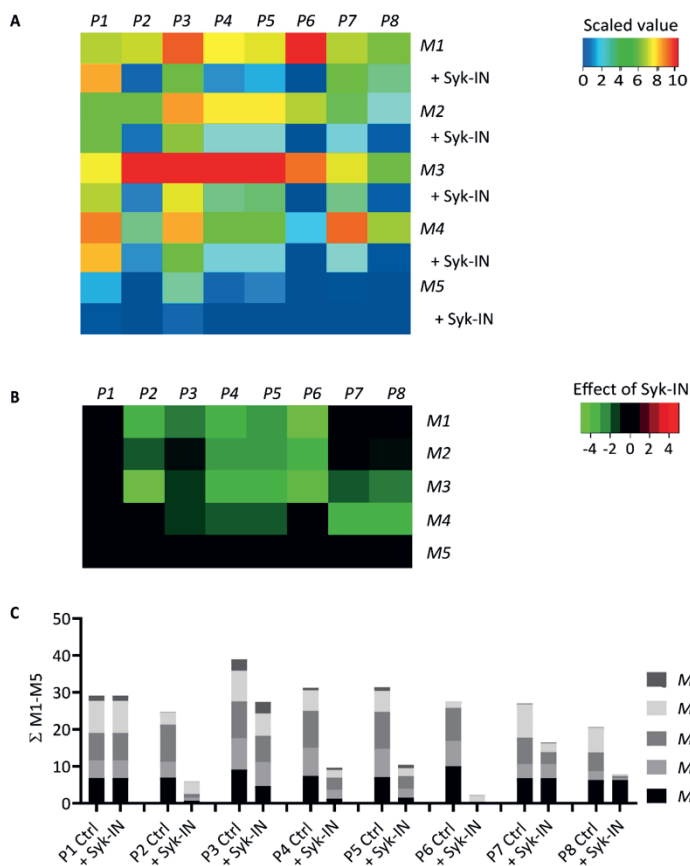µM) flowed over microspots *M1–5*, and the thrombi formed were imaged to obtain parameters *P1–8*, as in Figure 2. The effects of Syk-IN were assessed per blood sample, surface, and parameter. Mean values from individual blood samples (n=5–7) were univariate-scaled to 0–10 per parameter across all surfaces *M1–9*. (**A**) Heatmap of scaled parameters, demonstrating the mean effects of Syk-IN. The rainbow color code indicates scaled values between 0 (blue) and 10 (red). (**B**) Subtraction heatmap representing the scaled effects of Syk-IN, filtered for relevant changes (*p*<0.05, paired Student's *t*-test per surface and parameter). The color code represents decreases (green) or increases (red) in comparison to control runs. (**C**) Cumulative inhibitory effect per parameter over all microspots, indicating relevant changes.

GPVI-induced and Syk-dependent platelet activation by different collagens

Subendothelial collagen types I and III are considered to be the major platelet-activating collagens in the vessel wall, acting via GPVI and α2β1 [39]. Equine standard collagen (collagen-H), likely a modified type I collagen, is the most commonly used collagen in studies of GPVI-induced platelet activation. This prompted us to compare four collagen preparations for their ability to support the GPVI-PLCγ2-Ca^{2+} activation pathway: The fibrous collagen-H (*M6*), human fibrillar collagen-I (*M7*), a degraded collagen-I (M8), and human fibrillar collagen-III (*M9*). Realizing that the very high molecular mass of collagens results in a heterogeneous interaction with platelets in suspension, we evaluated the [Ca^{2+}]$_i$

rises induced by these collagens. Markedly, the four collagens (*M6–9*) evoked a biphasic rise in $[Ca^{2+}]_i$, with an initial plateau level and a later second phase that was highest for *M7* and *M9* (Figure 4A, B).

In absolute levels, the rises in $[Ca^{2+}]_i$ obtained with *M6,7,9* at a late time point of 600 s were 2–3-fold lower than those seen with the $(GPO)_n$-containing collagen peptides (Figure 4 *vs*. Figure 1). This difference was likely due to the high molecular mass of the fibrillar-type collagens, which slowed down the rate and extent of diffusion-limited interactions with platelets, but it was also likely due to the higher density of the activation motif within the peptides. In addition, it appeared that Syk inhibition completely suppressed the $[Ca^{2+}]_i$ transients induced by the standard collagen-H (*M6*), but it did not alter the transients of other collagens (Figure 4). In the presence of indomethacin (10 μM, a thromboxane A_2 pathway inhibitor), AR-C69931MX (10 μM, a $P2Y_{12}$ receptor inhibitor), or MRS2179 (100 μM, a $P2Y_1$ receptor inhibitor), the rises in $[Ca^{2+}]_i$ with collagens I–III were suppressed by 15%–28%, 31%–32%, or 17%–31%, respectively, in a nonredundant way (data not shown). Taken together, this suggested the presence of a Syk-independent pathway for Ca^{2+} mobilization of suspended natural collagens, which in part came from autocrine activation mechanisms.

GPVI- and Syk-dependent platelet responses in thrombus formation on collagens

The same collagen preparations (*M6–9*) were also applied as microspots to test their ability to support thrombus formation under flow. As indicated in Figure 5, collagen-H (*M6*) was the most potent in provoking the formation of large aggregates of platelets with high PS exposure, granule secretion, and fibrinogen binding, in agreement with the known high GPVI- and α2β1-activating potency of this collagen when immobilized [9,11,12]. In comparison, the fibrillar type I (*M7*) and III (*M9*) collagens formed only small aggregates of platelets with remaining secretion and fibrinogen binding, with *M9* causing residual PS exposure (Figure 5). The degraded collagen-I (*M8*) caused mostly single-platelet adhesion with incidental small-sized aggregates. The same information was obtained from the raw mean values of individual parameters with these surfaces (Figure S3).

Heatmapping of the eight scaled parameter values confirmed that overall microspot thrombogenicity decreased in the order of *M6* > *M7,9* > *M8* (Figure 6A). Treatment of the blood with Syk-IN left platelet deposition (*P1*) unchanged, but it decreased the thrombus signature and the platelet activation parameters (*P2–5, P7,8*) for several collagens. A subtraction heatmap was built with a filter for relevant changes ($p<0.05$). For collagen-H (*M6*) as well as for fibrillar collagen-I and -III (*M7,9*), it showed a reduction in almost all parameters except for *P1* in the presence of Syk-IN (Figure 6B). The parameters of platelet aggregation and contraction (*P2,4,5*) and platelet activation (*P6* for *M6*; and *P7,8* for *M7,9*) were the most reduced.

In view of the possible role of GPVI also for platelet interaction with collagen type IV, additional whole-blood flow runs (n=3 donors) were performed with collagen-IV

microspots. Under control conditions, we noticed a pattern of thrombus formation resembling that of collagen-I (*M7*) or collagen-III (*M9*). In the presence of Syk-IN, all parameters on collagen-IV were significantly reduced ($p<0.01$), with the exception of *P2* and *P6*. Across all parameters, the median inhibitory effect of Syk-IN for collagen-I, -III, and -IV was 87.8%, 88.0%, and 85.7%, respectively (data not shown). Hence, we observed a similar extent of thrombus inhibition by Syk-IN for all of these fibrillar collagens.

To obtain an overall insight into the effect of Syk inhibition, a summative plot was again constructed for each scaled parameter across all collagen microspots (Figure 6C). Importantly, this revealed a highly similar effect of Syk inhibition, as previously seen for the collagen peptides. Summing up the values for *M6–9*, we noticed a near-complete reduction in *P6* (*M6*, PS exposure), along with strong reductions in *P2* (platelet aggregate coverage), *P4* (thrombus multilayer), *P5* (thrombus contraction), *P7* (CD62P expression), and *P8* (fibrinogen binding) compared to vehicle-treated blood. Less affected by Syk inhibition was *P3* (thrombus morphology), while platelet adhesion (*P1*) was unchanged.

Modeling of the role of GPVI in thrombus formation on various collagens

We then applied a regression analysis to provide a systematic examination of the generated data (*M1–9*), which consisted of 416 data points (52 mean control flow runs of 9 surfaces, 8 parameters), to reveal the GPVI dependency of each surface. First, a partial least square (PLS) regression model was generated for collagen peptides *M1–3* (which had an assumed high GPVI dependency) and for *M4,5* (with supposedly no role for GPVI), after which the data from *M6* (collagen-H) were entered into the model. This analysis resulted in relevant components 1 and 2, explaining 68% and 15% of the variation, respectively (Figure S4). A principal component plot indicated a tight cluster of flow runs with *M1–3,6*. The data for *M5* (negative component 1) and *M4* (negative component 2) lay further out in the model. This agreed with the large observed differences in (the parameters of) thrombus formation on *M4* and *M5*. The calculated beta matrix indicated that *P2–6* contributed to the modeled results to a similar extent.

Because of the separation of *M4–5* parameters, the component 1 model was used for further analysis. Prediction testing of the model showed near complete prediction accuracy for all surfaces, except for *M4* (because there was no component 2) (Table 2). The model was further used to predict the role of GPVI in the remaining collagen surfaces, *M7–9*. For both fibrillar collagens (*M7,9*), the prediction of GPVI dependency was mixed, while it was negative for the degraded collagen-I (*M8*). Subsequently, we integrated into the model the second set of 416 data points of Syk-inhibited blood samples (52 mean flow runs with Syk-IN for 9 surfaces, 8 parameters) to predict the absence of GPVI activity. Markedly, across all surfaces, 51 out of 52 samples predicted a negative GPVI dependency, wherein the only incorrectly predicted sample was just above the conventional 0.5 threshold value for right prediction. Taken together, the constructed PLS model indicated, in addition to complete GPVI-independency of all Syk-inhibited samples, no role of GPVI on surfaces *M5* and *M8*.
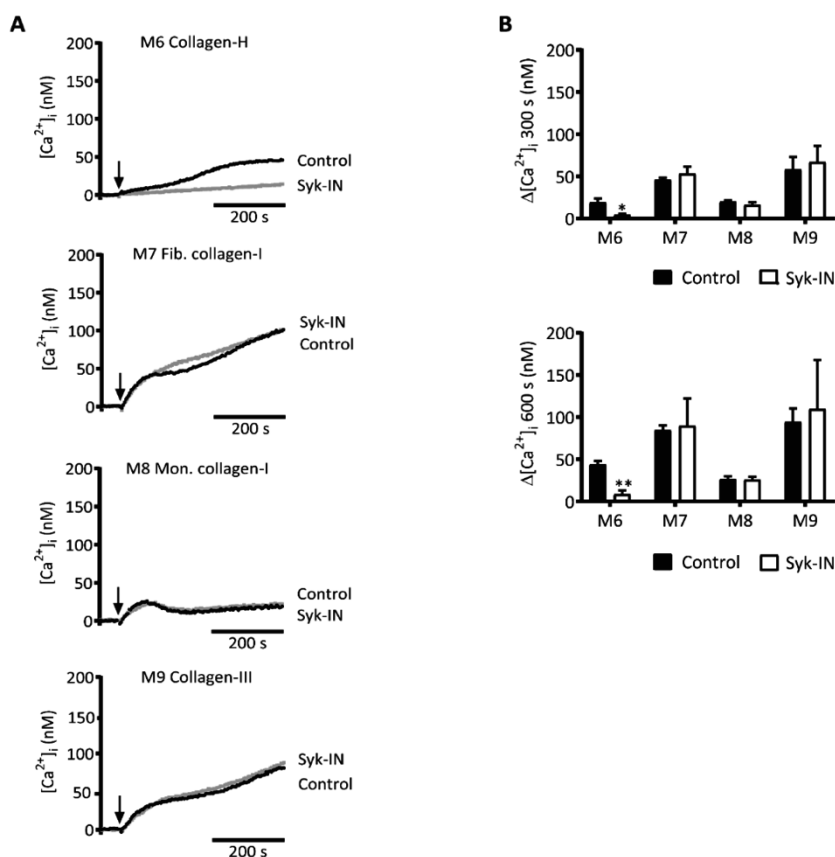
Figure 4. Syk inhibition differently affects platelet Ca²⁺ rises by collagens. Fura-2-loaded platelets in 96-well plates were pre-incubated with Syk-IN (5 µM) or were left untreated before stimulation with different collagens (*M6–9*, 10 µg/mL). Changes in $[Ca^{2+}]_i$ were continuously monitored per well-plate row by ratio fluorometry using a FlexStation 3. Collagens were injected at 60 s (arrow), and they reached platelets in a diffusion-limited way. (**A**) Calibrated $[Ca^{2+}]_i$ traces recorded for 600 s in the absence (black, control) or presence (grey) of a Syk inhibitor. Traces are representative of three experiments. (**B**) Quantification of $[Ca^{2+}]_i$ rises after 300 s (top graph) and 600 s (bottom graph) for *M1–5*. Means ± SEM (n=3). Paired Student's *t*-tests; * *p<0.05*, ** *p<0.01*.
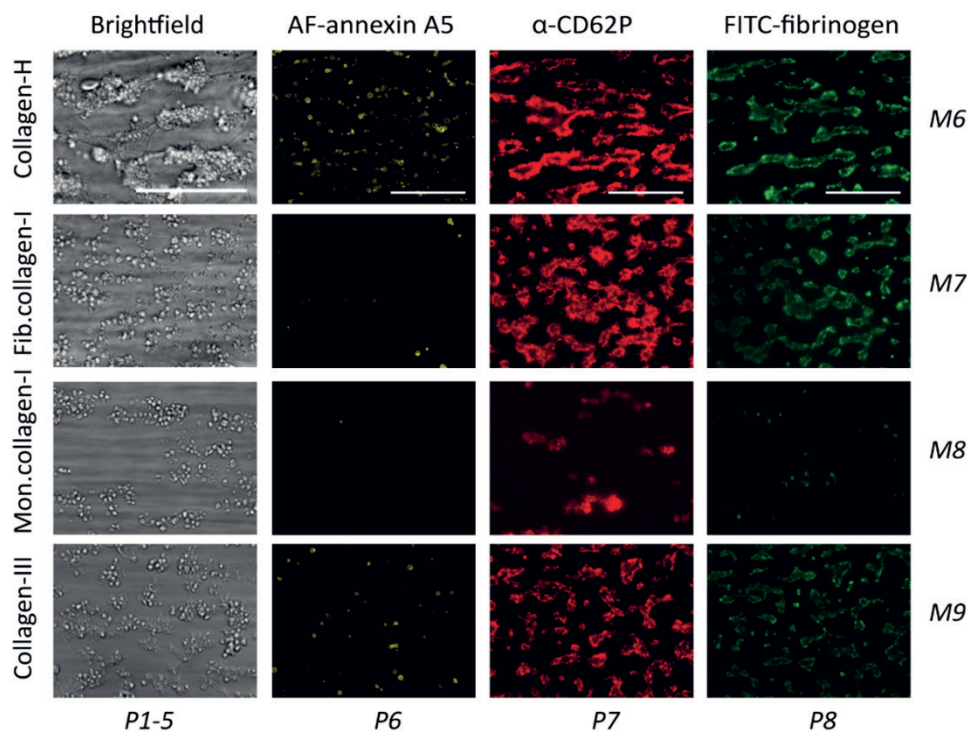
Figure 5. Thrombus formation on immobilized collagens. Whole blood was perfused over microspots *M6* (collagen-H), *M7* (fibrillar collagen-I), *M8* (degraded collagen-I), and *M9* (collagen-III). The wall-shear rate was 1000 s^{-1}, and the perfusion time was 3.5 min. Representative bright-field microscopic images at the end stage are shown for analysis of platelet deposition (parameter *P1*) and thrombus characteristics (*P2–5*). In addition, end-stage three-color fluorescence images for analysis of PS exposure (AF568 annexin A5, *P6*), CD62P expression (AF647 α-CD62P, *P7*), and fibrinogen binding (FITC, *P8*) are shown. Scale bars represent 50 μm.

3
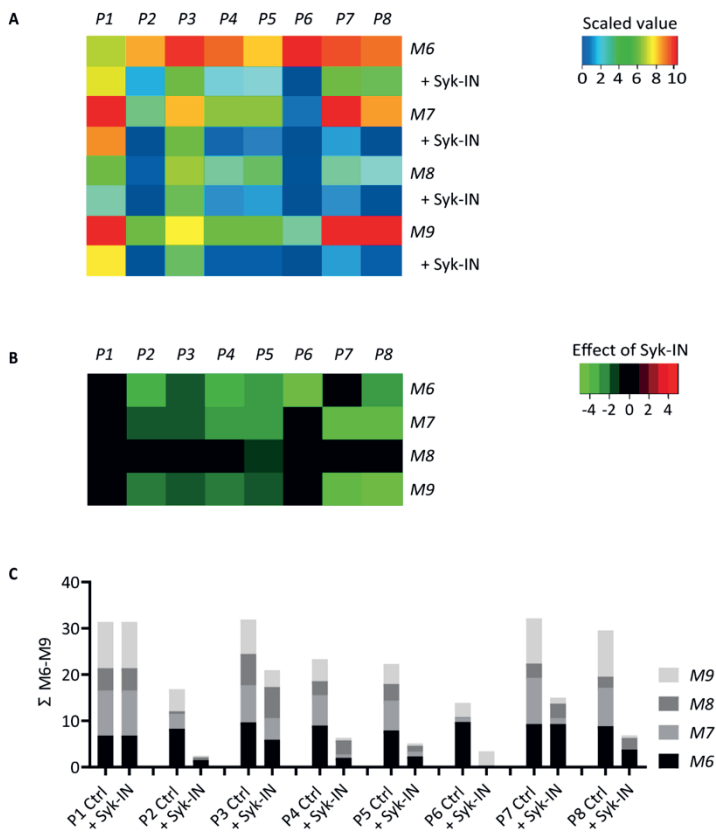
Figure 6. Effect of Syk inhibition on parameters of thrombus formation on immobilized collagen. Whole blood pre-incubated with vehicle (Ctrl) or Syk-IN (20 µM) was perfused over microspots *M6–9*, and thrombus formation was imaged to obtain parameters *P1–8*, as in Figure 5. The effects of Syk-IN were calculated per blood sample, surface, and parameter. Mean values for all blood samples (n=5–7) were univariate-scaled to 0–10 per parameter across all surfaces of *M1–9*. (A) A heatmap of the scaled parameters showing the mean effects of Syk-IN. The rainbow color code gives scaled values between 0 (blue) and 10 (red). (B) A subtraction heatmap representing the scaled effects of Syk-IN, filtered for relevant changes ($p<0.05$, paired Student's *t*-tests per surface and parameter). The color code represents decreases (green) or increases (red) in comparison to control runs. (C) Cumulative inhibitory effect over all microspots per parameter, indicating relevant changes from control runs.

Table 2. Modeled partial least square (PLS) analysis, based on component 1 principal component analysis (PCA) of range-scaled data for collagen peptides (*M1–5*) plus collagen-H (*M6*), with assumed GPVI dependency. The ranges of prediction values are shown. Predicted accuracy is given by the numbers of mean flow runs per donor (control and Syk-IN). By default, a correct prediction was set at >0.5. In addition, the back-prediction of GPVI dependency of mean flow runs per donor for *M7–9* is shown. Prediction outcomes are given here in italics. The contributions of parameters to the prediction model were in the order of *P2–6 > P1,7,8*.

Microspot	GPVI dependency	Correctly predicted		
		range	ctrl	Syk-IN
M1	positive	0.41–1.06	5/6	6/6
M2	positive	0.27–0.76	4/5	5/5
M3	positive	0.86–1.07	5/5	5/5
M4	negative	0.57–0.97	0/6	6/6
M5	negative	0.21–0.34	5/5	5/5
M6	positive	0.68–1.11	7/7	6/7
M7	mixed	0.44–0.85	5/7	7/7
M8	negative	0.13–0.41	0/5	5/5
M9	mixed	0.49–0.67	3/5	5/5

Discussion

Collagen peptides and GPVI-dependent platelet activation

The data obtained indicated a clear separation between the effects of triple-helical collagen peptides that contained the established GPVI recognition motif, $(GPO)_n$ [15], and peptides that had a $(GPP)_n$ backbone instead. We found that the $(GPO)_n$-containing collagen peptides (*M1–3*) *(i)* induced high platelet Ca^{2+} rises under stasis, *(ii)* accomplished a fast build-up of thrombi with aggregated and activated platelets under flow, and *(iii)* evoked platelet responses both under flow and static conditions that were highly sensitive to the inhibition of Syk. Accordingly, these peptides provided strong proof-of-principle evidence for potent stimulation of the GPVI-Syk-PLCγ2-Ca^{2+} pathway of platelet activation.

Immobilized, the $(GPO)_n$ peptide CRP-XL (*M2*), lacking an α2β1 interaction motif, produced smaller-sized thrombi (low parameter values in *P2–6*) than the other collagen peptides did, which was in agreement with the known synergy between GPVI, integrin α2β1, and GPIb-V-IX receptors in thrombus formation at a high shear rate [9-11]. The synergy of GPVI and α2β1 could also explain why peptides containing the integrin-binding motif G(F/A)OGER evoked a faster Ca^{2+} signal when compared to CRP-XL. Seemingly in contrast with its lower binding affinity to platelets under stasis [17], we observed higher parameters of thrombus formation with GAOGER-GPO (*M3*) than with GFOGER-GPO (*M1*). The explanation for this higher activity remains unclear.

In contrast, the $(GPP)_n$-containing peptides GFOGER-GPP (*M4*) and VWF-BP (*M5*) did not evoke detectable Ca^{2+} rises in platelets under stasis. Yet, when immobilized under flow, the integrin-binding peptide GFOGER-GPP evoked low-parameter thrombus formation in terms of platelet activation and aggregation, and this activity was again suppressed by Syk inhibition. This may have reflected the weak interaction of the $(GPP)_n$ motif with GPVI, reinforced by strong integrin-binding activity.

Jointly, these results pointed to a Syk-dependent role via GPVI in the support of

thrombus formation. This conclusion was supported by a reanalysis of earlier experiments, where the effects of the single-chain variable fragment antibody 10B12 were studied for the surfaces *M1*, *M5,* and *M6* [16]. Markedly, image reanalysis providing the parameters *P1,3–6* indicated a similar effect pattern of 10B12 as presently seen with Syk-IN (not shown).

Collagens and GPVI-dependent platelet activation

Fibrillar type I and type III collagens are among the vessel wall components that most strongly activate platelets [7,39]. Due to the structural complexity of multiple adjacent triple helices in these collagens, little is known about how platelet receptors bind to the fibrils, although there is evidence that the copresence of multiple binding sites in a collagen fiber enforces platelet adhesion and activation [40,41]. Recent high-resolution microscopy has indicated that multiple copies of GPVI dimerize and cluster along the fibers of such collagens, a process that is considered to enforce GPVI-dependent platelet activation [42,43]. Previous sequence analysis has shown that both type I and III collagens are made for up to 10% of GPO triplets, with α2β1 binding sequences present in both cases, *e.g.*, GFOGER in collagen-I and GAOGER in collagen-III [44].

Here, we compared the effects of preparations of human fibrillar collagen-I and collagen-III to the standard collagen-H, *i.e.*, a commercial equine type I-enriched preparation with fewer defined supramolecular characteristics [45]. Markedly, added to suspended platelets, collagen-H (*M6*) was the only collagen that induced Syk-dependent $[Ca^{2+}]_i$ rises, whereas the other collagens (*M7,9*) induced low $[Ca^{2+}]_i$ rises that were insensitive to Syk inhibition. When microspotted, collagen-H triggered the formation of large-size thrombi, with high parameters of platelet aggregation and activation, *i.e.*, responses that are known to be strongly GPVI-dependent [9] and that in the present setting were consistently affected by Syk inhibition.

In addition, we tested a protease-treated, monomeric collagen-I preparation (*M8*), which appeared to be inactive in supporting thrombus formation with no appreciable effect of Syk inhibition. This finding supports the notion that the fibrillar structure of immobilized collagens helps to expose receptor (GPVI) binding sites upon stretching under flow conditions.

In comparison to collagen-H, the immobilized type I (*M7*) and type III (*M9*) collagens triggered the formation of smaller thrombi with lower platelet activation parameters. Yet, for the fibrillar collagens, the summed suppressive effects of Syk inhibition were remarkably similar to those seen for collagen-H and the $(GPO)_n$-containing collagen peptides. Given the similar abundance of GPO triplets in both collagen-I and -III [15], these findings point to a limited role of GPVI-induced activation under flow conditions. In agreement with such a role for GPVI, others have shown that immobilized collagens can induce GPVI dimer clustering in adhered and spreading platelets [34]. In this setting, immobilized collagen-III was found to be more effective in cluster formation than collagen-H or CRP-XL. Furthermore, the inhibition of Syk did not abrogate the GPVI clustering.

These findings suggest that there is not a direct link between GPVI cluster formation and the strength of the GPVI-Syk-PLCγ2 signal. However, under flow conditions, the additional involvement of VWF/GPIb-V-IX and integrin α2β1 interactions [13,16] might enforce the GPVI clustering pattern, but this still needs to be demonstrated.

Comparative roles of GPVI and Syk in platelet activation

A remarkable finding was that Syk inhibition also affected parameters of thrombus formation on surfaces that were considered to act independently of GPVI (*i.e.*, GFOGER-GPP, *M4*) or with a low GPVI dependency (collagen-I, *M7*; collagen-III, *M9*). As another approach to examine this, a PLS model was constructed and used for principal component analysis. The PCA plots indicated a narrow cluster for all high GPVI-activating surfaces (*M1–3,6*), with the data of *M4,5* partly centering out. A prediction of the role of GPVI for other surfaces gave a mixed outcome for the fibrillar collagens (*M7,9*), whereas this was negative for the degraded collagen-I (*M8*). Importantly, the prediction model revealed a consistent GPVI independence for the Syk-inhibited samples, regardless of the type of microspot composition. Accordingly, this analysis supported the indication of low-level GPVI and Syk activity at these weakly thrombogenic surfaces.

In recent years, evidence has accumulated on the role of GPVI signaling in platelets in (also) contacting non collagen surfaces. For instance, GPVI dependency has been discovered for platelets interacting with laminin [46], fibrin [38,47], or fibrinogen [48,49]. In this context, it is also likely that for (GPP)$_n$-containing surfaces, Syk-dependent platelet responses can be traced back to residual GPVI activity. On the other hand, based on early studies, it cannot yet be excluded that (part of) the Syk-dependent platelet responses in thrombus formation at "weaker" surfaces are mediated by signaling via integrin αIIbβ3 [50-52], hence bypassing GPVI. This needs to be studied using specific GPVI-inhibitory tools.

Conclusion

The present data revealed typical differences in the preparations of collagens or collagen peptides if used in suspension with platelets or when immobilized as microspots and subjected to whole-blood flow (Figure 7). Especially for the "weaker" fibrillar collagens, immobilization appeared to enhance the signaling capability of GPVI, thus stimulating Syk-dependent platelet activation processes in thrombus formation. Apart from changes in the (immobilized) collagen structure, other factors that may have contributed to enhanced signaling capacity were the shear-dependent interaction of GPIb-V-IX with collagen-bound VWF and the priming of platelet activation via integrin α2β1. These, and perhaps also other receptor interactions with collagen fibers, may have ensured increased activation of the GPVI-PLCγ2-Ca^{2+} pathway.
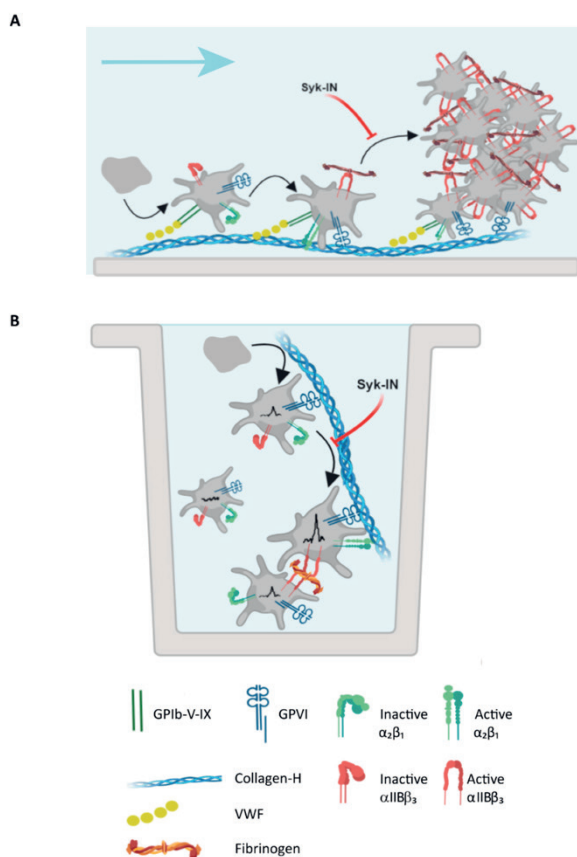
Figure 7. Schematic platelet adhesion and activation by collagen under flow or in suspension. (**A**) Under flow conditions, immobilized collagen-H interacted with VWF to capture platelets via GPIb-V-IX and activate platelets via GPVI and integrin α2β1. Thrombi built up through the recruitment of flowing platelets interacting with collagen/VWF-adhered platelets. Syk inhibition suppressed initial platelet activation and platelet aggregate formation. (**B**) Collagen-H added to a suspension of platelets transiently interacted with GPVI, resulting in Syk-dependent Ca^{2+} rises. Autocrine agonists stimulated non-adhered platelets, responding through Syk-independent signals.

Author contributions

Conceptualization, JWMH, PEJvdM, and MJEK. Methodology, NJJ, IDS, IP, and DIF. Formal analysis, NJJ, IDS, IP DIF, SLB, and RC. Investigation, NJJ, IDS, IP, and DIF. Resources, RWF and JWMH. Data curation, NJJ. Writing - original draft preparation, NJJ, IDS, IP, and DIF. Writing - review and editing, JWMH, RWF. Visualization, NJJ, IDS, IP, and DIF. Supervision, JWMH, YMCH, PEJvdM, MJEK and HtC. Funding acquisition, JWMH, PEJvdM, MJEK, and HtC.

Funding

Acknowledgments

Conflicts of interest

JWMH is a cofounder and shareholder of FlowChamber. The other authors declare no relevant conflicts of interest.

References

1. Versteeg HH, Heemskerk JW, Levi M, Reitsma PS. New fundamentals in hemostasis. *Physiol Rev.* 2013;93:327-358.
2. Van der Meijden PE, Heemskerk JW. Platelet biology and functions: new concepts and future clinical perspectives *Nat Rev Cardiol.* 2019;16:166-179.
3. Savage B, Almus-Jacobs F, Ruggeri ZM. Specific synergy of multiple substrate-receptor interactions in platelet thrombus formation under flow. *Cell.* 1998;94:657-666.
4. Atkinson BT, Jarvis GE, Watson SP. Activation of GPVI by collagen is regulated by α2β1 and secondary mediators. *J Thromb Haemost.* 2003;1:1278-1287.
5. Auger JM, Kuijpers MJ, Senis YA, Watson SP, Heemskerk JW. Adhesion of human and mouse platelets to collagen under shear: a unifying model. *FASEB J.* 2005;19:825-827.
6. Kehrel B, Wierwille S, Clemetson KJ, et al. Glycoprotein VI is a major collagen receptor for platelet activation: it recognizes the platelet-activating quaternary structure of collagen, whereas CD36, glycoprotein IIb/IIIa, and von Willebrand factor do not. *Blood.* 1998;91:491-499.
7. Nieswandt B, Watson SP. Platelet-collagen interaction: is GPVI the central receptor? *Blood.* 2003;102:449-461.
8. Baaten CC, Meacham S, de Witt SM, et al. A synthesis approach of mouse studies to identify genes and proteins in arterial thrombosis and bleeding. *Blood.* 2018;132:e35-46.
9. De Witt SM, Swieringa F, Cavill R, et al. Identification of platelet function defects by multi-parameter assessment of thrombus formation. *Nat Commun.* 2014;5:4257.
10. Pugh N, Simpson AM, Smethurst PA, de Groot PG, Raynal N, Farndale RW. Synergism between platelet collagen receptors defined using receptor-specific collagen-mimetic peptide substrate in flowing blood. *Blood.* 2010;115:5069-5079.
11. Siljander PR, Munnix IC, Smethurst PA, et al. Platelet receptor interplay regulates collagen-induced thrombus formation in flowing human blood. *Blood.* 2004;103:1333-1341.
12. Munnix IC, Kuijpers MJ, Auger JM, et al. Segregation of platelet aggregatory and procoagulant microdomains in thrombus formation. Regulation by transient integrin activation. *Arterioscler Thromb Vasc Biol.* 2007;27:2484-2490.
13. Fuchs B, de Witt S, Solecka BA, et al. Distinct role of von Willebrand factor triplet bands in glycoprotein Ib-dependent platelet adhesion and thrombus formation under flow. *Semin Thromb Hemost.* 2013;39:306-314.
14. Knight CG, Morton LF, Onley DJ, et al. Collagen-platelet interaction: Gly-Pro-Hyp is uniquely specific for platelet GPVI and mediates platelet activation by collagen. *Cardiovasc Res.* 1999;41:450-457.
15. Smethurst PA, Onley DJ, Jarvis GE, et al. Structural basis for the platelet-collagen interaction. The smallest motif within collagen that recognizes and activates platelet glycoprotein VI contains to glycine-proline-hydroxyproline triplets. *J Biol Chem.* 2007;282:1296-1304.

16.   Munnix IC, Gilio K, Siljander PR, et al. Collagen-mimetic peptides mediate flow-dependent thrombus formation by high- or low-affinity binding of integrin α2β1 and glycoprotein VI. *J Thromb Haemost.* 2008;6(12):2132-2142.

17.   Siljander PR, Hamaia S, Peachey AR, et al. Integrin activation state determines selectivity for novel recognition sites in fibrillar collagens. *J Biol Chem.* 2004;279:47763-47772.

18.   Ichinohe T, Takayama H, Ezumi Y, et al. Collagen-stimulated activation of Syk but not c-Src is severely compromised in human platelets lacking membrane glycoprotein VI. *J Biol Chem.* 1997;272:63-68.

19.   Melford SK, Turner M, Briddon SJ, Tybulewicz VL, Watson PS. Syk and Fyn are required by mouse megakaryocytes for the rise in intracellular calcium induced by a collagen-related peptide. *J Biol Chem.* 1997;272:27539-27542.

20.   Watson SP, Herbert JMJ, Pollitt AY. GPVI and CLEC-2 in hemostasis and vascular integrity. *J Thromb Haemost.* 2010;8:1457-1467.

21.   Badolia R, Kostyak JC, Dangelmaier C, Kunapuli SP. Syk activity is dispensable for platelet GPIb-IX-V signaling. *Int J Mol Sci.* 2017;18:1238.

22.   Yanaga F, Poole A, Asselin J, et al. Syk interacts with tyrosine-phosphorylated proteins in human platelets activated by collagen and cross-linking of the FcγIIA receptor. *Biochem J.* 1995;311:471-478.

23.   Munnix IC, Strehl A, Kuijpers MJ, et al. The glycoprotein VI-phospholipase Cγ2 signaling pathway controls thrombus formation induced by collagen and tissue factor in vitro and in vivo. *Arterioscler Thromb Vasc Biol.* 2005;25:2673-2678.

24.   Rayes J, Watson SP, Nieswandt B. Functional significance of the platelet immune receptors GPVI and CLEC-2. *J Clin Invest.* 2019;129:12-23.

25.   Reilly MP, Sinha U, André P, et al. PRT-060318, a novel Syk inhibitor, prevents heparin-induced thrombocytopenia and thrombosis in a transgenic mouse model. *Blood.* 2011;117:2241-2246.

26.   Ishikawa C, Senba M, Mori N. Anti-adult T-cell leukemia/lymphoma activity of cerdulatinib, a dual SYK/JAK kinase inhibitor. *Int J Oncol.* 2018;53:1681-1690.

27.   Knight CG, Morton LF, Onley DJ, et al. Identification in collagen type I of an integrin alpha2 beta1-binding site containing an essential GER sequence. *J Biol Chem.* 1998;273:33287-33294.

28.   Smethurst PA, Joutsi-Korhonen L, O'Connor MN, et al. Identification of the primary collagen-binding surface on human glycoprotein VI by site-directed mutagenesis and by a blocking phage antibody. *Blood.* 2004;103:903-911.

29.   De Witt S, Swieringa F, Cosemans JM, Heemkerk JW. Thrombus formation on microspotted arrays of thrombogenic surfaces. *Nat Protocol Exchange.* 2014;2014:3309#.

30.   Siljander P, Lassila R. Studies of adhesion-dependent platelet activation: distinct roles for different participating receptors can be dissociated by proteolysis of collagen. *Arterioscler Thromb Vasc Biol.* 1999;19:3033-3043.

31.   Gilio K, Harper MT, Cosemans JM, et al. Functional divergence of platelet protein kinase C (PKC) isoforms in thrombus formation on collagen. *J Biol Chem.* 2010;285:23410-23419.

32.   Van Geffen JP, Brouns S, Batista J, et al. High-throughput elucidation of thrombus formation reveals sources of platelet function variability. *Haematologica.* 2019;104:1256-1267.

33.   Feijge MA, van Pampus EC, Lacabaratz-Porret C, et al. Inter-individual variability in Ca^{2+} signalling in platelets from healthy volunteers, relation with expression of endomembrane Ca^{2+}-ATPases. *Br J Haematol.* 1998;102:850-859.

34.   Grynkiewicz G, Poenie M, Tsien RY. A new generation of Ca^{2+} indicators with greatly improved fluorescence properties. *J Biol Chem.* 1985;260:3440-3450.

35.   Chin WW. Bootstrap cross-validation indices for PLS path model assessment. *In: Handbook of Partial Least Squares (Eds Vinci, EV, et al)* 2010;Springer, Berlin: pp. 83-92.

3

36. Pollitt AY, Poulter NS, Gitz E, et al. Syk and Src family kinases regulate C-type lectin receptor 2 (CLEC-2)-mediated clustering of podoplanin and platelet adhesion to lymphatic endothelial cells. *J Biol Chem.* 2014;289:35695-35710.

37. Andre P, Morooka T, Sim D, et al. Critical role for Syk in responses to vascular injury. *Blood.* 2011;118:5000-5010.

38. Onselaer MB, Hardy AT, Wilson C, et al. Fibrin and D-dimer bind to monomeric GPVI. *Blood Adv.* 2017;1:1495-1504.

39. Farndale RW, Sixma JJ, Barnes MJ, de Groot PG. The role of collagen in thrombosis and haemostasis. *J Thromb Haemost.* 2004;2:561-573.

40. Jung SM, Takemura Y, Imamura Y, Hayashi T, Adachi E, Moroi M. Collagen-type specificity of glycoprotein VI as a determinant of platelet adhesion. *Platelets.* 2008;19:32-42.

41. Herr AB, Farndale RW. Structural insights into the interactions between platelet receptors and fibrillar collagen. *J Biol Chem.* 2009;284:19781-19785.

42. Jung SM, Moroi M, Soejima K, et al. Constitutive dimerization of glycoprotein VI (GPVI) in resting platelets is essential for binding to collagen and activation in flowing blood. *J Biol Chem.* 2012;287:30000-30013.

43. Poulter NS, Pollitt AY, Owen DM, et al. Clustering of glycoprotein VI (GPVI) dimers upon adhesion to collagen as a mechanism to regulate GPVI signaling in platelets. *J Thromb Haemost.* 2017;15:549-564.

44. Farndale RW, Lisman T, Bihan D, et al. Cell-collagen interactions: the use of peptide Toolkits to investigate collagen-receptor interactions. *Biochem Soc Trans.* 2008;36:241-250.

45. Heemskerk JW, Sakariassen KS, Zwaginga JJ, et al. Collagen surfaces to measure thrombus formation under flow: possibilities for standardization. *J Thromb Haemost.* 2011;9:856-858.

46. Ozaki Y, Suzuki-Inoue K, Inoue O. Novel interactions in platelet biology: CLEC-2/podoplanin and laminin/GPVI. *J Thromb Haemost.* 2009;Suppl. 1:191-194.

47. Mammadova-Bach E, Ollivier V, Loyau S, et al. Platelet glycoprotein VI binds to polymerized fibrin and promotes thrombin generation. *Blood.* 2015;126:683-691.

48. Induruwa I, Moroi M, Bonna A, et al. Platelet collagen receptor glycoprotein VI-dimer recognizes fibrinogen and fibrin through their D-domains, contributing to platelet adhesion and activation during thrombus formation. *J Thromb Haemost.* 2018;16:389-404.

49. Mangin PH, Onselaer MB, Receveur N, et al. Immobilized fibrinogen activates human platelets through glycoprotein VI. *Haematologica.* 2018;103:898-907.

50. Gao J, Zoller KE, Ginsberg MH, Brugge JS, Shattil SJ. Regulation of the pp72syk protein tyrosine kinase by platelet integrin $\alpha IIb\beta 3$. *EMBO J.* 1997;16:6414-6425.

51. Obergfell A, Eto K, Mocsai A, et al. Coordinate interactions of Csk, Src, and Syk kinases with aIIbb3 initiate integrin signaling to the cytoskeleton. *J Cell Biol.* 2002;157:265-275.

52. Van der Meijden PE, Feijge MA, Swieringa F, et al. Key role of integrin $\alpha IIb\beta 3$ signaling to Syk kinase in tissue factor-induced thrombin generation. *Cell Mol Life Sci.* 2012;69:3481-3492.

Supplemental Figures and Tables of Chapter 3
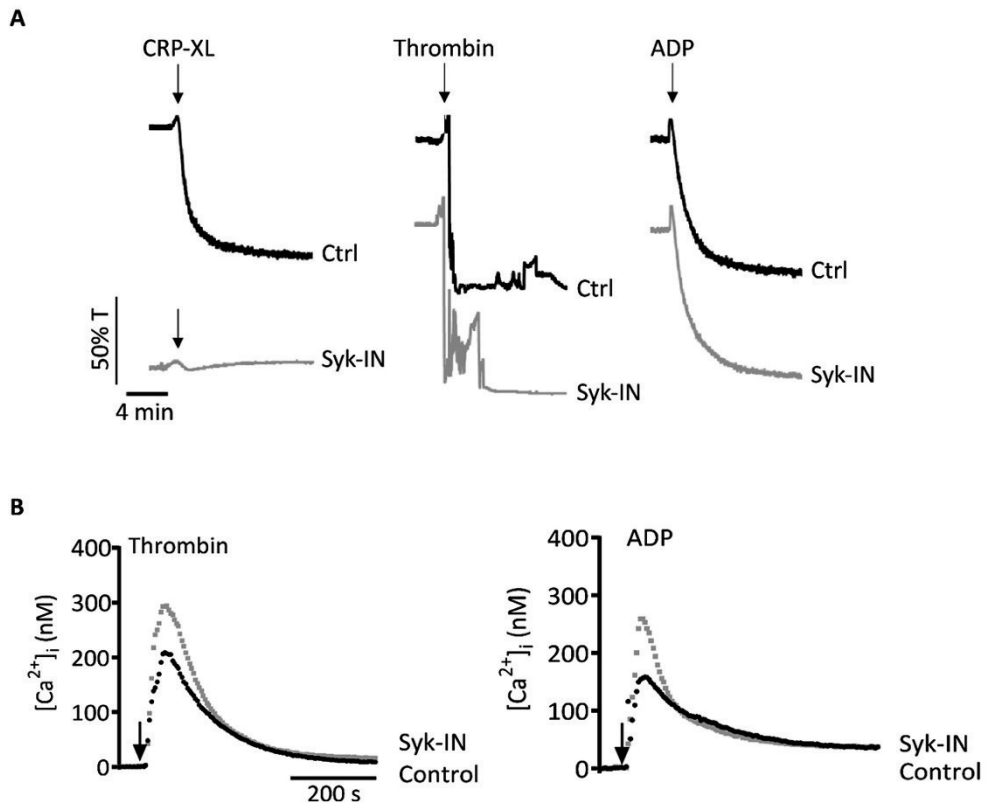
Figure S1. Effect of Syk inhibitor PRT-060318 (Syk-IN) on agonist-induced platelet responses. (**A**) Platelets in plasma (2.5×10^8/mL) were pre-incubated with vehicle (DMSO) or Syk-IN (5 µM) for 10 min, and then activated with CRP-XL (10 µg/mL), thrombin (8 nM) or stable ADP (5 mM), as indicated. Shown are representative traces from light transmission aggregometry. (**B**) Fura-2-loaded platelets in 96-well plates were pre-incubated with Syk-IN (5 µM) or left untreated before injection of thrombin (4 nM) or stable ADP (5 µM), as in Figure 1. Shown are representative traces of changes in $[Ca^{2+}]_i$ of control (black) and Syk-IN (grey) incubations. Arrows indicate the addition of agonists.

Figure S2. Parameters of thrombus formation on immobilized collagen peptides: raw data. Whole-blood was perfused over microspots M1 (GFOGER-GPO + VWF-BP),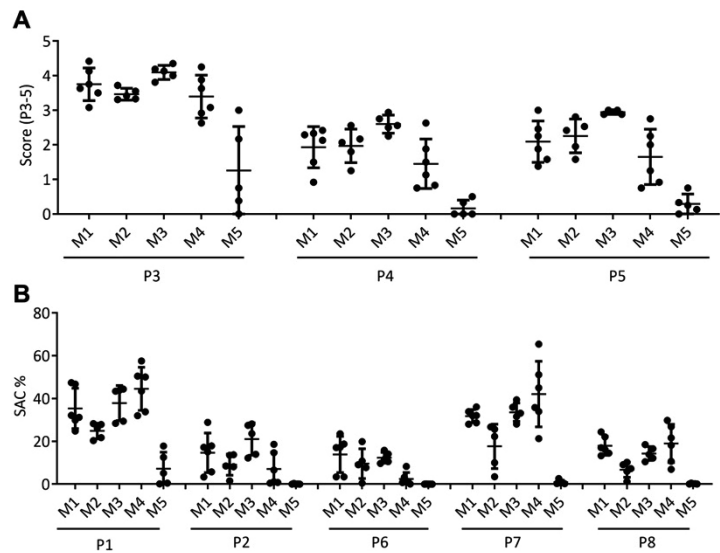 *M2* (CRP-XL + VWF-BP), *M3* (GAOGER- GPO + VWF-BP), *M4* (GFOGER-GPP + VWF-BP), and M5 (VWF-BP). Microscopic images were analyzed for parameters *P1-8*, as in Figure 2. Shown are raw mean outcome values from individual blood donors. (**A**) Parameters providing surface area coverage (SAC%) information: *P1*, platelet deposition; *P2*, platelet aggregate coverage; *P6*, PS exposure; *P7*, CD62P expression; *P8*, fibrinogen binding. (**B**) Score parameters: *P3*, thrombus morphological score (range 0-5); *P4*, thrombus multilayer score (range 0-3); *P5*, thrombus contraction score (range 0-3). Means ± SD (n=5-7 donors).
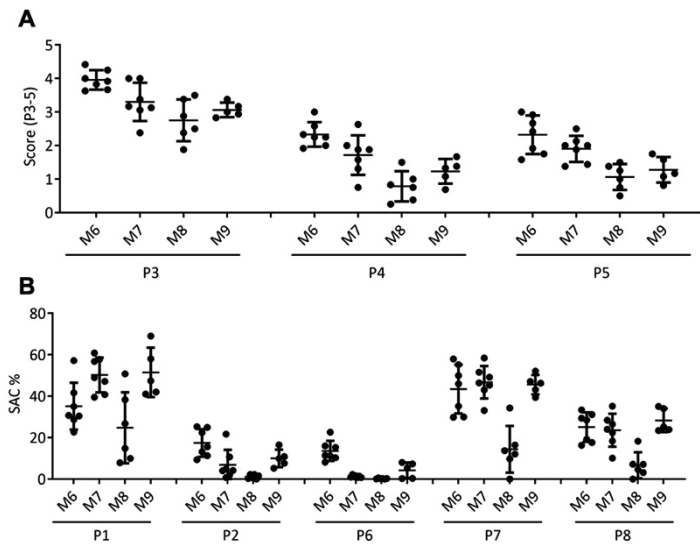
Figure S3. Parameters of thrombus formation on immobilized collagens: raw data. Whole blood was perfused over microspots *M6* (collagen-H), *M7* (fibrillar collagen-I), *M8* (monomeric collagen-I), and *M9* (collagen-III). Microscopic images were captured and analyzed for parameters *P1-8*, as in Figure 5. Shown are raw mean outcome values from individual blood donors. (**A**) Parameters providing surface area coverage (SAC%) information. (**B**) Score parameters. See further Figure S2. Means ± SD (n=5-7 donors).
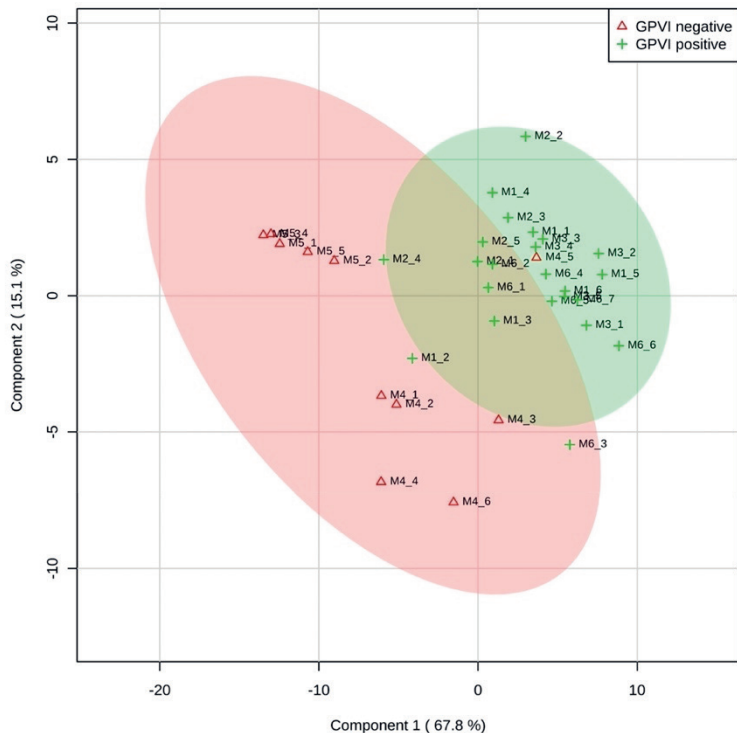
Figure S4. Partial Least Squares with components 1 and 2, indicating the distribution of thrombus formation parameters at microspots *M1-6* for 5-7 individual blood samples per microspot. Note, the clustering (green area) of flow runs over (GPO)$_n$ containing surfaces *M1-3* and *M6*, whereas flow runs with other surfaces *M4* and *M5* out-clustered with more negative contributions to component 2 or 1, respectively (red area). Red triangles indicate an assumed negative GPVI contribution, green plusses indicate a positive contribution.

Table S1. Scale subtracted parameter values of thrombus formation (means), indicating effects of Syk-IN, for microspots *M1-9* and parameters *P1-8*.

	P1	*P2*	*P3*	*P4*	*P5*	*P6*	*P7*	*P8*
M1	1.18±0.46	0.10±0.14	0.51±0.17	0.15±0.16	0.21±0.20	0.03±0.05	0.71±0.49	0.62±0.66
M2	1.15±0.24	0.16±0.13	0.77±0.15	0.30±0.20	0.30±0.15	0.04±0.06	0.69±0.39	0.31±0.28
M3	0.94±0.24	0.10±0.07	0.71±0.17	0.37±0.23	0.34±0.12	0.01±0.00	0.47±0.27	0.11±0.08
M4	0.93±0.29	0.17±0.29	0.73±0.09	0.34±0.34	0.37±0.40	0.13±0.16	0.25±0.18	0.04±0.03
M5	0.97±1.18	1.27±2.13	0.13±0.12	0.00±0.00	0.00±0.00	0.63±0.79	1.40±2.65	0.36±0.43
M6	1.12±0.33	0.19±0.10	0.61±0.15	0.22±0.17	0.28±0.18	0.02±0.02	0.65±0.35	0.42±0.44
M7	0.88±0.21	0.03±0.06	0.60±0.20	0.10±0.11	0.17±0.12	0.03±0.02	0.13±0.08	0.02±0.02
M8	0.87±0.56	2.91±6.23	0.61±0.35	0.64±0.74	0.42±0.28	0.16±0.15	0.25±0.16	0.12±0.17
M9	0.79±0.20	0.07±0.07	0.49±0.06	0.13±0.23	0.11±0.13	0.03±0.03	0.14±0.12	0.05±0.05

4

Chapter 4

Ultra-high throughput Ca^{2+} assay in platelets to distinguish ITAM-linked or G- protein coupled receptor activation

Fernández DI, Provenzale I*, Cheung HYF*, van Groningen J, Tullemans BME, Veninga, A, Dunster JL, Honarnejad S, van den Hurk H, Kuijpers MJE, Heemskerk JWM

Abstract

Antiplatelet drugs targeting G-protein coupled receptors (GPCR), used for the secondary prevention of arterial thrombosis, coincide with an increased bleeding risk. Targeting ITAM-linked receptors, such as the collagen receptor glycoprotein VI (GPVI), is expected to provide a better antithrombotic-hemostatic profile. Here, we developed and characterized an ultra-high throughput (UHT) method based on intracellular $[Ca^{2+}]_i$ rises to differentiate GPVI and GPCR effects on platelets. In 96-, 384-, or 1536-well formats, Calcium-6-loaded human platelets displayed a slow-prolonged or fast-transient $[Ca^{2+}]_i$ rise when stimulated with the GPVI agonist collagen-related peptide (CRP), or with thrombin and other GPCR agonists, respectively. Semi-automated curve fitting revealed five parameters describing the Ca^{2+} responses. The verification of the UHT assay was done with a robustness compound library and clinically relevant platelet inhibitors. Taken together, these results present proof-of-principle of distinct receptor-type dependent Ca^{2+} signaling curves in platelets, which allow the identification of new inhibitors in a UHT way.

Visual abstract
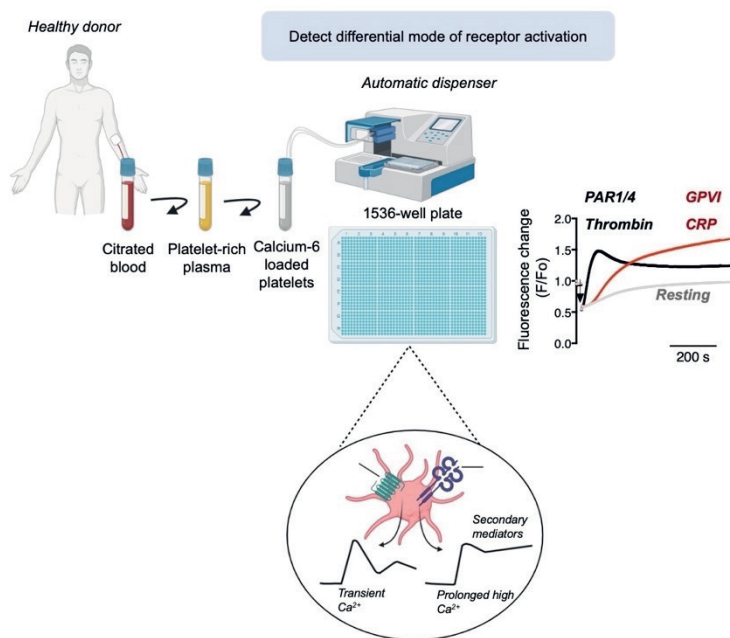
Highlights

- Tools are needed to screen for the anti-thrombotic potential of small molecules.
- Ultra-high throughput assay to discriminate between GPVI and GPCR pathways.
- Calcium signaling as a profiling method to follow real-time platelet activation.
- Platelet calcium assays are highly sensitive to evaluate inhibitory drug effects.

Introduction

Antiplatelet therapy is a frontline antithrombotic strategy in the secondary prevention of arterial thrombosis [1]. All currently used oral anti-platelet drugs target G-protein coupled receptor (GPCR) pathways, such as those evoked by the ADP receptor P2Y$_{12}$ (clopidogrel, ticagrelor, prasugrel) and the prostanoid TP receptor (aspirin, inhibiting formation of the TP receptor's ligand thromboxane A$_2$) [2,3]. However, these drugs, especially in dual therapy, increase the risk of bleeding in a substantial number of patients [4,5]. In development are antagonists of the GPCR activated by thrombin, protease-activated receptor (PAR)1 and 4, but their antithrombotic profile is still unclear [1,5]. This urges for a continued need to discover and develop drugs that target the role of platelets in thrombosis without compromising hemostasis [6].

In addition to GPCR, also the ITAM-linked receptor (ILR) for collagen, glycoprotein (GP)VI, regulates platelet activation [7]. In mice, deficiency of platelet GPVI suppresses arterial thrombosis with limited effect on hemostasis [8,9]. Similarly, in patients with a genetic GPVI defect only a mild bleeding phenotype is observed [10], in contrast to the major bleedings observed in patients with defective ADP receptors [11]. Recent clinical trials with antibody-based or recombinant protein-based drugs to target the GPVI interaction with collagen have provided proof-of-principle evidence for the antithrombotic potential of such ILR-affecting compounds [12,13]. However, because of the immunogenicity of antibody-based drugs, there is continued interest in searching for small molecules with effective drug-like properties [14,15]. To facilitate the search of large libraries of small molecule compounds for antiplatelet effects, methods in ultra-high throughput (UHT) screening format need to be developed that can discriminate between GPCR- and ILR-induced platelet responses.

In platelets, elevated cytosolic free Ca^{2+} concentration [Ca^{2+}]$_i$ acts as a common second messenger in response to both GPCR and ILR agonists. Agonist-induced rises in [Ca^{2+}]$_i$ precede essentially all functional platelet responses, such as cytoskeletal reorganization, platelet adhesion, aggregation, secretion and procoagulant and proinflammatory activity, and clotting [1,16]. A substantial amount of literature has detailed the upstream signaling and downstream effects of [Ca^{2+}]$_i$ rises for platelet functions after stimulation of GPCRs with thrombin and ADP [17-21] and after stimulation of the ILR GPVI [22-24]. In brief, the platelet agonists thrombin, TRAP6, ADP, and thromboxane A$_2$ all stimulate platelets via Gqα and phospholipase Cβ (PLCβ) isoforms, resulting in cytosolic Ca^{2+} mobilization (via inositol triphosphate formation and intracellular Ca^{2+} release from the endoplasmic reticulum) and PKCα/β activation. The agonist CRP for ITAM-linked GPVI acts in a tyrosine-kinase-dependent way, which results in activation of the PLCγ2 isoform and again causes inositol triphosphate-mediated Ca^{2+} mobilization and PKCα/β activation. A common subsequent event is store-operated Ca^{2+} entry [24]. Although it is understood that the GPCR-induced platelet signaling response is of shorter duration than the GPVI-induced response [9,25], this difference has not in detail been examined so far. In the present paper, we hypothesized that detailed analysis of the cytosolic free Ca^{2+} dynamics can help in the

screening for drugs discriminating between platelet GPCR and ILR agonists.

Historically, agonist-induced $[Ca^{2+}]_i$ rises in platelets are measured in cuvette-based assays using the fluorescent ratio dye Fura-2, allowing to record calibrated $[Ca^{2+}]_i$ responses in platelets from healthy subjects or patients [17,26,27]. Single wavelength dyes such as Fluo-4 provide reliable quantitative information on platelet Ca^{2+} responses by pseudo-rationing analysis [28]. For several years, robot instruments such as FlexStation 3 and FLIPR-Tetra are available to enable the simultaneous fluorescence analysis of multiple cell samples in 96-well plates [29]. However, their application for a proper comparison of GPCR- and ILR-induced signaling is still missing.

In the present study, we developed a UHT-based method for platelet $[Ca^{2+}]_i$ rises using the dye Calcium-6, for operation in 384- and 1536-well formats to establish the characteristics of Ca^{2+} signaling, and to evaluate the effects of antiplatelet drugs. To achieve this, we downscaled the platelet sample size to 6 µL, and used robot machines to automatically stimulate dye-loaded platelets with agonists and to read fluorescence changes in multiple wells at a time. We evaluated key GPCR agonists (thrombin, TRAP6, U46619, 2-MeS-ADP); and the ILR agonist, collagen-related peptide (CRP). After establishing time-dependent outcome parameters, we validated these using a robustness compound library and a reference set of clinically relevant antiplatelet agents. Our results provide proof-of-principle evidence that new receptor-type dependent antiplatelet drugs can be identified by this UHT screening.

Materials and methods

Materials availability

This study did not generate new unique reagents.

Data and code availability

All data and code reported in this paper are available and will be shared by the lead contact upon request. This paper does not report original code. Any additional information required to reanalyze the data reported in this paper is available from the lead contact upon request.

Human subjects

Blood was obtained by venipuncture from healthy male and female volunteers who had not received anti-platelet medication for at least two weeks, after full informed consent according to the Helsinki declaration. The study was approved by the Medical Ethics Committee of Maastricht University. According to the approval, blood donor age and sex were not recorded. Blood samples were collected into 3.2% trisodium citrate (Vacuette tubes, Greiner Bio-One, Alphen a/d Rijn, The Netherlands). All subjects had normal platelet counts, as measured with a Sysmex XN-9000 analyzer (Sysmex, Kobe, Japan). Where indicated, platelet concentrates from unknown healthy subjects were obtained from Sanquin (Amsterdam, the Netherlands), after written permission from Sanquin and full informed

consent. A concentrate unit contained >2.5×10^{11} platelets in 300 mL PAS-E solution and 30-35% plasma [30]. Concentrates were obtained two days after blood drawing and were kept at room temperature by gently shaking.

Platelet preparation

Platelet-rich plasma (PRP) was separated from citrated blood by centrifugation at 240 g for 15 min [62]. Alternatively, where indicated, platelet concentrates (pooled from 5 healthy donors of identical ABO and Rh(D) compatible blood types) were used from the Sanquin blood bank. Collected PRP or platelet concentrates were supplemented with 1:10 vol./vol. acid citrate dextrose (ACD; 80 mM trisodium citrate, 183 mM glucose, 52 mM citric acid), and centrifuged at 870 g for 15 min [31]. The platelet pellet was resuspended into HEPES buffer pH 6.6 (10 mM HEPES, 136 mM NaCl, 2.7 mM KCl, 2 mM MgCl$_2$, 5.5 mM glucose, and 0.1% bovine serum albumin). After the addition of apyrase (1 U/mL) and ACD (1:15 vol./vol.), another centrifugation step was performed to obtain washed platelets [32]. Platelet pellets were resuspended into HEPES buffer pH 7.45 at desired platelet concentration (10 mM HEPES, 126 mM NaCl, 2.7 mM KCl, 2 mM MgCl$_2$, 5.5 mM glucose, and 0.1 % bovine serum albumin) [31].

Cytosolic Ca^{2+} measurements with Fura-2

Washed platelets (200 $\times$ 10^9/L) were loaded with Fura-2-AM (3 µM) with Pluronic (0.4 µg/mL) for 40 min at room temperature. After another wash step and resuspension of the platelets at 200 $\times$ 10^9/L, changes in [Ca^{2+}]$_i$ were measured in the presence of 1 mM CaCl$_2$ in 96-well plates using a FlexStation 3 (Molecular Devices) at 37 °C during 10 min [33]. In brief, 200 µL of Fura-2-loaded cells were stimulated by automated pipetting with 20 µL of indicated agonist solution. Mixing of agonist with cells was thus provided by high-speed injection of 10% volume of the agonist solution. Prior to default use, injection volume, and speed were optimized to obtain the highest platelet responses. Ratiometric changes in Fura-2 fluorescence were measured over time at dual excitation wavelengths of 340 and 380 nm, and emission wavelength of 510 nm. For nanomolar calibration of ratio values to [Ca^{2+}]$_i$, Fura-2-loaded platelets in separate wells were lysed by 0.1% Triton-X-100 in the presence of either 1 mM CaCl$_2$ or 9 mM EGTA/Tris. The same method and machine, but at single wavelength excitation at 488 nm and no calibration, was used to measure fluorescence changes in Calcium-6 loaded platelets in 96-well plates.

Cytosolic Ca^{2+} measurements at UHT with Calcium-6

For UHT 384- or 1536-well plate formats, freshly obtained, washed platelets (400 $\times$ 10^9/L) were incubated at 1:1 vol./vol. with Calcium-6 dye solution for 2 h at room temperature, according to the manufacturer's instructions. After another wash, the loaded platelets in buffer containing 1 mM CaCl$_2$ were resuspended at 200-400 $\times$ 10^9 platelets/L and distributed over 384-well or 1536-well plates. Dispersion of the platelet suspension over the 384-well plates was using a multi-pipette; dispersion over the 1536-well plates was with a Certus

device (Gyger AG, Gwatt, Switzerland). In each setting, a camera-equipped FLIPR-Tetra machine (Molecular Devices) was used to measure fluorescence increases, representing rises in $[Ca^{2+}]_i$, in all wells simultaneously [34]. In the 384-well format, 50 µL of dye-loaded platelets (200×10^9/L) per well were injection pipetted with 5 µL agonist or vehicle solution. In the 1536-well format, 6 µL of dye-loaded platelets (400×10^9/L) per well were injection pipetted with 2 µL of agonist or vehicle solution. As a default procedure for this machine, mixing the platelets with the agonist was achieved by high-speed injection of a relatively large volume of agonist solution. In a pilot test, injection speed and volume were optimized per well-plate format to obtain the highest and most reproducible platelet responses. Using a suitable optical filter set, the increases in Calcium-6 fluorescence were continuously measured at excitation and emission wavelengths of 485 nm and 525 nm, respectively (room temperature). All conditions were repeated in duplicate to quadruplicate wells (16 wells for Z' assessment). Off-line, the time traces per well were semi-ratioed in comparison to the baseline fluorescence (F/F_o) of the agonist medium-diluted signal [28]. Of note, the injection mixing in UHT assays can result in a diffusion-limited delay in response in comparison to stirred measurements, but the high curve reproducibility compensates for the fastest kinetics.

Quantification and analysis of UHT platelet assay

Raw traces of changes in $[Ca^{2+}]_i$ in Calcium-6 loaded platelets were used to determine the initial slope of the increase, maximal fluorescence signal increase (maximum - minimum), and area under the curve (over 5-10 min). For each of these parameters, the assay's suitability was determined from the statistical effect size as Z' factor. This coefficient integrates the signal dynamic range and the test variation associated with the measured signal [35]. An assay's Z' factor is considered to be excellent with a large dynamic range and small data variability when $1 > Z' \geq 0.5$. Assays with $Z' < 0$ are not useful for screening. The equation is as follows:

$$Z' = 1 - \frac{3(\theta p + \theta n)}{|\mu p - \mu n|}$$

Herein, θ is the standard deviation; μ is the average signal value; p is a positive, minimum signal (resting platelets); and n is a negative, maximum signal (stimulated platelets).

For the modeling of $[Ca^{2+}]_i$, traces were separated into early and late slopes (rates of change, RoC). Traces of F/F_0 over time were regressed to a smoothed curve (using a locally weighted regression algorithm (loess, span = 0.1 and degree = 1, implemented in R version 3.2.5). Early RoC was determined as the maximum differential between 50-200 s; late RoC as the mean change over 200-450 s.

Use of robustness set compound library

A 263 chemical compound library for assessment of assay liabilities and suitability of UHT assays for screening of small molecules was composed by Pivot Park Screening Center (Oss, The Netherlands) [36]. For use of this robustness set, 4 µL of dye-loaded platelets (400×10^9/L), obtained from platelet concentrates, in 1536-well format were pre-incubated by automated

pipetting with 2 µL of each compound (10 µM, f.c.) or vehicle in selected wells, and after 5 min stimulated with either CRP or thrombin, as described above.

Effect percentages per compound and agonist were calculated from the mean traces of replicate wells. Three curve parameters (slope of initial increase, maximum - minimum signal, and area under the curve) were always obtained, and each parameter was used to calculate a so-called Z-score. The Z-score or standard score represents the number of standard deviations above or below the mean [37]. Compounds were named 'active' (*i.e.* assay interfering) when they surpassed a Z-score threshold of > 4 or <-4, in agreement with earlier UHT protocol standards [36].

Light transmission aggregometry and flow cytometry

For comparative measurements of platelet functions and $[Ca^{2+}]_i$ rises, aggregation of platelets in platelet-rich plasma or wash platelets was determined by light transmission aggregometry. In brief, washed platelets or PRP (250×10^9 platelets/L) were pre-incubated with indomethacin (10 µM) or DMSO (vehicle) for 10 min at 37 ºC. Maximal aggregation was induced by CRP (1 µg/mL) or thrombin (1 nM) while stirring at 1200 rpm at 37 ºC. Platelet aggregation was monitored using a Chronolog optical aggregometer (Havertown, PA, USA). The maximal amplitude was quantified at 10 min after the addition of the agonist. In other platelet subsamples, washed platelets (100×10^9/L) were stimulated for 15 min with CRP (1 µg/mL), thrombin (1 nM), or left unstimulated, in the presence of 1 mM $CaCl_2$. After stimulation, platelets were stained for Alexa Fluor-647 anti-CD62P mAb (2.5 µg/mL) and fluorescein isothiocyanate (FITC)-PAC1 mAb (1.25 µg/mL) to measure a-granule secretion and integrin αIIβb3 activation, respectively. Measurements were in duplicates with an Accuri C6 flow cytometer (10,000 events) and data were analyzed with FlowJo software.

Quantification and statistical analysis

Data were expressed as means ± SEM. GraphPad Prism 8 (San Diego, CA, USA) was used for the statistical analyses. Data normality was verified using a Shapiro-Wilk test, after which a one-tailed Student's t-test or non-parametric Mann-Whitney test was used. For more than one group comparison, a one-way repeated ANOVA test was used. Statistical significance was defined as $p<0.05$. Data sets were compared using Pearson or Spearman correlation analysis. The software R version 3.2.5 was used to calculate rates of changes, correlation analyses, and for heatmap visualization. Statistical details per experiment are indicated in the figure legends.

Results

High throughput assessment of [Ca²⁺]ᵢ rises in CRP- and thrombin-stimulated platelets with Calcium-6

For comparison with a UHT assay of agonist-induced Ca^{2+} responses, washed human platelets were first loaded with the ratiometric dye Fura-2, thus allowing measurement of calibrated nanomolar changes in $[Ca^{2+}]_i$ [38,39]. These Fura-2-loaded platelets were then screened for agonist-induced responses in 96-well plate format (200 µL of 200 × 10⁹ platelets/L) using a FlexStation 3 robot, which allowed the simultaneous measurement of one column at a time. The agonists were added by high-speed injection in order to obtain reproducible and highest responses. This resulted in relatively rapid and partially transient $[Ca^{2+}]_i$ traces in response to the GPCR agonist thrombin, but in slower and more persistently high $[Ca^{2+}]_i$ traces with the ILR agonist CRP (Figure 1A-C), which is in agreement with earlier results using dye-loaded platelets in 96-well plates [29,33]. A limitation of Fura-2 is its high sensitivity to light-absorbing compounds below 480 nm.

To overcome this limitation, we determined again in a 96-well format the high wavelength dye Calcium-6, also loaded as acetoxymethyl ester with low leakage rate after de-esterification, and commonly used in high-throughput assays with other cell types [40]. Platelet suspensions loaded with Calcium-6 again showed a fast and transient Ca^{2+} response upon injection with thrombin and a slow-onset prolonged bi-phasic Ca^{2+} response upon injection with CRP (Figure 1D-F). Pseudo-rationing was applied to obtain F/F_0 time curves, representing the relative increases in $[Ca^{2+}]_i$ [28]. The higher K_d (330 nM) of Calcium-6 for Ca^{2+} in comparison to Fura-2 (224 nM) may be responsible for the small differences in response curves between probes. The clearly distinct shapes obtained with thrombin and CRP motivated us to further explore the use of Calcium-6 as an intracellular Ca^{2+} dye.

Next, we established dose-response curves by taking the maximal calibrated or pseudo-ratioed $[Ca^{2+}]_i$ increases over 10 min as an output parameter. For Fura-2 and Calcium-6, EC_{50} concentrations were highly similar for both agonists, *i.e.* 2-3 µg/mL for CRP (Figure 1B, E) and 1-1.5 nM for thrombin (Figure 1C, F). This was confirmed by dose-response analyses based on the curve slope or the area-under-the-curve parameters (data not shown). Thus, we concluded that Calcium-6 adequately monitored the distinct Ca^{2+} responses of platelets dispersed over 96-well plates.

Suitability of 384-well plate format for measuring agonist-induced [Ca²⁺]ᵢ rises

To achieve higher throughput, we downscaled the test volume to 50 µL per well of Calcium-6-loaded platelets using 384-well plates. A camera-based FLIPR-Tetra robot was used, which allowed quantification of the fluorescence changes from all wells at the same time. The platelet count was kept at 200 × 10⁹/L as a compromise between sufficient fluorescent signal intensity and the availability of cells. In the 384-well format and quadruplicate wells, we compared the Ca^{2+} responses to commonly used GPCR agonists, *i.e.* thrombin (activating PAR1/4), TRAP6 (for PAR1), 2-MeS-ADP (for P2Y₁ receptor) and U46619 (for TP

receptor). Agonist addition again was by optimized high-speed injection with the robot. Markedly, all GPCR agonists showed faster and more transient $[Ca^{2+}]_i$ rises when compared to the slower-onset and prolonged $[Ca^{2+}]_i$ rises obtained with CRP (Figure 2A-E). As expected, the Ca^{2+} signals of weak agonists, 2-MeS-ADP and U46619 (Figure 2D, E), were lower and shorter in duration than those with more potent PAR agonists. To further characterize the differences between GPCR and ILR (CRP) mediated Ca^{2+} responses, in the same 384-well format we investigated the effect of the Syk tyrosine kinase inhibitor PRT060318. Markedly, this compound increased the Ca^{2+} responses with all four GPCR agonists, but completely annulled the Ca^{2+} response with CRP (Figure S1). Additional control experiments indicated that: *(i)* the CRP-induced Ca^{2+} signal was completely dependent on tyrosine kinase signaling (Figure S2A), *(ii)* the thrombin-induced Ca^{2+} signal was fully blocked by treatment with the catalytic site thrombin inhibitor, PPACK (Figure S2B), and *(iii)* the addition of 1 mM extracellular $CaCl_2$ to the dye-loaded platelets in wells was sufficient to reach a plateau level of intracellular Ca^{2+} signals with both CRP and thrombin (Figure S2C, D). The dosing effects of the two agonists were similar to those in 96-well plates (see Figure 1).
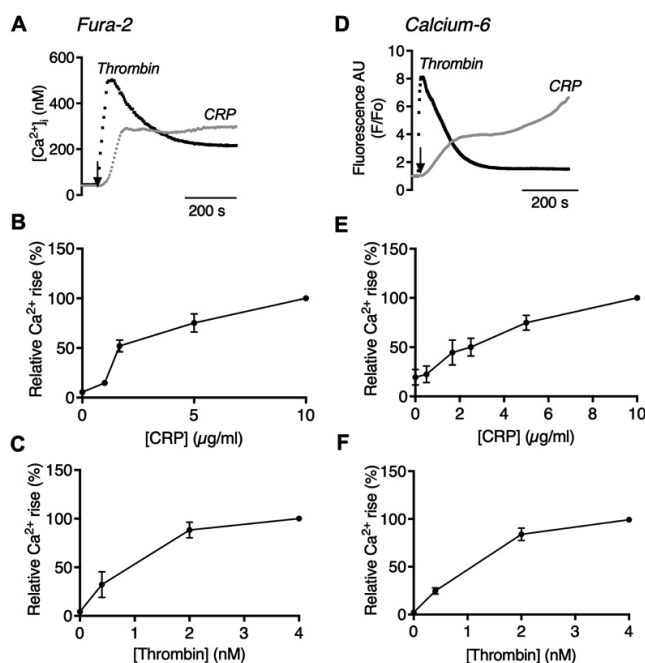

Figure 1. Comparison of agonist-induced $[Ca^{2+}]_i$ rises of platelets loaded with Fura-2 or Calcium-6 in 96-well format.
Washed human platelets (200×10^9/L) were loaded with Fura-2 (**A-C**) or Calcium-6 (**D-F**). Aliquots in 96-well plates were evaluated for changes in fluorescence upon stimulation with maximally effective CRP (10 μg/mL) or thrombin (4 nM) by automated pipetting in a FlexStation 3 robot. (**A**) Calibrated nanomolar rises in $[Ca^{2+}]_i$ with Fura-2 by 340/380 nm ratio fluorometry. (**D**) Pseudo-ratioed F/F_o rises with Calcium-6 obtained by single wavelength recording. Shown are representative traces. (**B, D**) Dose-response curves of $[Ca^{2+}]_i$ rise with CRP (0.5-10 μg/mL), expressed as % of the maximal increase. (**C, F**) Dose-response curves of $[Ca^{2+}]_i$ rise with thrombin (0.4-4 nM), expressed as % of the maximal increase. Means ± SEM, n=3-6 donors.
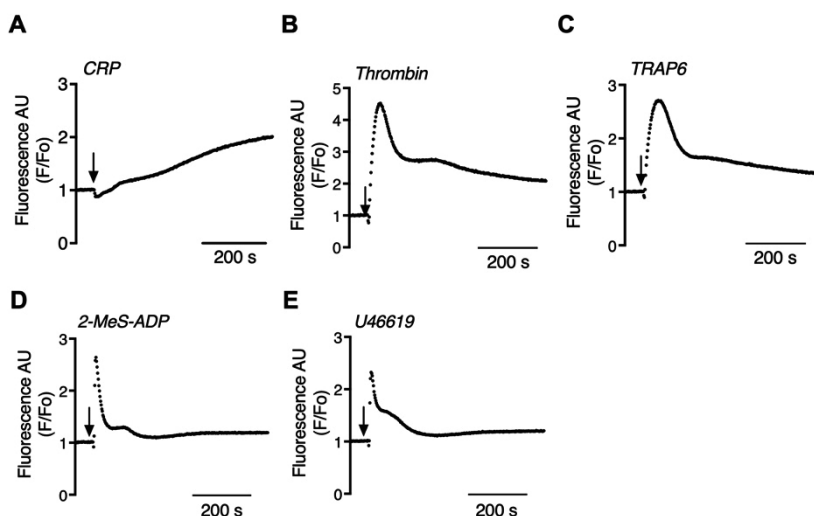
Figure 2. Rises in $[Ca^{2+}]_i$ in Calcium-6 loaded platelets by a range of agonists in 384-well format. Calcium-6-loaded platelets (200×10^9/L) were injection-stimulated with physiologically relevant receptor agonists CRP 10 μg/mL (**A**), thrombin 4 nM (**B**), TRAP6 10 μM (**C**), Me-S-ADP 10 μM (**D**), or U46619 10 μM (**E**) in 384-well plates. Arrows indicate the addition of agonists. Pseudo-ratioed rises in F/F_o were measured using a FLIPR-Tetra robot over 600 s. Representative traces of at least 3 experiments.

UHT assay miniaturization to 1536-well plates and quality analysis

Aiming to further downscale the assay, we moved to a 1536-well format, which was possible by using the FLIPR-Tetra machine. Per well, 6 μL of Calcium-6-loaded platelets (concentration doubled to 400×10^9/L) were used, and a minimal volume of 2 μL of agonist solution was injection pipetted for achieving maximal responses. For analysis again pseudo-rationing was applied, which in this case resulted in a sudden drop in fluorescence intensity due to the 33% dilution with agonist. A direct comparison of the overall assays' performances in 384- and 1536-well formats is shown in Figure 3. Notably, in the 1536-well format, the different fluorescence kinetics in response to thrombin (fast-transient) and CRP (slow-persistent) were well maintained. The use of relatively high concentrations of platelets showed a small gradual increase in fluorescence over 10 min in resting platelets, which was ascribed to dye leakage. Single-donor comparison of Calcium-6 loaded platelet responses in 384- and 1536-well plates showed the same typical shape differences in responses to thrombin and CRP (Figure S3). For the same batch of platelets, it was also confirmed by flow cytometry that CRP and thrombin addition caused functional responses such as integrin αIIbβ3 activation (PAC1 mAb binding) and granular secretion (P-selectin expression) (Figure S4).

For a detailed analysis of the pseudo-ratioed F/F_o $[Ca^{2+}]_i$ traces, we examined three parameters: *(i)* maximal curve slope after agonist addition, *(ii)* maximal fluorescence increase over time (maximum - minimum), and *(iii)* area under the curve (AUC), the latter as an approximation of the net integrated $[Ca^{2+}]_i$ rise over 10 min. Quantification showed

that curve slopes were 16- and 9-fold higher with thrombin than with CRP, when measured in 384-well (Figure 3A-B) or 1536-well plates (Figure 3E-F), respectively. The ratio of AUCs for thrombin *vs.* CRP was 2.3 and 1.2 for 384- and 1536-well formats (Figure 3C, G); and the maximal $[Ca^{2+}]_i$ rises with thrombin were 2.5- and 1.4-fold higher than with CRP in 384- or 1536-well plates, respectively (Figure 3D, H).

In order to further dissect the different shapes of the curves, we fitted these by obtaining smoothed, average-weighted curves. We then determined the rate of change (RoC) after agonist addition. We furthermore separated the biphasic curves into two parts, resulting in an early RoC (over 50-200 s) and a late RoC (over 200-450 s). The late RoC was considered as a best estimate of the later second-phase $[Ca^{2+}]_i$ response. When comparing the 384- and 1536-well formats, the early RoC was invariably higher with thrombin than with CRP, in agreement with the observed fast onset (Figure 4A, D). The late RoC was similar in size with thrombin and CRP in either well-plate format (Figure 4B, E).

Comparing the effects of CRP and thrombin, we observed that slope and early RoC significantly differed in 384- and 1536-well plates ($p<0.01$), while the other parameters were significantly different for CRP and thrombin only in 384-well plates ($p<0.05$). Accordingly, the slope was the parameter that most consistently discriminated between the two agonists. A regression analysis of all curve parameters obtained with platelets from all investigated donors indicated positive correlations with low p values ($p<0.05$) for maximal signal, slope, area under the curve, and early/late RoC in case of CRP or thrombin, regardless of the type of well plate (Figure 4C, F). However, this correlation was absent between both agonists in 384-well plates agonists. In 1536-well plates, negative correlations were observed between the agonists, because the agonist-specific effects of early and late rises operating at different parts of the curves were more prominent in the 1536-well format. This confirmed the different trace characteristics between both agonists.

To evaluate the overall measurement performance per type of well plate, we calculated the Z' factor, as a combined measure of the signal dynamic range and the intra-test variation [34]. In 384 wells, the Z' factors for the maximal signal were within the range of excellence ($1 > Z' \geq 0.5$), *i.e.* 0.63 ± 0.03 for CRP and 0.71 ± 0.06 for thrombin (means ± SEM, n=6). For the Calcium-6 loaded platelets in 1536-wells, Z' factors were slightly lower, *i.e.* 0.39 ± 0.13 for CRP and 0.37 ± 0.14 for thrombin (means ± SEM, n=3). For the 1536-well format, this pointed to a somewhat higher, but still acceptable curve variation between wells.

Robustness assessment of UHT measurement

The success of a UHT campaign relies on effective hit-triaging evaluation. It is important to check for a method's liabilities to detect undesired properties of chemical compounds with assay-interfering properties [36]. Pivot Park Screening Centre has created a proprietary robustness set compound collection for the evaluation of a wide variety of UHT assays [36]. The collection comprises 263 DMSO-soluble compounds with well-documented

interference in different types of tests. The compounds were classified as: aggregator, metal ion chelator, fluorescent, luciferase quenching, chemically reactive, metals, colored or visible light absorbing, redox active, and salt compounds. The set further contained clean compounds, which are chemically diverse lead-like compounds without known assay-interfering properties. In order to evaluate the liability of the UHT platelet Ca^{2+} assay, we determined the effects of these 263 compounds in 4 quadruplicate wells per compound, spread over the 1536-well plate.

For this purpose, platelets from concentrates were loaded with Calcium-6 loaded for CRP- and thrombin-induced $[Ca^{2+}]_i$ rise measurements. Effects of the agonists on functional platelet responses were confirmed by flow cytometry (not shown). For all 263 investigated compounds, effect values in quadruplicate were obtained of the three curve parameters (maximal increase, initial slope, area-under-the-curve) upon stimulation with thrombin or CRP. For the mean effects of these three parameters, the Z-score was calculated (number of standard deviations), in order to identify actively interfering compounds. Presentation of the data as a univariate scaled heatmap showed that the majority of compounds were without relevant effect, *i.e.* with |Z| < 4 (Figure 5A). Regression analysis using all compound-modified curves showed again high positive correlations between the various parameters per agonist, but not between agonists (Figure 5B).

Evaluating the Z-scores for all 263 compounds per class indicated some differences between CRP- and thrombin-induced $[Ca^{2+}]_i$ curves. For the majority of compound classes, interference in terms of Z-scores was lower in CRP- than in thrombin-stimulated conditions (Figure S5). Restricting the set to active compounds (compounds with |Z| > 4) indicated that, for CRP, some luciferase compounds were assay interfering (7% active compounds) as well as an aggregator compound (2%). For thrombin, on average 12% of active compounds per class were interfering (Figure 5C). Classes with the highest interfering rates were chelators (12.5%), luciferase quenching (20%), metals (21%), and colored (16%). Furthermore, the data pointed to a lower predicted hit rate for CRP (1%), based on the percentage of actives in the clean class, than for thrombin (12 %). Overall, the CRP-induced Ca^{2+} signal was less liable, as only some aggregator and luciferase compounds interfered with the assay in comparison to the thrombin assay with more compound classes interfering. The protein identity of thrombin as a large 37.4 kDa protease, sensitive to catalytic or regulatory site inactivation by chemical compounds, can explain its higher sensitivity to inhibition. Overall, this screening analysis pointed to an overall high liability of the Calcium-6 platelet UHT measurement, taking into account the intrinsic method's limitations: *(i)* interference of compounds with high absorbance at >480 nm (excitation wavelength of Calcium-6), and *(ii)* compounds affecting the agonist activity. Accordingly, using an appropriate hit triage cascade, a UHT-based screening procedure for novel antiplatelet drugs has now become possible.

Effects of specific antiplatelet drugs in UHT assay

To further confirm the usefulness and strength of the 384- and 1536-well plate

measurements, we compared the effects of established antiplatelet drugs with proven antiaggregatory effects on platelets in clinically relevant conditions (Table 1). The examined drugs were next to the tyrosine kinase Syk inhibitor PRT060318, the cyclooxygenase/thromboxane synthase inhibitor indomethacin (equivalent to aspirin), and the reversibly blocking P2Y$_{12}$ receptor antagonist ticagrelor. Indomethacin and ticagrelor interfere with platelet activation responses via GPCRs and effectively block the effects on platelets of autocrine-produced thromboxane A$_2$ and ADP via P2Y$_{12}$ signaling respectively. The drugs were applied at maximally effective doses [41].
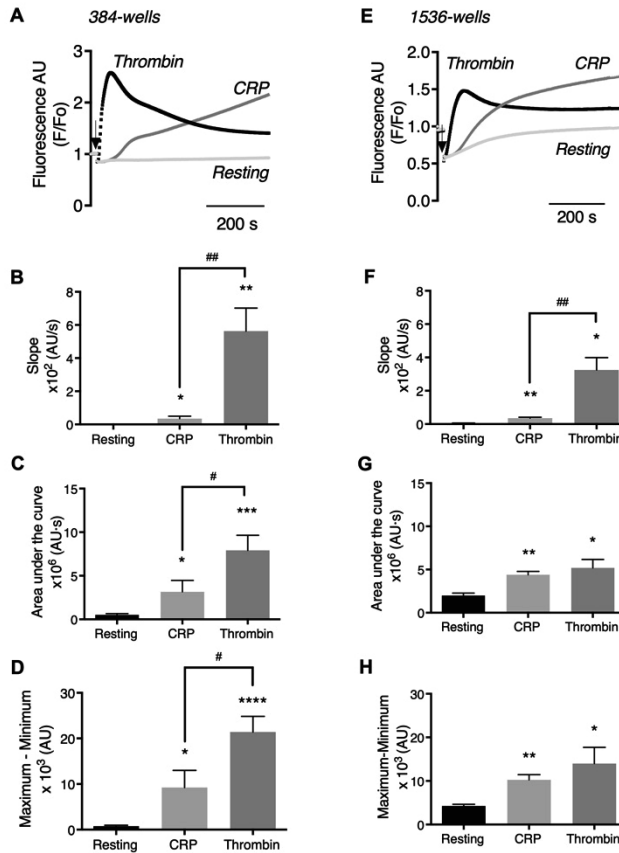

Figure 3. Comparative thrombin- and CRP-induced [Ca²⁺]$_i$ rises of platelets in 384- and 1536-well formats. Using 384- or 1526-well plates, Calcium 6-loaded platelets were stimulated with CRP (10 µg/mL, f.c.), thrombin (4 nM, f.c), or vehicle medium (resting). Agonist injection volume and rate were optimized per well-plate format to obtain the highest fluorescence increases with the FLIPR-Tetra machine. Time-dependent traces per well were constructed of pseudo-ratio fluorescence (F/F$_o$), indicative of changes in [Ca²⁺]$_i$. (**A-D**) Results from 384-well plates with 50 µL platelets (200×10^9/L) and 5 µL agonist solution injected. Data are means ± SEM (n=6). (**E-H**) Results from 1536-well plates with 6 µL platelets (400×10^9/L) and 2 µL agonist solution injected. Means ± SEM (n=3). (**A, E**) Representative [Ca²⁺]$_i$ traces of resting and CRP- or thrombin-stimulated platelets. (**B, F**) Measured slopes of pseudo-ratioed increases in fluorescence. (**C, G**) Maximum-minimum rises with CRP (over 600 s) or thrombin (peak level). Minimal fluorescence levels were determined after injection to exclude dilution effects. (**D, H**) Area-under-the-curve of response over 600 s. One-tailed Student's t-test, *$p<0.05$, **$p<0.01$, ***$p<0.001$, ****$p<0.0001$ vs. resting; #$p<0.05$, ##$p<0.01$ CRP vs. thrombin.
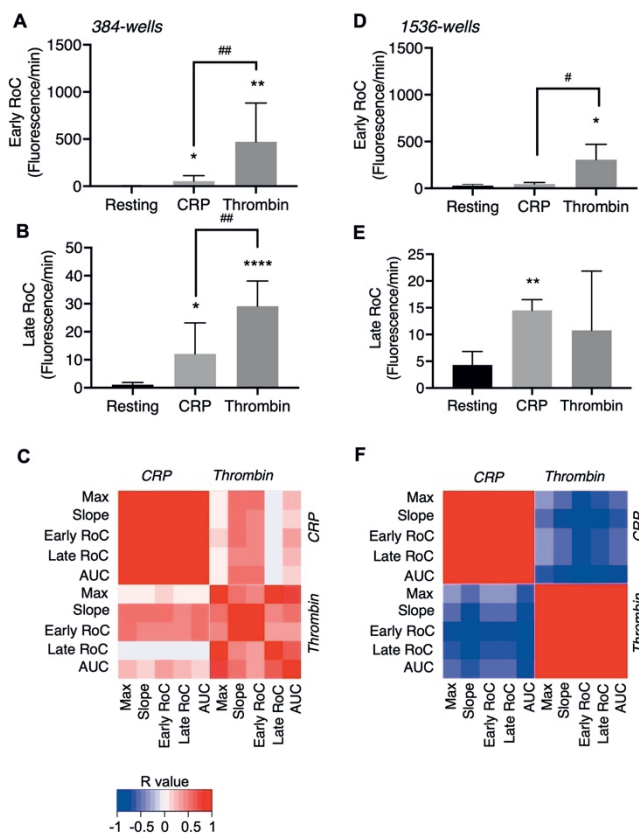
Figure 4. Comparative analysis of [Ca^{2+}]$_i$ curve parameters of thrombin- and CRP-induced platelet responses in 384- and 1536-well formats. Calcium 6-loaded platelets in 384-well (**A-C**) or 1536-well (**D-F**) plates were stimulated with CRP, thrombin, or left unstimulated, as in Figure 3. Fluorescence changes measured for 600 s were regressed to smoothed curves for the calculation of early (**A, D**) and late (**B, E**) rates of change (RoC) of the [Ca^{2+}]$_i$ rises per agonist. (**C, F**) Pearson correlation analyses were performed for all curve parameters used for Ca^{2+} response quantification: maximum - minimum rise (Max), slope of increase (slope), early and late RoC, and area under the curve (AUC). (**C, F**). Shown are heatmapped Pearson correlation matrices of R values of the various curve parameters, with blue/red colors indicating negative or positive correlations for 384- and 1536-well plates, respectively. Means ± SEM (n=3-6). Non-parametric Mann-Whitney test (**A, D**) or one-tailed Student's *t*-test (**B, E**), *$p< 0.05$, **$p<0.005$, ****$p<0.0001$ *vs.* resting. One-tailed Student's t-test, #$p<0.05$, ##$p<0.01$ CRP *vs.* thrombin (**A-E**).

Comparing the drug effects on CRP- and thrombin-induced rises in [Ca^{2+}]$_i$ in the 384- (Figure 6A-D) and 1536-well plates (Figure 6E-H) formats led to interesting results. Representative Ca^{2+} traces showed different inhibitory effects in response to CRP or thrombin, regardless of the type of well plate (Figure 6A, E). With CRP, the inhibition increased in the order of indomethacin < ticagrelor < PRT060318, while with thrombin only ticagrelor was inhibitory (Figure 6B, F). Systematic evaluation of the Ca^{2+} curve parameters underlined the selective inhibitory effect of PRT060318 with CRP, as described above. Indomethacin did not significantly affect the CRP- and thrombin-induced maximal Ca^{2+} signals (Figure 6). On the other hand, antagonism of P2Y$_{12}$ by ticagrelor suppressed these

signals with either agonist by 40-60%. A control experiment showed that, with Calcium-6 loaded platelets from one donor, essentially the same effects in 384-well and 1536-well plate formats were obtained of PRT060318, indomethacin, and ticagrelor regarding the various Ca^{2+} curve parameters (Figure S3A-H).
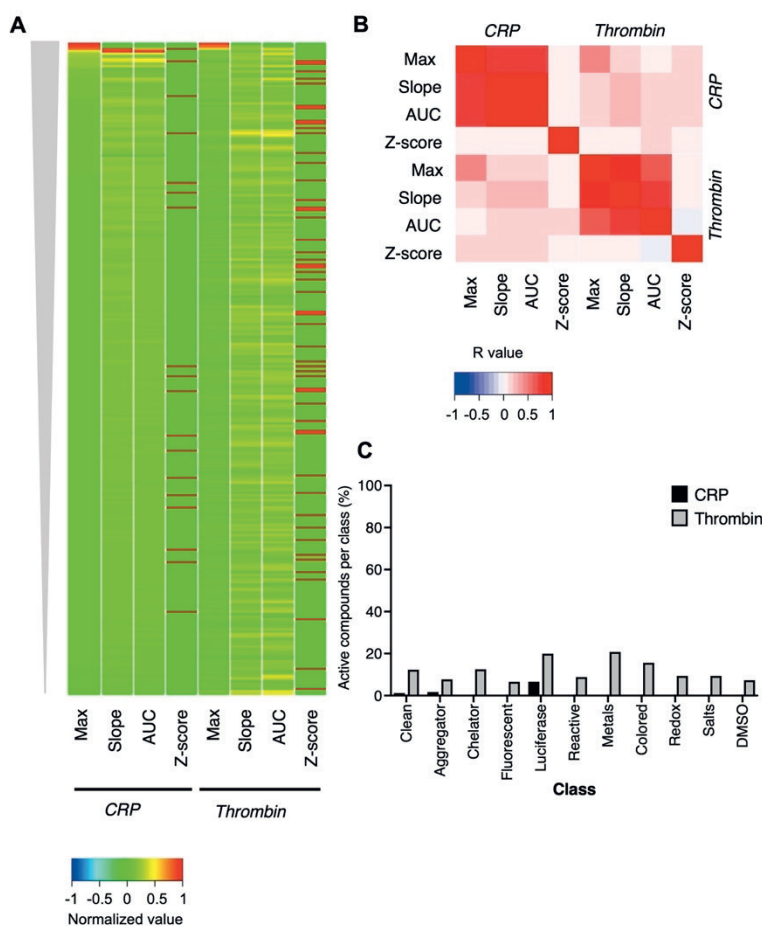

Figure 5. Robustness assessment of CRP- and thrombin-induced measurements of Calcium-6 loaded platelets in 1536-well plates. Rises in [Ca^{2+}]$_i$ of Calcium-6 loaded platelet concentrates in response to CRP (10 μg/mL), or thrombin (4 nM) were measured in 1536-well plates. Multiplicate wells (n=4) were preincubated with one of 263 compounds from a robustness set compound library (all 10 μM). Compounds were classified according to their potential assay interference: clean compounds (non-interfering); aggregating; metal ion chelating; fluorescent; luciferase quenching; chemically reactive; metal; colored or visible light absorbing; redox active; salt compounds; and DMSO controls. (**A**) Univariate scaled heatmap (-1 to 1) of mean interference of all 263 compounds in [Ca^{2+}]$_i$ rises induced by CRP or thrombin. Effects are represented by maximal increase (Max), initial slope (slope), area under the curve (AUC), and Z-score. Compounds were clustered according to decreasing size effects on the maximal increase. (**B**) Spearman correlation analysis of the four curve parameters for CRP and thrombin. Color bar represents calculated R values. (**C**) Percentages of active, assay-interfering compounds per class (Z-score >4 or <-4), calculated as means of three parameters for CRP- (black) and thrombin- (grey) stimulated platelets. For further details, see Figure S1.

In order to distinguish between the early and late contribution of the thromboxane A_2 and ADP/P2Y$_{12}$ pathways to the $[Ca^{2+}]_i$ curves, we again determined the early and late 'slopes' as RoC per agonist and well-plate format (Figure 7). The expected strong inhibition by PRT060318 of CRP-stimulated platelets was observed in both the early and late RoC (Figure 7A, C). In contrast, PRT060318 enhanced both the early and late RoC of thrombin-stimulated platelets (Figure 7B, D). Analyzing the smoothed curves, indomethacin did not notably change the early or late RoCs. In contrast, ticagrelor lowered the late RoC in response to CRP, and the early RoC in response to thrombin. This pointed to a more prominent role of autocrine-produced ADP (acting via P2Y$_{12}$ receptors) than of released thromboxane A_2 (inhibited with indomethacin) under the assay conditions. To control for the effects of indomethacin on functional platelet responses, we measured in parallel experiments platelet aggregate formation using washed platelets or PRP under stirred conditions. As shown in Suppl Figure 6, indomethacin moderately lowered the CRP-induced platelet aggregation of washed platelets but not of PRP, while it did not alter the thrombin-induced aggregation. This pointed to a small contribution of the thromboxane pathway in suspensions of stirred, washed platelets. Altogether, these data supported the suitability of the UHT assays with Calcium-6 loaded platelets in 384- or 1536-well formats for resolving agonist-dependent inhibitory effects of antiplatelet compounds.

Table 1. Overview of clinically relevant antiplatelet drugs tested. Information obtained from (pre)clinical studies and mouse *in vivo* thrombosis assays.

| Compound	Target	Receptor pathways	Effect on platelet aggregation	(Pre)clinical outcome and mouse	Refs.
PRT060318	Selective inhibitor of Syk tyrosine kinase	GPVI/FcRγ, CLEC2	Collagen, CRP ↓ ADP, thrombin =	In mouse, reduced arterial thrombosis with low bleeding.	32,53,54
Indomethacin	Reversible cyclooxygenase inhibitor	Arachidonic acid (AA)	Collagen, AA ↓ ADP, thrombin =/↓	Non-steroidal anti-inflammatory drug, acting on platelets as aspirin. Moderate risk of bleeding.	55-57
Ticagrelor	Reversible P2Y$_{12}$ receptor antagonist	P2Y$_{12}$	ADP ↓ Collagen, thrombin =/↓	Reduced ischemic events after percutaneous coronary intervention. Moderate risk of bleeding.	58 59 60
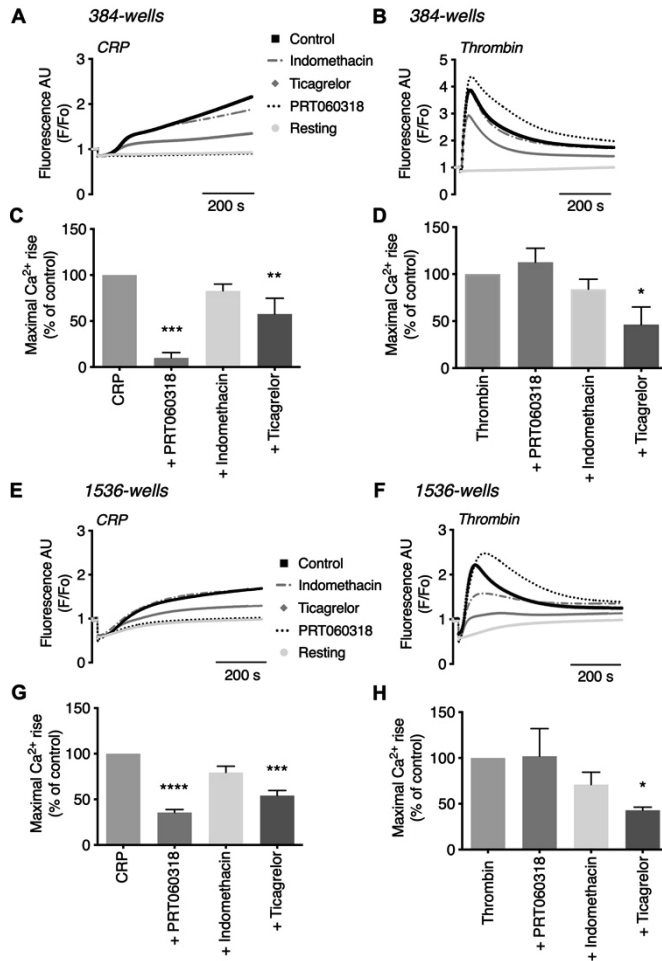
Figure 6. Drug-dependent inhibitory profiles on platelet Ca²⁺ responses in 384- and 1536-well formats. Calcium-6 loaded platelets were pretreated for 10 min with indicated compounds or vehicle (control) and injected with CRP (10 μg/mL), thrombin (4 nM) or remained unstimulated (resting) using a FLIPR-Tetra robot, and 384- or 1536-well plates, as described for Figure 3. Changes in pseudo-ratio fluorescence (F/F_o) per well were determined for 600 s. (**A-D**) Platelet responses in 384-well plates; means ± SEM (n = 6). (**E-H**) Platelet responses in 1536-well plates; means ± SEM (n=3). For 384-well (**A**, **B**) and 1536-well (**E**, **F**) formats are given representative $[Ca^{2+}]_i$ traces of resting (grey), CRP- or thrombin-stimulated platelets. Drugs used were (final concentrations): PRT060318 (5 μM, black dotted), indomethacin (10 μM, grey dotted), or ticagrelor (10 μM, grey diamonds). Drug effects on maximum $[Ca^{2+}]_i$ rises in 384-wells (**C**, **D**) or 1536-wells (**G**, **H**); values are expressed as percentages relative to the corresponding control. One-way ANOVA, *$p<0.05$, **$p<0.005$, ***$p<0.001$, ****$p<0.0001$ *vs*. agonist.
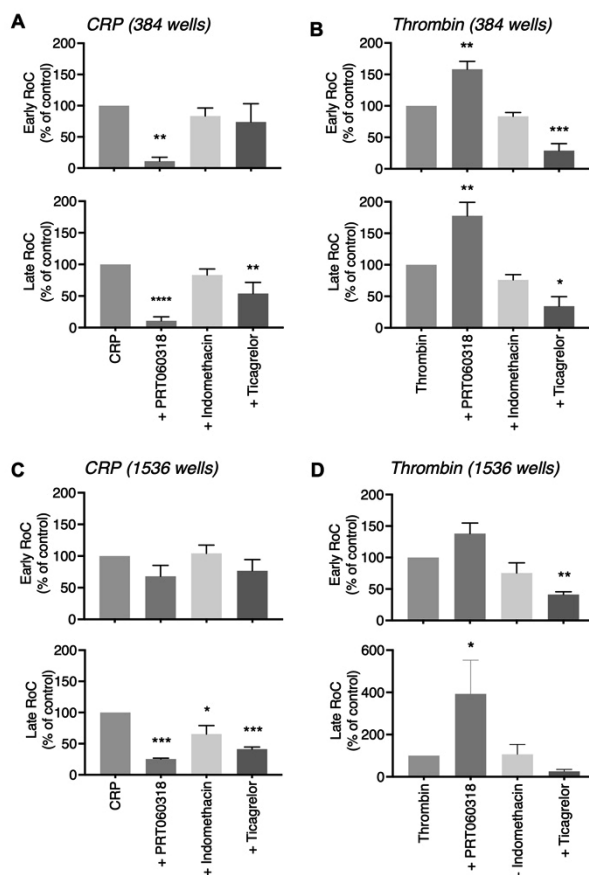
Figure 7. Drug-dependent effects on early and late slopes of platelet Ca^{2+} responses in 384- and 1536-well formats. Calcium-6 loaded platelets were pretreated for 10 min with PRT0606318, indomethacin, or ticagrelor, and activated with CRP or thrombin in 384- wells or 1536-well plates, as described in Figure 6. Pseudo-ratioed fluorescence traces over 600 s were regressed to smoothed curves for the calculation of early and late rates of change (RoC). Shown are data of early RoC (upper panels) and late RoC (lower panels) for platelets stimulated with CRP (**A**, **C**) or thrombin (**B**, **D**) in 384- or 1536-well formats. Values are expressed as percentages relative to controls. Means ± SEM (n=3). One-way ANOVA, *$p<0.05$, **$p<0.005$, ***$p<0.001$, ****$p<0.0001$ *vs.* agonist.

Discussion

In this paper, we describe a UHT assay for platelet signaling responses, operating as 96-, 384- or 1536-well plate formats, based on the different profiles of [Ca^{2+}]$_i$ rises as evoked by GPCR or ILR agonists. In 96- and 384-well plates, we detected comparable, short-term [Ca^{2+}]$_i$ transients induced by a range of physiologically relevant GPCR agonists: the PAR1/4 agonist thrombin, the PAR1 agonist TRAP6, the TP thromboxane receptor agonist U46619, and the P2Y$_1$ receptor agonist 2-MeS-ADP. With all these agonists, the [Ca^{2+}]$_i$ rises were not suppressed but slightly increased by the Syk tyrosine kinase inhibitor PRT060318. Because of this response similarity, we chose to perform further UHT assay development with the GPCR agonist thrombin only. On the other hand, the commonly used ILR agonist CRP for

GPVI evoked a more prolonged Ca^{2+} signal that was completely blocked by PRT060318. The ILR C-type lectin-like receptor 2 (CLEC2) was not investigated, since the known, physiological ligands such as podoplanin are no more than weak platelet agonists.

As described in the introduction, receptor-induced $[Ca^{2+}]_i$ rises comprise an essential signaling step, preceding almost all functional platelet responses [9]. We developed a semi-automated way of curve profiling to separate early and late RoC values, which allowed us to better characterize and quantify the fast and transient $[Ca^{2+}]_i$ rises in response to GPCR and PLCβ stimulation with thrombin, and the slow-persistent rises by ILR and PLCg2 stimulation with CRP. The fast kinetics of the Ca^{2+} signal with thrombin, a ligand formed upon coagulation, is in agreement with earlier single-cuvette studies of stirred platelet suspensions [21,26,42]. The more delayed Ca^{2+} signal with CRP is compatible with the slow-onset Ca^{2+} traces of single platelets contacting the GPVI agonist collagen [43]. In the present experiments, carried out at a plateaued level of extracellular $CaCl_2$, we did not discriminate between separate components of the $[Ca^{2+}]_i$ rises, *i.e.* Ca^{2+} mobilization from intracellular stores and Ca^{2+} entry modes [43,44].

The conventional high throughput method in 96-well plates, as earlier described [29], still needed large sample volumes per well (200 µL, 200×10^9 platelets/L). However, the 384-well measurements could be carried out at 50 µL per well (200×10^9/L), while the 1536-well assay only required 6 µL per well (400×10^9/L). In the 384-well format, agonist-induced traces appeared to be highly reproducible, as apparent from the excellent, high Z' factors. In the 1536-well format, Z' factors were slightly lower, but within the acceptable range [45]. The latter was a consequence of the small volumes of platelet suspension (6 µL) and agonist (2 µL) present per well, and the known inter-well variability in automated pipetting and cell concentrations [46]. In general, it is considered that the UHT-well formats enable a higher capability of testing with a reduction of costs and time [47,48].

The suitability of the developed UHT 1536-well assay for screening purposes was further assessed using an in-home developed robustness compound collection. We found that the CRP-induced $[Ca^{2+}]_i$ traces were essentially insensitive to the set of possible assay-interfering compounds, while the thrombin-induced responses showed limited but still acceptable compound interference. A likely explanation for this difference is that CRP consists of a cross-linked triple-helical peptide with high molecular stability [49]. On the other hand, thrombin as a large 37.4 kDa protease is by default more sensitive to catalytic or regulatory site inactivation by chemical compounds. The fraction of active, assay-interfering, compounds per class of 12%, is still lower than seen in other UHT tests [36]. In other words, in comparison to other cell systems, the platelet $[Ca^{2+}]_i$ assay in 1536-well format does not appear to be inferior.

Application of the 384- and 1536-well plate measurements with relevant anti-platelet inhibitors, *i.e.* indomethacin, ticagrelor, and PRT060318, provided detailed insight into the time-dependent contribution of autocrine-dependent signaling routes after CRP or

thrombin activation. The ADP/P2Y$_{12}$ antagonist ticagrelor suppressed only the late RoC with CRP, and both the early and late RoC with thrombin. This pointed to an unknown high contribution of the ADP/P2Y$_{12}$ enforcement pathway in the early stage of thrombin-induced signal generation. These assay results, in agreement with platelet functional measurements, demonstrated that platelet assays based on receptor-type specific [Ca^{2+}]$_i$ rises are highly sensitive to evaluate inhibitory effects of compounds in each phase of [Ca^{2+}]$_i$ curve in an agonist-dependent way.

In future use, the present UHT assays in 384- or 1536-well plate formats can be employed for large small molecule screening approaches. The 1536-well format is the gold-standard in the academic drug discovery community and the pharmaceutical industry to reduce costs in reagents, consumables, and biological materials, and make it time-efficient due to the high number of samples [50]. So far, similar Ca^{2+}-based small molecule screening has only been performed with cultured transfected cells to find novel PAR4 antagonists and as a secondary assay for PAR1 antagonists [51,52]. Other UHT Ca^{2+} dye assays have been used with cardiomyocytes and stem-induced pluripotent cells, amongst one developed by PPSC [34,40]. For platelets as primary human cells, this has not yet been achieved at the level described in our manuscript. Of note, the useful 96-well plate Optimul assay earlier developed for measuring platelet aggregation [53], uses platelet-rich plasma, has not been downscaled to 6 µL, and acts as an integral end-function test of platelet responses rather than a direct signaling test. Overall, advantages of the present UHT test are the application of receptor-dependent signaling responses in platelets, as easily accessible primary human differentiated cells, the use of a longer wavelength Ca^{2+} probe, the absence of blood plasma, and the ability to discriminate between vital cell activation and necrosis or toxicity (resulting in unphysiologically high Ca^{2+} levels). With small adaptations, the current UHT Ca^{2+} signaling method can also be applied to cultured human cell lines and differentiated iPSCs.

In general, UHT screening assays, such as the one described here, render many positive hits, which may not only result in lead compounds, but also false-positive leads due to each particular assay [54,55]. After initial compound screening, the further validation of hit antagonists involves a long process by applying several methodologies. In research on platelet GPCRs or ILR signaling inhibitors with antithrombotic potential, conventional further assays in hit-to-lead identification are light transmission aggregometry and whole blood microfluidics assays [56]. Bioavailability and toxicity assays as well as medicinal chemical improvements also need to be done before continuing the drug development process [55].

Limitations of the study

In this study, we developed a UHT fluorescence method to measure agonist-induced [Ca^{2+}]$_i$ rises in platelets in 384- and 1536-well plate formats. Herein, we were able to distinguish between GPVI- and PAR1/4-induced Ca^{2+} signaling, and characterize the inhibitory effects of compounds in the early and late phases of the [Ca^{2+}]$_i$ curves. Limitations of the study are the focus on only one ILR (CRP) and GPCR (thrombin) platelet agonist in both UHT

formats, the absence of discrimination between individual receptor isoforms (PAR1 and 4 for thrombin), and the absence of discrimination between intracellular Ca^{2+} mobilization and Ca^{2+} entry. Another limitation of such UHT assays is the absence of continuous stirring, resulting in slightly delayed responses, although the mixing of platelet suspensions with agonists was optimized by high-speed injection of relatively high volumes (10-33%) of agonist solution. On the other hand, the absence of stirring suppressed the system heterogeneity *i.e.* prevented the formation of large platelet aggregates (with CRP) or fibrin clots (with thrombin). Prolonged, biphasic Ca^{2+} curves of GPVI-stimulated platelets and aberrations in these with patients carrying genetic mutations in *ORAI1* or *STIM1* were previously obtained in stirred, single cuvette measurements [27]. For the present paper, experimental choices were made to evaluate the full Ca^{2+} signals in response to CRP, as a widely used collagen-like GPVI agonist, and thrombin as a physiological, coagulation-dependent agonist on platelets.

Acknowledgments

Author contributions

DIF, MJEK, S H, HvdH, and JWMH designed research; DIF, IP, HYFC, BMET, JvG, and AV performed experiments; DIF, IP, JLD, and SH analyzed data; DIF, MJEK, and JWMH wrote the manuscript.

Conflicts of interests

JWMH is a cofounder and shareholder of FlowChamber B.V. The other authors declare no relevant conflicts of interest.

References

1. Van der Meijden PE, Heemskerk JW. Platelet biology and functions: new concepts and clinical perspectives. *Nat Rev Cardiol*. 2019;16:166-179.

2. Michelson AD. Antiplatelet therapies for the treatment of cardiovascular disease. *Nat Rev Drug Discov*. 2010;9:154-169.

3. Anderson JL, Morrow DA. Acute myocardial infarction. *N Engl J Med*. 2017;376:2053-2064.

4. Cattaneo M. Aspirin and clopidogrel: efficacy, safety, and the issue of drug resistance. Arterioscler *Thromb Vasc Biol.* 2004;24:1980-1987.

5. McFadyen JD, Schaff M, Peter K. Current and future antiplatelet therapies: emphasis on preserving haemostasis. *Nat Rev Cardiol.* 2018;15:181-191.

6.   Gachet C. Antiplatelet drugs: which targets for which treatments? *J Thromb Haemost.* 2015;13 Suppl. 1:S313-322.

7.   Nieswandt B, Brakebusch C, Bergmeier W, et al. Glycoprotein VI but not α2β1 integrin is essential for platelet interaction with collagen. *EMBO J.* 2001;20:2120-2130.

8.   Baaten CC, Meacham S, de Witt SM, et al. A synthesis approach of mouse studies to identify genes and proteins in arterial thrombosis and bleeding. *Blood.* 2018;132:e35-e46.

9.   Fernandez DI, Kuijpers MJ, Heemskerk JW. Platelet calcium signaling by G-protein coupled and ITAM-linked receptors regulating anoctamin-6 and procoagulant activity. *Platelets.* 2020;32:1-9.

10.   Matus V, Valenzuela G, Saez CG, et al. An adenine insertion in exon 6 of human GP6 generates a truncated protein associated with a bleeding disorder in four Chilean families. *J Thromb Haemost*. 2013;11:1751-1759.

11.   Nurden AT, Nurden P. Inherited disorders of platelet function: selected updates. *J Thromb Haemost.* 2015;13 Suppl. 1:S2-9.

12.   Ungerer M, Rosport K, Bultmann A, et al. Novel antiplatelet drug revacept (dimeric glycoprotein VI-Fc) specifically and efficiently inhibited collagen-induced platelet aggregation without affecting general hemostasis in humans. *Circulation.* 2011;123:1891-1899.

13.   Voors-Pette C, Lebozec K, Dogterom P, et al. Safety and tolerability, pharmacokinetics, and pharmacodynamics of ACT017, an antiplatelet GPVI (glycoprotein VI) Fab. *Arterioscler Thromb Vasc Biol.* 2019;39:956-964.

14.   Arkin MR, Tang Y, Wells JA. Small-molecule inhibitors of protein-protein interactions: progressing toward the reality. *Chem Biol.* 2014;21:1102-1114.

15.   Gurevich EV, Gurevich VV. Therapeutic potential of small molecules and engineered proteins. *Handb Exp Pharmacol.* 2014;219:1-12.

16.   Versteeg HH, Heemskerk JW, Levi M, Reitsma PH. New fundamentals in hemostasis. *Physiol Rev.* 2013;93:327-358.

17.   Sargeant P, Sage SO. Calcium signalling in platelets and other nonexcitable cells. *Pharmacol Ther.* 1994;64:395-443.

18.   Heemskerk JW, Vis P, Feijge MA, Hoyland J, Mason WT, Sage SO. Roles of phospholipase C and Ca^{2+}-ATPase in calcium responses of single, fibrinogen-bound platelets. *J Biol Chem.* 1993;268:356-363.

19.   Gachet C. Identification, characterization, and inhibition of the platelet ADP receptors. Int J Hematol. 2001;74:375-381.

20.   Offermanns S. Activation of platelet function through G protein-coupled receptors. *Circ Res.* 2006;99:1293-1304.

21.   Covic L, Gresser AL, Kuliopulos A. Biphasic kinetics of activation and signaling for PAR1 and PAR4 thrombin receptors in platelets. *Biochemistry.* 2000;39:5458-5467.

22.   Siljander PR, Munnix IC, Smethurst PA, et al. Platelet receptor interplay regulates collagen-induced thrombus formation in flowing human blood. *Blood.* 2004;103:1333-1341.

23.   Varga-Szabo D, Braun A, Nieswandt B. Calcium signaling in platelets. *J Thromb Haemost.* 2009;7:1057-1066.

24.   Mammadova-Bach E, Nagy M, Heemskerk JW, Nieswandt B, Braun A. Store-operated calcium entry in thrombosis and thrombo-inflammation. *Cell Calcium*. 2019;77:39-48.

25.   Zou J, Wu J, Roest M, Heemskerk JW. Long-term platelet priming after glycoprotein VI stimulation in comparison to protease-activating receptor (PAR) stimulation. *Plos One.* 2021;16:e0247425.

26.   Heemskerk JW, Feijge MA, Henneman L, Rosing J, Hemker HC. The Ca^{2+}-mobilizing potency of alpha-thrombin and thrombin-receptor-activating peptide on human platelets: concentration and time effects of thrombin-induced Ca2+ signaling. *Eur J Biochem.* 1997;249:547-555.

27.   Nagy M, Mastenbroek TG, Mattheij NJ, et al. Variable impairment of platelet functions in patients with severe, genetically linked immune deficiencies. *Haematologica.* 2018;103:540-549.

28. Heemskerk JW, Willems GM, Rook MB, Sage SO. Ragged spiking of free calcium in ADP-stimulated human platelets: regulation of puff-like calcium signals in vitro and ex vivo. *J Physiol.* 2001;535:625-635.

29. Bye AP, Unsworth AJ, Gibbins JM. Screening and high-throughput platelet assays. *Methods Mol Biol.* 2018;1812:81-94.

30. Curvers J, van Pampus EC, Feijge MA, Rombout-Sestrienkova E, Giesen PL, Heemskerk JW. Decreased responsiveness and development of activation markers of PLTs stored in plasma. *Transfusion.* 2004;44:49-58.

31. Gilio K, van Kruchten R, Braun A, et al. Roles of platelet STIM1 and Orai1 in glycoprotein VI- and thrombin-dependent procoagulant activity and thrombus formation. *J Biol Chem.* 2010;285:23629-29638.

32. Feijge MA, Ansink K, Vanschoonbeek K, Heemskerk JW. Control of platelet activation by cyclic AMP turnover and cyclic nucleotide phosphodiesterase type-3. *Biochem Pharmacol.* 2004;67:1559-1567.

33. Jooss NJ, De Simone I, Provenzale I, et al. Role of platelet glycoprotein VI and tyrosine kinase Syk in thrombus formation on collagen-like surfaces. *Int J Mol Sci.* 2019;20:2788.

34. Famili F, Lam TW, van Loenen P, et al. High throughput screening in calcium transient assay to assess cardiotoxicity of compounds using hiPSC-derived cardiomyocytes. *J Pharmacol Toxicol Methods.* 2019; 99:106595.

35. Zhang JH, Chung TD, Oldenburg KR. A simple statistical parameter for use in evaluation and validation of high throughput screening assays. *J Biomol Screen.* 1999;4:67-73.

36. Honarnejad S, van Boeckel S, van den Hurk H, van Helden S. Hit discovery for public target programs in the European Lead Factory: experiences and output from assay development and ultra-high-throughput screening. *SLAS Discov.* 2021;26:192-204.

37. DeVore GR. Computing the Z score and centiles for cross-sectional analysis: a practical approach. *J Ultrasound Med.* 2017;36:459-473.

38. Mahaut-Smith MP, Ennion SJ, Rolf MG, Evans RJ. ADP is not an agonist at P2X₁ receptors: evidence for separate receptors stimulated by ATP and ADP on human platelets. *Br J Pharmacol.* 2000;131:108-114.

39. Sage SO, Pugh N, Mason MJ, Harper AGS. Monitoring the intracellular store Ca²⁺ concentration in agonist-stimulated, intact human platelets by using Fluo-5N. *J Thromb Haemost.* 2011;9:540-551.

40. Daily NJ, Santos R, Vecchi J, Kemanli P, Wakatsuki T. Calcium transient assays for compound screening with human iPSC-derived cardiomyocytes: evaluating new tools. *J Evol Stem Cell Res.* 2017;1:1-11.

41. Gilio K, Munnix IC, Mangin P, et al. Non-redundant roles of phosphoinositide 3-kinase isoforms alpha and beta in glycoprotein VI-induced platelet signaling and thrombus formation. *J Biol Chem.* 2009;284:33750-33762.

42. Shapiro MJ, Weiss EJ, Faruqi TR, Coughlin SR. Protease-activated receptors 1 and 4 are shut off with distinct kinetics after activation by thrombin. *J Biol Chem.* 2000;275:25216-25221.

43. Van Kruchten R, Braun A, Feijge MA, et al. Antithrombotic potential of blockers of store-operated calcium channels in platelets. *Arterioscler Thromb Vasc Biol.* 2012;32:1717-1723.

44. Mahaut-Smith MP. The unique contribution of ion channels to platelet and megakaryocyte function. *J Thromb Haemost.* 2012;10:1722-1732.

45. Iversen PW, Beck B, Chen YF, et al. HTS assay validation. In: *Assay Guidance Manual (eds Markossian S, Sittampalam GS, Grossman A, et al).* 2004; Bethesda (MD, USA): Eli Lilly & Company and the National Center for Advancing Translational Sciences.

46. Martis EA, Radhakrishnan R, Badve RR. High-throughput screening: the hits and leads of drug discovery: an overview. *J Appl Pharmac Sci.* 2011;1:2-10.

47. Bhambure R, Kumar K, Rathore AS. High-throughput process development for biopharmaceutical drug substances. *Trends Biotechnol.* 2011;29:127-135.

48. Mayr LM, Fuerst P. The future of high-throughput screening. *J Biomol Screen.* 2008;13:443-448.

4

49. Smethurst PA, Onley DJ, Jarvis GE, et al. Structural basis for the platelet-collagen interaction: the smallest motif within collagen that recognizes and activates platelet glycoprotein VI contains two glycine-proline-hydroxyproline triplets. *J Biol Chem.* 2007;282:1296-1304.

50. Coussens NP, Sittampalam GS, Guha R, et al. Assay guidance manual: quantitative biology and pharmacology in preclinical drug discovery. *Clin Transl Sci.* 2018;11:461-470.

51. Wong PC, Seiffert D, Bird JE, et al. Blockade of protease-activated receptor-4 (PAR4) provides robust antithrombotic activity with low bleeding. *Sci Transl Med.* 2017;9:371.

52. Dowal L, Sim DS, Dilks JR, et al. Identification of an antithrombotic allosteric modulator that acts through helix 8 of PAR1. *Proc Natl Acad Sci USA.* 2011;108:2951-2956.

53. Lordkipanidzé M, Lowe GC, Kirkby NS, et al. Characterization of multiple platelet activation pathways in patients with bleeding as a high-throughput screening option: use of 96-well Optimul assay. *Blood.* 2014;123:e11-22.

54. Hoelder S, Clarke PA, Workman P. Discovery of small molecule cancer drugs: successes, challenges and opportunities. *Mol Oncol.* 2012;6:155-176.

55. Choi S, Choi KY. Screening-based approaches to identify small molecules that inhibit protein-protein interactions. *Expert Opin Durg Discov.* 2017;12:293-303.

56. Provenzale I, Brouns SL, van der Meijden PE, Swieringa F, Heemskerk JW. Whole blood based multiparameter assessment of thrombus formation in a standard microfluidic device to proxy in vivo haemostasis and thrombosis. *Micromachines.* 2019;10:e787.

57. Andre P, Morooka T, Sim D, et al. Critical role for Syk in responses to vascular injury. *Blood.* 2011;118:5000-5010.

58. Liu D, Mamorska-Dyga A. Syk inhibitors in clinical development for hematological malignancies. *J Hematol Oncol.* 2017;10:145.

59. Bourn J, Cekanova M. Cyclooxygenase inhibitors potentiate receptor tyrosine kinase therapies in bladder cancer cells in vitro. *Drug Des Devel Ther.* 2018;12:1727-1742.

60. Falcinelli E, Iannone A, Mezzasoma AM, et al. Inhibition of platelet function after ocular administration of non-steroidal anti-inflammatory drugs. *Thromb Res.* 2019;175:1-5.

61. Perrone MG, Scilimati A, Simone L, Vitale P. Selective COX1 inhibition: a therapeutic target to be reconsidered. *Curr Med Chem.* 2010;17:3769-3805.

62. Gresele P, Momi S, Malvestiti M, Sebastiano M. Platelet-targeted pharmacologic treatments as anti-cancer therapy. *Cancer Metastasis Rev.* 2017;36:331-355.

63. Scavone M, Femia EA, Caroppo V, Cattaneo M. Inhibition of the platelet P2Y$_{12}$ receptor for adenosine diphosphate does not impair the capacity of platelet to synthesize thromboxane A$_2$. *Eur Heart J.* 2016;37:3347-3356.

64. Nergiz-Unal R, Cosemans JM, Feijge MA, et al. Stabilizing role of platelet P2Y$_{12}$ receptors in shear-dependent thrombus formation on ruptured plaques. *Plos One.* 2010;5:e10130.

Supplemental Figures of Chapter 4

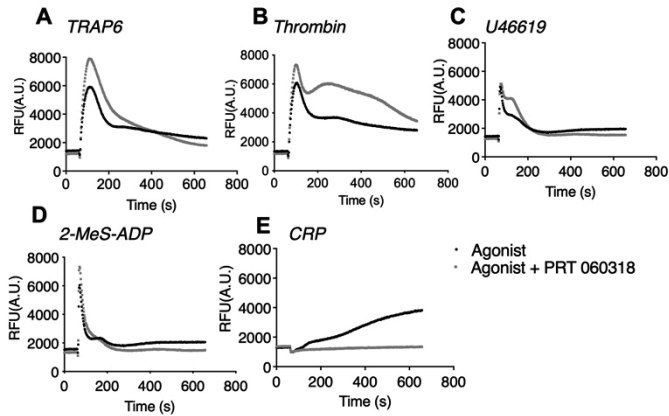**Figure S1. Differential inhibitory effect of Syk inhibitor PRT060318 on platelet [Ca²⁺]ᵢ rises induced by ILR in comparison to GPCR agonists.** Calcium-6 loaded platelets in 384-well plates were stimulated with GPCR agonists TRAP6 (10 mM) (**A**), thrombin (4 nM) (**B**), U46619 (10 mM) (**C**), or 2-MeS-ADP (10 µM) (**D**), as well as stimulated with ILR agonist CRP (10 mg/mL) (**E**). The loaded platelets were pretreated for 10 min with PRT060318 (5 mM), where indicated. Changes in fluorescence per well were simultaneously recorded over time using the FLIPR-Tetra machine. Raw fluorescence traces of a representative experiment are shown.
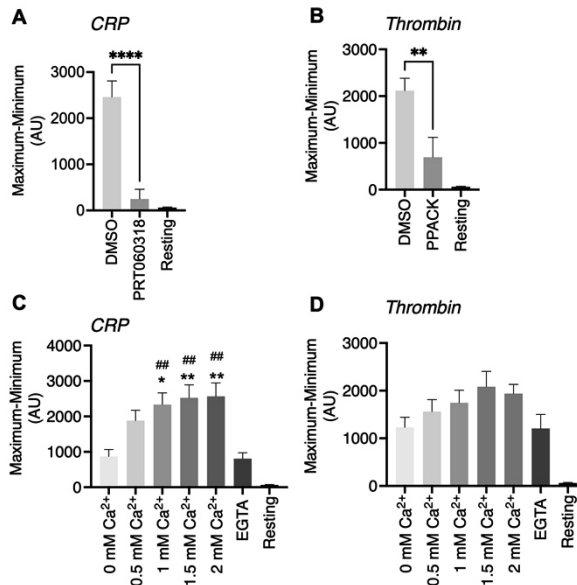
Figure S2. Agonist and CaCl₂-dependent characterization of platelet [Ca²⁺]ᵢ rises. Calcium-6 loaded platelets in 96-well plates were pre-treated for 10 min with Syk tyrosine kinase inhibitor PRT060318 (10 µM), DMSO (vehicle), or thrombin inhibitor PPACK (50 nM). The cells were subsequently stimulated with CRP (10 µg/mL) or thrombin (4 nM) or left untreated (resting) (**A**, **B**). Means ± SEM (n=3 donors), Student-*t*-test, **$p<0.01$, ****$p<0.0001$ *vs.* DMSO control. (**C**, **D**) Calcium-6 loaded washed platelets were suspended in buffer medium containing 0-2 mM CaCl₂ or 0.1 mM EGTA, and subsequently stimulated with CRP or thrombin as above. Means ± SEM (n=3 donors), One-way ANOVA, *$p<0.05$, **$p<0.01$ *vs.* 0 mM Ca²⁺, ## $p<0.01$ *vs.* EGTA. Shown are maximum - minimum increases in dye fluorescence over 600 s by CRP (**A**, **C**) or thrombin (**B**, **D**).

Figure S3. Single donor comparison of drug effects on agonist-induced [Ca^{2+}]$_i$ rises in 384- and 1536-well formats. Calcium-6 loaded platelets from one anonymous donor were distributed over a 384-well plat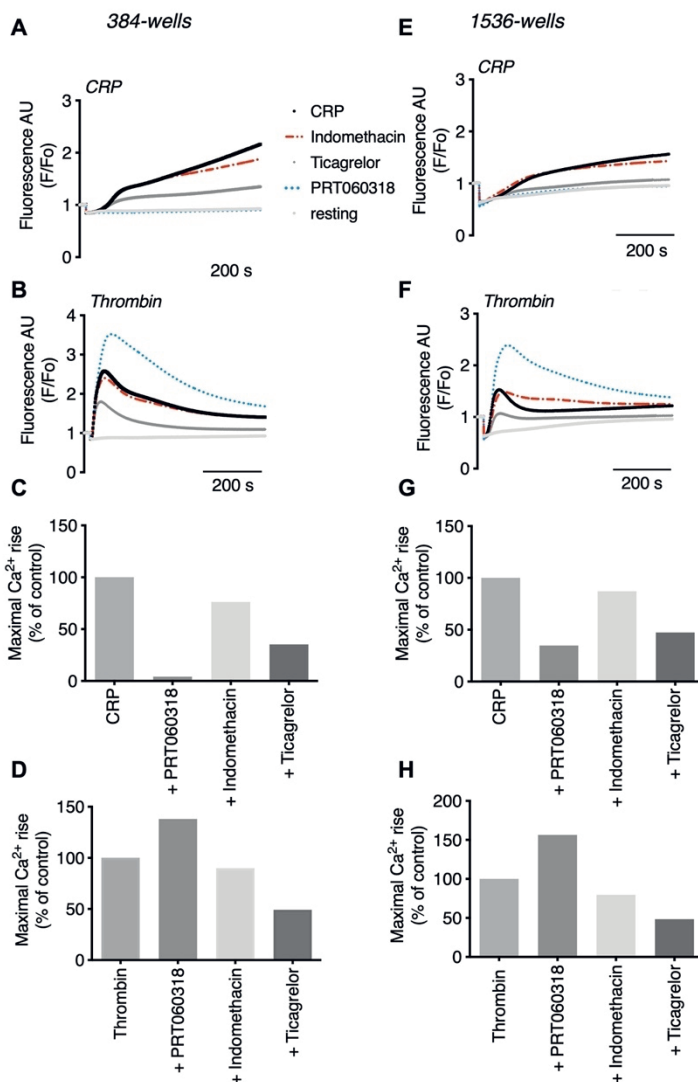e (200 × 10^9/L) and a 1536-well plate (400 x 10^9/L). The cells were pretreated for 10 min with indicated drug or vehicle (control), after which fluorescence changes per well were measured upon injection with CRP (10 µg/mL) or thrombin (4 nM) using a FLIPR-Tetra machine for 600 s, as described for Figure 6. Time traces of changes in pseudo-ratio fluorescence (F/F$_o$) were then constructed per well. (**A-D**) Platelet responses in 384-wells (50 µL platelet suspension, injection of 5 µL agonist solution). (**E-H**) Platelet responses in 1536-wells (6 µL platelet suspension, injection of 2 µL agonist solution). Representative F/F$_o$ traces of resting, CRP- or thrombin-stimulated platelets, as measured in 384-wells (**A, B**) or 1536-wells (**E, F**). Drugs were used as in Figure 6 (final concentrations): PRT060318 (5 µM, blue), indomethacin (10 µM, red), and ticagrelor (10 µM, grey). (**C, D**) Drug effects on CRP- and thrombin-induced maximum [Ca^{2+}]$_i$ rises in 384-well plates. (**G, H**) Drug effects on CRP- and thrombin-induced maximum [Ca^{2+}]$_i$ rises in 1536-well plates. Values are % relative to the corresponding control.
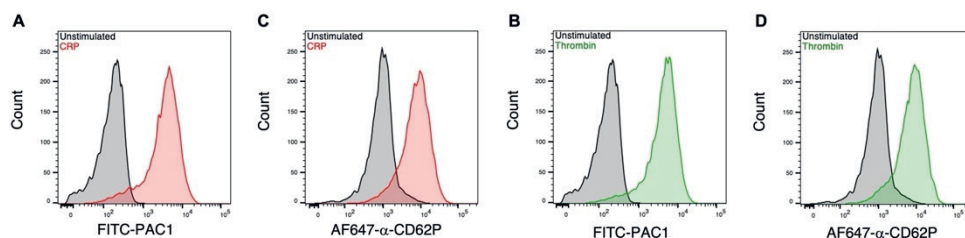
Figure S4. Agonist-induced effects on platelet activation markers by flow cytometry. Washed platelets were stimulated with CRP (1 µg/mL) or thrombin (1 nM) for 15 minutes. After stimulation, the cells were labeled FITC-PAC1 mAb (integrin αIIbβ3 activation marker) or AF647-anti-CD62P mAb (P-selectin exposure). Shown are representative histograms. Color code representing different samples: unstimulated platelets (grey), platelets stimulated with CRP (red), and platelets stimulated with thrombin (green). Platelets stimulated with CRP (**A**) or thrombin (**B**) and stained with FITC-PAC1mAb. Platelets stimulated with CRP (**C**) or thrombin (**D**) and stained with AF- anti-aCD62P mAb.
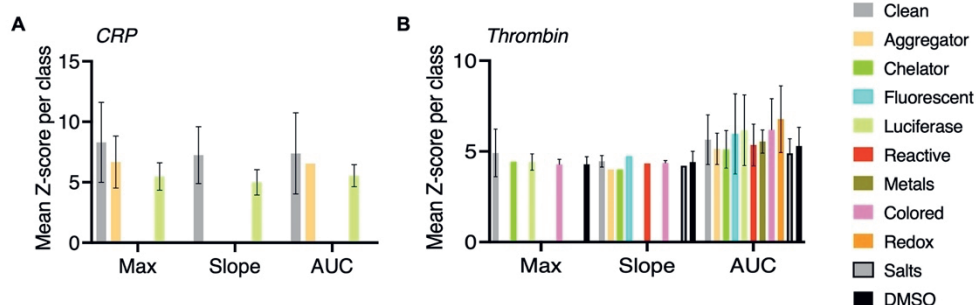
Figure S5. Interference sensitivity of UHT agonist-induced [Ca²⁺]ᵢ assaying of Calcium-6 loaded platelets per class in UHT assay. Rises in [Ca²⁺]ᵢ of Calcium-6 loaded platelets were measured in response to CRP (10 µg/mL), or thrombin (4 nM) in the 1536-well format during 600 s. Replicate wells were preincubated with one of 263 compounds from a robustness set compound library, as in Figure 5. Compounds were classified according to their potential assay interference: clean compounds (non-interfering); aggregator; metal ion chelator; fluorescent; luciferase quenching; chemically reactive; metal; colored or visible light absorbing; redox active; salts; and DMSO controls. Effects of active compounds (Z-score>4 or <-4) per class (see Figure 5) are shown on Z-scores for means of [Ca²⁺]ᵢ curve parameters, namely maximal increase (Max), curve slope, and area-under-the-curve (AUC). Data were resolved for CRP stimulation (**A**) and thrombin stimulation (**B**).
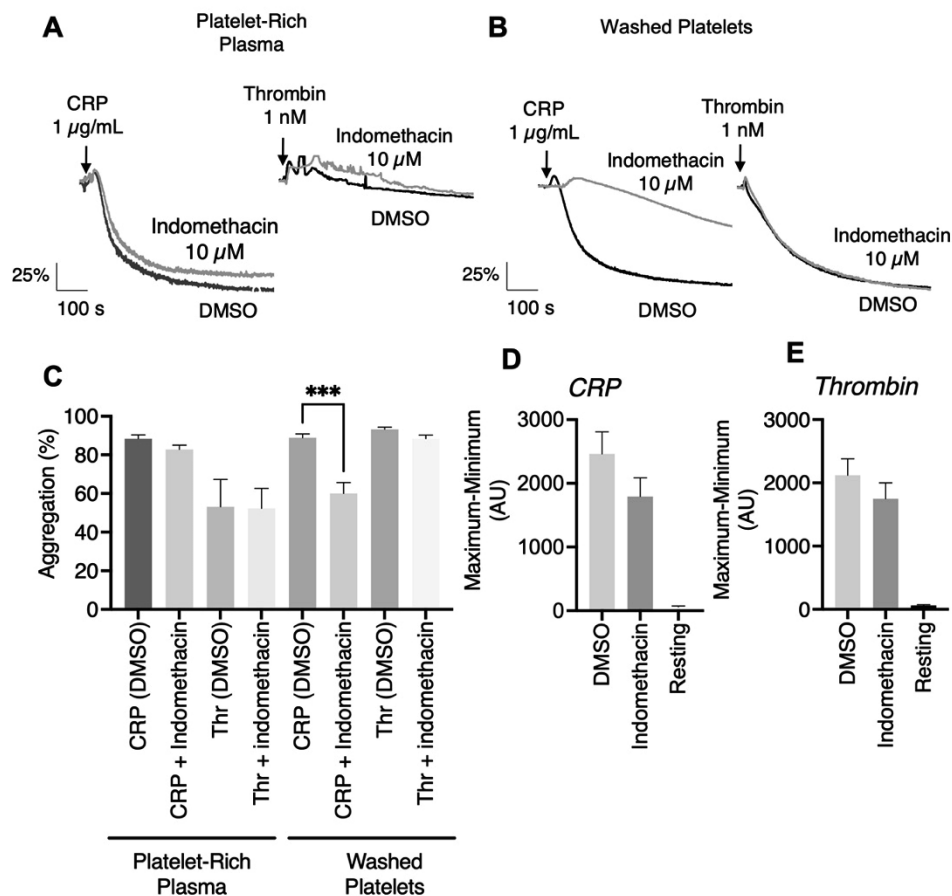
Figure S6. Comparative effects of indomethacin on agonist-induced platelet aggregation and [Ca²⁺]ᵢ rises in Calcium-6 loaded platelets. (**A-C**) Platelet-rich plasma or suspended washed platelets were pre-treated with indomethacin (10 µM) or DMSO vehicle for 10 min, and then stimulated with CRP (1 µg/mL) or thrombin (1 nM). Platelet aggregation was determined by light transmission aggregometry. Shown are (A, B) representative aggregation traces in PRP (**A**) or washed platelets (**B**), and maximal changes in % aggregation as % transmission (**C**). (**D**, **E**) Calcium-6 loaded platelets from the same donors in 96-well plates were pretreated with indomethacin (10 µM) or DMSO (vehicle), and then stimulated with CRP (10 µg/mL) or thrombin (4 nM). Changes in Calcium-6 fluorescence during 600 s were recorded. Means ± SEM (n=3 donors), Student-t-test, *** $p<0.005$ vs agonist (DMSO).

5

Chapter 5

Ultra-high throughput screening to identify antiplatelet drugs with discriminative receptor-dependent action mechanism

Fernández DI, Sobota V, Tullemans BME, van Groningen J, Troitiño S, Zou J, van den Hurk H, García A, Hornanejad S, Kuijpers MJE, Heemskerk JWM

6

Chapter 6

Role of SHP2 (PTPN11) in glycoprotein VI-dependent thrombus formation: restored platelet response in Noonan patients by the allosteric drug SHP099

Fernández DI, Diender M, Hermida-Nogueira L, Huang J, Veiras S,Henskens YMC, te Loo MWM, Heemskerk JWM*, Kuijpers MJE*, García A*

*Equal contribution

Abstract

The protein tyrosine phosphatase SHP2 (PTPN11) is a negative regulator of glycoprotein VI (GPVI)-induced platelet signal under certain conditions. Clinical trials with derivatives of the allosteric drug SHP099, inhibiting SHP2, are ongoing as a potential therapy for solid cancers. Gain-of-function mutations of the *PTPN11* gene are observed in part of the patients with the Noonan syndrome, associated with a mild bleeding disorder. We assessed the effects of SHP2 inhibition in platelets from controls and Noonan syndrome patients. Washed human platelets were incubated with SHP099 and stimulated with collagen-related peptide (CRP) for stirred aggregation and flow cytometric measurements. Whole-blood microfluidics assays using a dosed collagen and tissue factor coating were performed to assess shear-dependent thrombus and fibrin formation. Effects on clot formation were evaluated by thromboelastometry. Pharmacological inhibition of SHP2 did not alter GPVI-dependent platelet aggregation under stirring, but it enhanced integrin αIIbβ3 activation in response to CRP. Using whole-blood microfluidics, SHP099 increased the thrombus buildup on collagen surfaces. In the presence of tissue factor and coagulation, SHP099 increased thrombus size as well as time to fibrin formation. Blood from *PTPN11*-mutated Noonan patients, with low platelet responsiveness, after *ex vivo* treatment with SHP099, showed a normalized platelet function. In thromboelastometry, SHP2 inhibition tended to enhance tissue factor-induced blood clotting profiles with tranexamic acid, preventing fibrinolysis. Pharmacological inhibition of SHP2 by the allosteric drug SHP099 enhances GPVI-induced platelet activation under shear conditions with the potential to improve the platelet function of Noonan patients.

Visual abstract
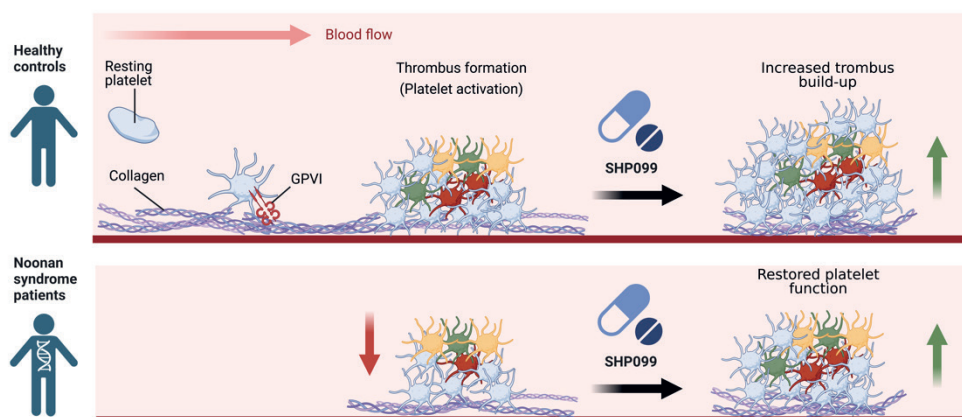
Introduction

The Src homology-2 containing protein tyrosine phosphatase-2 (SHP2), encoded by the gene *PTPN11*, is an oncogenic tyrosine phosphatase with pleiotropic roles in organism development and cell homeostasis [1]. Thus, SHP2 has been implicated in disease states such as autoimmunity, diabetes, and cancer [2-4]. In platelets, SHP2 has poorly understood roles, *e.g.* in co-regulating protein tyrosine kinase-dependent signaling pathways involving the Ras-ERK pathways.

The eight non-receptor protein phosphatases in platelets can have both positive and negative modulatory roles, which are also dependent on the agonist type [5,6]. Platelets express two structurally related Src homology-2 containing protein tyrosine phosphatases, SHP1 and SHP2, encoded by the genes *PTNP6* and *PTPN11*, respectively. Platelet SHP1 has been recognized as a positive regulator of the immunoreceptor tyrosine-based activation motif (ITAM)-coupled signaling through the collagen receptor glycoprotein VI (GPVI), for instance by stimulating integrin αIIbβ3 signaling [7]. In contrast, various authors have shown that SHP2 can negatively regulate platelet signaling via GPVI and CLEC-2 [7-10]. In the latter case, regulation occurs via the recruitment of SHP2 to immunoreceptor tyrosine-based inhibition motif (ITIM)-coupled receptors, including PECAM1, G6b-B, and CEACAM1 [7,11,12]. Recently, (murine) SHP2 has been described to negatively regulate thrombus formation at high shear by suppressing the thromboxane A_2 (TxA_2)-induced dense granule secretion [9]. Furthermore, SHP2 conditional knock-out mice displayed macrothrombocytopenia likely due to defective thrombopoiesis, however not resulting in a bleeding diathesis [7].

In humans, germline gain-of-function mutations are described for the *PTPN11* gene in part of the patients with Noonan syndrome (OMIM #163950), which is an autosomal dominant genetic disorder with a prevalence of 1 per 2500 live births [13]. Around half of the Noonan patients present with mild bleeding symptoms, while severe hemorrhage is rare (3%) [14]. Platelets from these patients can have a reduced aggregation after stimulation with low collagen. In a recent study, collagen-induced platelet adhesion and thrombus formation were lower in blood from *PTPN11*-mutated Noonan patients [10]. On the other hand, somatic gain-of-function mutations of *PTPN11*, activating the function of SHP2, are also found in several cancers, including leukemias, neuroblastomas, lung and breast cancers, being present in one-third of the non-syndromic juvenile myelomonocytic leukemia cases [13,15,16].

The drug SHP099 was first characterized as a novel allosteric, selective, potent, and orally available small molecule inhibitor of SHP2. SHP099 stabilizes the phosphatase SHP2 in its auto-inhibited conformation through an allosteric mechanism of action [17,18]. The blocked SHP2 activity with SHP099 was found to suppress tumor cell growth *in vitro* and animal models [18,19]. Currently, clinical trials are ongoing with four allosteric inhibitors of SHP2, investigated as a possible therapy for advanced metastatic or solid tumors, and also in combination with other chemotherapeutic agents [20,21]. SHP099 has been shown to increase

thrombus growth *in vitro* [10]. However, only limited information is available on the effects of SHP099 on ITAM-linked activation of human platelets. Here, we set out to characterize its effects on platelets from control subjects and Noonan syndrome patients, specifically investigating whether treatment of the patient's blood with SHP099 can improve the extent of thrombus formation as a proxy measurement for hemostasis.

Materials and methods

Materials

Bovine serum albumin (BSA), D(+)-glucose, D-phenylalanyl-prolyl-arginyl chloromethyl ketone (PPACK), heparin, human recombinant von Willebrand factor, and human thrombin were purchased from Sigma-Aldrich (Saint Lous, MI, USA). The agonist collagen-related peptide cross-linked (CRP-XL) was obtained from CambCol Laboratories (Cambridge, United Kingdom). Collagen Horm was from Takeda (Hoofddorp, The Netherlands). Human fibrinogen was from Enzyme Research Laboratories (South Bend, IN, USA). Recombinant human tissue factor (Innovin) was purchased from Siemens Healthineers (Erlangen, Germany). Fura-2-AM was obtained from Invitrogen, Fisher Scientific (Carlsbad, CA, USA). Fluorescein isothiocyanate (FITC)-labeled PAC1 monoclonal antibody (mAb) against activated human integrin αIIbβ3 was purchased from BD Bioscience (340507; Franklin Lakes, NJ, USA), while FITC-conjugated a-fibrinogen mAb was from ThermoFisher Scientific (RRID: AB 10984426). AF647-labeled CD62P mAb was from Biolegend (London, United Kingdom). 3,3-dihexyloxacarbocyanine iodide (DiOC$_6$) was purchased from Anaspec (Reeuwijk, The Netherlands). AF568-conjugated annexin A5 and AF647-labeled fibrinogen were purchased from Molecular Probes, Life Technologies (New York, NY, USA). Eptifibatide was from Cayman Chemical (Ann Arbor, MI, USA). Antibodies for western blotting were monoclonal phosphotyrosine antibody (clone 4G10, 05-321, Millipore), rabbit anti-human p-PLCγ2 (Y^{759}, Mab7277, R&D Systems); mouse anti-PLCγ2 (sc-5283, Santa Cruz Biotechnology); rabbit anti-p-Syk (Y^{525} + Y^{526}, ab58575, Abcam); mouse anti-Syk (sc-1240, Santa Cruz Biotechnology); rabbit anti-p-Src (Y^{418}, 44660G, Fisher Scientific); rabbit anti-Src pan (44-656G, Invitrogen); anti-p-LAT (Y^{191}, 07-278, Millipore); anti-LAT (sc-7948, Santa Cruz Biotechnology); or GAPDH (Sigma, G9545).

Ethical committees

Blood samples were obtained by venipuncture from healthy volunteers who had not received anti-platelet medication for at least two weeks. Approval was obtained from the medical ethics committees from the University of Santiago de Compostela (Galician Investigation Ethics Committee, code 2009-270) and Maastricht University Medical Centre$^+$ (MUMC$^+$, code: 2017-0285). Permission for blood drawing from Noonan patients was obtained from the medical ethics committees of Radboud University (Evaluation of Bleeding Disorders in Noonan Patients, non-WMO) and MUMC$^+$ (ProBe-AHP: Predictors of Bleeding Evaluation in Adult Hematologic Patients with Bleeding Tendencies, METC 14-4-036, Dutch Trial

Register, NL9643). All blood donors gave informed consent according to the declaration of Helsinki to participate in the study.

Blood collection and platelet isolation

Blood samples were collected into 3.2% (w/v) trisodium citrate (Vacuette tubes, Greiner Bio-One, Kremsmünster, Austria). Part of the samples were directly used for flow-perfusion assays. Washed platelets were obtained by centrifugation of platelet-rich plasma (PRP) in the presence of 0.2 μg/mL prostacyclin and resuspended in modified Tyrode's buffer (134 mM NaCl, 0.34 mM Na_2HPO_4, 2.9 mM KCl, 12 mM $NaHCO_3$, 20 mM HEPES, 5 mM glucose, 1 mM $MgCl_2$, pH 7.3) at the desired concentration. Washed platelets were allowed to rest for 30 min at room temperature.

Platelet aggregation by light transmission aggregometry

Washed platelets (2.5×10^8/mL) were pre-incubated with vehicle (DMSO) or SHP099 (10 μM, 25 min), ticagrelor (1 μM, 5 min), apyrase (2 U/mL, 5 min), or indomethacin (10 μM, 5 min) at room temperature with last 5 min at 37 ºC. Dosing of CRP-XL was performed to choose a submaximal concentration (0.5-0.2 μg/mL) per donor [range: 58-77% aggregation]. Platelet aggregation was measured under stirring conditions of 1200 rpm at 37 ºC using a Chronolog optical aggregometer (Chrono-log Corporation, Havertown, PA, USA).

Integrin αIIbβ3 activation by flow cytometry

Washed platelets (2×10^7/mL) were pre-incubated with vehicle (DMSO) or SHP099 (10 μM, 30 min). Then, platelets were stimulated with CRP-XL (3 μg/mL) or left unstimulated at 37 ºC for 15 min in presence of 1 mM $CaCl_2$. After agonist addition, the platelets were stained for activated integrin αIIbβ3 using FITC-labeled PAC1 mAb. Samples were prepared in triplicate. Per sample, 10,000 events were measured using a BD Accuri C6 flow cytometer (BD Bioscience, San Jose, CA, USA).

Platelet preparation for western blotting

Washed platelets (8×10^8/mL) were pre-incubated with SHP099 (10 μM, 25 min), and then treated with 9 μM eptifibatide (to avoid platelet aggregation) at room temperature. The platelet samples were heated for 4 min at 37 ºC in a Chronolog aggregometer. After 1 min of stirring, activations were performed for 90 s with CRP-XL (0.5, 1, or 3 μg/mL). Lysates were obtained, and proteins were separated by SDS 11% polyacrylamide gel electrophoresis, followed by immunoblotting using polyvinylidene difluoride membranes [22]. After blocking with 5% BSA in TBS-T (20 mM Tris-HCl pH 7.6, 150 mM NaCl, 0.1% Tween 20), the membranes were incubated using a primary antibody, as stated. The immune-stained membranes were treated with horseradish peroxidase-labeled goat anti-mouse antibody (31430, dilution 1/5000) or goat anti-rabbit antibody (31460, Pierce, Rockford, IL, USA). The membranes were then washed and processed using an enhanced chemiluminescence system (ECL, Pierce, Rockford, USA).

Cytosolic Ca²⁺ measurements

Cytosolic $[Ca^{2+}]_i$ measurements of Fura-2 loaded platelets (2×10^8/mL) were performed in 96-well plates, using a FlexStation 3 (Molecular Devices, San Jose, CA, USA). The loaded platelets were pre-incubated with vehicle (DMSO) or SHP099 for 30 min at room temperature. Samples were stimulated by CRP-XL (10 µg/mL). Changes in Fura-2 fluorescence were measured in duplicate, and levels of calibrated $[Ca^{2+}]_i$ concentration (in nM) were obtained from fluorescence ratio values [23].

Collagen- or fibrinogen-induced thrombus formation under flow

Microfluidic whole-blood thrombus formation without coagulation was assessed using the parallel-plate Maastricht flow chamber, as described before [24]. In brief, glass coverslips were coated overnight at 4 °C with two microspots; one with 1 µL of collagen type I at either 100 µg/mL or 30 µg/mL and another with 1 mL human recombinant VWF (50 µg/mL) with human fibrinogen (250 µg/mL). In all flow runs the most active microspot was placed downstream. Previously, it has been shown that the presence of two microspots did not influence the thrombus parameters on either microspot [25]. After coating, the coverslips were incubated in a humid chamber for 1 h and blocked for 30 min with 1% BSA-blocking buffer. For blood flow, 500 µL of citrated blood was anticoagulated with PPACK (40 µM) and recalcified with 3.75 mM MgCl₂ and 7.5 mM CaCl₂, and then perfused for 3.5 min at a wall shear rate of 1000 s⁻¹. Blood was preincubated with vehicle (DMSO 0.5%) or SHP099 (10 µM) for 30 min at room temperature. Thrombi formed on the surfaces were poststained with HEPES rinse buffer (10 mM HEPES pH 7.45, 136 mM NaCl, 2.7 mM KCl, 2 mM MgCl₂, 2 mM CaCl₂, 1 mg/mL glucose, 1 mg/mL BSA, and 1 U/mL heparin), supplemented with fluorescent labels: FITC-labeled anti-fibrinogen mAb (1:100), AF568 annexin A5 (1:200), and AF647 anti-CD62P mAb (1:80). Unbound label was removed by post-perfusion with rinse. Brightfield and 3-color fluorescence images were taken with a LeicaDFC360FX widefield microscope (Leica Microsystems, L'Hospitalet de Llobregat, Spain) or an EVOS-FL microscope (Life Technologies, Bleiswijk, The Netherlands), equipped with Cy5, RFP and GFP LEDs, an Olympus UPLSAP 60× oil-immersion objective, and a 1360 × 1024 pixel CCD camera. Per condition, flow runs were performed at least in duplicate.

Collagen-induced thrombus formation under flow with coagulation

Whole blood microfluidic experiments under coagulating conditions were performed as described before [26]. In brief, coverslips were coated with two spots of collagen-H (250 µg/mL, 1 µL) of which the downstream spot contained tissue factor (250 pM, 1 µL). Samples of citrated blood were supplemented with AF647-fibrinogen (16.5 µg/mL), DiOC₆ (0.5 µg/mL), and AF568-annexin A5 (1:200) and co-perfused (1:10) with buffer containing 63 mM CaCl₂ and 32 mM MgCl₂ to obtain a shear rate of 1000 s⁻¹. Images of each spot were captured every 2 min using a Leica-DFC360FX widefield microscope (Leica Microsystems) equipped with a 60× oil-immersion objective.

Image analysis and delineation of multiparameter outcome of microfluidic assay

Semi-automated scripts, using a manual threshold setting, were used for standardized image analysis in the open-access program Fiji (based on ImageJ) [25]. In brief, brightfield images provided five outcome parameters: *P1*, platelet surface area coverage (SAC%), obtained from thresholded, binary images, representing identified regions of all adhered platelet and thrombus structures; *P2*, platelet multilayer coverage (SAC%), representing identified regions of multi-layered platelets; *P3*, thrombus multilayer score (scale 0-3); *P4*, thrombus contraction score (scale 0-3); *P5*, thrombus morphological score (scale 0-5). Scoring (half units) of the auto-enhanced brightfield images was based on a predefined image gallery [25]. Threshold, binary fluorescence images, indicative of platelet activation stages, gave percentage surface area coverage (SAC%) per label. Processing of the brightfield and fluorescence images (background equalization, thresholding, region-of-interest settings) was as in the supplement of Ref. [27].

In the non-coagulation setting, further parameters obtained were *P6*, PS exposure (AF568-annexin A5); *P7*, P-selectin expression (AF647 anti-CD62P mAb); and *P8*, integrin $\alpha IIb\beta 3$ activation (FITC anti-fibrinogen mAb). For the coagulation setting, these parameters were *P6*, AF647-fibrinogen monitoring fibrin formation; *P7*, $DiOC_6$ monitoring platelet deposition; and *P8*, AF568-annexin A5 for PS exposure.

Rotational thromboelastometry

Whole blood clot formation and firmness were analyzed using a ROTEM delta device (Werfen, Munich, Germany). Whole blood was preincubated with vehicle (DMSO) or inhibitor (SHP099, 10 µM) for 30 min at room temperature. After incubation, blood was added into a cuvette and treated with tissue factor and tranexamic acid (APTEM mode). Measurement runs were performed for 20 min. Samples were tested in duplicate. The APTEM mode measures platelet-dependent clot retraction in the presence of a fibrinolysis inhibitor.

Statistical analyses

Data are shown as means ± SD. Comparative heatmaps were generated in the R program (version 1.2.5033) from mean values per parameter, which were univariate scaled 0-10. Effects in subtracted heatmaps were filtered based on statistical analysis either paired Student's t-test or standard deviation of controls, as indicated. GraphPad Prism 9.3.1 software (La Jolla, CA, USA) was used for statistical analysis. Parametric or non-parametric tests were used according to normality tests of data. For more than one group comparison, a one-way ANOVA was used. Statistical significance was set as *p*-value <0.05.

6

Results

Pharmacological inhibition of SHP2 limitedly increases GPVI-induced platelet activation

To assess the effects of the selective allosteric inhibitor of SHP2, SHP099, on CRP-induced activation of washed platelets, a submaximal concentration of the agonist was used. No relevant effect of the inhibitor was found under these conditions (Figure 1A, B). Similarly, when the secondary mediators ADP or TxA2 were inhibited (using apyrase or indomethacin), pretreatment with SHP099 could not restore the CRP-induced aggregation process. Along the same line, blocking of the $P2Y_{12}$ receptor with ticagrelor in combination with SHP099 did not result in an altered CRP-induced aggregation pattern (Figure 1A, B). When monitoring the CRP-induced Ca^{2+} responses in Fura-2-loaded platelets, pretreatment with SHP099 also did not alter the $[Ca^{2+}]_i$ traces (Figure S1A-D). Moreover, no effect of this SHP099 concentration was observed on the CRP-induced (0.5 to 3 µg/mL) tyrosine phosphorylation of signaling proteins downstream of GPVI (Figure S2).

Finally, we measured the effects of SHP099 on CRP-induced activation of washed platelets by flow cytometry. In this test, the presence of SHP099 resulted in a slightly increased αIIbβ3 activation (Figure 1C). These results jointly point to only minor activating effects of SHP2 on the responses of platelets in suspension induced by the GPVI agonist CRP.
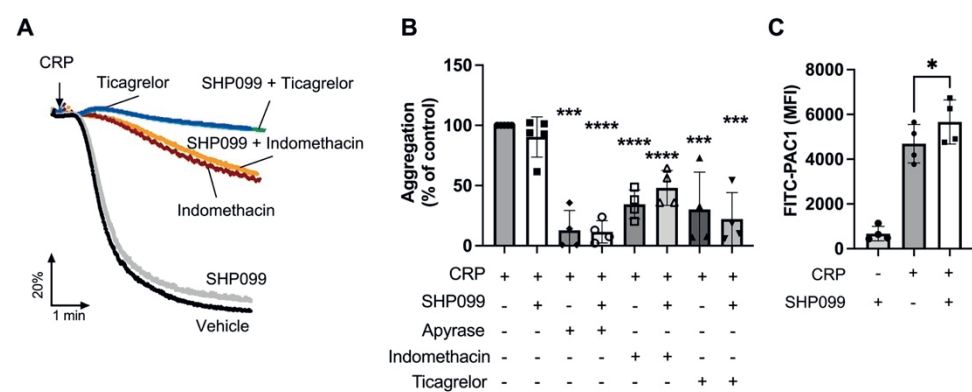
Figure 1. Subtle effect of SHP099 on GPVI-dependent platelet aggregation and integrin αIIbβ3 activation. Washed platelets (2.5×10^8/mL) were incubated with SHP099 (10 µM), apyrase (0.1 U/mL), indomethacin (10 µM), ticagrelor (1 µM), or control (DMSO <0.5%), as indicated. Platelet aggregation was induced with CRP at a submaximal dose, adjusted per donor [range: 58-77% aggregation]. (**A**) Representative traces of CRP-induced aggregation at indicated conditions. (**B**) Histograms showing maximal aggregation as a percentage of the DMSO control. (**C**) Washed platelets (2×10^7/mL) were stimulated with CRP (3 µg/mL) for 15 min at 37 ºC. The stimulated platelets were labeled with FITC-PAC1 mAb (αIIbβ3 activation marker) and analyzed by flow cytometry. Histograms show mean fluorescence intensity (MFI). Data are means ± SD (n = 4-5 donors); *$p<0.05$; **$p<0.01$; ***$p<0.005$; ****$p<0.001$ (one-way ANOVA).

Inhibition of SHP2 enhances thrombus characteristics on collagen surfaces

To study the role of SHP2 in platelet responses in a physiologically relevant setting, we used a microspot-based microfluidics method, previously developed for high throughput evaluation of surface- and subject-dependent characteristics of thrombus formation [24,25]. Recalcified whole blood was perfused through the flow chambers containing two microspots at high shear rate in the absence of coagulation. Thrombus formation was monitored after 3.5 min by multicolor microscopic imaging from in total three microspots containing: *(i)* collagen at high coating concentration (100 μg/mL), *(ii)* collagen at low coating concentration (30 μg/mL), and *(iii)* a mixture of VWF (50 μg/mL) plus fibrinogen (250 μg/mL). The recorded images provided 8 parameters (*P1-8*) of platelet deposition, thrombus size, and type, and platelet activation (see methods). The raw parameter data per surface are shown in Figure S3.

Examination of the brightfield microscopic images indicated subtle changes in platelet deposition in terms of more contracted thrombi in the presence of SHP099 (Figure 2A). Quantification of parameters *P1-5* from these images indicated no significant effect in platelet deposition on any of the three surfaces (Figure S3A-C). On the contrary, SHP099-treated blood did show significant increases in *P3-5*, representing thrombus activation characteristics, at high collagen concentration ($p<0.05$), and an increase in thrombus multilayer for the low collagen concentration (*P5*, $p<0.05$). Other thrombus characteristics parameters had a tendency to be increased ($p=0.05$ to 0.10). No differences with SHP099 were seen for the VWF/fibrinogen surface (Figure S3C).

Platelet activation was monitored from fluorescence images using markers of P-selectin, phosphatidylserine exposure, and integrin αIIbβ3 activation. No statistical significance was observed in the presence of SHP099-treated for any of the spots (Figure S3).

To investigate whether SHP2 has a more prominent regulatory role under conditions where autocrine effects via the P2Y$_{12}$ ADP receptor are blocked, we used the reversible P2Y$_{12}$ antagonist, ticagrelor. As expected, preincubation of the blood with ticagrelor alone significantly reduced thrombus contraction (*P3*, $p<0.05$) and multilayer formation (*P4*, only low collagen) on the collagen surfaces (Figure S3A-B). On the other hand, at high collagen concentrations, ticagrelor increased the coverage of P-selectin-expressing platelets (*P7*), due to the formation of a more extended platelet monolayer. For the VWF/fibrinogen spots, ticagrelor reduced the majority of parameters (Figure S3C). As shown in the subtraction heatmap of all univariate scaled parameters *P1-8*, the extra addition of SHP099 to ticagrelor-preincubated blood resulted in a slight increase of only platelet deposition (*P2*, $p<0.05$) and fibrinogen binding (*P8*, $p<0.05$) for the high collagen concentration versus control conditions (Figure 2B). Together, these results indicated that inhibition of SHP2 increased the thrombus characteristics parameters on collagens in a manner that was independent of the P2Y$_{12}$ pathway.

6

Inhibition of SHP2 with SHP099 restores low thrombus formation of Noonan patients

Noonan syndrome patients with a gain-of-function mutation in the *PTPN11* gene encoding for SHP2, are described to display hemostatic abnormalities including a platelet function defect and an impaired thrombus growth [10,14]. Based on previously described cohorts [28,29], we included six Noonan patients with characteristic phenotypes and defined (likely) pathogenic mutations in the *PTPN11* gene, linked to a gain-of-function, and a variable but mild bleeding tendency (Table 1). Hematological characteristics of the patient blood samples showed mostly similar values in comparison to the day-control subjects, with the exception of a lower mean corpuscular volume and hemoglobin of the red blood cells (Table 2). Platelet aggregation tests, as a diagnostic routine performed with the blood samples showed low values for at least one of the agonists, ADP, collagen, or TRAP6, for NS patients 2, 4, and 5 (Table 3). Other platelet function tests, such as PFA closure time and release of ADP and platelet factor 4 (PF4) were within normal ranges.

Blood samples from the 6 patients (NS1-6) and 6 daily control subjects were perfused over high and low collagen microspots, and thrombus parameters were examined as described above. Note that because of the young age of the patients (6-13 years old), only small blood samples were available. On both high and low collagen surfaces, the blood from patient 1, with normal diagnostic values of platelet function tests, showed low platelet adhesion, aggregate formation, and platelet activation staining when compared to the blood from day control 1 (Figure 3A). Interestingly, pre-incubation of the patient's blood with SHP2 inhibitor SHP099 increased these processes (in comparison to the vehicle) similar to the thrombus formation seen for the control subject.

Comparing the scaled thrombus parameters for each of the 6 patients to the mean values of control subjects, we observed a variable reduction regarding one or more parameters at high and low collagen concentrations, which disappeared in the presence of SHP099 (Figure 3B). The alterations were more clearly visible when expressed as subtracted heatmaps versus means of control subject values. For patients NS1-6, one to seven parameters were lower than controls for each collagen concentration (Figure 3C, green color). The exception was platelet deposition (*P1*), which always was unchanged. On the other hand, in the presence of SHP099, this reduction versus controls disappeared with the high collagen concentration and turned into an increase for three to seven parameters at low collagen concentration (Figure 3C, red color). The exception was patient NS4, where SHP099 addition was without clear effect, with consequently a reduction in most parameters when compared to the control subjects. All these differences were observed even when for each patient a threshold of mean ± SD of the daily control was applied (Figure S4). Hence, this heatmap pointed to an overall SHP099-dependent normalization or even increase (at low collagen) of the thrombus-forming process for the majority of patients.
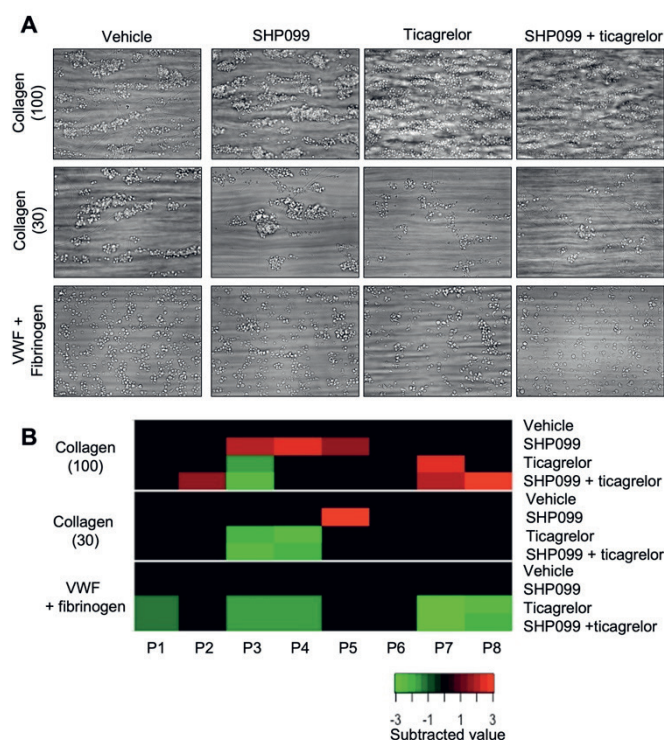
Figure 2. Increased collagen-induced thrombus characteristics by SHP2 inhibitor SHP099. Whole blood was perfused over in total three 1 μL microspots of collagen (100 μg/mL), collagen (30 μg/mL), and VWF (50 μg/mL) plus fibrinogen (250 μg/mL), at a wall-shear rate of 1000 s^{-1} for 3.5 min under non-coagulating conditions. Blood samples were pre-treated with SHP099 (10 μM, 30 min), ticagrelor (10 μM, 10 min), or vehicle (DMSO <0.5%) at room temperature. Platelet deposition, thrombus formation, and platelet activation were monitored by brightfield and multicolor microscopy. (**A**) Representative brightfield microscopic images per surface at end stage. Scale bar = 50 μm. (**B**) Subtraction heatmap of SHP099 effects for univariate-scaled parameters, filtered for relevant changes ($p<0.05$, paired Student's t-test). Parameters: *P1*, morphological score; *P2*, platelet deposition (SAC%); *P3*, thrombus contraction score; *P4*, thrombus multilayer score; *P5*, thrombus multilayer (SAC%); P6, phosphatidylserine exposing platelets (SAC%); *P7*, P-selectin (SAC%); *P8*, fibrinogen binding (SAC%). Color codes represent a decrease (green) or increase (red) in comparison to the control condition (n = 5 donors). See Figure S3A-C for raw data per surface and parameter.

Table 1. Genetics and bleeding scores of included Noonan syndrome (NS) patients. Bleeding score based on bruising. For a description of the analysis of patient diagnosis and genetics, see Ref. [29]. All variants are reported in ClinVar [30] and evidence of increased catalytic activity has been reported experimentally or *in silico* [15,31-35].

Patients	Gene	Mutation in DNA	Mutation in protein	Bleeding score
NS1	*PTPN11*	c.1510A>G	p.Met504Val	1
NS2	*PTPN11*	c.205G>C	p.Glu69Gln	1
NS3	*PTPN11*	c.1510A>G	p.Met504Val	0
NS4	*PTPN11*	c.922A>G	p.Asn308Asp	2
NS5	*PTPN11*	c.1507G>A	p.Gly303Arg	0
NS6	*PTPN11*	c.1529A>G	p.Gln510Arg	1

Table 2. Hematological parameters for Noonan syndrome (NS) patients and daily controls. Values (reference ranges) WBC (4.0-10.0), white blood cell count; RBC (3.5-5.9), red blood cell count; HGB (7.4-18), hemoglobin; HCT (0.35-0.52), hematocrit; MCV (80-100), mean corpuscular volume, MCH (1600-2100), mean corpuscular hemoglobin; MCHC (19-23), mean corpuscular hemoglobin concentration; PLT (150-400), platelet count. Red = below the reference range. *Abbreviations:* M, male; F, female.

	NS1	NS2	NS3	NS4	NS5	NS6	Day controls (SD)
WBC (10^9/L)	4.1	6.0	6.8	3.5	8.2	4.6	3.3-7.4 (1.5)
RBC (10^{12}/L)	4.52	4.50	4.57	5.22	4.95	3.72	3.74-4.80 (0.37)
HGB (mM)	7.5	7.8	7.5	8.5	8.8	<u>5.8</u>	7.0-8.8 (0.69)
HCT (L/L)	0.35	0.35	0.36	0.40	0.36	<u>0.28</u>	0.34-0.41 (0.03)
MCV (fL)	<u>77.2</u>	<u>78.2</u>	<u>79.4</u>	<u>76.2</u>	<u>73.1</u>	<u>76.3</u>	84.6-95.3 (4.4)
MCH (amol)	<u>1639</u>	1733	<u>1641</u>	<u>1628</u>	1778	<u>1559</u>	1773-1962 (62)
MCHC (mM)	21.5	22.2	20.7	21.4	24.3	20.4	19.8-21.7 (0.7)
PLT (10^9/L)	157	<u>138</u>	219	206	224	309	143-377 (93)
Sex	M	M	F	M	M	F	M (2) F (4)
Age	13	12	13	13	5	4	>22

Table 3. Platelet function analyzer (PFA) and light transmission aggregometry results of Noonan syndrome (NS) patients. Platelet release of ADP, ATP, and platelet factor 4 (PF4) was measured by mass spectrometry. For use of diagnostics tests, see Refs. [13,29]. Values of diagnostic tests below normal ranges are indicated in red (low). AA, arachidonic acid; Coll., collagen; Eph, epinephrine. Low levels below reference ranges are underlined.

| NS Patient	PFA coll.-ADP (s)	PFA coll.-eph. (s)	Light transmission aggregometry					Release (per 10^8 platelets)		
			ADP (5 µM)	Coll. (2 µg/mL)	AA (1 mM)	TRAP6 (15 µM)	Eph. (5 µM)	ADP (nmol)	ATP/ADP (ratio)	PF4 (µg)
NS1	91	125	Normal	Normal	Normal	Normal	Normal	4.3	1	1.6
NS2	137	202	Normal	Normal	Normal	<u>Low</u>	Normal	3.5	1.1	-
NS3	74	127	Normal	Normal	Normal	Normal	Normal	2.6	1.4	1.1
NS4	158	198	<u>Low</u>	<u>Low</u>	Normal	<u>Low</u>	Normal	3.5	1.3	1.3
NS5	93	132	Normal	<u>Low</u>	Normal	<u>Low</u>	Normal	2.5	1.2	1.1
NS6	122	168	Normal	Normal	Normal	Normal	Normal	3.3	1.2	1.1
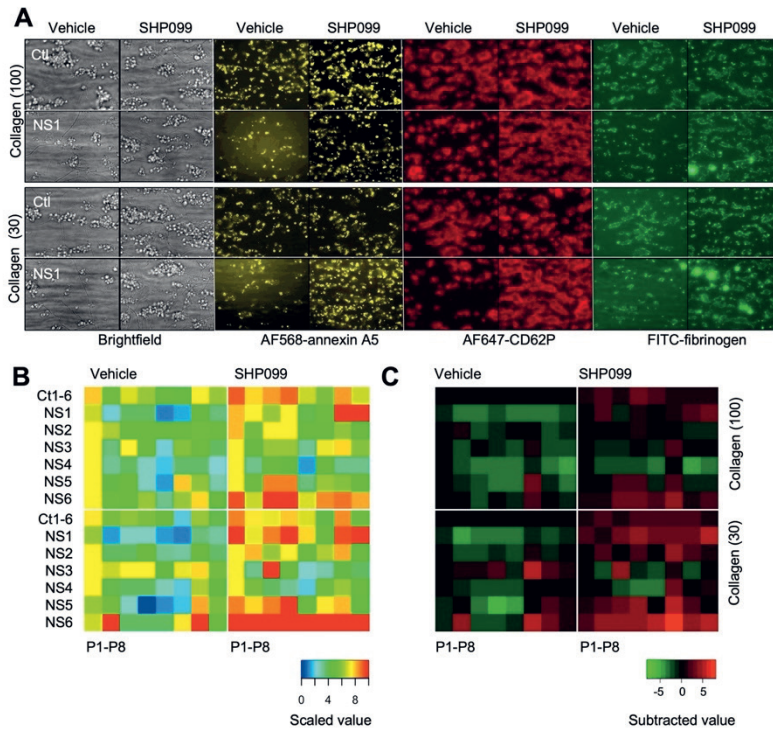
Figure 3. Restored whole-blood thrombus formation in Noonan patients by SHP099. Whole blood from day control subjects and Noonan patients was perfused over microspots of collagen (100 µg/mL) and collagen (30 µg/mL) at 1000 s^{-1} for 3.5 min under non-coagulating conditions. Samples were pre-treated with vehicle (DMSO <0.5%) or SHP099 (10 µM). Microscopy was performed as in Figure 2. (**A**) Representative brightfield and fluorescence microscopic images at end stage. Scale bar = 50 µm. Mean values from individual samples with(out) SHP099 were univariately scaled (0-10) per parameter across surfaces. (**B**) Heatmap of scaled thrombus parameters for high and low collagen microspots in the absence or presence of SHP099. (**C**) Subtraction heatmap illustrating difference versus the mean of control subjects. Color codes represent decreases (green) or increases (red) in comparison to control subjects (n=6 day control subjects, 6 patients). Parameters *P1-8* as in Figure 2.

Enhanced thrombus parameters and blood clotting under coagulation conditions by SHP099

Considering that in hemostasis also tissue factor-induced thrombin generation can play a role, we also studied the effects of SHP099 on thrombus formation parameters in the presence of tissue factor and coagulation. For this purpose, a modification of the microfluidic assay was used in which microspots of collagen were co-coated with tissue factor and the citrated blood sample was continuously recalcified during flow [26]. Microscopic images were taken every 2 min to follow the kinetics of platelet deposition, thrombus buildup, and platelet-dependent fibrin formation over time [36]. In this protocol, the SHP099-treated blood from control subjects showed a shorter time to fibrin formation (Figure 4A). This was accompanied by a higher platelet deposition (Figure 4B) and a tendency to increase thrombus multilayer formation (Figure 4C) at later time points.

Finally, we assessed the contribution of platelet SHP2 in clot contraction using the whole-blood rotational thromboelastometry viscoelastic test in the so-called APTEM mode with tranexamic acid to inhibit fibrinolysis. The obtained thromboelastic curves indicated consistent, but small SHP099 effects such as an increased clot firmness, degree of fibrin-clot cross-linking, thromboelastic clotting amplitude, and area under the clotting curve (Figure 5). Given that clot-contracting platelets are responsible for most of the amplitude of thromboelastic curves [37], these results agree with the platelet-dependent and clot-suppressing role of SHP2.
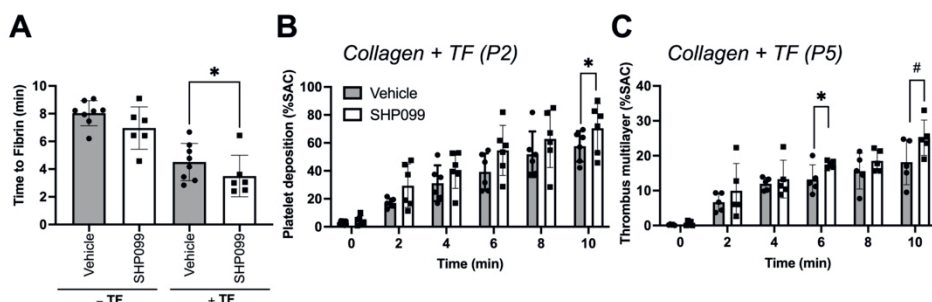
Figure 4. Increased collagen-induced whole-blood clot formation under flow by SHP099. Whole blood was co-infused with recalcification medium and perfused through a flow chamber containing 1 μL microspots of collagen (50 μg/mL, upstream) and collagen plus tissue factor (TF, 250 pM, downstream) at a wall-shear rate of $1000 \ s^{-1}$. Blood samples were pre-treated with vehicle (DMSO <0.5%) or SHP099 (10 μM). Brightfield images were captured every 2 min. (**A**) Bar graphs of time to fibrin formation per surface. (**B**, **C**) Platelet deposition and thrombus multilayer (SAC%) were measured over time for the microspot containing TF. Data are means ± SD (n=6 donors), *$p<0.05$ *vs.* control, #$p=0.076$ (paired Student's t-test).
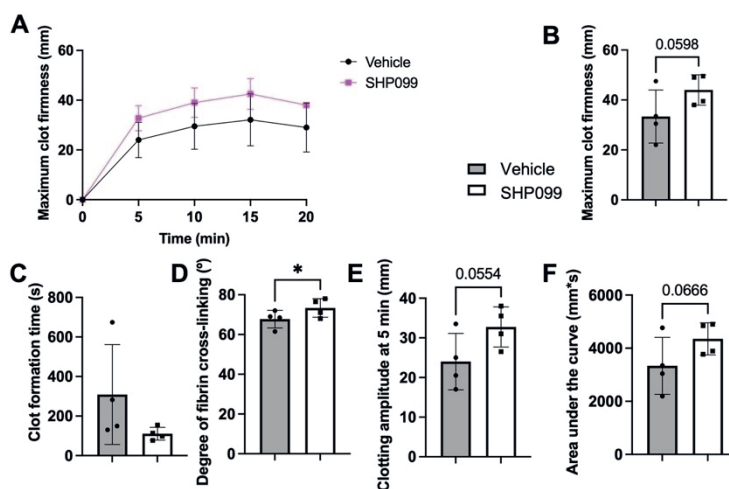
Figure 5. Tendency to increase whole-blood clot elasticity by SHP099. Whole-blood samples were analyzed by thromboelastometry using ROTEM in APTEM mode. Stimulation was with tissue factor in the presence of tranexamic for 20 min. Blood samples were pre-treated with vehicle (DMSO <0.5%) or SHP099 (10 μM). (**A**) Changes in elastometric amplitude over time. Bar graphs of (**B**) final maximum clot firmness, (**C**) clot formation time, (**D**) degree of fibrin cross-linking parameter, (**E**) clotting amplitude at 5 min, and (**F**) final area under the curve. Data are means ± SD (n=4 donors), *$p<0.05$ *vs.* vehicle (paired Student's t-test).

Discussion

The present study indicates that the pharmacological inhibition of the platelet tyrosine phosphatase SHP2 by SHP099 resulted in minor stimulating effects on low-dose CRP-induced platelet responses. On the other hand, in whole-blood perfusion over collagen the compound SHP099 caused a consistent increase in thrombus build-up and accelerate platelet-dependent fibrin formation in tissue factor conditions. Moreover, SHP2 inhibition with SHP099 led to a normalization of thrombus formation on collagen in the majority of Noonan syndrome patients with a gain-of-function mutation in *PTPN11*. Thus, these results indicate that the consequences of a hyperactive SHP2 due to gain-of-function mutations in the patient's platelets were antagonized by pharmacological inhibition of the phosphatase.

Noonan syndrome is an autosomal dominant disorder that in about half of the cases is linked to gain-of-function mutations in the *PTPN11* gene. Noonan patients present with developmental defects such as facial dysmorphism, heart defects, and short stature, suggesting a modulating role of SHP2 in development [4,38,39]. On a biochemical level, the gain-of-function variants are considered to result in a hyperactive SHP2 form, in which the auto-inhibitory status of the enzyme is disrupted or the substrate binding ability in the catalytic pocket is enhanced [40]. The mutations also predispose to juvenile myelomonocytic leukemia-like myeloproliferative neoplasm [41], and the risk of blood tumors or solid tumors is estimated to be eight times higher than in the general population [41,42]. Guidelines for the symptomatic treatment of Noonan syndrome indicate the use of recombinant human growth hormone [43]. In addition, part of the patients suffer from easy cutaneous bruising and mucosal bleeding, and bleeding diathesis, which has been linked to a partial platelet dysfunction [13].

Although in the present study patient numbers are too low to draw clinical conclusions, it is interesting to note that we observed a relatively low collagen-induced thrombus formation using blood from three of the patients (NS1, 2, 4, and 5) with a mild bleeding phenotype. However, the blood from NS4 did not appear to respond to SHP099 addition, for unknown reasons that could be either acquired or genetic. Nevertheless, the current data overall suggest that pharmacological SPH2 inhibition in such patients may help to regulate the hemostatic process caused by mutated SHP2.

The targeting of SHP2 is proposed to be beneficial in myeloproliferative disorders, characterized by the overproduction of platelets due to elevated signaling of the thrombopoietin receptor MPL, in which SHP2 is involved [44,45]. On the other hand, SHP2 inhibitors are reported to be specific but due to high similarity with SHP1 caution is needed for off-target effects caused by SHP1, due to its negative regulatory role in signaling pathways of hematopoietic cells and autoimmune regulation [8]. Previous studies using single and double SHP2 and SHP1 platelet/megakaryocyte knockout mice revealed a complex phenotype and non-redundant functions of the two phosphatases in platelet functions [7].

Our results indicate that SHP2 inhibition increased the collagen-induced thrombus build-up and contraction, which is in agreement with a role in thrombus formation in

6

published mice models [7,9,10]. It is reported that loss of SHP2 catalytic activity amplifies platelet responses to collagen in a shear stress-dependent manner in mutated mice or SHP2-inhibited human blood [9,10]. Currently, SHP2 inhibitors are being tested in clinical trials as a single treatment or as combination therapy with other anti-cancer/chemotherapeutic agents to enhance the SHP2 inhibitory potential, such as reviewed elsewhere [4,46]. Given that the SHP2 phosphatase is abundantly expressed and is involved in various physiological processes, potential side effects may arise during the treatment of cancers in different cell types [4]. Local drug administration may be one of the ways to reduce these side effects [47]. The clinical trials will also reveal how pharmacological inhibition of SHP2 affects human megakaryocytopoiesis, in a way as observed in SHP2 knockout mice [7]. Preliminary results of TNO155, a selective, allosteric, oral inhibitor of SHP2 indicated that a decreased platelet count was observed in only 4% of the patients undergoing treatment [48].

Patients with a loss-of-function mutation of *PTPN11*, presenting with the rarer Noonan Syndrome with Multiple Lentigines (previously called Leopard syndrome) appear to have normal platelet aggregation responses to low collagen [10]. Also, ablation in the megakaryocyte/platelet lineage of the *Ptptn11* gene in mice resulted in platelets with normal responses to low CRP [7,10]. However, a loss-of-function mutation of *Ptpn11* in mice resulted in enhanced platelet aggregation with CRP accompanied by an increased $\alpha IIb\beta 3$ activation [10]. These findings are in general agreement with our results, indicating a slight increase by SHP2 inhibition of CRP-induced integrin $\alpha IIb\beta 3$ activation. On the other hand, we observed no clear changes in tyrosine phosphorylation patterns in SHP2-inhibited platelets upon stimulation with low or high CRP concentrations.

Although the role of platelet SHP2 on platelet activation has been explored in previous reports, most of them have used mouse models [7,9,10]. Only one study used Noonan syndrome patients to assess the effect of gain- and loss-of-function mutations in platelets [10]. Inter-species differences may reveal different results, accordingly, pharmacological studies can help establish SHP2's role in platelet function avoiding also the developmental defects observed in megakaryocytes due to SHP2 knockout in mice models [7]. By using the pharmacological SHP2 inhibitor SHP099, our study showed the conserved role of SHP2 in humans and mice. In the present study, we mainly focus on SHP2-dependent GPVI and CRP-induced integrin $\alpha IIb\beta 3$ activation effects. Other studies in mice have found that SHP2-integrin-dependent effects are mediated by TxA_2 pathway [9], so further research is needed to corroborate this in human platelets.

Conclusion

In conclusion, this study presents an extensive evaluation of SHP2 inhibition in human platelets, particularly on collagen-dependent thrombus formation in blood from control subjects and Noonan patients. The main observed effects of SHP2 inhibition require the presence of shear and/or coagulation. In Noonan patients, *ex vivo* SHP099 treatment showed normalization of platelet function to control levels in microfluidic assays. This result

underlines the value of a potential treatment option for these patients to improve their platelet function and hemostatic potential.

Acknowledgments

Authors contributions

Conceptualization and formal analysis, DIF, MD. Investigation, DIF, MD, LHN, JH, SV. Resources, JWMH, AG, MWMtL. Writing - original draft preparation, DIF, MJEK, AG. Writing - review and editing, DIF, MJEK, JWMH, AG. Visualization, DIF, JWMH. Supervision, JWMH, YMCH, MJEK, AG. Funding acquisition, JWMH, MWMtL, AG. All authors have read and agreed to the submitted version of the manuscript.

Conflicts of interest

The authors declare no relevant conflicts of interest.

References

1.   Saxton TM, Henkemeyer M, Gasca S, et al. Abnormal mesoderm patterning in mouse embryos mutant for the SH2 tyrosine phosphatase Shp2. *EMBO J.* 1997;16:2352-2364.

2.   Song Y, Wang S, Zhao M, Yang X, Yu B. Strategies targeting protein tyrosine phosphatase SHP2 for cancer therapy. *J Med Chem.* 2022;65:3066-3079.

3.   Shen D, Chen W, Zhu J, et al. Therapeutic potential of targeting SHP2 in human developmental disorders and cancers. *Eur J Med Chem.* 2020;190:112117.

4.   Liu Q, Qu J, Zhao M, Xu Q, Sun Y. Targeting SHP2 as a promising strategy for cancer immunotherapy. *Pharmacol Res.* 2020;152:104595.

5.   Faria AV, Andrade SS, Peppelenbosch MP, Ferreira-Halder CV, Fuhler GM. The role of phospho-tyrosine signaling in platelet biology and hemostasis. *Biochim Biophys Acta.* 2021;1868:118927.

6.   Heemskerk JW. More than reverting tyrosine kinases. *Blood.* 2022;140:939-941.

7.   Mazharian A, Mori J, Wang YJ, et al. Megakaryocyte-specific deletion of the protein-tyrosine phosphatases Shp1 and Shp2 causes abnormal megakaryocyte development, platelet production, and function. *Blood.* 2013;121:4205-4520.

8.   Tautz L, Senis YA, Oury C, Rahmouni S. Perspective: tyrosine phosphatases as novel targets for antiplatelet therapy. *Bioorg Med Chem.* 2015;23:2786-2797.

9.   Hu M, Liu P, Liu Y, et al. Platelet Shp2 negatively regulates thrombus stability under high shear stress. *J Thromb Haemost.* 2019;17:220-231.

10. Bellio M, Garcia C, Edouard T, et al. Catalytic dysregulation of SHP2 leading to Noonan syndromes affects platelet signaling and functions. *Blood.* 2019;134:2304-2317.

11. Wong C, Liu Y, Yip J, et al. CEACAM1 negatively regulates platelet-collagen interactions and thrombus growth in vitro and in vivo. *Blood.* 2009;113:1818-1828.

12. Mazharian A, Wang YJ, Mori J, et al. Mice lacking the ITIM-containing receptor G6b-B exhibit macrothrombocytopenia and aberrant platelet function. *Sci Signal.* 2012;5:ra78.

13. Tartaglia M, Mehler EL, Goldberg R, et al. Mutations in PTPN11, encoding the protein tyrosine phosphatase SHP2, cause Noonan syndrome. *Nat Genet.* 2001;29:465-468.

14. Artoni A, Selicorni A, Passamonti SM, et al. Hemostatic abnormalities in Noonan syndrome. *Pediatrics.* 2014;133:e1299-1304.

15. Tartaglia M, Niemeyer CM, Fragale A, et al. Somatic mutations in PTPN11 in juvenile myelomonocytic leukemia, myelodysplastic syndromes and acute myeloid leukemia. *Nat Genet.* 2003;34:148-150.

16. Bentires-Alj M, Paez JG, David FS, et al. Activating mutations of the Noonan syndrome-associated SHP2/PTPN11 gene in human solid tumors and adult acute myelogenous leukemia. *Cancer Res.* 2004;64:8816-8820.

17. Garcia Fortanet J, Chen CH, Chen YN, et al. Allosteric inhibition of SHP2: identification of a potent, selective, and orally efficacious phosphatase inhibitor. *J Med Chem.* 2016;59:7773-7782.

18. Chen YN, LaMarche MJ, Chan HM, et al. Allosteric inhibition of SHP2 phosphatase inhibits cancers driven by receptor tyrosine kinases. *Nature.* 2016;535:148-152.

19. Chen H, Libring S, Ruddraraju KV, et al. SHP2 is a multifunctional therapeutic target in drug resistant metastatic breast cancer. *Oncogene.* 2020;39:7166-7180.

20. Liu C, Lu H, Wang H, et al. Combinations with allosteric SHP2 inhibitor TNO155 to block receptor tyrosine kinase signaling. *Clin Cancer Res.* 2021;27:342-354.

21. Kong J, Long YQ. Recent advances in the discovery of protein tyrosine phosphatase SHP2 inhibitors. *RSC Med Chem.* 2022;13:246-257.

22. Izquierdo I, Barrachina MN, Hermida-Nogueira L, et al. A comprehensive tyrosine phosphoproteomic analysis reveals novel components of the platelet CLEC-2 signaling cascade. *Thromb Haemost.* 2020;120:262-276.

23. Grynkiewicz G, Poenie M, Tsien RY. A new generation of Ca^{2+} indicators with greatly improved fluorescence properties. *J Biol Chem.* 1985;260:3440-3450.

24. Van Geffen JP, Brouns S, Batista J, et al. High-throughput elucidation of thrombus formation reveals sources of platelet function variability. *Haematologica.* 2019;104:1256-1267.

25. De Witt SM, Swieringa F, Cavill R, et al. Identification of platelet function defects by multi-parameter assessment of thrombus formation. *Nat Commun.* 2014;5:4257.

26. Swieringa F, Baaten CC, Verdoold R, et al. Platelet control of fibrin distribution and microelasticity in thrombus formation under flow. *Arterioscler Thromb Vasc Biol.* 2016;36:692-699.

27. Huang J, Jooss NJ, Fernandez DI, et al. Roles of focal adhesion kinase PTK2 and integrin aIIbb3 signaling in collagen- and GPVI-dependent thrombus formation under shear. *Int J Mol Sci.* 2022;23:8688.

28. Van den Burgt I, Berends E, Lommen E, van Beersum S, Hamel B, Mariman E. Clinical and molecular studies in a large Dutch family with Noonan syndrome. *Am J Med Genet.* 1994;53:187-191.

29. Van der Burgt I. Noonan syndrome. *Orphanet J Rare Dis.* 2007;2:4.

30. Landrum MJ, Lee JM, Benson M, et al. ClinVar: improving access to variant interpretations and supporting evidence. *Nucleic Acids Res.* 2018;46:D1062-D1067.

31. Tartaglia M, Martinelli S, Stella L, et al. Diversity and functional consequences of germline and somatic PTPN11 mutations in human disease. *Am J Hum Genet.* 2006;78:279-290.

32. Niihori T, Aoki Y, Ohashi H, et al. Functional analysis of PTPN11/SHP-2 mutants identified in Noonan syndrome and childhood leukemia. *J Hum Genet.* 2005;50:192-202.

33. Musante L, Kehl HG, Majewski F, et al. Spectrum of mutations in PTPN11 and genotype-phenotype correlation in 96 patients with Noonan syndrome and five patients with cardio-facio-cutaneous syndrome. *Eur J Hum Genet.* 2003;11:201-206.

34. Athota JP, Bhat M, Nampoothiri S, et al. Molecular and clinical studies in 107 Noonan syndrome affected individuals with PTPN11 mutations. *BMC Med Genet.* 2020;21:50.

35. Bertola DR, Pereira AC, Passetti F, et al. Neurofibromatosis-Noonan syndrome: molecular evidence of the concurrence of both disorders in a patient. *Am J Med Genet A.* 2005;136:242-245.

36. Brouns S, van Geffen JP, Campello E, et al. Platelet-primed interactions of coagulation and anticoagulation pathways in flow-dependent thrombus formation. *Sci Rep.* 2020;10:11910.

37. Ninivaggi M, Feijge MA, Kuiper GJ, et al. Principal roles of platelets and fibrinogen in whole-blood fibrin clot formation in dilutional coagulopathy determined by thromboelastometry. *Thromb Haemost.* 2014;111:447-457.

38. Grossmann KS, Rosario M, Birchmeier C, Birchmeier W. The tyrosine phosphatase SHP2 in development and cancer. *Adv Cancer Res.* 2010;106:53-89.

39. Roberts AE, Allanson JE, Tartaglia M, Gelb BD. Noonan syndrome. *Lancet.* 2013;381:333-342.

40. Guo W, Liu W, Chen Z, et al. Tyrosine phosphatase SHP2 negatively regulates NLRP3 inflammasome activation via ANT1-dependent mitochondrial homeostasis. *Nat Commun.* 2017;8:2168.

41. Strullu M, Caye A, Lachenaud J, et al. Juvenile myelomonocytic leukaemia and Noonan syndrome. *J Med Genet.* 2014;51:689-697.

42. Kratz CP, Franke L, Peters H, et al. Cancer spectrum and frequency among children with Noonan, Costello, and cardio-facio-cutaneous syndromes. *Br J Cancer.* 2015;112:1392-1397.

43. Andelfinger G, Marquis C, Raboisson MJ, et al. Hypertrophic cardiomyopathy in Noonan syndrome treated by MEK inhibition. *J Am Coll Cardiol.* 2019;73:2237-2239.

44. Butterworth S, Overduin M, Barr AJ. Targeting protein tyrosine phosphatase SHP2 for therapeutic intervention. *Future Med Chem.* 2014;6:1423-1437.

45. Kanumuri R, Kumar Pasupuleti S, Burns SS, Ramdas B, Kapur R. Targeting SHP2 phosphatase in hematological malignancies. *Expert Opin Ther Targets.* 2022;26:319-332.

46. Wu J, Zhang H, Zhao G, Wang R. Allosteric inhibitors of SHP2: an updated patent review (2015-2020). *Curr Med Chem.* 2021;28:3825-3842.

47. Song Z, Wang M, Ge Y, et al. Tyrosine phosphatase SHP2 inhibitors in tumor-targeted therapies. *Acta Pharm Sin B.* 2021;11:13-29.

48. Brana I, Shapiro G, Johnson ML, et al. Initial results from a dose finding study of TNO155, a SHP2 inhibitor, in adults with advanced solid tumors. *J Clin Oncol.* 2021;39 (Suppl. 15):3005.

6

Supplemental Figures of Chapter 6
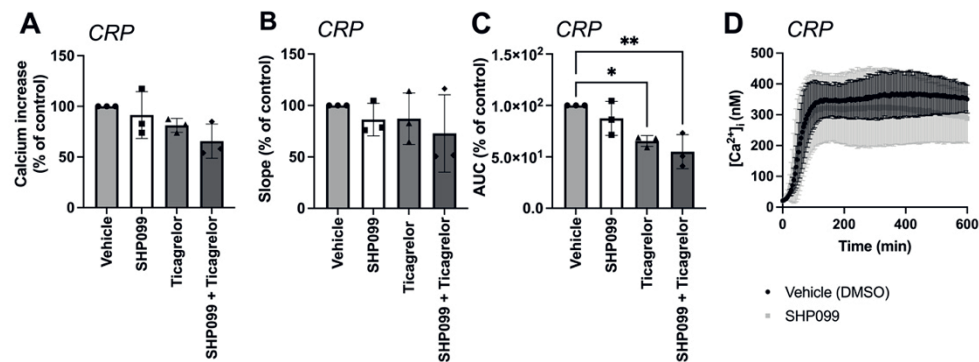
Figure S1. Effect of SHP099 on CRP-induced Ca^{2+} rises in platelets. Fura-2-loaded platelets (2×10^8/mL) were pre-incubated with vehicle (DMSO <0.5%), SHP099 (10 µM), ticagrelor (1 µM), or the combination of SHP099 and ticagrelor, and Changes in [Ca^{2+}]$_i$ in response to CRP (10 µg/mL) were recorded over 600 s using a FlexStation 3. (**A**) Quantification of maximal [Ca^{2+}]$_i$ rises at 600 s; (**B**) quantification of curve slope; and (**C**) and area under the curve. (**D**) Average Ca^{2+} traces. Data are means ± SD (n=3 donors), *p<0.05 (one-way ANOVA).
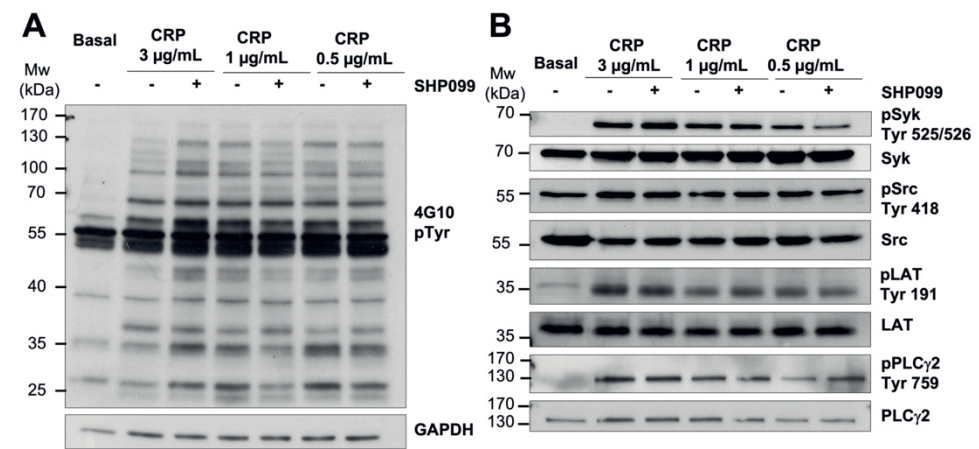
Figure S2. Effect of SHP099 on CRP-induced tyrosine phosphorylation in platelets. Representatives immunoblot from 5 independent experiments of platelet lysates (4×10^8/mL) pre-treated with vehicle (DMSO <0.5%) or SHP099 (10 µM) and stimulated with CRP (3, 1 and 0.5 µg/mL). Lysates were run by SDS-PAGE, transferred to a PVDF membrane, and incubated (**A**) with anti-tyrosine antibody (4G10), or (**B**) with antibodies against (p)Syk, (p)Src, (p)LAT, or (p)PLCγ2. Also indicated is the staining for loading control GAPDH.
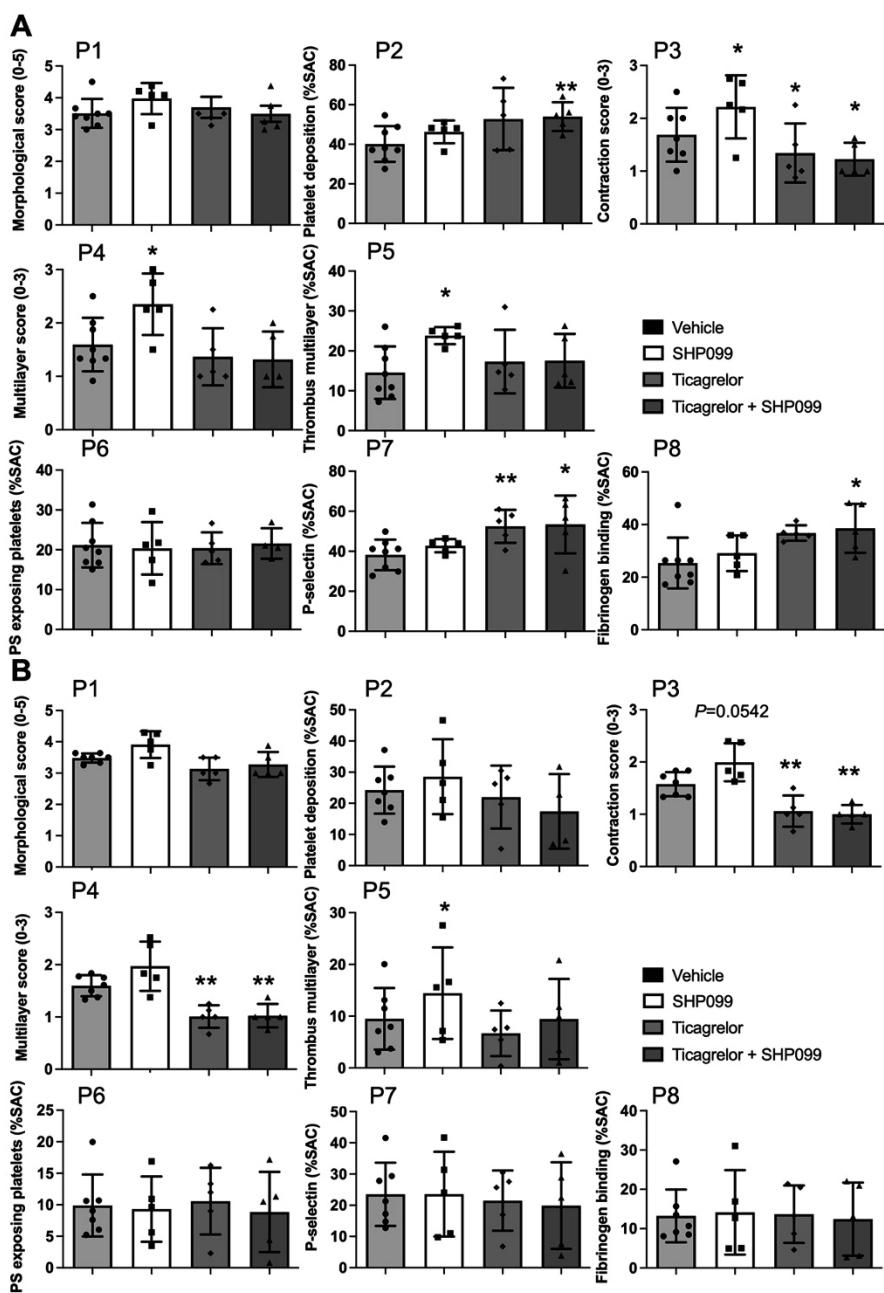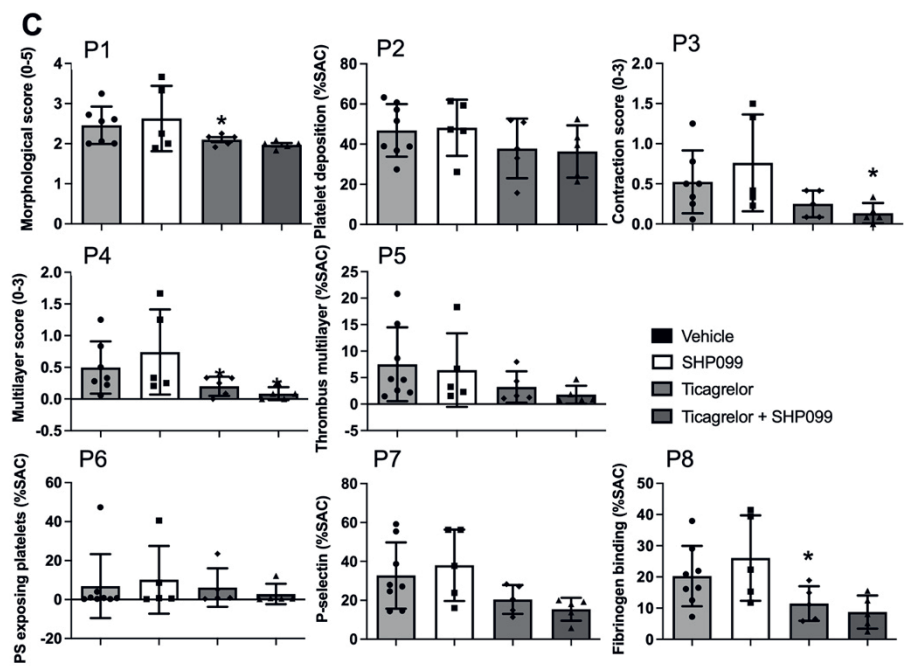
Figure S3. **Quantification of SHP099 effects on parameters of whole-blood thrombus formation under flow.** Whole blood thrombus formation was performed, as described in Figure 2. Histograms of parameter quantifications of thrombus formation in the presence of SHP099 (10 μM), ticagrelor (10 μM), or combination *vs.* control for (**A**) collagen (100 μg/mL), (**B**) collagen (30 μg/mL), (**C**) and VWF (50 μg/mL) plus fibrinogen (250 μg/mL) per parameter (*P1-8*). Data are means ± SD (n=5 donors), *$p<0.05$, **$p<0.01$ *vs.* control group (paired Student's t-test).
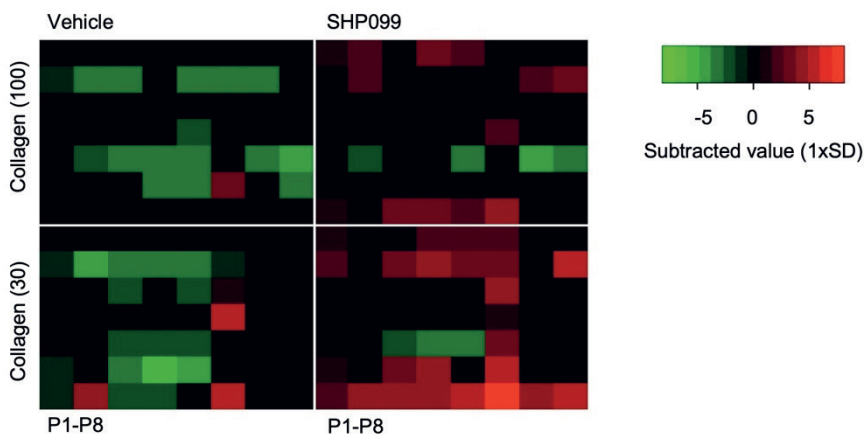
Figure S4. Restored whole-blood thrombus formation in Noonan patients by SHP099. Whole blood from day control subjects and Noonan patients was perfused over microspots of collagen (100 μg/mL) and collagen (30 μg/mL) at 1000 s^{-1} for 3.5 min under non-coagulating conditions. Samples were pre-treated with vehicle (DMSO <0.5%) or SHP099 (10 μM). Subtraction heatmap of thrombus parameters for high and low collagen microspots in the absence or presence of SHP099, as in Figure 3, filtered for 1 SD of the mean of daily controls. Color codes represent decreases (green) or increases (red) in comparison to control subjects (n=6 day control subjects, 6 patients). Parameters *P1-8* as in Figure 2.

6

7
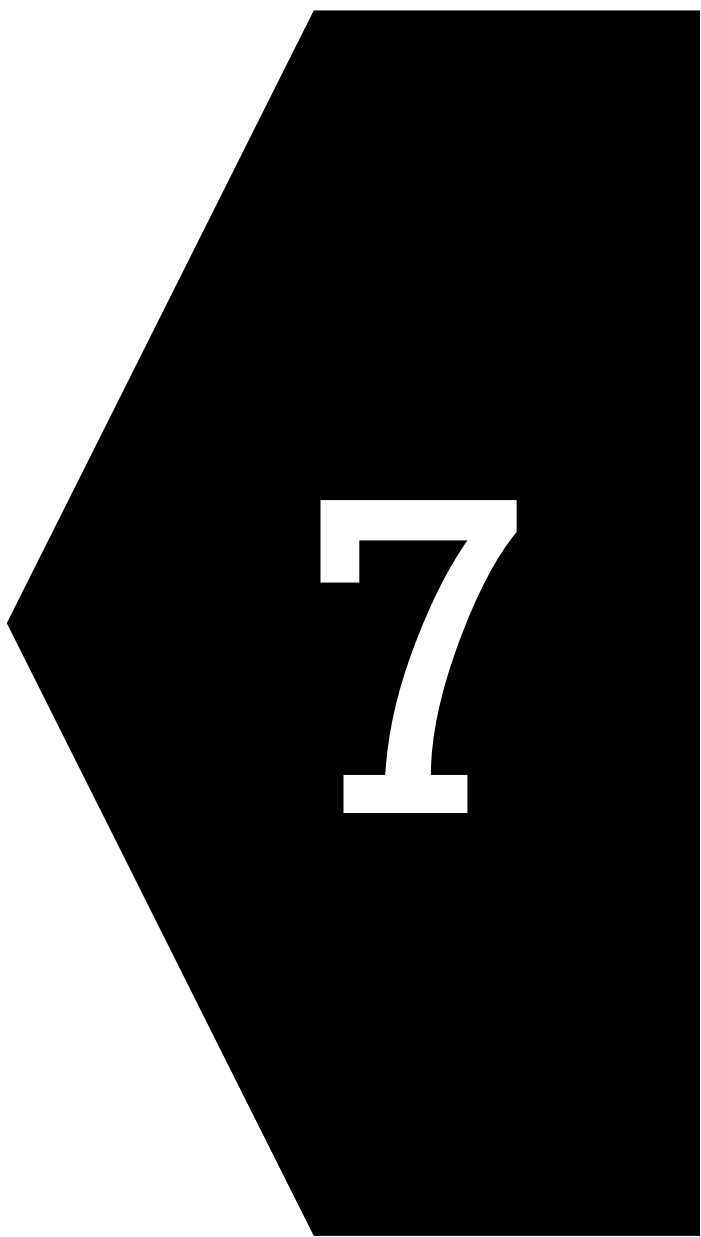
Chapter 7

Structure-based cyclic glycoprotein Ibα-derived peptides interfering with von Willebrand factor binding, affecting platelet aggregation under shear

Hrdinova J*, **Fernández DI***, Ercig B, Tullemans BME, Suylen DPL, Agten, SM, Jurk K, Hackeng TM, Vanhoorelbeke K, Voorberg J, Reutelingsperger, CPM, Wichapong K*, Heemskerk JWM*, Nicolaes GAF

Abstract

Plasmatic von Willebrand factor (VWF) circulates in a compact form unable to bind platelets. Upon shear stress, the VWF A1 domain is exposed, allowing VWF-binding to platelet glycoprotein Ib-V-IX (GPIbα chain). For a better understanding of the role of this interaction in cardiovascular disease, molecules are needed to specifically interfere with the opened VWF A1 domain interaction with GPIbα. Therefore, we *in silico* designed and chemically synthesized stable cyclic peptides interfering with the platelet-binding of the VWF A1 domain per se or complexed with botrocetin. Selected peptides (26–34 amino acids) with the lowest-binding free energy were: the monocyclic mono- vOn Willebrand factoR-GPIbα InTerference (ORbIT) peptide and bicyclic bi-ORbIT peptide. Interference of the peptides in the binding of VWF to GPIb-V-IX interaction was retained by flow cytometry in comparison with the blocking of anti-VWF A1 domain antibody CLB-RAg35. In collagen and VWF-dependent whole-blood thrombus formation at a high shear rate, CLB-RAg35 suppressed stable platelet adhesion as well as the formation of multilayered thrombi. Both peptides phenotypically mimicked these changes, although they were less potent than CLB-RAg35. The second-round generation of an improved peptide, namely opt-mono-ORbIT (28 amino acids), showed an increased inhibitory activity under flow. Accordingly, our structure-based design of peptides resulted in physiologically effective peptide-based inhibitors, even for convoluted complexes such as GPIbα-VWF A1.

Introduction

Von Willebrand factor (VWF) plays an important role in the control of hemostasis and onset of pathological arterial thrombosis [1,2]. Endothelial cells release VWF as ultra-large multimers into the blood, which are normally degraded by ADAMTS13 (a disintegrin and metalloprotease with thrombospondin type 1 motif 13) to a mixture of circulating large and small multimers [3,4]. In the blood, the VWF multimers assume a compact form, which prevents the binding to platelets [5]. However, at a high arterial shear rate and upon binding to collagen, the multimers elongate and undergo a conformational change. As a consequence, the VWF A1 domain becomes exposed and is able to bind to platelets via the large glycoprotein (GP)Ibα subunit of the GPIb-V-IX complex [6-8]. The antibiotic ristocetin induces a similar conformational change in VWF, which likewise induces GPIbα-VWF A1 binding [9]. The venom botrocetin binds to the VWF A1 domain potentiating its interaction with GPIbα chain [10,11].

Upon vascular damage or atherosclerotic plaque rupture, collagen-bound VWF, in a shear-dependent way, initiates thrombus formation through a fast onset of GPIb-V-IX binding and platelet adhesion [12-14]. The transient adhesion of platelets is considered to be stabilized by integrin αIIbβ3 binding to the RGD-sequence in the VWF C4 domain, which facilitates platelet activation via signaling of the collagen receptor, glycoprotein VI (GPVI) and the adhesive collagen receptor, integrin α2β1 [15-18]. Platelet activation leads to outside-in signaling via αIIbβ3 binding to VWF and fibrinogen, which then facilitates stable platelet arrest and ensuing platelet aggregate formation. At shear rates of 1000 s^{-1} and higher, initial platelet adhesion is known to be triggered by the interaction between unrolled filamentous VWF A1 and GPIbα [19]. In addition, it is proposed that under flow also homotypic VWF interactions support shear-dependent platelet aggregation and thrombus formation, *i.e.* at sites distant from the exposed collagen [15]. How these proposed multiple roles of VWF A1 contribute to the thrombosis process is still unclear.

For studying the molecular function of platelet GPIb-V-IX, it is important to have suitable drugs that interfere with the VWF-GPIbα interaction. Such drugs will also be of therapeutic interest, for example for the treatment of patients with immune-mediated thrombotic thrombocytopenic purpura (iTTP). Such patients are known to have hyperactive ultra-large multimers of VWF due to autoantibody-mediated inactivation or clearance of the VWF-cleaving protease ADAMTS13 [20,21]. Candidate drugs tested in this respect are mostly targeting the VWF A1 domain and aim to suppress ultra-large VWF-dependent platelet activation. These include nano/antibodies such as caplacizumab and KB-VWF-006bi [22,23], and the aptamers ARC1779 [24], ARC15105 [25], and BT200 [26]. In addition, a snake venom-derived peptide antagonist anfibatide (agkisacucetin) targets the GPIb-V-IX complex [27]. Yet, the precise molecular effects of these drugs are incompletely understood, and well-designed peptide-based antagonists affecting the VWF A1 domain may help to improve understanding of the multifaceted ligand interactions of platelets in arterial thrombus formation and, ultimately, provide a guide for novel therapeutics.

In recent years, peptide-based drugs are becoming of high interest, because of their small size, their ease of synthesis and modification, and good biocompatibility [28,29]. Peptides offer several advantages over antibody treatment, as they provide limited steric hindrance and low manufacturing costs. In the present study, we designed and synthesized several peptides interfering with the 'active' conformation of VWF, for functional studies of thrombus formation. The peptides were designed by utilization of *in silico* approaches, which we have successfully used to develop novel inhibitors for coagulation factor VIII [30], the signaling protein TRAF6 [31,32], the chemokine CCL5 [33], and extracellular histones [34,35]. For the present purpose, we employed two different strategies to design cyclic peptides that mimic the GPIbα binding surface at the VWF A1 domain (ORbIT: vOn Willebrand factoR-GPIbα Interference): one strategy used GPIbα as a structural template (mono-ORbIT), and the other used GPIbα in complex with botrocetin (bi-ORbIT). The latter mode is of interest, since botrocetin reduces the VWF A1-GPIb off-rate by two-folds. It initially binds to the VWF A1 domain, after which the complexed botrocetin forms a new interaction with GPIbα [11]. Two best-performing binding peptides *in silico* were selected for chemical synthesis, and subsequently experimentally tested for studying the GPIbα-VWF A1 interaction *in vitro* in a physiologically relevant whole-blood assay that operates at high wall-shear rate conditions. Based on the functional performance of the peptides, we performed another round of *in silico* design and synthesis using mono-ORbIT as a template, and again evaluated the inhibitory potential of the new *opt*-mono-ORbIT towards the VWF A1-GPIbα axis.

Materials and Methods

An extended version of the Materials section is available in the Supplement.

Materials

Collagen I (Horm-type) derived from equine tendon was obtained from Nycomed (Hoofddorp, The Netherlands). Human placenta-derived collagen-III (C4407) and bovine serum albumin (BSA) were obtained from Sigma-Aldrich (Zwijndrecht, The Netherlands). Human VWF native protein was purchased from ThermoFisher Scientific (RP-43132, Eindhoven, The Netherlands). Fibrinogen was obtained from Sigma-Aldrich (F-4129-16); DiOC$_6$ (3,3'-dihexyloxacarbocyanine iodide) from AnaSpec (AS-84715, Seraing, Belgium) and PPACK (D-phenylalanyl-L-propyl-L-arginine chloromethyl ketone) from Calbiochem (520222, Amsterdam, The Netherlands). For fluorescence staining, we used Alexa Fluor (AF)647-conjugated anti-CD62P mAb (304918, Biolegend, London, United Kingdom), FITC-labeled anti-fibrinogen mAb (F0111, Dako, Amstelveen, The Netherlands), and AF568-labeled annexin A5 (A13202, ThermoFisher). FITC-conjugated sheep anti-human VWF antibody was from Bio-Rad laboratories (AHP062F, Feldkirchen, Germany). Tirofiban (aggrastat) was from Iroko Cardio (Philadelphia, PA, USA). Ristocetin was from American Biochemical & Pharmaceuticals (London, United Kingdom). Other materials were also from Sigma-Aldrich.

Molecular dynamics and binding free energy calculations

The GPIbα-VWF A1 domain complex and the GPIbα-VWF A1-botrocetin complex (PDB code 1U0N) were subjected to molecular dynamics (MD) simulations, in order to identify key interacting residues at the interface, according to a previously established method [36,37]. Herein, AMBER14SB force fields were assigned for proteins and a TIP3P water model was used and added to a 10 Å radius of the molecular surface of the complex. Counter ions (Na^+ or Cl^-) were added in replacement of water to neutralize the system. Prior to running MD simulations, the complexes were relaxed by performing two consecutive steps: *(i)* 4000 steps of energy minimization (2000 steps of steepest descent, followed by 2000 steps of conjugate gradient algorithm) to minimize and adjust the positions of water molecules, while partially fixing the positions of proteins by use of a weak force constraint (10 kcal/mol·A^2); followed by *(ii)* energy minimization (5000 steps of steepest descent, followed by 5000 steps of conjugate gradient algorithm) of the whole complex without applying force constraint to fix the positions of atoms. Initial MD simulation was performed for 100 ps, while applying a weak force constraint (10 kcal/mol) to restrain the structure and slowly heat the system from 0 to 300 K. Subsequently, a free MD simulation phase was performed for 100 ns by setting the temperature at 300 °K, the pressure at 1 bar, and the time step at 2 fs with a SHAKE constraint.

The identified key interacting residues of GPIbα with VWF A1 domain [32] were used as a template to design a range of mono-cyclic peptides. Similarly, two sets of GPIbα and botrocetin residues were connected via different linkers – the disulfide bond or chemical linkage of peptides onto scaffolds [38] – to create bi-cyclic peptides. Several peptides were *in silico* designed and were consequently subjected to MD simulations (5 ns) and binding free energy (BFE) calculation to predict the relative binding affinity of the designed peptides with the VWF A1 domain. The peptides with the lowest BFE (predicted to be potent inhibitors) were selected for further synthesis and functional characterization.

The BFE of GPIbα-VWF A1, GPIbα-VWF A1-botrocetin, and VWF A1-peptide complexes was calculated by application of the method of molecular mechanics/generalized Born surface area (MM/GBSA). A generalized Born model 8 was applied using default parameter settings. Regarding the GPIbα-VWF A1 and GPIbα-VWF A1-botrocetin complexes, 100 snapshots were extracted from the last 10 ns (90-100 ns) of the molecular dynamics and taken for the BFE calculations. As described before [39], such a molecular dynamics simulation is sufficient to optimize the design of peptides and to estimate the relative BFE. Snapshots of 0-5 ns (500 snapshots) of the *in silico* VWF A1-peptide complexes were utilized for BFE assessments, using the program AMBER16.

Blood and platelet isolation

Blood from healthy volunteers was drawn through venipuncture. All volunteers did not receive antiplatelet medication for at least two weeks. All study subjects gave their full informed consent according to the Declaration of Helsinki and the studies were approved by

7

the local Medical Ethics Committee (Maastricht University Medical Centre[+], NL31480.068.10). Blood was collected into 3.2% trisodium citrate (Vacuette tubes, Greiner Bio-One, Alphen a/d Rijn, The Netherlands). All subjects had platelet counts within the reference range as measured by the Sysmex XN-9000 analyzer (Sysmex, Cho-ku, Kobe, Japan). Platelet-rich plasma (PRP) was isolated from citrate-anticoagulated blood samples, as previously described [10].

Flow cytometric assessment of platelet GPIbα-VWF A1 interaction

The PRP was diluted 1:8 with phosphate-buffered saline (PBS) and treated with tirofiban (1.25 µg/mL) to prevent integrin αIIbβ3-mediated aggregation of platelets. The GPIbα-derived peptides (200 µg/mL) or CLB-RAg35 mAb (5 µg/mL) were pre-incubated with the diluted PRP for 10 min at room temperature. The mixtures were subsequently activated with either ristocetin (0.5 mg/mL) or botrocetin (5 µg/mL) for 6 min at room temperature. The samples were then fixed with 0.5% formaldehyde for 30 min at room temperature. Fixed platelets were washed with 500 µL PBS and pelleted at 800 g for 10 min. Supernatants were then discarded, leaving a residual volume of 100 µL of platelet-containing pellet. The platelets were then labeled with FITC anti-VWF antibody (1:2000) for 30 min, and analyzed using a FACS Canto II (BD Biosciences, San Jose, CA, USA) [10].

Assessment of shear-dependent whole blood thrombus formation

Microspots of collagen-I, -III, and VWF were applied on glass coverslips as 0.5 µL microspots, as described previously [40]. Briefly, three consecutive microspots of collagen-I (100 µg/mL), collagen-III (100 µg/mL), and VWF/fibrinogen (50/250 µg/mL) were applied on washed coverslips. The coated amount was chosen to obtain maximal platelet adhesion in flow assays [41]. The most active microspot, in this case, collagen-I, was located downstream to prevent the cross-activation of platelets during perfusion [41]. Coated coverslips were maintained in a humid chamber for 1 h at room temperature, and then blocked with blocking buffer (HEPES buffer pH 7.45, 1% BSA) for 30 min before assembly into the Maastricht microfluidic chamber [42].

Samples of 600 µL of citrated whole blood were pre-incubated for 10 min with either saline, inhibitory CLB-RAg35 mAb (10 µg/mL), or one of the GPIbα-derived peptides (20 µg/mL). The 10-min pre-incubation time was employed to allow homogeneous dispersion of the bicyclic peptide that tended to form aggregates in stock solution. After incubation, 40 µM PPACK was added and the blood was recalcified (final concentrations: 3.75 mM MgCl$_2$ and 7.5 mM CaCl$_2$). Whole-blood perfusion through the microspot-containing flow chamber was performed for 3.5 min at a high wall-shear rate of 1600 s^{-1}. Staining was then performed by 2 min perfusion with AF647 anti-CD62P mAb (for P-selectin expression), FITC anti-fibrinogen mAb (for integrin αIIbβ3 activation), and AF568-annexin A5 (for phosphatidylserine exposure) [40]. The residual label was removed by postperfusion at 1000 s^{-1} with HEPES buffer pH 7.45, containing 2 mM CaCl$_2$ and 1 U/mL heparin. All conditions were measured in duplicate using blood obtained from ≥ 5 healthy

donors.

Real-time brightfield and fluorescence microscopy

Per microspot, two brightfield images and three fluorescence images (overlays) were taken using an EVOS-FL microscope (Life Technologies, Bleiswijk, The Netherlands) equipped with three LED diode cubes (Cy5 626 nm, GFP 470 nm, and RFP 531 nm); an Olympus UPLSAPO 60× oil-immersion objective and a 1360 × 1024-pixel CCD camera [40,43]. The images were analyzed with standardized, semi-automated scripts in Fiji (ImageJ) calculating surface area coverage (%) platelet deposition (*P1*), thrombus aggregate (*P5*) and platelet activation (CD62P expression, fibrinogen binding, and phosphatidylserine exposure; *P6-8*), and by visual inspection compared with representative images for morphology score (*P2*), thrombus contraction score (*P3*) and thrombus multilayer score (*P4*), as described [40].

Statistics and data analysis

Statistical analysis was performed in GraphPad Prism 8 (GraphPad Software, La Jolla, CA, USA). Heatmaps were generated in R package version 2.3. In the heatmap representation, mean parameter values were univariate-normalized at a scale of 0-10 [40]. Parameter sets for one donor were obtained by averaging the values of duplicate (or triplicate) flow runs of controls and intervention, per microspot. Data normality was verified using a Shapiro-Wilk test. Across donors, mean values of control and antibody/peptide runs were compared per each blood sample using paired Student's *t*-test. Values of $p<0.05$ were considered to be significant.

Results

Design and synthesis of cyclic GPIbα-mimicking peptides binding to the VWF A1 domain

The binding of VWF to platelet GPIb-V-IX is characterized by fast on- and off-rates. Based on published molecular structures of the GPIbα chain in interaction with the exposed VWF A1 domain [11,44], we employed an *in silico* approach to design peptides with: *(i)* a sufficiently high affinity to interfere with the rapid interaction, and *(ii)* a cyclic form to enhance their stability. As a structural template, we used the X-ray structure of the known ternary complex between GPIbα, VWF A1 domain, and botrocetin (PDB code 1U0N), to design a series of interfering mono- and bi-cyclic peptides. As shown in Figure 1, for the design of the mono-cyclic peptides, we used, as a template, the binary interaction of GPIbα with VWF A1 domain, while for the design of bi-cyclic peptides we used that of the ternary complex between GPIbα, VWF A1 domain, and botrocetin.

To predict the binding efficacy, we subjected published structures of the bimolecular GPIbα-VWF A1 complex and the trimolecular GPIbα-VWF A1-botrocetin complex, and we used molecular dynamic simulations to reveal key interacting regions at the complexed inter-molecular interfaces. The simulations were based on established and

7

published protocols using standard parameter settings [36].

The known structure of amino acids 221-246 of GPIbα, which sequence interacts with VWF A1, was used to design a first set of interacting mono-cyclic peptides which are connected via a disulfide bond. For the ternary complex, amino acids 225-231 and 237-241 of GPIbα and residues 2069-2077 and 2089-2098 of botrocetin were used and designed as being connected by employing the method of the chemical linkage of peptides onto scaffolds (CLIPS) [38]. Per procedure, more than fifty peptides were designed *in silico* and all products were subjected to molecular dynamics simulation (5 ns) and binding free energy (BFE) calculation to predict the relative binding affinity with the VWF A1 domain. The selected mono-cyclic peptide mono-ORbIT (26 amino acids) and the bi-cyclic peptide bi-ORbIT (34 amino acids) were found to exhibit the lowest BFE of -76 and -81 kcal/mol, respectively, thus predicting a high binding strength (Figure 1). These two peptides were synthesized and characterized (Table 1). The BFE value of the monocyclic GPIbα peptide was calculated as -35 ± 6 kcal/mol. The BFE of the botrocetin-based peptide sequence could not be calculated, since it was composed of distinct small peptides derived from the botrocetin and the GPIbα chain.

For the bi-ORbIT peptide, the determination of sites for the formation with the linker occurred by a combination of structural analysis and per-residue energy decomposition analysis. Therein, we selected those amino acid residues that had a lesser contribution for interacting with the VWF A1 domain for mutation to conjugate with the linker. In this case, we rationally changed the positions of amino acid residues for connection by CLIPS. For the mono-ORbIT peptide, we did not optimize the disulfide bond positions

Chemical synthesis of the linear peptide chains was performed by manual BOC-mediated solid-phase peptide synthesis. After cleavage from the solid support, the linear peptides were purified and cyclized. The cyclization was achieved by the oxidation of two free cysteines to form a disulfide bond (mono-ORbIT) or by allowing to react of three free cysteines in the linear peptide chain with 1,3,5-tris(bromomethyl)benzene (T3) to form a 2-CLIPS constrained peptide (bi-ORbIT; Figures S1 and S2). The purified peptides were finally dissolved into the saline water.

Figure 1. Design of GPIbα-mimicking peptides to interfere with VWF A1 domain. Molecular structures of the ternary complexes of GPIbα-VWF A1 and GPIbα-VWF A1–botrocetin (PDB code: 1U0N) were subjected to molecular dynamics simulations. Low energy structures are shown in GPIbα (blue), botrocetin (yellow), and VWF A1 domain (purple). The indicated residues of GPIbα with(out) botrocetin identified as interacting with VWF A1 were used for the *in silico* design of (>100) mono- and bi-cyclic peptides. All designed peptides were subjected to molecular dynamics simulations and binding free-energy (BFE) calculations. Peptide mutants with the lowest BFE were selected for optimization and synthesis: mono-ORbIT (-76±6 kcal/mol) and bi-ORbIT (-81±7 kcal/mol).
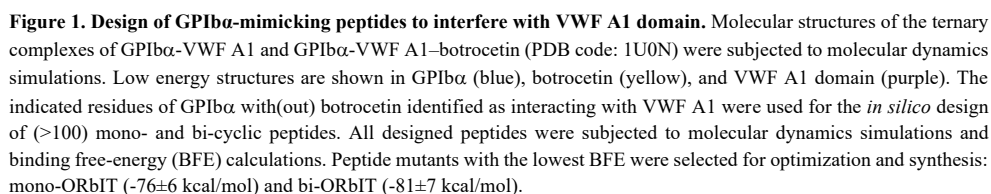
Table 1. Amino acid sequences of mono-ORbIT and bi-ORbIT peptides with a schematic representation of the peptide cyclizations.

Sequence	Peptide	BFE (kcal/mol)
	Monocyclic	
GPIbα	[221]QDNAENVYVWKQGVDVKAMTSNVASV[246]	-35 ± 6
Template peptide	H-QDNAENCYVWKQGVDVKAMTSNCAEE-OH Disulfide bond between Cys7 and Cys23	-62 ± 5
Mono-ORbIT	H-DDNAENCYVWKQGDEVRAMRSNCAEE-OH Disulfide bond between Cys7 and Cys23	-76 ± 6
	Bicyclic	
Botrocetin	[2070]DVWNKCRF[2077] [2089]DYYLIAEYEC[2098]C[2113]-T[2114]	-
GPIbα	[225]ENVYVWK[231] [237]KAMTS[241]	
Template peptide	Ac-CDVWNESAFDYYSIAEYECSTENCYVWEPSDTSC-OH Disulfide bond between Cys1-Cys19 and Cys24-Cys34	-76 ± 9
Bi-ORbIT	Ac-CDVWNESAFDEYSIAESESSECNEYVDEPSYTSC-OH CLIPS(T3*) connection between Cys1-Cys22-Cys34	-81 ± 7

*T3 = 1,3,5-tris(bromoethyl)benzene

GPIbα-derived inhibitory peptides interfere with ristocetin- and botrocetin-induced VWF binding

As a proof-of-principle that the new cyclic peptides interfered with the binding of VWF to platelets, we made use of the ability of ristocetin and botrocetin to 'open up' and activate multimeric VWF, enabling it to bind to platelet GPIbα. The monoclonal antibody (mAb) CLB-RAg35 directed against the VWF A1 domain, previously developed in the van Mourik lab [45], was used as a reference agent. For quantification of the binding of plasma-derived VWF to platelets in the presence of ristocetin or botrocetin, we employed a recently optimized flow cytometric assay [10]. Platelets in diluted plasma (containing autologous VWF) were therefore incubated with ristocetin or botrocetin and after fixation, VWF binding to the platelets was quantified by flow cytometry using a FITC-labeled anti-VWF antibody.
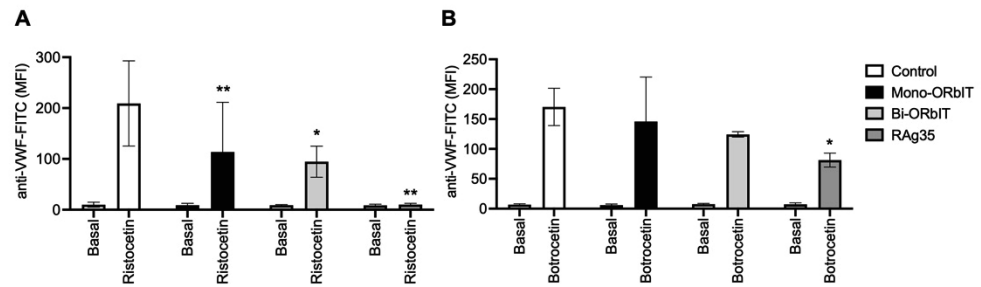
Figure 2. Reduced ristocetin- and botrocetin-induced VWF binding to platelet GPIb by mono-ORbIT and bi-ORbIT. Diluted PRP containing tirofiban (1.25 μg/mL) was pre-incubated with the GPIbα-derived peptides (mono-ORbIT or bi-ORbIT at 200 μg/mL) or CLB-RAg35 mAb (RAg35, 5 μg/mL) for 10 min at room temperature. The mixtures were activated for 6 min with either ristocetin (0.5 mg/mL) or botrocetin (5 μg/mL). Platelet samples were fixed before labeling with FITC-conjugated anti-VWF Ab. For flow-cytometric analysis, a gating of selected single platelets was used, and fluorescence was measured in the F1 channel. VWF binding was obtained as mean fluorescence intensities (MFI) for ristocetin- (**A**) or botrocetin-stimulated platelets (**B**). Paired Student's *t*-test, *$p<0.05$, **$p<0.01$ (n=3-5 donors).

As indicated in Figure 2, we found that the binding of VWF-ristocetin to platelets was strongly inhibited by mono-ORbIT (49% fluorescence reduction vs the control, p<0.01) as well as by bi-ORbIT (58% fluorescence reduction vs. the control, p<0.05). On the other hand, we observed only a minor reduction in the binding of VWF-botrocetin to platelets with mono-ORbIT (14% fluorescence reduction vs the control) or bi-ORbIT (27% fluorescence reduction vs the control). In comparison, the CLB-RAg35 mAb almost completely prevented the ristocetin-dependent VWF binding (95% fluorescence reduction vs. the control, p<0.01) and strongly inhibited the botrocetin-induced VWF binding (52% inhibition vs. the control, p<0.05).

Interference in the VWF A1 domain interaction with GPIbα affecting thrombus formation at high shear flow

To better understand the role of the VWF-GPIbα interaction at high-shear arterial flow conditions, we applied a previously validated method of microspot-whole-blood thrombus formation. This multiparameter test provides simultaneous information on the processes of flow-dependent platelet adhesion, aggregation, and activation [41,43]. For this study, we used a combination of three microspots, encompassing a wide range of GPIb-V-IX dependent surfaces, *i.e.* collagen-I (Horm-type collagen-I as a standard, microspot *M1*) [43], human collagen-III (with high VWF binding, *M2*) [8], and the combination of VWF and fibrinogen (*M3*) [41]. At first, we tested the anti-A1 domain CLB-RAg35 antibody, which is described to inhibit VWF-dependent platelet adhesion to the sub-endothelial matrix [45,46]. The high-shear perfusion of whole blood over microspots *M1-3* resulted in different types of thrombi. Using multicolor microscopic imaging per microspot and standard image analysis, we phenotyped these thrombi according to eight different parameters at end-stage (Table 2). Brightfield images provided parameters informing on platelet adhesion (*P1-2*) and platelet aggregation or thrombus buildup (*P3-5*); while three-color fluorescence images (AF647 anti-CD62P mAb, *P6*; FITC anti-fibrinogen mAb, *P7* and phosphatidylserine exposure AF568 annexin A5, *P8*) provided parameters of platelet activation.

Table 2. Assignment of thrombus parameters obtained from end-stage brightfield and fluorescence microscopic images. Indicated are ranges with mean values per parameter for collagen-I microspots and scaling used for heatmap presentation. Abbreviations: SAC: surface area coverage; PS: phosphatidylserine.

Parameter	Range	Scaling
Brightfield images (platelet adhesion)		
P1 Platelet deposition (%SAC)	0-66	0-10
P2 Morphology score (0-5)	0-3.8	0-10
Brightfield images (platelet aggregation)		
P3 Thrombus contraction score (0-3)	0-2.2	0-10
P4 Thrombus multilayer score (0-3)	0-1.9	0-10
P5 Thrombus aggregate coverage (%SAC)	0-12	0-10
Fluorescence images (platelet activation)		
P6 CD62P expression (%SAC)	0-50	0-10
P7 Fibrinogen binding (%SAC)	0-21	0-10
P8 PS exposure (%SAC)	0-17	0-10

Representative microscopic images from each of the three microspots under control conditions illustrated the marked differences in thrombus buildup (Figure 3A-C). This concerned the formation of larger size platelet aggregates or thrombi on collagen-I (*M1*), smaller size aggregates on collagen-III (*M2*), and mostly single platelets adhering to VWF/fibrinogen (*M3*). On all three surfaces, we detected noticeable platelet activation in terms of P-selectin expression (CD62P), fibrinogen binding, and phosphatidylserine exposure, the latter of which though was highest on collagen-I (*M1*).

Quantification of the effects of CLB-RAg35 mAb addition to blood, at a maximally effective dose of 5 µg/mL, indicated strong inhibitory effects on the formed thrombi (Figure 3D, raw data with statistics in Figure S3). More precisely, on collagen-I (*M1*), CLB-RAg35 intervention decreased the values of platelet deposition (*P1*, 40% of control, $p<0.0001$) and morphology score (*P2*, 73%, $p<0.0001$). This was accompanied by a profound reduction in the platelet aggregation parameters, namely thrombus contraction score (*P3*, 40%, $p<0.0001$), thrombus multilayer score (*P4*, 36%, $p<0.0001$), and platelet aggregate coverage (*P5*, 14%, $p<0.0001$); and also, by a reduction in the activation parameters of CD62P expression (*P6*, 56%, $p<0.0001$) and fibrinogen binding (*P7*, 52%, $p<0.001$), while CLB-RAg35 did not have a significant effect on phosphatidylserine exposure (*P8*).

Essentially the same parameters were affected by CLB-RAg35 for the smaller size thrombi formed on collagen-III (Figure 3D): platelet deposition (*P1*, 37% of control, $p<0.0001$), morphology score (*P2*, 72%, $p<0.001$), thrombus contraction score (*P3*, 58%, $p<0.01$), thrombus multilayer score (*P4*, 44%, $p<0.001$), platelet aggregate coverage (*P5*, 19%, $p<0.001$), CD62P expression (*P6*, 45%, $p<0.001$), and fibrinogen binding (*P7*, 54%, $p<0.05$). For the VWF/fibrinogen microspots (*M3*), causing mostly single platelet adhesion (Figure 3D), only one parameter was significantly decreased by CLB-RAg35: platelet deposition (*P1*, 67% of control, p<0.001). The phosphatidylserine exposure (P8) observed with CLB-RAg35 on the VWF/fibrinogen coated surface (M3) points to a slightly increased platelet activation state on fibrinogen when the interaction with VWF is blocked. Jointly, these data revealed a major, unexpected role of GPIbα interaction with VWF A1 at high shear rate, extending from VWF-dependent platelet adhesion to platelet aggregate and thrombus formation, regardless of the type of collagen.

Designed GPIbα-derived peptides interfering with platelet aggregation and thrombus formation under high-shear flow

To assess the inhibitory potential of the newly designed mono-ORbIT (low concentration of 20 µg/mL) in whole-blood thrombus formation, we applied the same multiparameter output, as described above. Representative end-stage microscopic images indicated the presence of smaller-size thrombi and less-deposited platelets for *M1-3* (Figure 4A). Overall, across blood from seven donors tested, we noticed a consistent reduction with mono-ORbIT in platelet aggregation for the two thrombus-forming microspots *M1-2*. Quantification indicated a reduction of scaled parameters for platelet adhesion (*P1-2*) and aggregation (*P3-5*; Figure 4B). Representation of effect sizes as a subtraction heatmap showed a consistent inhibitory

pattern for mono-ORbIT (Figure 4C). In detail, for collagen-I (*M1*), we observed a significant reduction of *P2-4* to 77-92% ($p<0.05$) of the control condition. For collagen-III (*M2*), the adhesion parameters (*P1-2*) were significantly reduced to 92% ($p<0.05$) and 84% ($p<0.05$), while the aggregation parameters (*P3-5*) were decreased to 60-69% ($p<0.05$) of the control. For the VWF/fibrinogen microspot, where only single platelets adhered, none of the parameters was changed. Platelet activation markers (*P6-8*) were not significantly affected by this peptide. Dose-response curves indicated a persistent inhibitory effect of mono-ORbIT at up to ten times higher concentration (Figure S4; raw data in Table S1).

Regarding bi-ORbIT peptide (20 µg/mL), effects on whole-blood thrombus formation were similar in sign but smaller than those of mono-ORbIT (Figure 5A). The overall pattern of the scaled parameters with blood from 5 donors pointed to an apparent reduction of the aggregation-related parameters (*P3-5*) for microspots *M1-2* (Figure 5B). However, significance was only reached for *P4* (thrombus multilayer score) on *M1* (69% of control, $p<0.05$). As shown in a subtraction heatmap (Figure 5C), parallel runs carried out with CLB-RAg35 gave an expected reduction in most of the observed parameters. Further analyses of the effects of bi-ORbIT at higher concentrations were hindered by its poor solubility. Raw data per parameters of thrombus formation per microspot are shown in Table S2.

Additional optimization of mono-cyclic peptide to opt-mono-ORbIT

Given the twice high inhibitory effects of RAg35 mAb on thrombus parameters, we reasoned that there is room for higher efficacy of the synthesized peptides. We thus designed a set of novel mono-cyclic peptides *in silico* based on the mono-ORbIT peptide as a template. Similar protocols as described for mono-ORbIT and bi-ORbIT were applied. First, molecular dynamics simulations of several improved mono-cyclic peptides were performed for 5 ns, of which the BFE was calculated. As some of the peptides gave comparable BFE values, further molecular dynamics simulations were performed for 100 ns to distinguish the theoretically most stable peptides for binding to the VWF A1 domain. Extended analysis of these simulations and subsequent BFE calculations resulted in the selection of an improved peptide, namely *opt*-mono-ORbIT (Ac-EDDNAECAYVEAEGDEARDQR SNCQDED-COOH), which displayed the lowest BFE (-97.11 ± 8.44 kcal/mol) amidst a set of 20 mono-ORbIT-based peptides. The 28 amino-acid *opt*-mono-ORbIT was thus selected for synthesis. The peptide was cyclized with a disulfide bond between residues C_7 and C_{24} (Figure 6C), and the *opt*-mono-ORbIT was spectrally analyzed for purity (Figure S5).
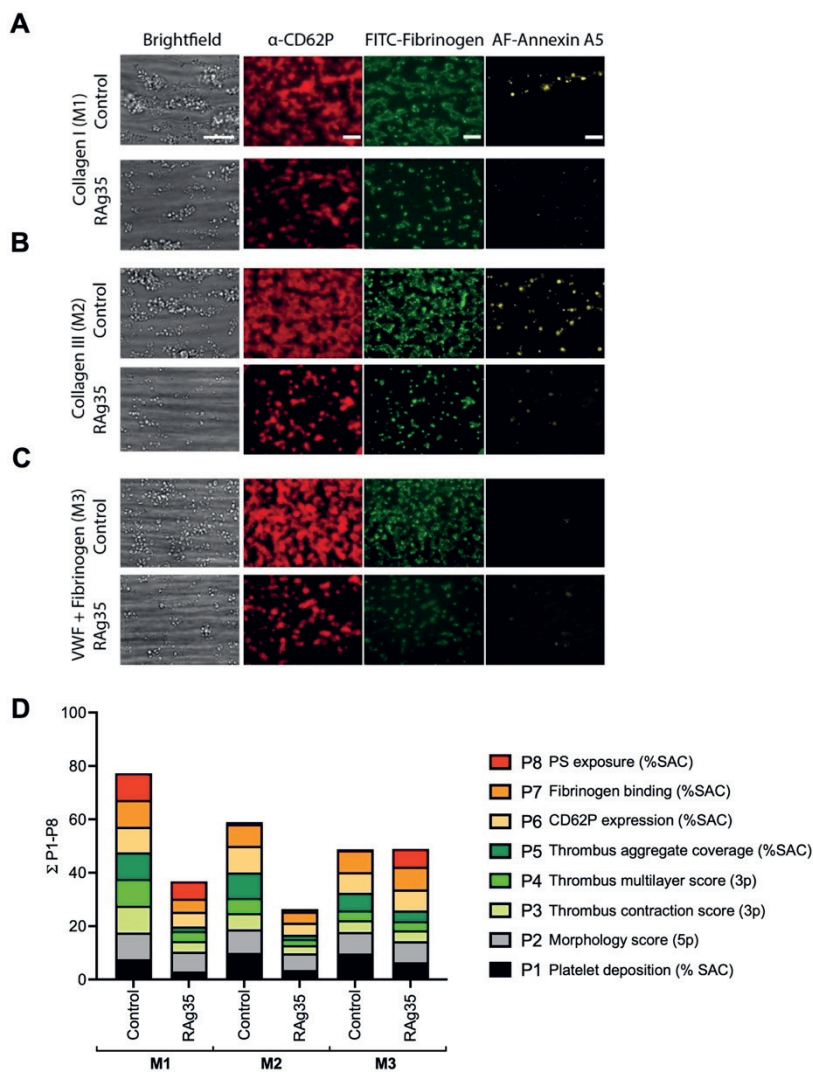
Figure 3. Thrombus and aggregation-reducing effect by blockage of the interaction of GPIbα with VWF A1 domain at high-shear flow. Whole blood was preincubated for 10 min with CLB-RAg35 mAb (CLB-RAg35, 10 µg/mL) or equal volume of saline. Blood samples flowed over microspots consisting of collagen-I (*M1*), collagen-III (*M2*), or VWF/fibrinogen (*M3*) for 3.5 min at a wall-shear rate of 1600 s^{-1}. (**A-C**) Representative brightfield microscopic images at end stage. Bars = 20 µm. Brightfield images were used for the analysis of adhesion-related parameters: platelet deposition (*P1*), morphological score (*P2*); and aggregation-related parameters (*P3-5*). End-stage three-color fluorescence images used for platelet activation assessment: CD62P expression (AF647 anti-CD62P mAb, *P6*), fibrinogen binding (FITC anti-fibrinogen mAb, *P7*), and phosphatidylserine exposure (AF568 annexin A5, *P8*). (**D**) Cumulative representation of scaled values (0-10) per parameter. Color reflects adhesion parameters *P1-2* (shades of black), aggregation parameters *P3-5* (shades of green), and activation parameters *P6-8* (shades of red). For details, see Figure S3.
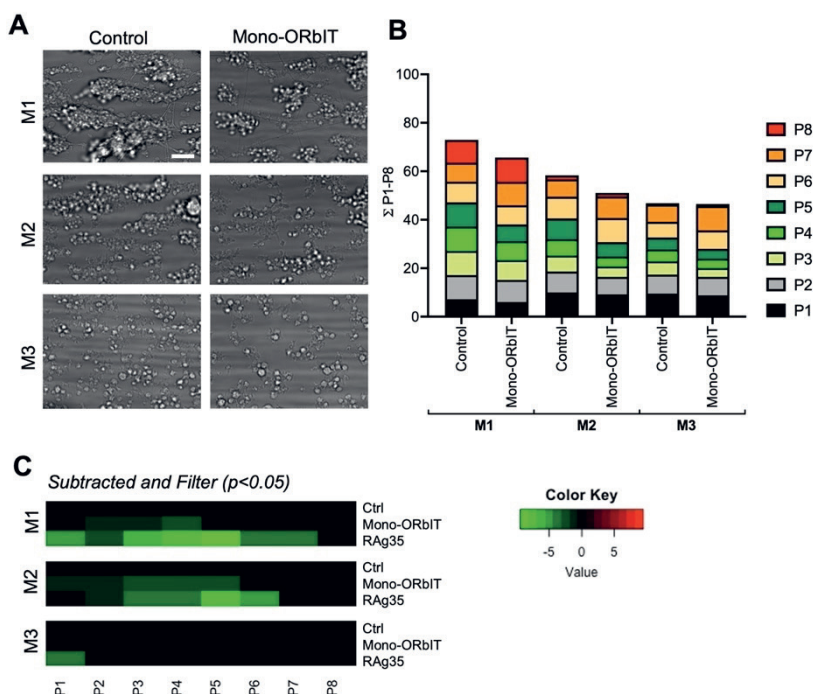
Figure 4. Suppressed thrombus formation and platelet aggregation by mono-ORbIT at high-shear flow. Whole blood was preincubated for 10 min in parallel with mono-ORbIT (20 µg/mL), CLB-RAg35 mAb (RAg35, 10 µg/mL), or saline (control). Duplicate blood samples flowed over microspots consisting of collagen-I (*M1*), collagen-III (*M2*), or VWF/fibrinogen (*M3*) for 3.5 min at a wall-shear rate of 1600 s^{-1}, and then stained, as in Figure 3. (**A**) Representative end-stage brightfield microscopy images per microspot in the absence or presence of mono-ORbIT. Bar = 10 µm. (**B**) Cumulative plots of scaled data per parameter (0-10), showing the effect of mono-ORbIT. Platelet adhesion parameters: *P1-2* (shades of black), aggregation parameters: *P3-5* (shades of green), and activation parameters: *P6-8* (shades of red). (**C**) Heatmap representation of control-subtracted data for mono-ORbIT and CLB-RAg35. Color coding indicates a decrease (green) or increase (red) in comparison to control runs. Mean values were compared per each blood sample using a paired Student's *t*-test, *p<0.05*, **p<0.005*, ***p<0.001* (n=7 donors). For raw data, see Table S1.

Flow cytometry indicated a notable inhibitory effect on VWF-platelet binding in response to ristocetin (Figure S6). In the microfluidics system, blood treatment with *opt*-mono-ORbIT caused dose-dependently a stronger inhibition of thrombus formation than mono-ORbIT (Figure 6, details in Table S3). On collagen-I (*M1*), consistent inhibition was observed with *opt*-mono-ORbIT (20 µg/mL) for the adhesion parameter P2 *(*83% of control, *p<0.05*), and importantly for the aggregation parameters *P3-4* (67-69%, *p<0.05*). Regarding the collagen-III surface (*M2*), inhibition was also seen for platelet adhesion *P2* (83%, *p<0.05*) and platelet aggregation *P3-4* (70-75%, *p<0.05*). Increasing concentrations of *opt*-mono-ORbIT revealed greater inhibitory potential in particular for spot *M2* (Figure 6). Inhibitory effects for the GPIb-specific surface *M3* were only achieved at 100 µg/mL for *P2-5* (77-85%, *p<0.05*). Together, the results with the constructed mono-ORbIT and *opt*-mono-ORbIT point to consistent inhibitory effects on collagen/VWF-dependent platelet aggregation and thrombus formation, exceeding the effects on VWF-dependent platelet adhesion.
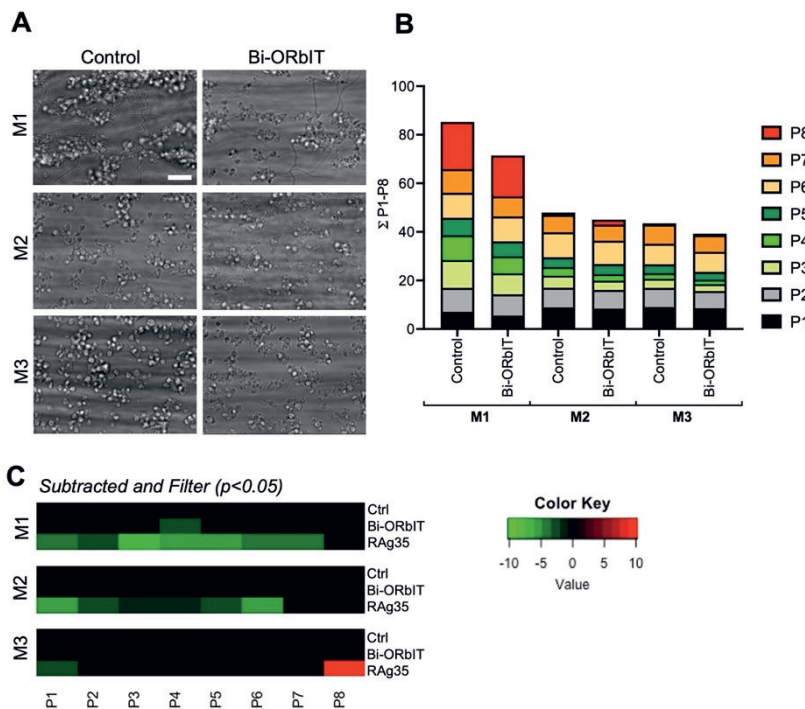
Figure 5. Moderately reduced platelet aggregation by bi-ORbIT at high-shear flow. Whole blood was preincubated for 10 min in parallel with bi-ORbIT (20 µg/mL), CLB-RAg35 mAb (RAg35, 10 µg/mL), or saline (control). Experimental setup and analysis as in Figure 3. (**A**) Representative end-stage brightfield microscopy images per microspot in the absence or presence of bi-ORbIT. Bar = 10 µm. (**B**) Cumulative plots of scaled data per parameter (0-10), showing the effects of bi-ORbIT. (**C**) Heatmap representation of control-subtracted data for bi-ORbIT and CLB-RAg35. Color coding indicates a decrease (green) or increase (red) in comparison to control runs (n=5 donors, paired Student's t-test, p<0.05). For raw data, see Table S2.
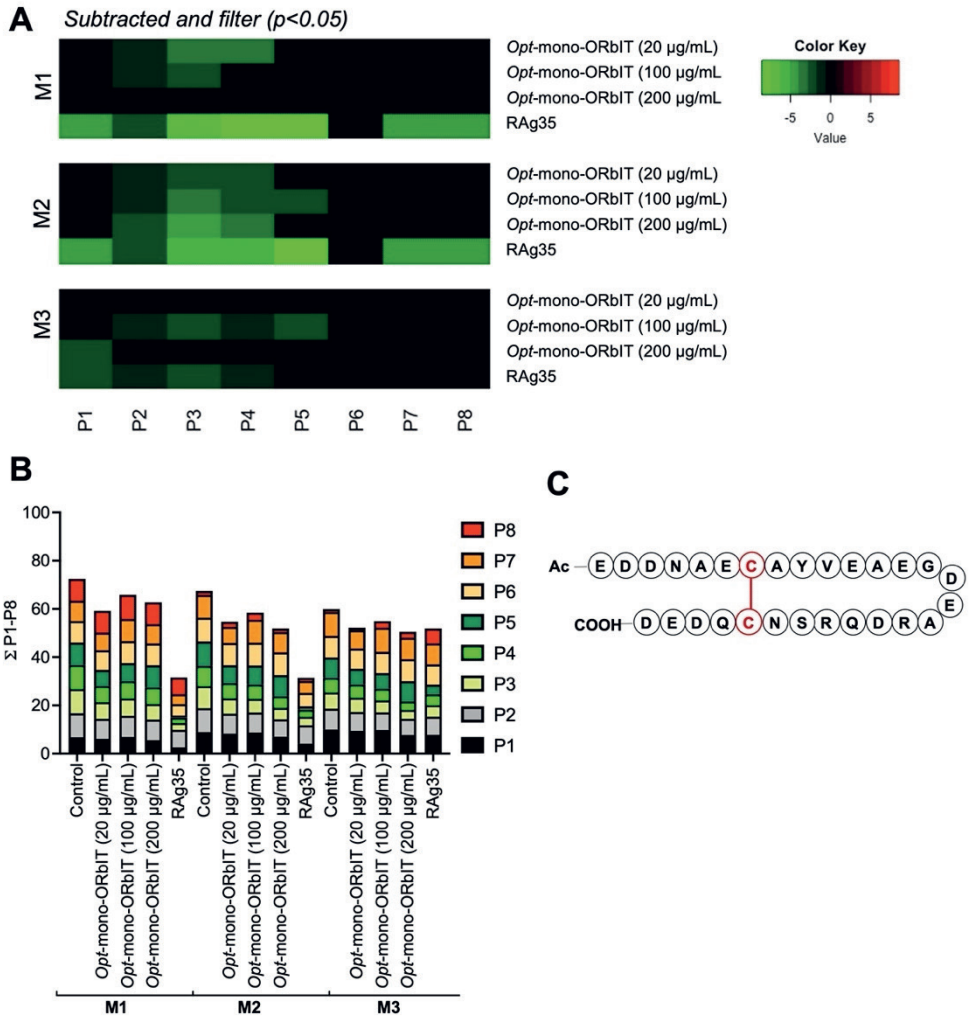
Figure 6. Additionally reduced platelet aggregation and thrombus formation by *opt*-mono-ORbIT at high-shear flow. Whole blood was preincubated for 10 min in parallel with *opt*-mono-ORbIT (20, 100, and 200 μg/mL), CLB-RAg35 (RAg35, 10 μg/mL), or control (saline). Blood samples were flowed at 1600 s^{-1} and stained, as indicated in Figure 3. Mean values from individual blood samples were scaled 0-10 per parameter across all surfaces *M1-3*. (**A**) Heatmap representation of control-subtracted data. Color coding indicates a decrease (green) or increase (red) in comparison to control runs. Filtering for relevant changes (n=3-7 donors, paired Student's *t*-test, *p*<0.05). (**B**) Cumulative plot of scaled data per parameter (0-10), showing the effect of *opt*-mono-ORbIT. Platelet adhesion parameters: *P1-2* (shades of black), aggregation parameters: *P3-5* (shades of green), and activation parameters: *P6-8* (shades of red). See further Table S3. (**C**) Schematic representation of *opt*-mono-ORbIT, in which a disulfide bond is indicated in red (C-C).

Discussion

Functional efficacy of in silico designed GPIba peptides interfering in binding to the VWF A1 domain

In order to explore a novel strategy for the development of inhibitors of the interaction of VWF with platelet GPIb-V-IX, which is pathologically in iTTP, we designed novel peptide-based inhibitors to target the VWF A1 domain rather than target the GPIb-V-IX complex on platelets. The advantage of this approach is that the binding site for GPIbα in the A1 domain is not accessible in circulating VWF multimers under physiological conditions. This approach hence may produce VWF inhibitors that are effective only after exposure to the A1 domain-binding site under shear stress or after interaction with vascular collagens, thereby theoretically leaving other VWF functions unchanged. For this purpose, we designed two distinct sets of peptides *in silico*, which resulted in the peptides mono-ORbIT (GPIbα-derived) and bi-ORbIT (botrocetin-GPIbα derived). The rationale for the second design was that botrocetin not only binds VWF, but also stabilizes the GPIbα-VWF A1 complex formation [10]. The two peptides, namely mono-ORbIT and bi-ORbIT, displayed, based on molecular dynamics simulations, a predicted low binding free energy, and hence, were selected for chemical synthesis and functional evaluation.

When establishing their efficacy to interfere with the GPIbα-VWF A1 interaction by flow cytometry, mono-ORbIT indeed suppressed the binding of ristocetin- and botrocetin-activated VWF to platelets by 49 and 14% fluorescence reduction, respectively. The synthesized bi-ORbIT displayed a stronger inhibitory effect on ristocetin-activated VWF (58% fluorescence reduction) than on botrocetin-activated VWF (27% fluorescence reduction). The reference CLB-RAg35 mAb inhibited ristocetin-induced VWF-binding to platelets by 95% and only partially inhibited the botrocetin-induced binding (52% fluorescence reduction). The generally lower inhibitory effect on botrocetin-induced binding observed for all inhibitors may be due to the mechanism of botrocetin action. Botrocetin first interacts only with VWF A1 and then slides around its A1 domain to form a new interface while interacting with GPIbα [11]. A higher peptide concentration than in the thrombus formation assay was used for the flow cytometric evaluation of the ristocetin- and botrocetin-induced VWF-binding flow cytometry assay due to the absence of shear conditions which greatly enforce VWF binding to GPIb-V-IX.

Role of VWF A1 domain in shear-dependent platelet aggregation and thrombus formation on collagen surfaces

The two synthesized peptides were tested under physiologically relevant shear conditions in whole blood using an established microfluidic-based platform [41]. With the established CLB-RAg35 mAb, we found that for the thrombogenic surfaces, collagen-I and collagen-III, it suppressed not only the shear-dependent stable adhesion of platelets but also the parameters of platelet aggregate formation and thrombus size. In addition, we noted the inhibitory effects

of CLB-RAg35 on secretion and fibrinogen binding by remaining platelets. The same pattern of changes in collagen-induced thrombus formation, although to a lesser extent, was also observed by the synthesized cyclic peptides, aimed to interfere with the VWF-GPIbα interactions. These results revealed an unexpected major role of VWF-binding to the platelet GPI-V-IX receptors in shear-dependent platelet activation and aggregation upon thrombus formation. An explanation for this finding is the earlier resolved formation of homotypic VWF-VWF interactions under shear conditions [15,45].

Both mono-ORbIT and bi-ORbIT appeared to reduce platelet aggregation and thrombus buildup under high-shear flow in a similar manner as CLB-RAg35. Yet, we noted a certain variation in inhibitory effects among blood samples tested, which may be due to inter-individual differences in VWF level and multimer composition, differences that are known to be related to blood type, genetic make [47], or sex-related platelet responses [48,49]. In support of the current data, we and others have previously shown that the role of GPIbα in flow-dependent platelet aggregation was most prominent at high pathological wall-shear rate gradients, *i.e.,* as present at stenotic sites in the arterial circulation [50,51]. A recently published single-chain antibody, scFV-A1, designed to target VWF activated by shear was shown to play an inhibiting effect in stenotic chambers, *i.e.*, at sites of sharp shear rate changes [52]. Therefore, stenotic flow chambers hence may be a useful tool to further study the effects of the present cyclic peptides under conditions of pathological VWF-dependent platelet activation.

Both mono- and bi-ORbIT peptides displayed VWF A1-GPIbα inhibitory effects that were smaller in effect size than those obtained with the anti-VWF mAb. Therefore, we set out to improve the inhibitory potential of the two peptides by implementing a second round of *in silico* design, based on the mono-ORbIT peptide. The peptide *opt*-mono-ORbIT was synthesized to assess its effect on thrombus formation under flow. This peptide showed improved efficacy as compared to mono-ORbIT but still did not approach the effects of the blocking CLB-RAg35 mAb. The difference between peptides and antibody is most likely due to the much higher, nanomolar range of affinity of an antibody in comparison to the micromolar range of affinity of the smaller designed peptides. Moreover, we hypothesized that the reversible peptide binding will also be more effective in inhibiting the more continued VWF-GPIbα interaction of already adhered platelets, as we observed with the higher inhibitory effect on aggregation parameters by these peptides than the sub-second interaction of GPIbα of high-shear flowed platelets.

An interesting question is whether the bi-ORbIT peptide has botrocetin-like activity. However, our flow cytometric evaluation indicated that the bi-ORbIT peptide reduced both the botrocetin- and ristocetin-induced VWF binding to platelets. Moreover, we did not see an increase in the basal sample incubated with bi-ORbIT only. We also expect no effect of this peptide on the di- or multimeric VWF-VWF interactions because it targets the A1 domain of VWF which has not been implicated in the multimer assembly of VWF. Protein-protein interactions have been difficult to target using small molecules. Therefore,

we *in silico* designed and synthesized cyclic peptides, which potentially bind to larger inter-protein surface areas in comparison to small molecules [53]. However, our flow cytometry data indicated that the peptide-induced blockade of the interaction between GPIbα and the VWF A1 is relatively weak, which is explained by the likely structural differences present *in silico* and *in vitro*. In other words, a slight difference in the calculated epitopes could affect the actual biological effect of the peptide. Accordingly, there is still room for improvement of the *in silico* design of peptides to better accommodate the complexities of *in vitro* and *in vivo* conditions. The advantage of cyclic over linear peptides is based on the knowledge that linear peptides are structurally more flexible, which allows them to also bind with low affinity to the surface or binding pockets of off-target proteins. Hence, linear peptides often have a high tendency to bind to off-target proteins [53]. On the other hand, the higher three-dimensional rigidity of cyclic peptides increases the specificity of binding to their target, *i.e.,* the VWF A1 domain.

Although a complete blocking of the VWF A1-GPIbα binding effect could be detrimental *in vivo*, as observed clinically with the nanobody caplacizumab, which causes bleeding-related events [23], the designed peptides tested in this study appear to be far from ready to be used in the clinic and several rounds of optimization are still needed to improve their efficacy. Yet, our results show that the combination of *in silico* and *in vitro* testing is a useful strategy. We envision that the design of multiple peptides will lead to greater inhibitory effects in shear-based thrombus buildup.

In the future, after dealing with the initial hurdles with peptide design and consequent extensive peptide library testing, a future therapy with peptide inhibitors of the VWF A1-GPIbα interaction may ease the thrombotic complications in iTTP, avoiding adverse effects of other therapies. Peptides with mild inhibitory effects may prevent the side effects observed with the caplacizumab nanobody [54]. In iTTP, ultra-large multimers of VWF enhance the formation of GPIbα VWF A1 bonds in the microcirculation due to the presence of autoantibody-mediated clearance/inhibition of ADAMTS13 [23], which implies that targeting this binding can give beneficial results. On the other hand, it needs to be stated that the charged small peptides are likely to interact with other blood cells and plasma proteins, and are susceptible to degradation by proteases and clearance, all of which will influence their availability in plasma. Cyclization of peptides, as presented in this work, is an alternative approach to improve the stability and half-life of peptide drugs in plasma and tissue [29]. Nevertheless, for the present class of GPIbα interference peptides the *in vivo* half-life still needs to be determined.

Conclusion

The present combined data provide proof-of-principle evidence that *in silico* design methods can be used to obtain peptides that can interfere in the complex ligand-receptor interaction of VWF and platelet GPIb-V-IX, an interaction that is subjected to shear-dependent molecular configuration changes and is partly reproduced with the antibiotic ristocetin and the snake venom botrocetin. Future patient treatment with well-designed peptides is

considered to be cost-effective, of high target specificity, and with low toxicity in comparison to antibody-based drugs [55]. The peptides designed in this paper can further be modified to improve their inhibitory potential by optimization with repeated rounds of mutagenesis and selection, followed by shear-dependent whole blood testing.

Author Contributions

Conceptualization: KW, JWMH, CPMR, GAFN, and JV. Methodology: JH, DIF, BE, BT, DS, SMA, KJ, and KW. Formal analysis: JH, DIF, JWMH, BE, BT, DS, SMA, KJ, and KW. Investigation: JH, DIF, BE, BT, DS, SMA, KJ, and KW. Resources: JWMH, GAFN, and JV; Data curation: JH and DIF. Writing – original draft preparation: JH, DIF, and JWMH. Writing – review & editing: JWMH, KW, and GAFN. Visualization; JH, DIF, and JWMH. Supervision: KW, CPMR, GAFN, and JV. Funding acquisition: KV, CPMR, TMH, GAFN, and JV

Acknowledgments and Funding

Institutional Review Board Statement

The study was approved by the local Medical Ethics Committees (Maastricht University Medical Centre, NL31480.068.10). All subjects gave full informed consent according to the Declaration of Helsinki and all methods were performed in accordance with the relevant guidelines and regulations.

Informed Consent Statement

Informed consent was obtained from all subjects involved in the study. According to ethical permission, all subjects gave blood without tracing to individuals.

Data availability statement

All data are included in the manuscript as figures, tables, or supplement figures.

Conflicts of interest

The funders had no role in the design of the study; in the collection, analyses, or interpretation of data; in the writing of the manuscript, or in the decision to publish the results. JWMH was a co-founder and shareholder of FlowChamber. The other authors declare no conflict of interest.

7

References

1. Sadler JE. Biochemistry and genetics of von Willebrand factor. *Ann Rev Biochem*. 1998;67:395-424.

2. Wagner DD. Cell biology of von Willebrand factor. *Ann Rev Cell Biol*. 1990;6:217-246.

3. Dong J, Moake JL, Nolasco L, et al. ADAMTS-13 rapidly cleaves newly secreted ultra-large von Willebrand factor multimers on the endothelial surface under flowing conditions. *Blood*. 2002;100:4033-4039.

4. Crawley JT, de Groot R, Xiang Y, Luken BM, Lane D, de Groot R. Unravelling the scissile bond: how ADAMTS13 recognises and cleaves von Willebrand factor. *Blood*. 2011;118:3212-3221.

5. Slayter H, Loscalzo J, Bockenstedt P, Handin RI. Native conformation of human von Willebrand protein. Analysis by electron microscopy and quasi-elastic light scattering. *J Biol Chem*. 1985;260:8559-8563.

6. Siedlecki CA, Lestini BJ, Kottke-Marchant KK, Eppell SJ, Wilson DL, Marchant RE. Shear-dependent changes in the three-dimensional structure of human von Willebrand factor. *Blood*. 1996;88:2939-2950.

7. Savage B, Saldivar E, Ruggeri ZM. Initiation of platelet adhesion by arrest onto fibrinogen or translocation on von Willebrand factor. *Cell*. 1996;84:289-297.

8. Fuchs B, de Witt S, Solecka BA, et al. Distinct role of von Willebrand factor triplet bands in glycoprotein Ib-dependent platelet adhesion and thrombus formation under flow. *Semin Thromb Hemost*. 2013;39:306-314.

9. Dong JF, Berndt MC, Schade A, et al. Ristocetin-dependent, but not botrocetin-dependent, binding of von Willebrand factor to the platelet glycoprotein Ib-IX-V complex correlates with shear- dependent interactions. Blood. 2001; 97:162-168.

10. Trabold K, Makhoul S, Gambaryan S, et al. The direct thrombin inhibitors dabigatran and lepirudin inhibit GPIbα-mediated platelet aggregation. *Thromb Haemost*. 2019;119:916-929.

10. Read MS, Smith SV, Lamb MA, Brinkhous KM. Role of botrocetin in platelet agglutination: formation of an activated complex of botrocetin and von Willebrand factor. *Blood*. 1989;74:1031-1035.

11. Fukuda Ki, Doggett T, Laurenzi IJ, Liddington RC, Diacovo TG. The snake venom protein botrocetin acts as a biological brace to promote dysfunctional platelet aggregation. *Nat Struct Mol Biol*. 2005;12:152-159.

12. Ruggeri ZM, Orje JN, Habermann R, Federici AoB, Reininger AJ. Activation-independent platelet adhesion and aggregation under elevated shear stress. *Blood*. 2006;108:1903-1910.

13. Van der Meijden PE, Heemskerk JW. Platelet biology and functions: new concepts and future clinical perspectives. *Nat Rev Cardiol*. 2019;16:166-179.

14. Versteeg HH, Heemskerk JW, Levi M, Reitsma PS. New fundamentals in hemostasis. *Physiol Rev*. 2013;93:327-358.

15. Savage B, Sixma JJ, Ruggeri ZM. Functional self-association of von Willebrand factor during platelet adhesion under flow. *Proc Natl Acad Sci USA*. 2002;99:425-430.

16. Wu YP, Vink T, Schiphorst M, et al. Platelet thrombus formation on collagen at high shear rates is mediated by von Willebrand factor-glycoprotein Ib interaction and inhibited by von Willebrand factor-glycoprotein IIb/IIIa interaction. *Arterioscler Thromb Vasc Biol*. 2000;20:1661-1667.

17. Brouns S, van Geffen JP, Heemskerk JW. High throughput measurement of platelet aggregation under flow. *Platelets*. 2018;29:662-669.

18. Deng W, Xu Y, Chen W, et al. Platelet clearance via shear-induced unfolding of a membrane mechanoreceptor. Nat Commun. 2016;7:e12863.

19. Broos K, Feys HB, De Meyer SF, Vanhoorelbeke K, Deckmyn H. Platelets at work in primary hemostasis. *Blood Rev*. 2011;25:155-167.

20. Crawley JT, Scully MA. Thrombotic thrombocytopenic purpura: basic pathophysiology and therapeutic strategies. *Hematology*. 2013;2013:292-299.

21. Kremer Hovinga JA, Coppo P, Lammle B, Moake JL, Miyata T, Vanhoorelbeke K. Thrombotic thrombocytopenic purpura. *Nat Rev Dis Primers.* 2017;3:17020.

22. Ayme G, Adam F, Legendre P, et al. A novel single-domain antibody against von Willebrand factor A1 domain resolves leukocyte recruitment and vascular leakage during inflammation. *Arterioscler Thromb Vasc Biol.* 2017;37:1736-1740.

23. Scully M, Cataland SR, Peyvandi F, et al. Caplacizumab treatment for acquired thrombotic thrombocytopenic purpura. *N Engl J Med.* 2019;380:335-346.

24. Jilma-Stohlawetz P, Knöbl P, Gilbert JC, Jilma B. The anti-von Willebrand factor aptamer ARC1779 increases von Willebrand factor levels and platelet counts in patients with type 2B von Willebrand disease. *Thromb Haemost.* 2012;108:284-290.

25. Siller-Matula JM, Merhi Y, Tanguay JF, et al. ARC15105 is a potent antagonist of von Willebrand factor mediated platelet activation and adhesion. *Arterioscler Thromb Vasc Biol.* 2012;32:902-909.

26. Kovacevic KD, Buchtele N, Schoergenhofer C, et al. The aptamer BT200 effectively inhibits von Willebrand factor (VWF) dependent platelet function after stimulated VWF release by desmopressin or endotoxin. *Sci Rep.* 2020;10:11180.

27. Lei X, Reheman A, Hou Y, et al. Anfibatide, a novel GPIb complex antagonist, inhibits platelet adhesion and thrombus formation in vitro and in vivo in murine models of thrombosis. *Thromb Haemost.* 2014;111:279-289.

28. Muttenthaler M, King GF, Adams DJ, Alewood PF. Trends in peptide drug discovery. *Nat Rev Drug Discov.* 2021;20:309-325.

29. Henninot A, Collins JC, Nuss JM. The current state of peptide drug discovery: back to the future? *J Med Chem.* 2018;61:1382-1414.

30. Nicolaes GA, Kulharia M, Voorberg J, et al. Rational design of small molecules targeting the C2 domain of coagulation factor VIII. *Blood.* 2014;123:113-120.

31. Van den Berg SM, Seijkens TT, Kusters PJ, et al. Blocking CD40-TRAF6 interactions by small-molecule inhibitor 6860766 ameliorates the complications of diet-induced obesity in mice. *Int J Obes (Lond).* 2015;39:782-790.

32. Seijkens TT, van Tiel CM, Kusters PJ, et al. Targeting CD40-induced TRAF6 signaling in macrophages reduces atherosclerosis. *J Am Coll Cardiol.* 2018;71:527-542.

33. Alard JE, Ortega-Gomez A, Wichapong K, et al. Recruitment of classical monocytes can be inhibited by disturbing heteromers of neutrophil HNP1 and platelet CCL5. *Sci Transl Med.* 2015;7:317ra196.

34. Wichapong K, Poelman H, Ercig B, et al. Rational modulator design by exploitation of protein-protein complex structures. *Future Med Chem.* 2019;11:1015-1033.

35. Schumski A, Ortega-Gomez A, Wichapong K, et al. Endotoxinemia accelerates atherosclerosis through electrostatic charge-mediated monocyte adhesion. *Circulation.* 2021;143:254-266.

36. Wichapong K, Silvestre-Roig C, Braster Q, Schumski A, Soehnlein O, Nicolaes GA. Structure-based peptide design targeting intrinsically disordered proteins: Novel histone H4 and H2A peptidic inhibitors. *Comput Struct Biotechnol J.* 2021;19:934-948.

37. Liu X, Wichapong K, Lamers S, Reutelingsperger CP, Nicolaes GA. Autocitrullination of PAD4 does not alter its enzymatic activity: In vitro and in silico studies. *Int J Biochem Cell Biol.* 2021;134:105938.

38. Timmerman P, Puijk WC, Boshuizen RS, et al. Functional reconstruction of structurally complex epitopes using CLIPS technology. *Open Vaccine J.* 2009;2:56-67.

39. Wichapong K, Alard JE, Ortega-Gomez A, et al. Structure-based design of peptidic inhibitors of the interaction between CC chemokine ligand 5 (CCL5) and human neutrophil peptides 1 (HNP1). *J Med Chem.* 2016;59:4289-4301.

40. Van Geffen JP, Brouns S, Batista J, et al. High-throughput elucidation of thrombus formation reveals sources of platelet function variability. *Haematologica.* 2019;104:1256-1267.

7

41. De Witt SM, Swieringa F, Cavill R, et al. Identification of platelet function defects by multi-parameter assessment of thrombus formation. *Nat Commun.* 2014;5:e4257.

42. Van Kruchten R, Cosemans JM, Heemskerk JW. Measurement of whole blood thrombus formation using parallel-plate flow chambers: a practical guide. *Platelets.* 2012;23:229-242.

43. Nagy M, Mastenbroek TG, Mattheij NJ, et al. Variable impairment of platelet functions in patients with severe, genetically linked immune deficiencies. *Haematologica.* 2018;103:540-549.

44. Huizinga EG, Tsuji S, Romijn RA, et al. Structures of glycoprotein Ibα and its complex with von Willebrand factor A1 domain. *Science.* 2002;297:1176-1179.

45. Sixma JJ, Sakariassen KS, Stel HV, et al. Functional domains on von Willebrand factor. Recognition of discrete tryptic fragments by monoclonal antibodies that inhibit interaction of von Willebrand factor with platelets and with collagen. *J Clin Invest.* 1984;74:736-744.

46. Stel HV, Sakariassen KS, Scholte BJ, et al. Characterization of 25 monoclonal antibodies to factor VIII-von Willebrand factor: relationship between ristocetin-induced platelet aggregation and platelet adherence to subendothelium. *Blood.* 1984;63:1408-1415.

47. Bladbjerg EM, de Maat MP, Christensen K, Bathum L, Jespersen J, Hjelmborg J. Genetic influence on thrombotic risk markers in the elderly: a Danish twin study. *J Thromb Haemost.* 2006;4:599-607.

48. Zhou Z, Yu F, Buchanan A, et al. Possible race and gender divergence in association of genetic variations with plasma von Willebrand factor: a study of ARIC and 1000 genome cohorts. *Plos One.* 2014;9:e84810.

49. Jastrzebska M, Marcinowska Z, Oledzki S, et al. Variable gender-dependent platelet responses to combined antiplatelet therapy in patients with stable coronary-artery disease. *J Physiol Pharmacol.* 2018;69:26402.

50. Goto S, Ikeda Y, Saldívar E, Ruggeri ZM. Distinct mechanisms of platelet aggregation as a consequence of different shearing flow conditions. *J Clin Invest.* 1998;101:479-486.

51. Westein E, van der Meer AD, Kuijpers MJ, Frimat JP, van den Berg A, Heemskerk JW. Atherosclerotic geometries spatially confine and exacerbate pathological thrombus formation poststenosis in a von Willebrand factor-dependent manner. *Proc Natl Acad Sci USA.* 2013;110:1357-1362.

52. Hoefer T, Rana A, Niego B, et al. Targeting shear gradient activated von Willebrand factor by the novel single-chain antibody A1 reduces occlusive thrombus formation in vitro. *Haematologica.* 2021;106:2874-2884.

53. Gonzalez-Muniz R, Bonache MA, Perez de Vega MJ. Modulating protein-protein interactions by cyclic and macrocyclic peptides. Prominent strategies and examples. *Molecules.* 2021;26:445.

54. Elverdi T, Eskazan AE. Caplacizumab as an emerging treatment option for acquired thrombotic thrombocytopenic purpura. *Drug Des Devel Ther.* 2019;13:1251-1258.

55. Marqus S, Pirogova E, Piva TJ. Evaluation of the use of therapeutic peptides for cancer treatment. *J Biomed Sci.* 2017;24:21-21.

Supplemental Methods and Figures of Chapter 7

Supplemental Methods

Solid phase synthesis of mono- and bi-cyclic peptides

The reduced peptides mono-ORbIT (H$_2$N-DDNAENCYVWKQGDE VRAMR SNCAEE-COOH), *opt*-mono-ORbIT (Ac-EDDNAECAYVEAEGDEARDQRSNCQ DED-COOH), and the linear form of bi-ORbIT (Ac-CDVWNESAFDEYSIAESESS ECNEYVDEPSYTSC-COOH) were synthesized by manual solid-phase peptide synthesis on a 0.20 mmol scale using the *in situ* neutralization/activation procedure for Boc/Bzl peptide synthesis as previously described [29], but using HCTU instead of HBTU as a coupling reagent. Glu(OBzl)-PAM resin (0.71 mmol/g), Asp(OBzl)-PAM resin (0.72 mmol/g) and Cys(MeBzl)-PAM resin (0.73 mmol/g) were used as the solid support for mono-ORbIT, *opt*-mono-ORbIT and bi-ORbIT, respectively. After completion of the peptide chain, the resin-bound peptide was washed with dimethylformamide, treated with trifluoroacetic acid (2 × 1 min) to remove the N-terminal Boc group, washed with dimethylformamide, dichloromethane, and 1:1 *v/v* dichloro-methane/methanol and dried. *Opt*-mono-ORbIT and bi-ORbIT were N-terminally acetylated by treatment with 1:1 acetic anhydride : pyridine for 5 min. The peptides were then sidechain-deprotected and cleaved from the resin by treatment with anhydrous HF for 1 h at 0 °C, using 4 *vol*% *p*-cresol as a scavenger. Following cleavage, peptides were precipitated in ice-cold diethyl ether. Subsequently, peptides were extracted with 0.1 M sodium acetate buffer (pH 4) containing 6 M guanidine HCl and purified by preparative HPLC (mono-ORbIT and bi-ORbIT. Fractions containing the desired product were identified by UPLC-MS, pooled, and lyophilized. *Opt*-mono-ORbIT was extracted from diethyl ether using 50% MeCN in water plus 0.1% TFA and used in subsequent steps without further purification.

To facilitate the formation of the disulfide connection the reduced purified mono-ORbIT was dissolved at 0.3 mg/mL into 1 M guanidine HCl, 0.1 M Tris buffer (pH 8.0), and was stirred for 24 h at 4 °C in the presence of 8 mM cysteine and 1 mM cystine as redox couple. Folding progress was monitored by UPLC-MS, appearing as a mass decrease of -2 Da (2 protons, 1 disulfide bound) resulting in a final mass of 3029.32 Da (Figure S1B), corresponding to the calculated monoisotopic mass of the folded, cyclic mono-ORbIT peptide. After semi-preparative HPLC, the product-containing fractions were identified by UPLC-MS, pooled, and lyophilized.

For the bicyclic peptide, bi-ORbIT, Cys(Mebzl)-PAM resin (0.73 mmol/g) was used as the solid support. Next, the resin-bound peptide was acetylated on N-terminal acetylation using a 1:1 mixture of pyridine/acetic anhydride for 5 min. The peptide was washed with dimethylformamide, dichloromethane, and 1:1 *v/v* dichloromethane/methanol and dried. The peptide was further deprotected and cleaved from the resin by treatment with anhydrous HF for 1 h at 0 °C, using 4 *vol*% *p*-cresol as a scavenger. Following cleavage, the peptide was precipitated with ice-cold diethyl ether, dissolved in 0.1 M sodium acetate buffer

(pH 4) containing 6 M guanidine HCl, and purified by preparative HPLC. Fractions containing the desired product were identified by UPLC-MS, pooled, and lyophilized.

The crude linear peptide of the optimized construct, *opt*-mono-ORbIT, was dissolved at 3 mg/mL into 1 M guanidine HCl, 0.1 M Tris buffer (pH 8.0), and treated with 1% peroxide solution to oxidize the free thiols and form the desired disulfide bridge. Folding progress was monitored by UPLC-MS, appearing as a mass decrease of -2 Da (2 protons, 1 disulfide bound) resulting in a final mass of 3215.10 Da, corresponding to the calculated monoisotopic mass of the folded, cyclic *opt*-mono-ORbIT peptide. After semi-preparative HPLC, the product-containing fractions were identified by UPLC-MS, pooled, and lyophilized.

The linear peptide chain of bicyclic peptide, bi-ORbIT, was cyclized by reaction with a 1,3,5-tris(bromomethyl)benzene scaffold (T3) to connect three cysteine residues resulting in a generation of bicyclic peptides as previously described [40-42]. The peptide was dissolved at 2 mg/mL in 50 mM ammonium bicarbonate buffer pH 7.8. One equivalent T3 scaffold (stock solution of 2 mg/mL in acetonitrile) was added to the linear peptide every 30 min until full cyclization was realized. Cyclization progress was monitored by UPLC-MS, resulting in a final mass of 4042.50 Da, corresponding to the calculated monoisotopic mass of the cyclized peptide. After semi-preparative HPLC, product-containing fractions were identified by UPLC-MS, pooled, and lyophilized.

Semi-preparative HPLC purification and mass spectrometry

Semi-preparative reversed-phase HPLC was performed by using a Vydac C-18 column (250 × 10 mm, 10 μm). A linear gradient of acetonitrile in water/0.1% trifluoroacetic acid was used to elute the peptide using a flow rate of 12 mL/min. UPLC-MS was performed on a Waters XEVO QTOF G2 mass spectrometer, with an Acquity H-class solvent manager, FTN-sample manager, and TUV-detector. The system was equipped with a reversed-phase C_{18}-column (Waters, Acquity PST 130 A, 1.7 μm 2.1 × 50 mm), column temperature 40 °C. The mobile phases consisted of 0.1% formic acid in water and 90% acetonitrile. FTN-purge solvent was 10% acetonitrile in water. Gradient condition: starting with 10% acetonitrile to 55% acetonitrile in 15 min, absorbance detection at 220 nm wavelength.

Supplemental Figures

Figure S1. Representative spectra of chemically synthesized and purified mono-ORbIT. (**A**) UV spectrum and (**B**) mass spectrum of mono-ORbIT.

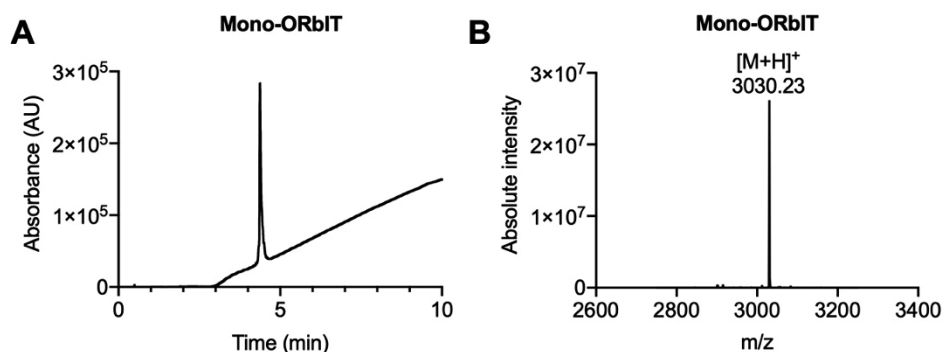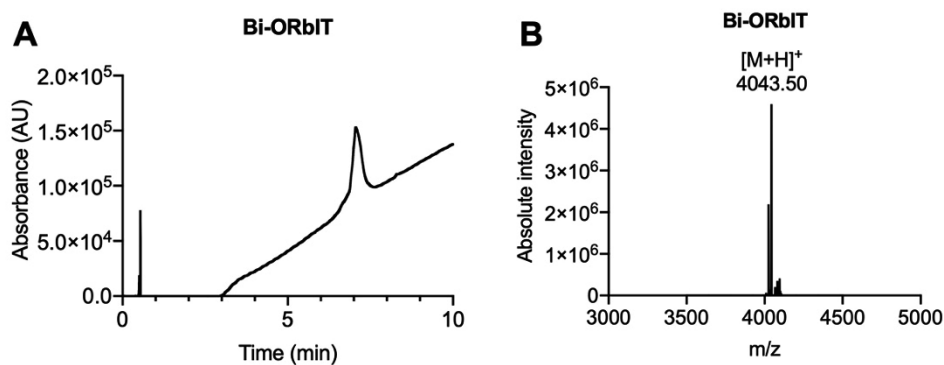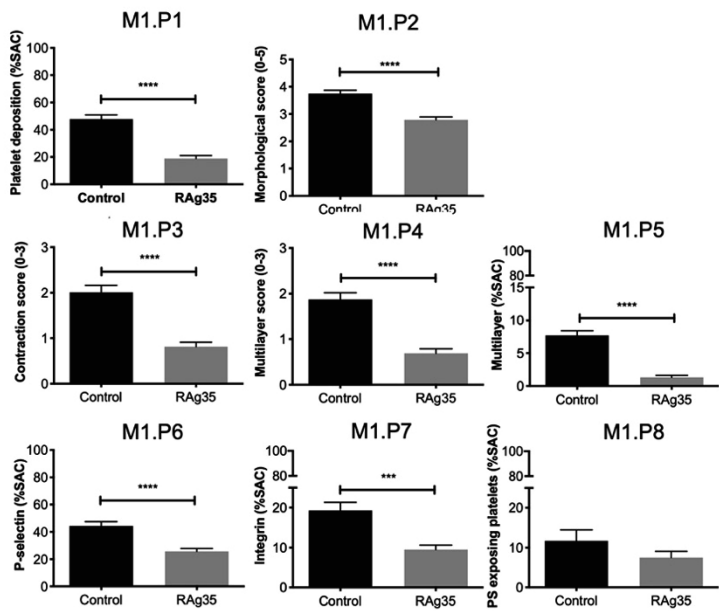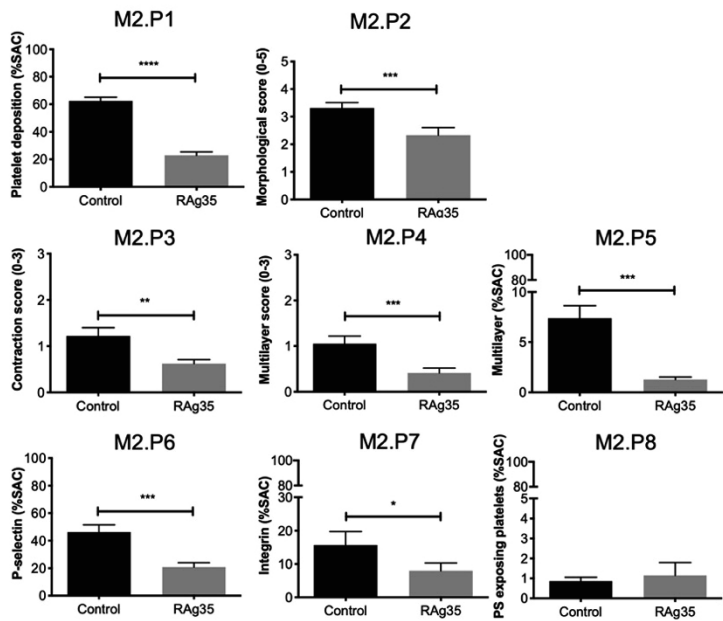**Figure S2. Representative spectra of chemically synthesized and purified bi-ORbIT.** (**A**) UV spectrum and (**B**) mass spectrum of bi-ORbIT.

A Collagen-I (M1)
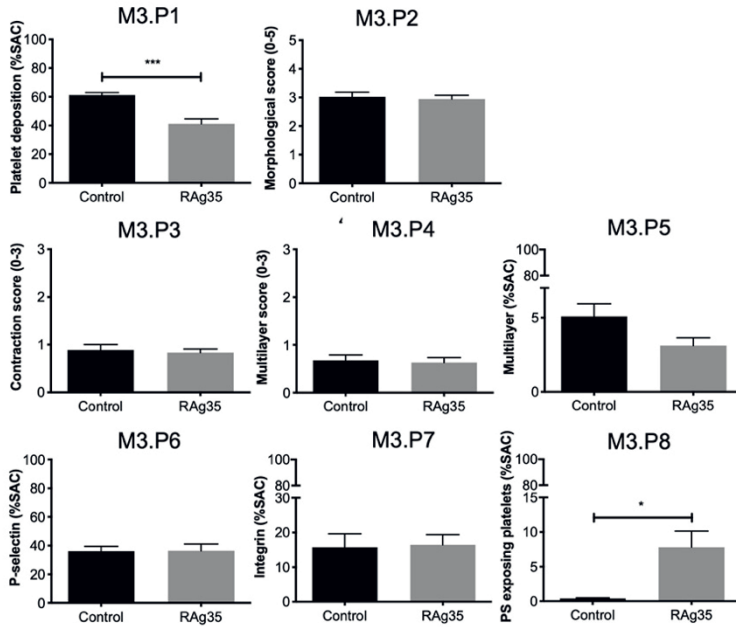

B Collagen-III (M2)

Figure S3. Effect of CLB-RAg35 on thrombus formation at high-shear flow. Microspot thrombus formation was performed, as described in Figure 1. Shown are the calculated effects of CLB-RAg35 *vs.* control for microspot *M1* (**A**), microspot *M2* (**B**), and microspot *M3* (**C**), per parameter (*P1-8*). Paired Student's t-test, *$p<0.05$, **$p<0.01$, ***$p<0.001$, ****$p<0.0001$ ($n=10$).
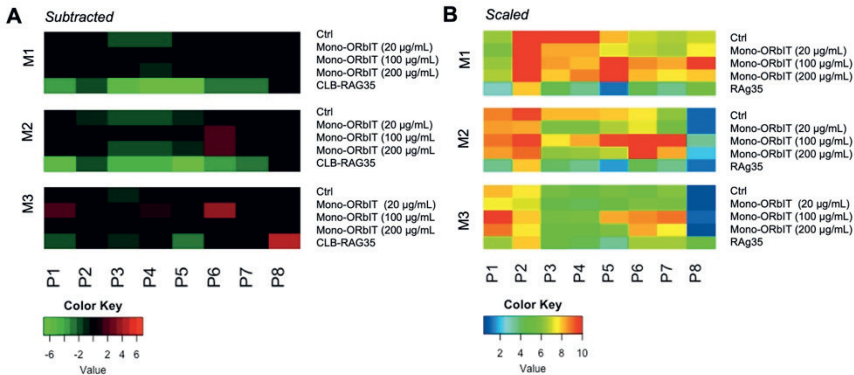
Figure S4. Effects of mono-ORbIT on thrombus formation under flow. Whole blood was preincubated for 10 min in parallel with mono-ORbIT (20, 100, and 200 μg/mL), CLB-RAg35 (RAg35, 10 μg/mL), or control (saline). Samples were perfused over microspots consisting of collagen-I (*M1*), collagen-III (*M2*), or VWF/fibrinogen (*M3*) for 3.5 min at a wall-shear rate of 1600 s^{-1}, and then stained, as indicated for Figure 3. Mean values from individual blood samples ($n=13$ donors) were scaled 0-10 per parameter across all microspots *M1-3*. (**A**) Heatmap representation of control-subtracted data. Color coding indicates a decrease (green) or increase (red) in comparison to control runs. (**B**) Heatmap of mean data per parameter and microspot of thrombus formation. Raw data were scaled on range 0-10 per parameter (*P1-8*) across all microspots. (n=6-13 donors). See Table S3.
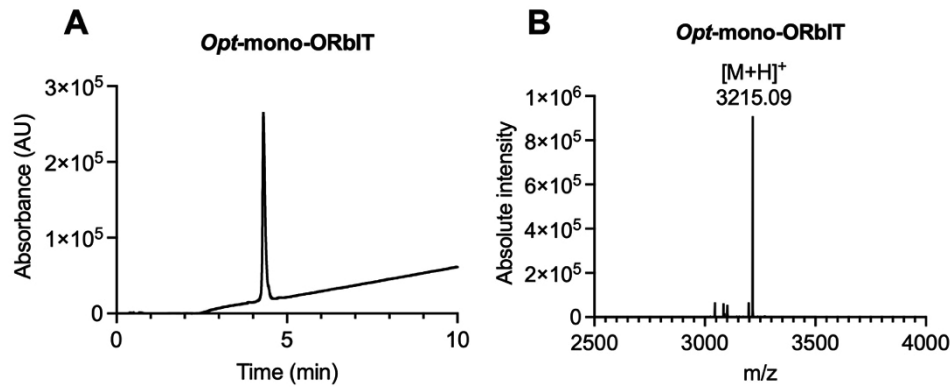
Figure S5. Representative spectra of chemically synthesized and purified *opt*-mono-ORbIT. (A) UV spectrum and **(B)** mass spectrum of *opt*-mono-ORbIT.
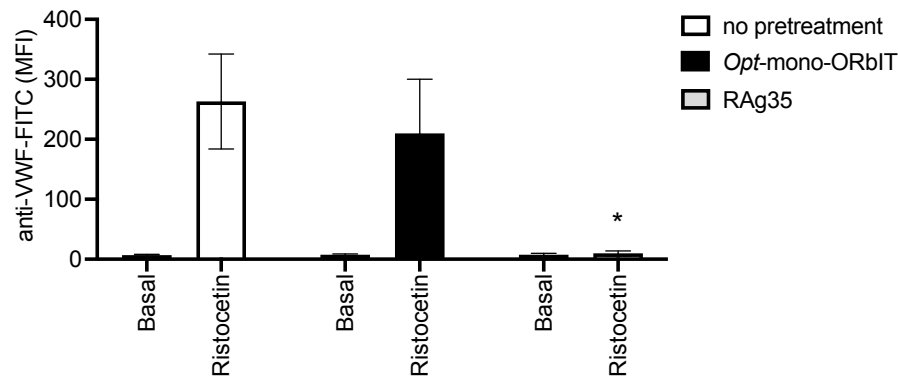
Figure S6. Effect of *opt*-mono-ORbIT on ristocetin-induced platelet binding to VWF. Diluted PRP containing tirofiban (1.25 µg/mL) was pre-incubated with 200 µg/mL *opt*-mono-ORbIT for 10 min at room temperature. The mixture was subsequently activated for 6 min with ristocetin (0.5 mg/mL). Samples were fixed and labeled with FITC-conjugated anti-VWF antibody. A selected gated population of single platelets was used for the analyses. VWF binding was calculated as mean fluorescence intensity (MFI). Paired Student's t-test, $*p<0.05$ (n=3 donors).

Supplemental Tables

Table S1. Raw data per microspot and parameter of control/mono-ORbIT peptide on whole-blood thrombus formation. Data are mean ± SD, n=7 donors for mono-ORbIT. For explanation, see Figure 4.

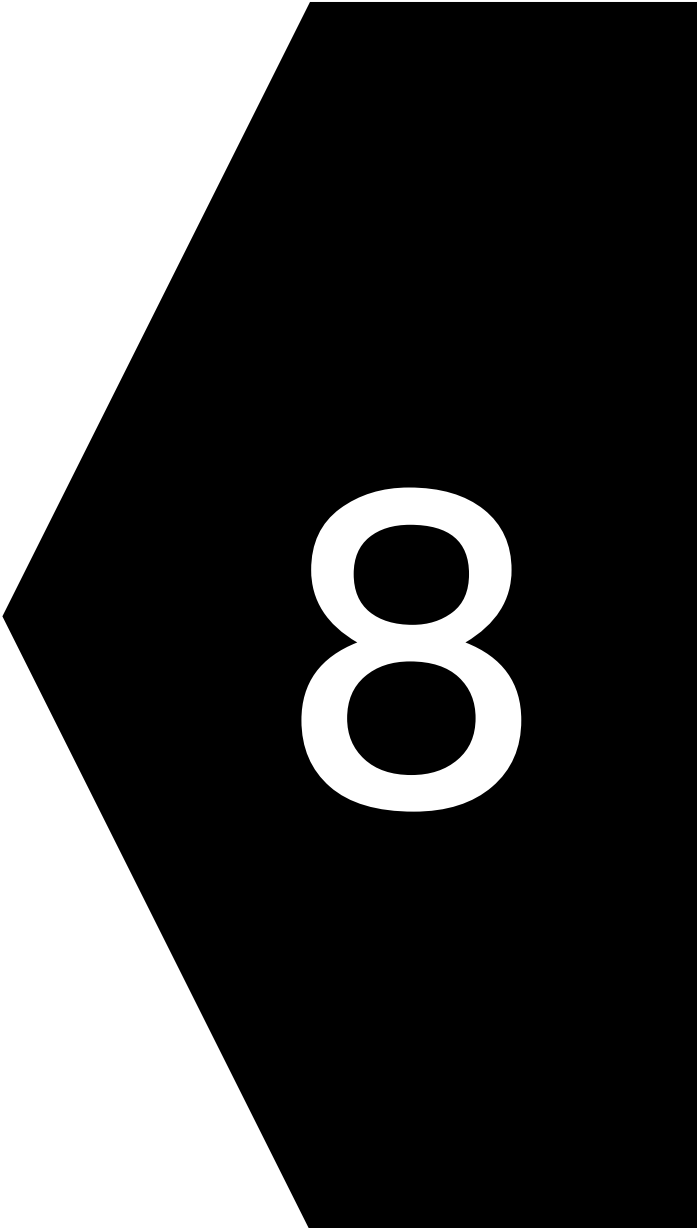|	Condition	P1	P2	P3	P4	P5	P6	P7	P8
M1	Control	44.99±8.62	3.62±0.22	1.75±0.39	1.76±0.30	11.33±4.50	45.22±9.12	22.84±10.73	8.83±4.21
M1	Mono-ORbIT 20 µg/mL	42.37±12.96	3.48±0.37	1.46±0.61	1.46±0.49	10.22±4.77	43.94±12.52	22.12±11.73	9.63±3.58
M1	Mono-ORbIT 100 µg/mL	44.87±6.15	3.58±0.30	1.48±0.32	1.44±0.27	13.47±1.99	55.25±8.94	28.50±6.12	12.69±5.55
M1	Mono-ORbIT 200 µg/mL	46.89±8.76	3.48±0.20	1.40±0.28	1.54±0.25	14.00±1.96	52.99±9.92	26.11±9.92	10.12±3.88
M2	Control	62.16±10.54	3.44±0.53	1.42±0.52	1.44±0.39	11.26±3.60	50.09±9.73	21.05±12.44	1.44±1.12
M2	Mono-ORbIT 20 µg/mL	59.31±10.19	3.02±0.83	1.04±0.67	1.04±0.65	9.44±4.50	47.14±17.09	19.47±11.29	1.30±0.97
M2	Mono-ORbIT 100 µg/mL	62.81±7.66	3.42±0.52	1.35±0.50	1.46±0.46	13.31±2.10	64.46±6.06	34.03±10.58	4.44±5.95
M2	Mono-ORbIT 200 µg/mL	59.85±10.60	3.29±0.37	1.08±0.13	1.13±0.14	9.65±1.68	62.40±3.14	28.34±11.00	2.61±2.48
M3	Control	57.26±17.33	2.79±1.14	0.99±0.54	0.92±0.50	8.17±5.53	35.16±17.35	20.55±14.39	0.54±0.55
M3	Mono-ORbIT 20 µg/mL	52.39±22.43	2.58±1.00	0.79±0.54	0.75±0.55	7.26±5.36	38.69±21.60	19.78±14.55	0.56±0.59
M3	Mono-ORbIT 100 µg/mL	70.55±10.30	2.88±0.38	0.98±0.34	1.02±0.32	11.59±3.34	55.76±11.77	30.07±10.71	1.32±1.25
M3	Mono-ORbIT 200 µg/mL	63.13±8.93	2.79±0.51	0.88±0.31	0.85±0.28	8.42±3.29	53.74±11.86	25.92±14.47	0.68±0.61

7

Table S2. Raw data per microspot and parameter of bi-ORbIT peptide on whole blood thrombus formation. Data are mean ± SD, n=5 donors for bi-ORbIT. For explanation, see Figure 5.

	Condition	P1	P2	P3	P4	P5	P6	P7	P8
M1	Control	46.80±10.18	3.78±0.48	2.19±0.33	2.01±0.7	8.57±2.67	49.75±7.12	20.31±6.55	13.83±2.45
M1	Bi-ORbIT	40.40±8.87	3.45±0.45	1.75±0.5	1.38±0.47	7.89±2.47	50.09±7.12	17.22±8.66	14.14±4.63
M2	Control	58.43±5.33	3.12±0.63	0.95±0.37	0.65±0.22	4.59±2.15	49.55±12.04	15.00±13.89	0.80±0.62
M2	Bi-ORbIT	56.87±6.11	3.03±0.61	0.69±0.19	0.51±0.24	5.16±0.84	50.39±10.94	13.80±10.94	1.69±4.22
M3	Control	51.68±12.37	3.03±0.68	0.72±0.14	0.43±0.19	3.84±1.79	41.14±11.56	16.51±15.22	0.44±0.28
M3	Bi-ORbIT	50.53±10.22	2.80±0.56	0.51±0.11	0.33±0.19	3.58±1.53	14.31±10.38	39.21±14.14	0.44±0.53

Table S3. Raw data per microspot and parameter of control/*Opt*-mono-ORbIT on whole-blood thrombus formation. Data are means ± SD, n=3-7 donors for *Opt*-mono-ORbIT2.

	Condition	P1	P2	P3	P4	P5	P6	P7	P8
M1	Control	44.35±11.96	3.93±0.37	2.01±0.31	2.17±0.48	15.47±3.86	9.85±2.23	54.25±6.97	28.06±7.16
M1	*Opt*-mono-ORbIT 20 µg/ml	40.07±12.57	3.27±0.28	1.39±0.48	1.45±0.48	11.10±3.63	9.84±4.07	49.91±7.19	24.22±8.43
M1	*Opt*-mono-ORbIT 100 µg/ml	44.99±12.37	3.46±0.47	1.45±0.44	1.55±0.44	12.49±2.65	10.93±5.02	55.05±6.76	30.60±8.68
M1	*Opt*-mono-ORbIT 200 µg/ml	36.45±15.93	3.38±0.33	1.29±0.51	1.50±0.33	15.26±1.76	9.87±6.14	54.76±8.69	26.74±12.58
M2	Control	58.62±15.08	3.90±0.40	1.85±0.45	1.81±0.43	16.78±6.77	1.75±1.04	60.39±10.05	31.27±7.81
M2	*Opt*-mono-ORbIT 20 µg/ml	54.37±16.61	3.25±0.25	1.29±0.42	1.36±0.38	12.32±3.31	2.28±1.79	56.22±9.58	22.08±10.79
M2	*Opt*-mono-ORbIT 100 µg/ml	57.32±17.83	3.27±0.48	1.14±0.38	1.29±0.46	13.09±4.05	3.21±2.52	57.44±8.77	31.53±10.16
M2	*Opt*-mono-ORbIT 200 µg/ml	46.02±20.93	2.83±0.19	0.96±0.31	1.04±0.19	14.56±4.18	1.62±2.11	57.61±11.13	27.79±15.59
M3	Control	65.43±13.27	3.40±0.26	1.36±0.26	1.31±0.28	14.03±7.06	1.28±1.18	54.45±8.09	32.98±8.80
M3	*Opt*-mono-ORbIT 20 µg/ml	61.54±20.01	3.09±0.76	1.20±0.58	1.18±0.59	10.86±5.60	1.06±1.40	51.02±7.21	25.29±8.37
M3	*Opt*-mono-ORbIT 100 µg/ml	63.94±13.54	2.89±0.57	1.00±0.38	1.04±0.36	10.83±5.10	2.97±4.18	53.73±10.58	33.17±9.12
M3	*Opt*-mono-ORbIT 200 µg/ml	50.29±18.69	2.67±0.63	0.75±0.45	0.75±0.50	13.97±6.46	2.58±3.62	55.54±13.96	29.52±18.4

7

8

Chapter 8

High-throughput microfluidic blood testing to phenotype patients with genetically linked or familial platelet disorders: an aid to diagnosis.

Fernández DI, Provenzale I, Canaul M, Fels S, Lenz A, Andresen F, Krümpke A, Dupuis A, Heemskerk JWM*, Boeckelmann D*, Zieger B*

* Equal contribution

Abstract

Linking the genetic background of patients with a platelet function disorder to a bleeding diathesis is still challenging. High-throughput microfluidic assays have the potential to link pathogenic variants or variants of uncertain significance (VUS) to platelet dysfunctions and distinguish between patients and variant-carrying relatives. In this study, we included 15 index patients, presenting with bleeding symptoms and/or albinism, and 16 relatives. Genotyping of patients by panel or candidate gene sequencing revealed a novel biallelic pathogenic variant in *RASGRP2* (splice site c.240-1G>A), abrogating CalDAG-GEFI expression; a compound heterozygosity (c.537del, c.571A>T) in *P2RY12*, affecting P2Y$_{12}$ signaling; and other heterozygous VUS in the *P2RY12* and *HPS3* genes. Included were also patients with genetically confirmed Hermansky-Pudlak syndrome type 1 or 3. In 5 patients no genetic variant was identified by panel sequencing. Routine laboratory measurements of platelet functions were performed. Furthermore, blood samples from all subjects and day controls were screened for multiparameter thrombus formation (48 outcome parameters) and compared to a reference cohort. Differential and principal component analysis of the multiparametric microfluidics data showed a compromised thrombus formation in the 15 index patients, which clustered differentially compared to heterozygous family members and the control subjects. The inclusion of hematological parameters and diagnostic laboratory measurements further segregated the clusters. Subject ranking based on thrombus outcome indicated that the microfluidic platelet function defects linked to the presence but not the severity of a bleeding diathesis. In conclusion, whole blood multiparametric thrombus formation was able to further diagnose symptomatic patients carrying different variants linked to platelet bleeding disorders.

Introduction

Platelet bleeding disorders are highly heterogeneous with clinical manifestations ranging from prolonged bleeding time, incidental mucocutaneous bleeding, easy bruising, and menorrhagia to life-threatening bleeding episodes [1,2]. Despite extensive efforts, the underlying genetic cause of abnormal bleeding disorders often remains elusive [3,4]. Standard panels of platelet function tests have been developed by consensus parties to provide an optimal diagnostic workflow for revealing platelet disorders [5-7].

Common platforms that analyze platelet function are light transmission aggregometry (LTA), and flow cytometry, often accompanied by measurement of von Willebrand factor (VWF), and standard coagulation times [7,8]. Flow cytometry in particular is useful to confirm a storage pool deficiency (SPD) with platelets impaired in δ-granule secretion (marker CD63) and/or α-granule secretion (marker CD62P) [9,10]. In addition, sequencing analysis of a defined set of platelet-expressed genes (panel sequencing) has become common to identify inherited platelet defects, although its power is still limited [11,12].

Large-scale point-of-care microfluidic testing to proxy hemostasis has so far only been performed with whole-blood from patients with von Willebrand disease (VWD) [13]. Recently, we have established a multiparameter microfluidic assay, based on six defined microspots for detailed platelet phenotyping from a cohort of 97 full-genetically characterized healthy subjects, which provided 48 outcome parameters of thrombus formation [14]. The analysis revealed that certain thrombus characteristics were associated with common genetic variants of *GP6* (encoding for glycoprotein VI, GPVI) and *FCER1G* (encoding for Fc receptor γ-chain). In addition, we performed microfluidic testing for patients with combined immunodeficiency and bleeding in patients with pathogenic variants in *STIM1* and *ORAI1* [15], which both encode for proteins regulating Ca^{2+} entry [16]. While this multiparameter assay can identify platelet abnormalities in families with platelet disorders because of its high-throughput characteristics [17], this testing has not been performed in larger patient cohorts.

Here, we describe three families with a CalDAG-GEFI defect (biallelic novel *RASGRP2* variant) and a P2Y$_{12}$ receptor defect (compound heterozygous variants in *P2RY12*). In addition, we investigated families with variants of uncertain significance (VUS) in *P2RY12* (monoallelic) and *HPS3* (compound heterozygous). Additionally, we included seven families with pathogenic variants in the *HPS1* and *HPS3* genes, and two families with genetically unclear SPD. Using whole-blood assays for thrombus formation, we evaluated the potential of microspot-based microfluidics as an additional tool to identify platelet disorders.

Materials and methods

A detailed description of the methods and patients is available in the Supplement.

8

Patients and control subjects

The study was conducted in accordance with the Declaration of Helsinki and approved by the Ethics Committee of Albert-Ludwigs-University Freiburg (584/17, 28th August 2018). Patients were recruited from the outpatient clinic of the Department of Pediatrics and Adolescent Medicine, University Medical Center in Freiburg. After written informed consent, high-throughput microfluidic blood testing for patients with familial qualitative or quantitative platelet defects, family members, and day controls, was performed at the Medical Center, Freiburg, in September 2019. An extensive phenotypic description of the included index patients and family members, for convenience all labeled as 'Pat', with genetic analysis is presented in the supplementary materials and Table S1. Reference data were obtained from included day-control subjects (so-called CCF) and from a previously published cohort of 97 healthy subjects with all blood type O (so-called CCB) [14].

Blood preparation and platelet aggregation

Blood samples were collected into 3.2% trisodium citrate Vacuette tubes and used for all assays. Common hematologic parameters were obtained using an automated cell counter (Sysmex KX-21 N, Norderstedt, Germany). For index patients and available family members, platelet aggregometry (APACT4) with normalized PRP was performed [18]; the agonist panel consisted of 2 μg/mL collagen (Takeda, Linz, Austria), 4 μM ADP (Sigma-Aldrich, St. Louis, MO, USA), 8 μM epinephrine (Sanofi-Aventis, Frankfurt, Germany), 1.2 mg/mL ristocetin (American Biochemical and Pharmaceutical, Frankfurt, Germany). Where indicated, 5 μM TRAP6 (Hart Biologicals, Hartlepool, UK) and 0.5 mg/mL arachidonic acid (MöLab, Langenfeld, Germany) were added to the panel.

Molecular genetic analysis

Genomic DNA was extracted from EDTA-anticoagulated blood using a QIAamp DNA Blood Mini Kit (Qiagen, Hilden, Germany). Next-generation sequencing (NGS) was performed using a 95 gene panel (custom-designed Nextera Rapid Enrichment Kit, Illumina) previously described [19]. For bioinformatics analysis, Sequence Pilot (JSI Medical Systems) and Alamut Visual Plus (Sophia Genetics) were used. *In silico* pathogenicity of variants was analyzed with CADD (combined annotation-dependent depletion), PolyPhen2, and SIFT. Variants were classified based on American College of Medical Genetics guidelines [20]. Confirmation of potentially pathogenic variants and segregation analysis was performed by direct sequencing.

For the patient with the biallelic *RASGRP2* canonical splice-site variant cDNA sequencing was performed. Total RNA was isolated from washed human platelets using Trizol reagent (Thermo Fisher, Waltham, MA, USA). Single-strand cDNA synthesis was generated with superscript III reverse transcriptase (Thermo Fisher). Amplification and sequencing were with the following primers: forward CTTCGATGACTCCGGGAAGG, reversed GATCATGAG-CTGCACCCACT, covering the coding region from exon 2 to exon 7 of *RASGRP2*. For family 2 with a suspected ADP receptor defect, direct sequencing of the

candidate gene *P2RY12* was performed. The genetic analysis results of remaining patients and family members has been reported before (Table S1).

Microspot-induced multiparameter thrombus formation under flow

Microfluidic whole-blood thrombus formation was assessed according to standard procedures, as described before [14]. Microspots in the flow chambers were coated as indicated in Table 2: *M1,* collagen type I; *M2,* GFOGER-GPO +VWF-BP; *M3,* collagen type III; *M4,* rhodocytin + VWF-BP; *M5,* laminin + VWF-BP; *M6,* human fibrinogen + VWF-BP. No cross-over effects were observed between the consecutive microspots. After recalcification in the presence of a thrombin inhibitor, blood samples from indicated subjects were perfused for 3.5 min at 1000 s^{-1}. Formed thrombi were triple-stained with FITC-labeled anti-fibrinogen mAb, Alexa Fluor (AF)568 annexin A5, and AF647 anti-CD62P mAb. Representative brightfield and fluorescence images from each of the microspots were taken before and after staining, respectively, as before [14]. Duplicate flow runs were performed when possible. Semi-automated scripts, using a manual threshold setting, were used for standardized image analysis in the open-access program Fiji (based on ImageJ) [14]. Images were evaluated by observers, blinded to the condition. The scoring of brightfield images was based on predefined images across microspots. Outcome parameters were, *P1,* platelet deposition (%SAC); *P2,* platelet multilayers (%SAC); *P3,* thrombus multilayer score (scale 0-3); *P4,* thrombus contraction score (scale 0-3); *P5,* thrombus morphological score (scale 0-5); *P6,* integrin αIIbβ3 activation (FITC anti-fibrinogen mAb); *P7,* P-selectin expression (AF647 anti-CD62P mAb); *P8,* phosphatidylserine exposure (AF568-annexin A5).

Results

Patient cohort and genetic variants

To evaluate the thrombus-forming potential of blood samples from patients with a platelet-related bleeding disorder, as a method for point-of-care evaluation, we included 16 patients (12 index patients and 4 affected family members in 11 families), 15 unaffected family members (either heterozygous carrier or wild type) and 5 day control subjects (Table 1). This assaying was performed in September 2019 in the outpatient clinic of the Department of Pediatrics and Adolescent Medicine from the University Medical Center of Freiburg, along with conventional measurements of hematological parameters, LTA, and flow cytometry. Full genetic and diagnostic information of the index patients and family members is given in the Supplementary Materials. For convenience, all members are labeled as Pat01-31 (index patients with *). A comprehensive description of the newly identified genetic variants is given below.

CalDAG-GEFI deficiency. Index patient Pat01* (family 1) presented to the outpatient clinic at the age of 3 years with a history of bleeding (ISTH-BAT score of 7) 21. Platelet aggregation in response to ADP, collagen, epinephrine, and TRAP6 was severely impaired, in contrast to ristocetin-induced agglutination (Figure 1A). Flow cytometry

8

showed normal platelet expression of the platelet receptor αIIbβ3 (Figure 1B), but impaired ADP-induced fibrinogen binding, (Figure 1C). Panel sequencing revealed a novel homozygous pathogenic variant in the *RASGRP2* gene, located at the acceptor splice site of intron 4 (NM_153819.1:c.240-1G>A) (Figure 1D). The variant (rs1490853368) was absent in Human Gene Mutation Database. Genotyping confirmed a familial *RASGRP2* variant (Figure 1E) and a founder effect was suspected based on a relationship six generations back. cDNA sequencing of platelet-derived RNA confirmed a skip of exon 5 (Figure 1F). Immunoblotting confirmed the absence of CalDAG-GEFI protein in the patient's platelets (Figure 1G). Of the three heterozygous family members (Pat02-04, no bleeding), only the father's platelets showed a slightly impaired platelet aggregation, while fibrinogen binding was normal (Supplement).

P2Y$_{12}$ receptor defects. Index patients Pat05* and Pat06* (family 2) are twins with severe bleeding after trauma and surgery (Table 1). Platelet aggregometry showed major impairments in response to ADP [22]. Flow cytometry indicated an essentially abolished fibrinogen binding in response to ADP in both patients (Supplement), suggestive of P2Y$_{12}$ receptor deficiency [23]. Direct sequencing of *P2RY12* (NM_022788.4) and family genotyping revealed compound heterozygosity of two novel (likely) pathogenic variants (c.537del and c.571A>T) in both children. The variants lead to a premature stop codon and an amino acid change, respectively (Table S1). The Asn191Tyr change is located in a transmembrane domain of the ADP ligand-binding pocket according to crystal structure analysis [24]. Pat07 (mother) was heterozygous for c.571A>T, but had no bleeding symptoms. Pat08* (family 3), had a history of mild bleeding after tonsillectomy. Sequencing revealed a heterozygous variant in *P2RY12* (c.853T>C; p.Trp285Arg), predicted to be deleterious (Supplement). Platelet fibrinogen binding upon stimulation with ADP was reduced. The variant segregated with the platelet phenotype in his two affected children (not included). Mild bleeding symptoms have been associated with the presence of a heterozygous *P2RY12* variant as reported before [25,26]. We classified c.853T>C as a variant of uncertain significant (VUS) because this variant has not been published before.

Unresolved storage pool deficiencies. Family 4 consisting of a mother (Pat09*) and her two affected sons (Pat10* and Pat11*), presented with a moderate to severe bleeding phenotype, combined with a platelet storage pool defect (reduced expression of CD62P and mildly of CD63) (Table 1). Platelet aggregometry was impaired in response to collagen, ADP, ristocetin, and epinephrine in all three probands (Datafile S1). The father, Pat12, was not affected. The molecular genetic analysis did not identify the cause for the SPD or the moderate thrombocytopenia, but revealed a heterozygous pathogenic variant (c.7987C>T, p.Arg2663Cys) in the *VWF* gene in the unaffected father and the two sons, but not in the mother. However, VWF parameters in the subjects were normal (Supplement). In family 5, the index patient (Pat13*) and his mother (Pat14*) had mild to moderate bleeding problems and a platelet δ-granule secretion defect, whereas the father (Pat15) was not affected. Panel sequencing did not reveal a pathogenic or likely pathogenic variant.

Hermansky-Pudlak syndromes 1 and 3. We investigated 5 patients with HPS type 1 (oculocutaneous albinism, platelet δ-SPD, genetically confirmed) and their family members (family 8-11). All pathogenic variants have been published by our group previously (supplemental references). For all index patients, platelet aggregation was impaired after stimulation with several agonists (Datafile S1). Five clinically healthy family members were heterozygous for a single variant and one family member (Pat26) showed wild type for the segregating variants (Table 1).

In addition, members from two other families (family 6 and 7) with δ-SPD and variants in the *HPS3* gene (Table 1) were included. The index patient (Pat16*) of family 6 suffered from oculocutaneous albinism and platelet δ-SPD) and was diagnosed with HPS type 3 (NM_032383.5:c.2771del; loss-of-function p.Asn924Ilefs*4) [27]. Both unaffected family members Pat17 and Pat18 were heterozygous for the variant. In family 7, Pat19* with δ-SPD (by flow cytometry) carried two novel compound heterozygous *HPS3* missense VUS (c.65C>G and c.1193G>A) (Datafile S1). Specialized ophthalmological examination showed atypical albinism.[19] Father Pat20 was heterozygous for c.65C>G.

Alterations in whole-blood thrombus formation in patients and family members

Based on whole-blood thrombus formation data from a reference control cohort (labeled as CCB) of 97 genotyped healthy subjects [14], we applied the same multiparameter test for the phenotyping of 31 patients and family members (Pat01-31) - *i.e.* a first cohort of this size - with familial-linked platelet function disorders. For comparison, we obtained blood samples from 5-day-control subjects (labeled as CCF).

Recalcified, anticoagulated blood samples from all subjects were perfused at a high shear rate (1000 s^{-1}) over six microspots (*M1-6*), composed of collagen-I (*M1*), collagen-like peptide GFOGERGPO + VWF-BP (*M2*), collagen-III (*M3*), rhodocytin + VWF-BP (*M4*), laminin + VWF (*M5*), and fibrinogen + VWF-BP (*M6*) (Table S2). Brightfield and fluorescence images of adhered platelets and thrombi, provided parameters of adhesion, aggregation, and thrombus type (*P1-5*) and platelet activation (fibrinogen binding, P-selectin expression indicative of α-granule secretion and phosphatidylserine exposure (*P6-8*). Thus, this analysis resulted in 48 thrombus parameters per blood sample (Table S2).

As described before [14], perfusion of blood from control subjects (CCF) resulted in microspots in multilayered thrombi with activated, fibrinogen-binding platelets and on *M3* in smaller-sized thrombi with also activated platelets (Figure 2, upper panels). Regarding the other microspots, platelet adhesion, and thrombus formation decreased in the order of *M2 > M5 > M4 > M6* (Figure S1). Perfusion of blood from index patients Pat01* (*RASGRP2* defect) and Pat10* (SPD with thrombocytopenia) over *M1* and *M3* resulted in essentially abolished thrombus formation (Figure 2). Less severe defects, with small-sized thrombi, were seen with blood from patients Pat06* (*P2RY12* defect), Pat13* (δ-SPD), Pat19* (*HPS3* variants, δ-SPD), and Pat29* (HPS-1, δ-SPD).

8

Table 1. General characteristics of included patients and control subjects. Indicated are controls (day control cohort CCF; reference control cohort CCB), index patients (in bold*), and relatives, arranged per family (Fam). Further indicated are sex, global phenotype, platelet (10^9/L), and red blood cell (10^{12}/L) counts. In addition, mean defects in platelet aggregation (scored for ADP, collagen, epinephrine, and ristocetin) or in secretion marker exposure by flow cytometry, estimating SPD (FC-SPD: thrombin-induced P-selectin and CD63 expression). Codes per measurement: 0, within the normal range; -1 below the normal range, -2, below 50% of the normal range. *Abbreviations*: n.d., not determined. AR, autosomal recessive; AD, autosomal dominant; CH, compound heterozygous. For an extended description of patients, genetic analyses, and references, see Suppl. Materials and Table S1.

Subject	Family	Diagnosis and genetics	Age	M/F	Phenotype	PLT	RBC	Mean LTA	FC-SPD mean
CCF	N/A	day controls CCF (n=5)	25-48	2/3	healthy controls	277 ± 42	4.2 ± 0.2	0	0
CCB	N/A	reference controls CCB (n=97)	25-79	38/59	healthy, blood type O	268 ± 58	4.6 ± 0.4	n.d.	n.d.
Pat01*	Fam1	CalDAG-GEFI deficiency (AR)	4	m	severe bleeding	263	4	-2	0
Pat02	Fam1	carrier *RASGRP2* pathogenic variant	49	m	healthy family member	145	4.7	-1.3	0
Pat03	Fam1	carrier *RASGRP2* pathogenic variant	44	f	healthy family member	190	4	0	0
Pat04	Fam1	carrier *RASGRP2* pathogenic variant	10	f	healthy family member	288	4.5	0	n.d.
Pat05*	Fam2	P2Y12 receptor defect (AR, CH)	9	m	severe bleeding	280	4.5	-1.3	0
Pat06*	Fam2	P2Y12 receptor defect (AR, CH)	9	m	severe bleeding	298	4.3	-1.3	0
Pat07	Fam2	carrier *P2RY12* likely pathogenic variant	42	f	healthy family member	217	4	n.d.	n.d.
Pat08*	Fam3	P2Y12 receptor defect variant of uncertain significance	33	m	mild bleeding	204	4.4	-1.3	-0.3
Pat09*	Fam4	SPD + thrombocytopenia	41	f	moderate bleeding	94	3.6	-1.3	-1.5
Pat10*	Fam4	SPD + thrombocytopenia; VWD-1 pathogenic variant	20	m	moderate bleeding	65	3.8	-1.3	-1.5
Pat11*	Fam4	SPD + thrombocytopenia; VWD-1 pathogenic variant	18	m	moderate bleeding	86	3.9	-1.3	-1.5
Pat12	Fam4	no SPD, VWD-1 pathogenic variant	46	m	healthy family member	163	4.4	0	0
Pat13*	Fam5	δ-SPD, no variant identified	18	m	moderate bleeding	198	4.8	-1.7	-1
Pat14*	Fam5	δ-SPD, no variant identified	60	f	moderate bleeding	212	3.9	-0.7	-0.5
Pat15	Fam5	unaffected family member	62	m	healthy family member	201	4.2	0	0
Pat16*	Fam6	HPS-3 (AR), δ-SPD	17	m	oculocutaneous albinism	213	4.5	-1.7	-0.7
Pat17	Fam6	carrier *HPS3* pathogenic variant	47	f	healthy family member	209	4	-1	0
Pat18	Fam6	carrier *HPS3* pathogenic variant	25	f	healthy family member	185	4	n.d.	n.d.
Pat19*	Fam7	δ-SPD, HPS3 (CH) variants of uncertain significance	7	f	ocular albinism	192	4.1	-1.3	-1
Pat20	Fam7	carrier variant in *HPS3*	47	m	healthy family member	221	4.5	-1	n.d.
Pat21*	Fam8	HPS-1 (AR, CH), δ-SPD	16	m	oculocutaneous albinism	228	4.4	-0.7	-1
Pat22	Fam8	carrier *HPS1* pathogenic variant	7	f	healthy family member	172	3.9	0	-1
Pat23	Fam8	carrier *HPS1* pathogenic variant	50	m	healthy family member	203	4.7	0	n.d.
Pat24*	Fam9	HPS-1 (AR, CH), δ-SPD	11	m	oculocutaneous albinism	329	4	-0.3	-1.5
Pat25	Fam9	carrier HPS1 pathogenic variant	49	f	healthy family member	261	4.5	n.d.	n.d.
Pat26	Fam9	wild type in family genotyping	19	m	healthy family member	183	4.9	0	n.d.
Pat27	Fam9	carrier *HPS1* pathogenic variant	53	m	healthy family member	210	4.7	0	n.d.
Pat28*	Fam10	HPS-1 (AR, CH), δ-SPD	9	m	oculocutaneous albinism	354	4.3	-1.3	-1.5
Pat29*	Fam10	HPS-1 (AR, CH), δ-SPD	5	m	oculocutaneous albinism	309	3.9	-1.7	-1.5
Pat30	Fam10	carrier *HPS1* pathogenic variant	33	f	healthy family member	227	4.1	n.d.	n.d.
Pat31*	Fam11	HPS-1 (AR, CH), δ-SPD	30	m	oculocutaneous albinism	181	4.8	-1.7	-1

According to standard analysis, the values from all patients and control subjects were univariate scaled 0-10 for each of the eight parameters (*P1-8*) across all six microspots (*M1-6*) for an integrative comparison. The resulting heatmap indicated substantial heterogeneity between blood samples, while pointing to overall higher thrombus parameters for *M1-3* in comparison to *M4-6* (Figure 3A). Construction of a subtraction heatmap, showing the changes per patient relative to the in-study controls (filtered for changes outside means ± 2 SD of controls) provided an overview of the most contributing parameters for individual patients Pat01-31 (Figure 3B). In general, the largest negative effect sizes (green colored) can be seen for microspots *M2* (GFOGERGPO + VWF-BP), *M3* (collagen-III), and *M5* (laminin + VWF). However, several positive effect sizes (red colored) were observed for *M4* (rhodocytin + VWF-BP). This subtraction heatmap also underlined the overall similarity of parameter values for day-control (CCF) and reference-control (CCB) subjects.

To assess the cohesion of the scaled dataset, we generated a Spearman correlation matrix, comparing all parameters within and across microspots (Figure S2A). Per microspot, this matrix showed for *M1-5* mostly strong correlations between *P1-8*, while for *M6* the brightfield parameters *P1-5* segregated from the fluorescence parameters *P6-8*. This was also apparent from a matrix of P values (Figure S2B). In a pairwise comparison of microspots, the highest cohesion of parameters was seen for the spots *M1-3*, which are all platelet GPVI-dependent surfaces. Across all microspots, parameters related to platelet aggregation (*P2*, platelet multilayer; *P3*, thrombus multilayer score; *P4*, thrombus contraction score, *P5*, thrombus morphological score; *P6*, integrin αIIbβ3 activation) correlated well with an R>0.40 (Figure S2A). This pointed to a subject-dependent factor determining the extent and progress of platelet aggregation independent of the microspot.

8
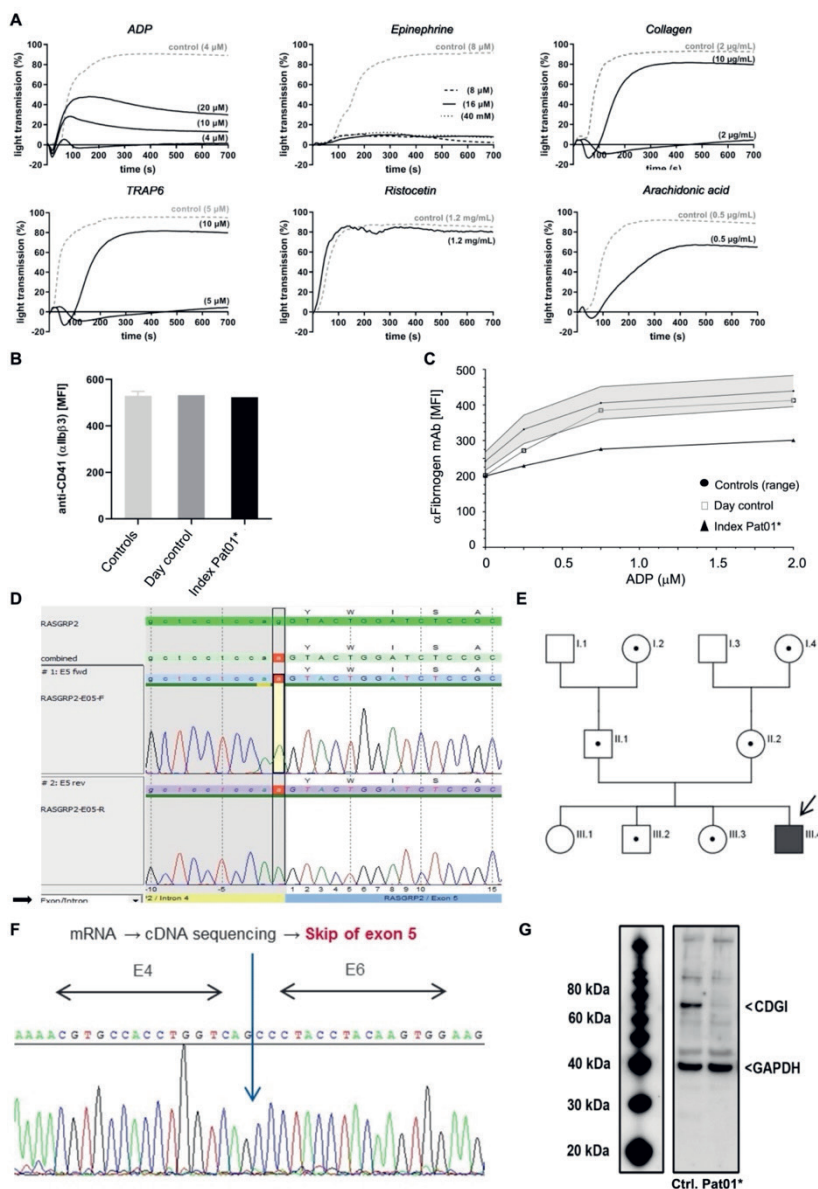
Figure 1. Platelet characterization and molecular genetic analysis of patient Pat01* with *novel RASGRP2* variant.
(**A**) Aggregation of platelet-rich plasma (PRP, light transmission %) from index patient Pat01* (black curves) and healthy control (dotted curve), induced by ADP (4-20 μM), epinephrine (8-40 μM), collagen H (2-10 μg/mL), TRAP6 (5-10 μM) or arachidonic acid (0.5 mg/mL). Platelet agglutination was induced by ristocetin (1.2 mg/mL). (**B**) Flow cytometric analysis of diluted PRP, showing normal expression of αIIbβ3 (CD41). (**C**) Flow cytometry indicating impaired ADP-induced fibrinogen binding to Pat1* platelets, compared to control subjects (day control and 20 measurements from 6 controls, mean ± SD). (**D**) Verification of a homozygous *RASGRP2* canonical splice site variant by direct sequencing. (**E**) Pedigree after segregation analysis (black symbol affected patient, III.4; dotted symbols heterozygous carrier). (**F**) Direct sequencing of platelet-derived cDNA, showing skip of exon 5. (**G**) Absence of CalDAG-GEFI protein (CDGI) in patient's platelets compared to a control subject, by western blotting.
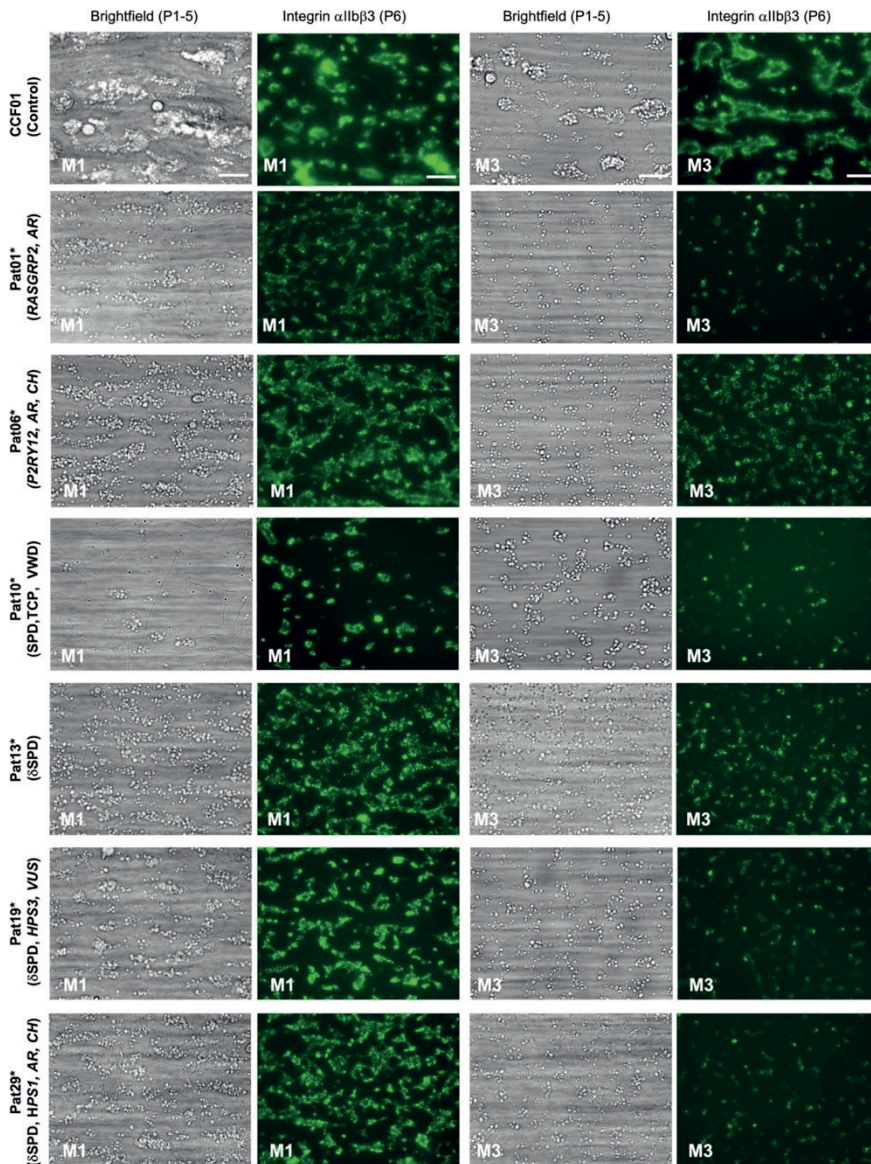
Figure 2. Altered thrombus formation in blood from index patients with confirmed genetics. Whole blood from patients and control subjects was perfused over microspots *M1-6* for 3.5 minutes at a wall-shear rate of 1000 s^{-1}. Brightfield and fluorescence images were captured and analyzed for platelet phenotypes. Shown are representative brightfield and fluorescence (FITC α-fibrinogen mAb for integrin αIIbβ3 activation) images at end stage (Scale bar = 20 µm) for microspots *M1* (collagen-I) and *M3* (collagen-III). Results for a control subject (CCF01), or index patients with a defect in *RASGRP2* (Pat01*) or *P2RY12* (Pat06*)*;* storage pool deficiency with thrombocytopenia (SPD, VWD, TCP) (Pat10*); δ-SPD (no variant identified, Pat13*); or compound heterozygous variants of the *HPS3* (Pat19*) or *HPS1* (Pat29*) genes.

A non-filtered display of all scaled parameters provided detailed insight into the differences in thrombus formation between patients. Per patient, scaled parameter values were subtracted from the controls (CCF) (Figure S3). The cumulative changes showed consistently reduced values for microspots M1-3 and M5 in most index patients and with fewer changes in unaffected family members. Strongest negative changes were seen in Pat01* (RASGRP2 defect), Pat05*, and Pat06* (P2RY12 defects), Pat08* (P2RY12, VUS), and in the carrier Pat07 (Figure S3A-B). Low cumulative values on M1-5 were also present for affected members of family 4 with a genetically unsolved SPD and thrombocytopenia (Pat0-11*), but not for the relative Pat12 (clinically unaffected). For the families with SPD (HPS-1 or HPS-3), most index patients, but not the carrier family members had low values on M2, M3, and M5 (Figure S3D-J). Overall, this subtraction analysis pointed to a separation of thrombus parameters between index patients and the unaffected family members plus control subjects.

Integration of thrombus formation and hematological parameters

To evaluate the contribution of blood cell count to thrombus formation [15], we combined the scaled 48 MP values with those of common hematological parameters (white and red blood cells and platelet count parameters) using subtraction analysis versus the means of day-controls (CCF). The resulting unsupervised clustered heatmap again showed two main clusters of index patients and most of the unaffected family members (Figure 4A).

For the reference CCB cohort, the overall extent of platelet aggregation was calculated as 'thrombus signature', i.e. the integrated scaled sums of P2-6 for all 6 microspots [14]. Ranking of the subjects by thrombus signature showed the highest rankings of heterozygous family members and controls, with Pat14* (mild δ-SPD, genetically unexplained) as the exception (Figure 4B). This correlated with the mild decrease of CD63 expression in flow cytometry. Essentially, all index patients ranked below the control groups. To validate this, we performed a principal component analysis based on all thrombus and hematologic parameters, using k-means analysis (Figure 5A). This revealed a first cluster consisting of controls, most heterozygous carriers, and Pat14*; a second cluster with the majority of index patients plus two carriers; and a third cluster composed of Pat09-11* (SPD with thrombocytopenia). The corresponding Euclidean distance matrix confirmed the high cohesiveness of data from subjects per cluster (Figure 5B). Accordingly, the combination of thrombus and hematological parameters resulted in a clear segregation between index patients (with RASGRP2, P2RY12, HPS1, HPS3 mutations or SPD) and unaffected family members and control subjects.

Linkage of thrombus parameters to clinical and laboratory phenotypes

Then, we evaluated the additive value of the routine laboratory measurements by performing additional principal component analyses, again using the k-means algorithm. In the first approach, we compared the datasets of thrombus formation, hematology, and conventional platelet phenotyping by LTA and flow cytometry (Datafile S1). We obtained similar clusters

with most index patients carrying *RASGRP2*, *P2RY12*, *HPS1,* or *HPS3* variants grouping together (Figure S4A). The values that contributed (>40%) to this grouping were: parameters from microspots *M1-3* and *M5*; platelet and red blood cell characteristics; collagen- and epinephrine-induced platelet aggregation by LTA; and the thrombin-induced CD62P and CD63 expression (Figure S5). Overall, the inclusion of LTA and flow cytometry data resulted in a notable limited contribution to the clustering (see color sidebars of Figure S4A). Furthermore, we compared only the hematological, LTA, and flow cytometry parameters, excluding the microfluidics results. Yet, this analysis did not discriminate between index patients and unaffected family members (Figure S4B).

Analyses of platelet function obtained so far in all patients revealed: *(i)* a consistent contribution of parameters from *M1-3* and *M5* parameters to the common phenotype; *(ii)* an additional contribution of blood cell counts, *(iii)* an informative subject ranking based on thrombus signature, and *(iv)* limited additive value of LTA and flow cytometry measurements. In a final analysis, we also included the data from individual CCF subjects ranked according to the summed parameters of *M1-3,5,* which resulted in a matrix with scaled blood cell counts (Figure 6A). By adding the aberrant traits per subject (impaired platelet aggregation, flow cytometry, bleeding, and oculoalbinism), almost all of these aberrations grouped with the lower set of summed thrombus parameters observed in most index patients. Interestingly, Pat09-11* with SPD and moderate thrombocytopenia ranked lowest, *i.e.* below the patients with HPS or with $P2Y_{12}$ or CalDAG-GEF1 defects.

8
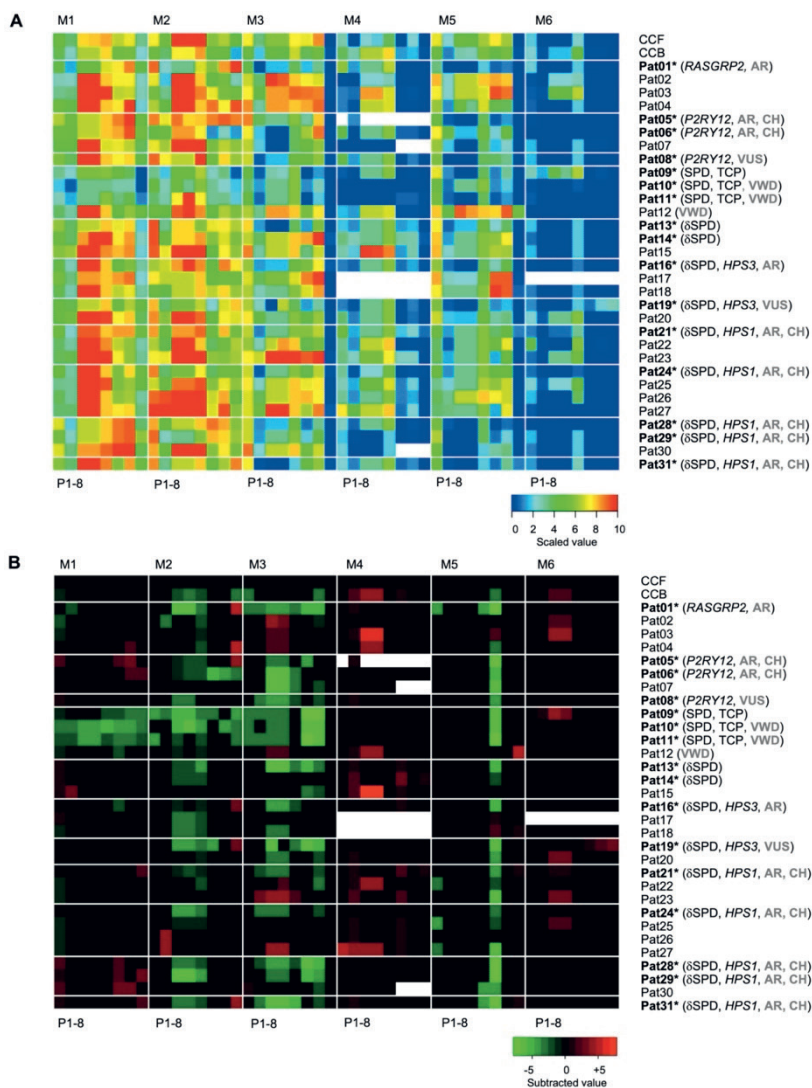
Figure 3. Impairments in multiparameter thrombus formation of patients with platelet function disorders. Whole blood from 31 patients plus family members or 5 day control subjects was perfused over microspots *M1-6* for 3.5 min at wall-shear rate of 1000 s^{-1}. Brightfield and tricolor fluorescence images were recorded and analyzed for platelet-related parameters (Table S2). Brightfield images were evaluated for the analysis of platelet deposition (*P1*), platelet multilayers (*P2*), and thrombus characteristics (*P3-5*). Fluorescence images provided parameters for integrin αIIbβ3 activation (*P6*), P-selectin expression (*P7*), and phosphatidylserine exposure (*P8*). Mean values were obtained from duplicate runs. Individual parameters across all surfaces (*M1-6*) and subjects were univariate scaled 0-10. (**A**) Heatmap drawing of scaled data per patient, microspot, and parameter (missing runs in white). Rainbow color code represents univariate-scaled values between 0 and 10. (**B**) Heatmap of subtracted, scaled data relative to means from day controls (CCF). Subtracted values were filtered for relevant changes, defined as outside the mean of day controls ± 2 SD. Also indicated are subtracted data from the reference cohort of 97 healthy subjects with blood type O (CCB). Color coding indicates a decrease (green) or increase (red) in comparison to CCF controls. Patients are ordered by family; index patients are shown in bold. *Abbreviations:* AR, autosomal recessive; CH, compound heterozygosity; SPD, storage pool deficiency; TCP, moderate thrombocytopenia; VUS, variant of unknown significance.
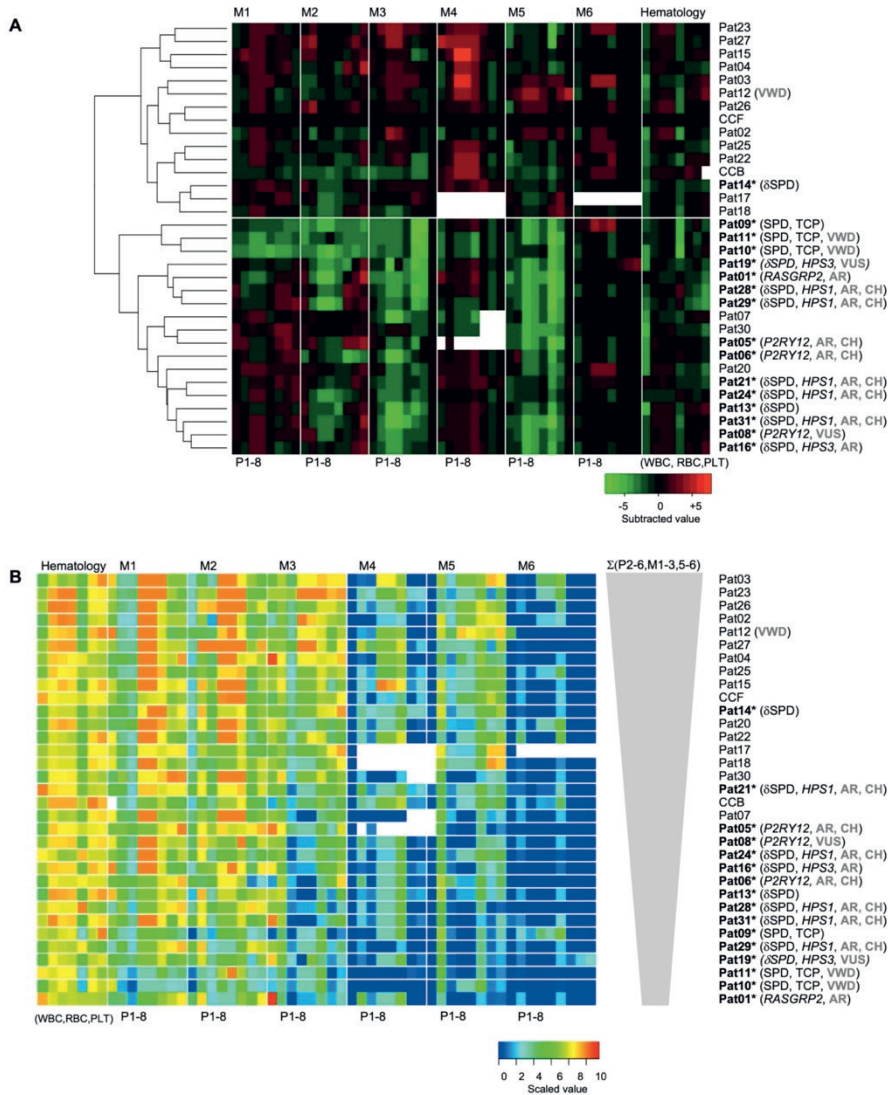
Figure 4. Unsupervised clustering analysis and signatures of thrombus formation with hematological parameters.
Thrombus formation and hematology data were obtained from 31 patients and family members or control subjects. (**A**) Unsupervised clustered heatmap of scaled thrombus parameters (*P1-8*) per microspot (*M1-6*) with added hematological parameters (WBC, RBC, HGB, HCT, PLT, MPV, RDW, P-LCR). Shown are subtraction values per patient/family member versus means of CCF controls. (**B**) Rearrangement of patient order according to decreasing thrombus signature (Σ*P2-6* for *M1-3,5-6*). Microspot M4 with missing data was excluded from the thrombus signature analysis. For scaling and abbreviations, see Figure 3.

8
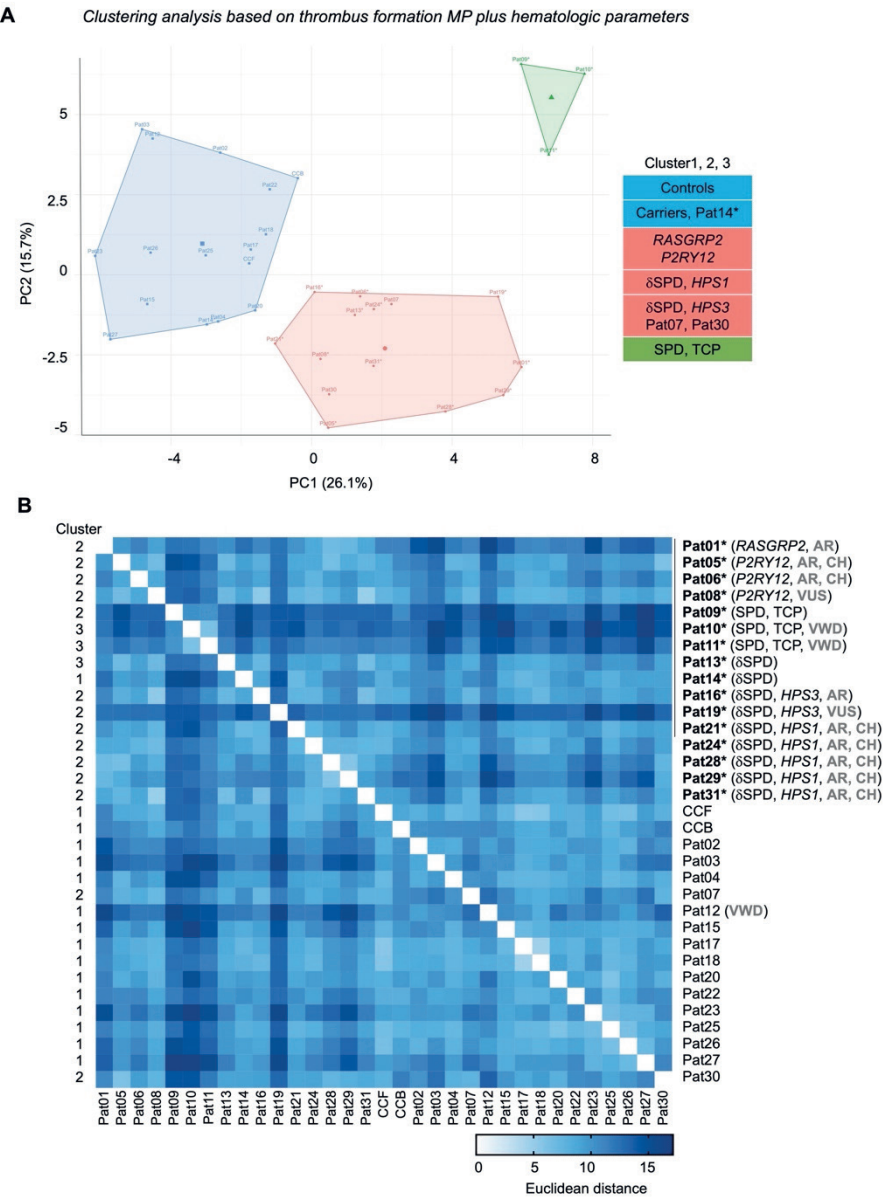
Figure 5. Principal component analysis for microspot and hematological traits of patients and controls. For all included patients, family members, and controls (CCF and CCB), multiparameter data (*P1-8*) of thrombus formation on *M1-6* together with hematological values were univariately scaled and clustered for principal component analysis using scaled and mean-centered data (k-means = 3). Missing values were imputed. (**A**) Default 2-component plot resulting in clusters of: *(1)* controls and most carriers of a heterozygous mutation; *(2)* majority of index patients and autosomal recessive, compound heterozygous carriers; *(3)* family members Pat09-11 with SPD and moderate thrombocytopenia (TCP). (**B**) Euclidean distance matrix of clustered scaled parameters comparing all individual patients. For values, see Datafile S1.
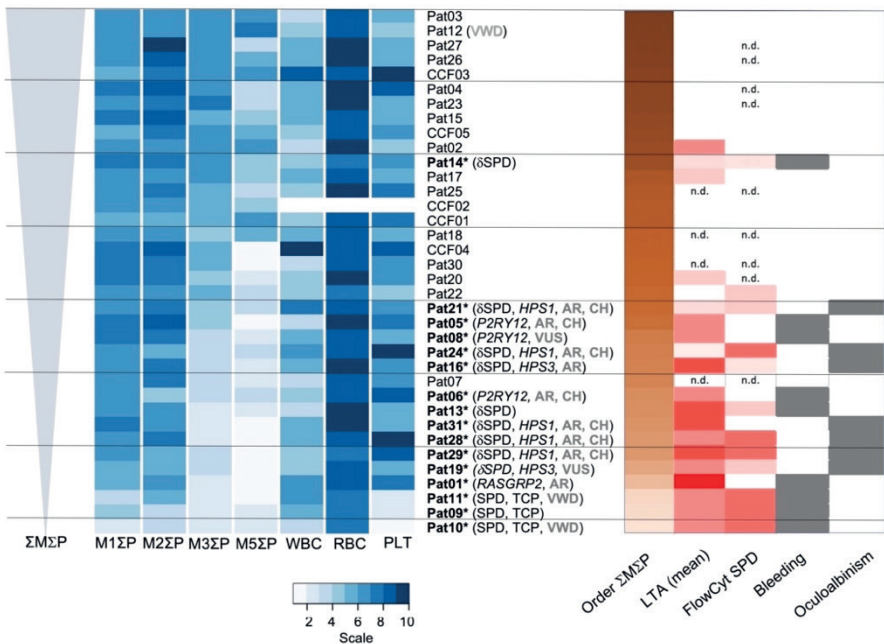
Figure 6. Principal component-based ranking of main microspot parameters separating index patients with bleeding or oculoalbinism. Based on the clustered plot of all compared datasets (Figure S4A), and the parameters mostly contributing to components 1-2 (Figure S5), mean parameters of *M1-3* and *M5* were integrated and ranked, together with hematological parameters of blood cell counts (WBC, RBC, PLT). Shown is a plot of the rescaled narrowed dataset, ranking individual patients (Pat01-31) and controls (CCF01-05) according to decreasing *ΣMΣP* values. Shown as sidebars are: *(1)* order of patient (brown color, lowest); *(2)* mean defects in platelet aggregation (LTA, scaled for ADP, collagen, epinephrine, and ristocetin); *(3)* mean defects in secretion marker exposure by flow cytometry (FlowCyt) to estimate SPD (thrombin-induced P-selectin and CD63 expression); *(4)* bleeding phenotype; *(5)* oculoalbinism phenotype. Color codes: dark red = severely impaired, white = within control range; grey = reported phenotype, n.d. = not determined.

Discussion

This study included 31 index patients with variable bleeding tendency, their relatives, and corresponding control subjects. All index patients and affected family members had been diagnosed before with a (likely) congenital platelet function disorder and presented with a bleeding and/or oculocutaneous albinism phenotype. We identified a novel homozygous splice variant of the *RASGRP2* gene in Pat01* (ISTH bleeding score 7), which encodes for the small GTPase regulator CalDAG-GEFI. This signaling protein was absent in the patient's platelets. The current variant expands the set of 29 earlier reported mutations in this gene [28,29]. The protein CalDAG-GEFI is essential for the Rap1b-dependent activation of integrin αIIbβ3 [30,31]. In the current microfluidic flow assay, we observed a severe defect in thrombus formation, regardless of the surface. The three heterozygous relatives (Pat02-04) showed normal thrombus formation profiles interestingly matching the low ISTH-bleeding scores (2, 2, 0).

Pat05* and Pat06* (family 2) with a bleeding phenotype were found to carry two

novel compound heterozygous pathogenic/likely pathogenic variants in the *P2RY12* gene, causing a platelet $P2Y_{12}$ receptor defect. Microfluidic analysis pointed to a clear, but incomplete reduction in thrombus formation with residual platelet activation via $P2Y_1$ receptors [32]. Other pathogenic variants of the *P2RY12* gene are relatively rare [12,25,33]. On the other hand, Pat08* who experienced bleeding after surgery and had reduced ADP-induced platelet aggregation was genotyped with only one heterozygous variant of *P2RY12*. Yet, in microfluidic testing, thrombus formation was similarly impaired as in index members of family 2. This is suggestive of dominant inheritance.

Genotyping of Pat09-12 (family 4), Pat09*, and Pat10-11 was unable to identify an underlying variant that may explain their phenotype. Although the family carried a pathogenic variant in the *VWF* gene, VWF parameters were within normal ranges and we reasoned that the VWF variant could not explain the severely impaired outcomes of microfluidic testing. This family hence requires further genetic investigation, *e.g.* whole exome sequencing (WES) or checking for super-enhancer sites [34]. Similarly for Pat13-15 (family 5), the bleeding symptoms and the δ-SPD are genetically unexplained. Index Pat13*, but not the mother Pat14*, had low parameters of thrombus formation (*M1-3, M5*). This is consistent with the lower CD63 expression of Pat13* compared to the mother, Pat14*.

The index patients from families 6 to 11 were diagnosed with HPS by flow cytometry and genetic analysis. Typical symptoms for HPS are oculocutaneous albinism and mild bleeding diathesis caused by a δ-granule secretion defect. Some of the HPS patients develop granulomatous colitis and pulmonary fibrosis depending on the gene affected [19,35,36]. HPS is caused by homozygous or compound heterozygous mutations in up to eleven genes, including *HPS1* and *HPS3* [36-38]. For index patients a compound heterozygous pathogenic variants in *HPS1* or *HPS3* were confirmed, while relatives were heterozygous for one variant or wild type. Pat19* had compound heterozygous missense variants in *HPS3,* which were classified as VUS. *HPS3* encodes a subunit of the BLOC-2 complex, of which missense variants may induce milder albinism phenotypes [37,38]. Platelets from the majority of HPS index patients performed poorly in microfluidics and co-clustered with the patients with *RASGRP2* or *P2RY12* mutations.

The present integrative analysis of microspot-dependent microfluidic testing linked to other platelet quantitative and qualitative traits had remarkable outcomes. It appeared that: *(i)* the parameters from collagen-like microspots (*M1-3*) and laminin microspots (*M5*) provided a consistent subject-dependent contribution in terms of capacity to thrombus formation; *(ii)* the inclusion of blood cell counts was of additive value in case of thrombocytopenia; *(iii)* principal component analyses provided a small additional separation between index patients and heterozygous carriers/controls by the inclusion of diagnostic laboratory measurements; *(iv)* the ranking of individual subjects based on cumulative parameters from the microspots was useful in identifying patients with a genotyped platelet disorder. Following the current ranking, thrombus formation was highest for control subjects and heterozygous carriers. It decreased in the order of *P2RY12* defect (heterozygous or

compound heterozygous) > HPS (compound heterozygous *HPS1* or *HPS3*) > *RASGRP2* defect (homozygous) > SPD with thrombocytopenia.

We conclude that microfluidic testing has added value for patients with a bleeding disorder. In addition, the co-clustering of patients with more severe bleeding (*RASGRP2*, *P2RY12* variants) with patients with δ-SPD (*HPS1* or *HPS3* variants), experiencing more moderate bleeding, indicated that the relative reduction in microfluidic thrombus formation revealed an impaired hemostasis, but not the severity of the bleeding diathesis. Accordingly, this work shows that appropriate microfluidic testing provides a valuable addition to the routine laboratory assays in cases of (suspected) platelet bleeding disorders.

Acknowledgments

Author contributions

BZ, FA, and AK took care of the patients and their families. DB, SF, AL, and AD performed molecular genetic analysis. MC performed western analysis and analyzed the data. IP and DF performed experiments, analyzed the data, and wrote the manuscript. DB, BZ, and JH provided supervision and wrote the manuscript.

Conflict of interest

The authors declare no competing financial interests.

References

1. Bastida JM, Benito R, Lozano ML, et al. Molecular diagnosis of inherited coagulation and bleeding disorders. *Semin Thromb Hemost.* 2019;45:695-707.
2. Nurden P, Stritt S, Favier R, Nurden AT. Inherited platelet diseases with normal platelet count: phenotypes, genotypes and diagnostic strategy. *Haematologica.* 2021;106:337-350.
3. Vries MJ, van der Meijden PE, Kuiper GJ, et al. Preoperative screening for bleeding disorders: a comprehensive laboratory assessment of clinical practice. *Res Pract Thromb Haemost.* 2018;2:767-777.
4. Bourguignon A, Tasneem S, Hayward CP. Screening and diagnosis of inherited platelet disorders. *Crit Rev Clin Lab Sci.* 2022:1-40.
5. Lordkipanidzé M, Lowe GC, Kirkby NS, et al. Characterization of multiple platelet activation pathways in patients with bleeding as a high-throughput screening option: use of 96-well Optimul assay. *Blood.* 2014;123:e11-22.
6. Hayward CP, Moffat KA, Brunet J, et al. Update on diagnostic testing for platelet function disorders: What is practical and useful? *Int J Lab Hematol.* 2019;41 Suppl 1:26-32.

8

7. Gresele P, Bury L, Mezzasoma AM, Falcinelli E. Platelet function assays in diagnosis: an update. *Expert Rev Hematol.* 2019;12:29-46.

8. Cattaneo M, Cerletti C, Harrison P, et al. Recommendations for the standardization of light transmission aggregometry: a consensus of the working party from the Platelet Physiology Subcommittee of SSC/ISTH. *J Thromb Haemost.* 2013;11:1183-1189.

9. Nakamura L, Sandrock-Lang K, Speckmann C, et al. Platelet secretion defect in a patient with stromal interaction molecule 1 deficiency. *Blood.* 2013;122:3696-3698.

10. Van Asten I, Schutgens RE, Baaij M, et al. Validation of flow cytometric analysis of platelet function in patients with a suspected platelet function defect. *J Thromb Haemost.* 2018;16:689-698.

11. Simeoni I, Stephens JC, Hu F, et al. A high-throughput sequencing test for diagnosing inherited bleeding, thrombotic, and platelet disorders. *Blood.* 2016;127:2791-2803.

12. Downes K, Megy K, Duarte D, et al. Diagnostic high-throughput sequencing of 2396 patients with bleeding, thrombotic, and platelet disorders. *Blood.* 2019;134:2082-2091.

13. Lehmann M, Ashworth K, Manco-Johnson M, Di Paola J, Neeves KB, Ng CJ. Evaluation of a microfluidic flow assay to screen for von Willebrand disease and low von Willebrand factor levels. *JThromb Haemost.* 2018;16:104-115.

14. Van Geffen JP, Brouns S, Batista J, et al. High-throughput elucidation of thrombus formation reveals sources of platelet function variability. *Haematologica.* 2019;104:1256-1267.

15. Nagy M, Mastenbroek TG, Mattheij NJ, et al. Variable impairment of platelet functions in patients with severe, genetically linked immune deficiencies. *Haematologica.* 2018;103:540-549.

16. Mammadova-Bach E, Nagy M, Heemskerk JW, Nieswandt N, Braun A. Store-operated calcium entry in blood cells in thrombo-inflammation *Cell calcium.* 2019;77:39-48.

17. Provenzale I, Brouns SL, van der Meijden PE, Swieringa F, Heemskerk JW. Whole blood based multiparameter assessment of thrombus formation in a standard microfluidic device to proxy in vivo haemostasis and thrombosis. *Micromachines.* 2019;10:e787.

18. Lahav J, Jurk K, Hess O, et al. Sustained integrin ligation involves extracellular free sulfhydryls and enzymatically catalyzed disulfide exchange. *Blood.* 2002;100:2472-2478.

19. Boeckelmann D, Wolter M, Neubauer K, et al. Hermansky-Pudlak syndrome: identification of novel variants in the genes HPS3, HPS5, and DTNBP1 (HPS7). *Front Pharmacol.* 2021;12:786937.

20. Richards S, Aziz N, Bale S, et al. Standards and guidelines for the interpretation of sequence variants: a joint consensus recommendation of the American College of Medical Genetics and Genomics and the Association for Molecular Pathology. *Genet Med.* 2015;17:405-424.

21. Boeckelmann D, Lenz A, Fels S, Loewecke F, Lausch E, Zieger B. Novel splice-site mutation in RASGRP2 leading to CalDAG-GEFI deficiency. *Blood.* 2020;136 (Suppl. 1):16-17.

22. Dupuis A, Boeckelmann D, Laeuffer P, Neubauer K, Gachet C, Zieger B. Two novel compound heterozygous pathogenic variants in P2YR12 gene. *Blood.* 2018;132 (Suppl. 1):1154.

23. Lecchi A, Femia EA, Paoletta S, et al. Inherited dysfunctional platelet P2Y$_{12}$ receptor mutations associated with bleeding disorders. *Hamostaseologie.* 2016;36:279-283.

24. Zhang J, Zhang K, Gao ZG, et al. Agonist-bound structure of the human P2Y$_{12}$ receptor. *Nature.* 2014;509:119-122.

25. Daly ME, Dawood BB, Lester WA, et al. Identification and characterization of a novel P2Y$_{12}$ variant in a patient diagnosed with type 1 von Willebrand disease in the European MCMDM-1VWD study. *Blood.* 2009;113:4110-4113.

26. Mundell SJ, Rabbolini D, Gabrielli S, et al. Receptor homodimerization plays a critical role in a novel dominant negative P2RY12 variant identified in a family with severe bleeding. *J Thromb Haemost.* 2018;16:44-53.

27. Sandrock-Lang K, Bartsch I, Buechele N, et al. Novel mutation in two brothers with Hermansky Pudlak syndrome type 3. *Blood Cells Mol Dis.* 2017;67:75-80.

28. Westbury SK, Canault M, Greene D, et al. Expanded repertoire of RASGRP2 variants responsible for platelet dysfunction and severe bleeding. *Blood.* 2017;130:1026-1030.

29. Sevivas T, Bastida JM, Paul DS, et al. Identification of two novel mutations in RASGRP2 affecting platelet CalDAG-GEFI expression and function in patients with bleeding diathesis. *Platelets.* 2018;29:192-195.

30. Crittenden JR, Bergmeier W, Zhang Y, et al. CalDAG-GEFI integrates signaling for platelet aggregation and thrombus formation. *Nat Med.* 2004;10:982-986.

31. Cifuni SM, Wagner DD, Bergmeier W. CalDAG-GEFI and protein kinase C represent alternative pathways leading to activation of integrin αIIbβ3 in platelets. *Blood.* 2008;112:1696-1703.

32. Fernandez DI, Kuijpers MJ, Heemskerk JW. Platelet calcium signalling by G-protein coupled and ITAM-linked receptors regulating anoctamin-6 and procoagulant activity. *Platelets.* 2021;32:863-871.

33. Lecchi A, Razzari C, Paoletta S, et al. Identification of a new dysfunctional platelet P2Y$_{12}$ receptor variant associated with bleeding diathesis. *Blood.* 2015;125:1006-1013.

34. Petersen R, Lambourne JJ, Javierre BM, et al. Platelet function is modified by common sequence variation in megakaryocyte super enhancer. *Nat Commun.* 2017;8:16058.

35. Oh J, Ho L, Ala-Mello S, et al. Mutation analysis of patients with Hermansky-Pudlak syndrome: a frameshift hot spot in the HPS gene and apparent locus heterogeneity. *Am J Hum Genet.* 1998;62:593-598.

36. Pennamen P, Le L, Tingaud-Sequeira A, et al. BLOC1S5 pathogenic variants cause a new type of Hermansky-Pudlak syndrome. *Genet Med.* 2020;22:1613-1622.

37. Huizing M, Malicdan MC, Wang JA, et al. Hermansky-Pudlak syndrome: mutation update. *Hum Mutat.* 2020;41:543-580.

38. Boeckelmann D, Wolter M, Käsmann-Kellner B, Koehler U, Schieber-Nakamura L, Zieger B. A novel likely pathogenic variant in the BLOC1S5 gene associated with Hermansky-Pudlak syndrome type 11 and an overview of human BLOC-1 deficiencies. *Cells.* 2021;10:2630.

8

Supplemental Materials, Methods, and Figures of Chapter 8

Patient description

Description of subjects including index patients per family

In addition to daily control subjects (CCF), 31 patients or their relatives from 11 families were included in this study in September 2019. Note that all 31 included subjects were labeled for convenience as Pat01-31, although not all were clinically categorized as patients. The complete diagnostic, laboratory, and genotype data are provided in Datafile S1. Below, a comprehensive description is given per family, with an overview in Table S1.

 Family 1: CalDAG-GEFI deficiency (novel pathogenic variant). The index patient (**Pat01***, P1040), was a 3-year-old boy who was referred to the Division of Pediatric Hematology and Oncology at the Freiburg Medical Center with the clinical presumption diagnosis of Glanzmann thrombasthenia. Postnatal he had developed petechiae and later recurrent infections, including pneumonia at the age of 8 months. After a tongue bite at the age of 1 year, he needed tranexamic acid to stop ongoing bleeding. At the time of counseling, he presented with hematomas of different stages located at the legs and the body. The ISTH-BAT score was 7. Family members, including parents, elder sisters, and a brother, did not have a history of bleeding. The index patient and three family members (**Pat02-04**) were enrolled in a follow-up diagnostic protocol to establish the biochemical and molecular genetic background of the suspected platelet disorder (see Figure 1).

 Patient **Pat01*** had normal values for platelet count, aPTT, INR, factor XIII, and VWF parameters. The Ivy bleeding time was markedly increased (>15 min, normal <6 min). Light transmission aggregometry (LTA) in response to ADP, epinephrine, and low dose collagen, and TRAP6 was severely reduced. His platelets expressed normal levels of GPIb-V-IX (CD42a/b) and fibrinogen receptor integrin αIIbβ3 (CD41). Ristocetin-induced VWF binding was normal, but ADP-induced fibrinogen binding was decreased compared to controls. After thrombin stimulation, secretion of α-granules (CD62P) and δ-granules (CD63) was normal. Because of these findings, a functional defect of integrin αIIbβ3 activation was suspected.

 Next-generation sequencing (NGS) revealed a novel homozygous pathogenic variant in the *RASGRP2* gene (NM_153819.1), located at the acceptor splice site of intron 4 (c.240-1G>A). The heterozygous parents were non-consanguine but were locally enrooted. The variant is listed in dbSNP (rs1490853368) and the Genome Aggregation Database (gnomAD, <1:245,050 subjects) with a minor allele frequency close to 0%. Entries in ClinVar or HGMD (Human Gene Mutation Database) are absent. Because of the rareness of the variant, a founder effect or a background relatedness among the parents was suspected which could be traced to related ancestors 6 generations back. Sequencing of the reverse transcribed cDNA from platelet RNA identified a skip of exon 5, while immunoblot analysis revealed the absence of the encoded protein CalDAG-GEFI in the platelets of the index patient. The patient has been diagnosed with CalDAG-GEFI deficiency (BDPLT18),

inherited autosomal recessive. The case has been described in abstract form [1]. Three included family members were heterozygous for the variant. LTA studies indicated a severe impairment in response to all agonists tested for index patient **Pat01*** (Figure 1) and a moderate impairment for the father (Pat02). The two other family members showed values within normal ranges.

Family 2: P2Y$_{12}$ receptor defect (novel *P2RY12* pathogenic/likely pathogenic variants). Index patients (**Pat05*** and **Pat06***, P1006 and P1007) are fraternal twins, both with an autosomal recessive inherited P2Y$_{12}$ receptor defect (BDPLT8). Both boys, but not the parents, suffered from easy bruising and prolonged bleeding events after trauma and surgery (tonsillectomy). LTA showed major impairments in response to 4-20 μM ADP (<15 %Tmax), and milder in response to collagen or epinephrine. Ristocetin-induced platelet agglutination was normal. Flow cytometry revealed a severely decreased fibrinogen binding to the platelets after stimulation with ADP (0.25–5.0 μM) for both twins, compared to control subjects. We performed VASP phosphorylation analysis (Stago, France) to evaluate the degree of inhibition of adenylyl cyclase (AC) by ADP, by measuring the phosphorylation of vasodilator-stimulated phosphoprotein (VASP) after the exposure of platelets to prostaglandin E$_1$ (PGE$_1$). The platelet reactivity index (PRI) for the twins was as low as 1.2% and 1%, respectively (control 73%) confirming that the P2Y$_{12}$ receptor is not functional. Direct sequencing of the candidate gene *P2RY12* (NM_022788.4) identified a compound heterozygosity for two novel variants: a one base pair deletion leading to a frameshift and a premature stop codon c.537del, p. Lys179Asnfs*6); and a likely pathogenic missense variant (c.571A>T, Asn191Tyr) [2]. The mother (**Pat07**, P1008), carrying the Asn191Tyr variant, was included in this study.

Family 3: P2Y$_{12}$ receptor defect (novel *P2RY12* variant of uncertain significance, VUS). Index patient **Pat08*** (P1028) suffered from postoperative bleeding after tonsillectomy as an adult. Laboratory results indicated an impaired platelet aggregation after stimulation with ADP or epinephrine. In flow cytometry, fibrinogen-binding after ADP activation was impaired. His son (not included in this study) also suffered from bleeding after tonsillectomy. Panel sequencing performed for **Pat08*** and his son identified a heterozygous variant (NM_022788.4:c.853T>C, p.Trp285Arg) in *P2RY12*. No other relevant variants were found in the gene panel. Family genotyping of Pat08*´s daughter (not included in the study) also identified the girl as a carrier. The missense variant is predicted to be deleterious (SIFT, PolyPhen2), the CADD score was 24.6, and the variant was absent in controls of the 1000 Genomes (dbSNP, gnomAD, v2.1.1). According to ACMG criteria, we classified the variant as of uncertain significance (PM1, PM2). Interestingly, the VASP assay performed with platelets from **Pat08*** revealed only a mild defect (RPI 60.5% compared to control 84%). This is in contrast to the twins (family 2) with a classical, autosomal recessive ADP receptor defect. Although the common inheritance for *P2RY12* defects is autosomal recessive, few heterozygous pathogenic variants have been reported that are associated with a bleeding phenotype [3,4].

8

Family 4: SPD and moderate thrombocytopenia. We included three affected family members with a complex platelet phenotype. The index patient (**Pat09***, P1000, mother) and two sons (**Pat10*** and **Pat11***, P1001 and P1004), all presented with a moderate bleeding tendency, moderate thrombocytopenia and a platelet storage pool defect (CD62P- and CD63-expression reduced). Pat09* suffered from easy bruising, gum bleeding, and menorrhagia. **Pat10*** reported easy bruising and bleeding after surgery. **Pat11*** suffered from bleeding after surgery (adenectomy), easy bruising, and gum bleeding. Platelet aggregation/agglutination in response to all tested agonists (collagen, ADP, epinephrine, ristocetin) was impaired for **Pat09-11**. The father (**Pat12**, P1005) was not affected. Panel sequencing was performed for all three affected family members without a disease-explaining finding. Therefore, the cause of the SPD is genetically unsolved, so far. Interestingly, panel sequencing identified a pathogenic heterozygous variant in the *VWF* gene (c.7987C>T, p.Arg2663Cys) to be present in the two brothers. Sequencing identified the father as a carrier as well. In HGMD, the variant is listed as associated with VWD type 1. *In vitro* work by other groups has shown that the heterozygous expression of this variant in HEK293 cells reduced the expression of ultra-large multimers in endothelium-elongated Weibel-Palade body-like granules [5]. The family has been investigated multiple times, but it appeared that VWF antigen, VWF function (VWF collagen-binding, CB), and factor VIII activity were within the normal ranges as well as VWF multimers. Also, the VWF:antigen/VWF:CB ratio of VWF Arg2663Cys carriers **Pat10***, **Pat11*,** and **Pat12** (Datafile S1) was in the normal high range.

Family 5: δ-SPD (no variant identified). We investigated the index patient (**Pat13***, P1021), with epistaxis, hematomas) who showed severely impaired LTA data and severely reduced CD63 expression. His mother (**Pat14***, P1022, with epistaxis and hematomas, and menorrhagia), showed borderline impaired LTA and a moderate δ-granule secretion defect by flow cytometry. Both patients had a normal platelet count. Panel sequencing did not reveal a pathogenic or likely pathogenic variant in the genes investigated. The father (**Pat15**,) was not affected.

Family 6: HPS type 3 (HPS-3). The index patient **Pat16*** (P1012) was diagnosed with HPS-3 and presented with a classic autosomal recessive inherited Hermansky-Pudlak syndrome phenotype, visual impairment, nystagmus, an increased bleeding symptom (prolonged bleeding after tonsillectomy, severe epistaxis requiring hospitalization). As a child of a consanguine marriage, he was homozygous for one base-pair deletion, resulting in a frameshift and premature stop codon (Suppl. Datafile S1). Additionally, he suffered from severe psychomotor retardation. Array-comparative genomic hybridization revealed a 0.482 Mb deletion on chromosome 17 [6]. The two heterozygous family members (**Pat17** and **Pat18** P1013 and 1014) were unaffected. The **Pat16*** showed a severe δ-granule secretion defect, whereas the **Pat17** did not show a δ-granule secretion defect (for Pat18 flow cytometry was not performed). **Pat16*** showed impaired aggregation (after stimulation with all agonists). LTA analysis for Pat17 showed normal and borderline values, respectively.

Family 7: δ-SPD with two compounds heterozygous VUS in *HPS3*. Index patient **Pat19*** (P1019) showed two compounds heterozygous *HPS3* variants of uncertain significance (NM_032383.5:c.65C>G and c.1193G>A). These two missense variants lead to amino acid changes in p.Pro22Arg and Cys398Tyr, respectively. While the patient did not present an apparent Hermansky-Pudlak phenotype with cutaneous albinism and nystagmus, the specialized ophthalmological examination did indicate ocular albinism (atypical albino-visual evoked potential) with normal visual acuity. A platelet δ-granule secretion defect was revealed by flow cytometry [7]. Platelet aggregation studies were impaired after stimulation with all agonists. The father (**Pat20**, P1020) was heterozygous for c.65C>G, without clinical phenotype. LTA platelet studies showed normal or borderline values.

Family 8: HPS type 1 (HPS-1). Index patient **Pat21*** (P1035) was diagnosed with HPS-1 (Suppl. Datafile S1). He presented with oculocutaneous albinism and mild bleeding symptoms (hematomas) [8]. The index patient carried two compound heterozygous pathogenic variants in the *HPS1* gene (NM_000195.5). These include the relatively common c.1189del variant (rs281865084, gnomAD v2.1.1 in Europe 0.014%), first reported in 1998 [9]. The ClinVar database lists 11 citations for this variant. The second variant concerned a 4 base-pair deletion (c.97_100delTCAG deletion), which is recorded in the 2020 mutation update from Huizing *et al* [10]. Included were two non-affected family members, **Pat22** (sister, P1033) and **Pat23** (father, P1034) of the index patient. The unaffected Pat22 was unborn at the time of the original publication and was genotyped as part of this study. Like the father, Pat22 was a heterozygous carrier of the c.1189del variant. Platelet aggregation responses of **Pat21** were mildly impaired after stimulation with collagen and epinephrine, whereas platelet aggregation of **Pat22-23** was within normal ranges. Flow cytometric assessment of CD63 expression showed a severe reduction for **Pat21** and only a mild decrease for **Pat22** (flow cytometry was not performed for **Pat23**).

Family 9: HPS type 1. Index patient **Pat24*** (P1029) presented with oculocutaneous albinism, nystagmus, and prolonged bleeding after dental surgery. We identified two relatively common pathogenic variants in the *HPS1* gene, *i.e.* c.1189del and a one base pair deletion c.355del (rs281865075). The clinically unaffected mother **Pat25** (P1030) was a heterozygous carrier of the c.1189del variant, whereas the clinically unaffected father **Pat27** (P1032) had the c.355del variant. The clinically unaffected brother **Pat26** (P1031) carried only wildtype alleles [11]. For **Pat24***, flow cytometry of activated platelets showed a severely reduced CD63 expression and a mild reduction in CD62P, whereas in LTA only collagen-induced platelet aggregation was slightly decreased. The brother´s (Pat26) platelets showed normal function. LTA and flow cytometry were not performed for **Pat25** and **Pat27**

Family 10: δ-SPD and HPS type 1. The index patient **Pat28*** (P1036) and his affected brother **Pat29*** (P1037) were investigated because of oculocutaneous albinism, nystagmus, and increased bleeding symptoms (easy bruising after minor trauma and prolonged bleeding after injuries). We identified two pathogenic variants in *HPS1*, namely

8

the relatively common variant c.1189del and a novel canonical splice site mutation c.987+1G>A, as published [11]. Direct sequencing identified the mother (**Pat30**) as a heterozygous carrier of the c.1189del variant. The father was not available. Platelet phenotyping indicated for **Pat28*** and **Pat29*** an aggregation defect (after stimulation with collagen, ADP, and epinephrine). Flow cytometry for both brothers (Pat28* and Pat29*) showed a severe reduction of CD63 expression and a mild reduction of CD62. For Pat30, no data were available.

Family 11: δ-SPD and HPS type 1. Index patient **Pat31*,** who presented with oculocutaneous albinism including nystagmus and a bleeding tendency, was diagnosed with HPS-1 [8]. He is a compound heterozygous carrier of two relatively common pathogenic *HPS1* variants, namely the deletions, c.1189del (rs281865084) and c.355del (rs281865075). LTA was impaired after stimulating with all agonists. CD63 expression was severely decreased and CD62 expression was normal.

Supplemental Materials and Methods

Flow cytometry

Flow cytometry analysis was performed according to Lahav *et al.* [12] using a FACSCalibur (Becton Dickinson, Heidelberg, Germany). For platelet analysis of subjects with suspected CalDAG-GEFI or $P2Y_{12}$ deficiency, aliquots of diluted PRP (5×10^7 platelets/mL) were fixed and stained with FITC-labeled monoclonal antibodies against CD41 (for integrin $\alpha IIb\beta 3$ complex) or against CD42a or CD42b (for GPIb-IX-V complex) (Coulter Immunotech, Marseille, France). For VWF-binding analyses, aliquots were stimulated with ristocetin (0-1 mg/mL) or ADP (0-2 µM) for 3 minutes. The platelets were then stained with FITC-labeled anti-VWF mAb (Bio-Rad AbD Serotec, Puchheim, Germany), followed by Alexa Fluor 488-labeled anti-fibrinogen mAb (Invitrogen, Waltham, MA, USA). For analysis of granule secretion, diluted PRP (5×10^7 platelets/mL) was stimulated with agonist. When using human thrombin (0-1 U/mL; Siemens Healthineers, Marburg, Germany), 1.25 mM Gly-Pro-Arg-Pro (Bachem, Bubendorf, Switzerland) was added. The activated platelets were stained with FITC-labeled anti-CD62P mAb (α-granule secretion) or anti-CD63 mAb (δ-granule secretion), both from Coulter Immunotech [12,13].

Immunoblot analysis

Citrated PRP was centrifuged at 1,000 g for 5 min. The collected platelets were lysed in 10 mM Tris-HCl, 150 mM NaCl, 3 mM EDTA, 6 mM N-ethylmaleimide, and 2.5% sodium dodecyl sulfate, pH 7.00, containing Pefabloc SC (Sigma-Aldrich, Zwijndrecht, The Netherlands). Western blotting was performed, as described [14]. In brief, total protein from cell lysates was determined using a bicinchoninic acid kit (Sigma-Aldrich). Aliquoted samples were then separated by SDS-PAGE and transferred onto polyvinylidene difluoride membranes. The separate proteins were visualized on the blots with antibodies against CalDAG-GEFI (Abcam, Cambridge, UK) and human glyceraldehyde-3-phosphate dehydrogenase (GAPDH, clone 6C5; Millipore, Burlington, MA, USA). Secondary antibodies were either goat anti-rabbit or anti-mouse IgG, horseradish peroxidase-coupled (Bio-Rad Laboratories, Hercules, CA, USA). Protein detection was by chemiluminescence.

Microspot-induced multiparameter thrombus formation under flow

Microfluidic whole-blood thrombus formation was assessed using the parallel-plate Maastricht flow chamber (depth 50 µm, width 3 µm, length 30 mm), as described before for the CCB cohort [15]. In brief, glass coverslips were coated with three microspots of 0.5 µL (3 mm center-to-center distance). Coating concentrations of the applied proteins were optimized [16]. With two coverslips, a total of six different microspots *M1-6* were used for whole blood perfusion (see Table 2). The spots were coded as: *M1*, collagen type I, applied at 100 µg/mL (Horm, Takeda, Hoofddorp, The Netherlands); *M2*, GFOGER-GPO +VWF-BP, coated at 250 µg/mL and 100 µg/mL, respectively; *M3*, collagen type III, at 100 µg/mL (Octapharma, Berlin, Germany); *M4*, rhodocytin + VWF-BP, at 250 and 100 µg/mL; *M5*,

8

laminin + VWF-BP, at 50 and 100µg/mL (laminin: Sigma-Aldrich, 511/521); and *M6*, human fibrinogen + VWF-BP, at 250 and 100 µg/mL (fibrinogen: Sigma-Aldrich F-4129-16). No cross-over effects were observed between the consecutive microspots. After coating, the coverslips were incubated in a humid chamber for 1 h at room temperature and blocked for 30 min with 1% bovine serum albumin blocking buffer.

For blood perfusion, the following standard operating procedures were used [15]. PPACK (D-phenylalanyl-L-prolyl-L-arginine chloromethylketone, 40 µM) anticoagulated blood samples (500 µL) were recalcified with 3.75 mM $MgCl_2$ and 7.5 mM $CaCl_2$, and then perfused for 3.5 min at wall shear rate of 1000 s^{-1}. This was followed by 1.5 min of perfusion with staining solution, during which two representative brightfield images per microspot were recorded. The staining solution was composed of rinse buffer: 10 mM HEPES pH 7.45, 136 mM NaCl, 2.7 mM KCl, 2 mM $MgCl_2$, 2 mM $CaCl_2$, 1 mg/mL glucose, 1 mg/ml BSA, 5 U/mL fragmin (Pfizer) and 1 U/mL heparin (Sigma-Aldrich). Added to this were FITC-labeled anti-fibrinogen mAb (1:100, Dako, F0111, Santa Clara, CA, USA), Alexa Fluor (AF)568 annexin A5 (1:200, Molecular Probes), and AF647 anti-CD62P mAb (1:80, Biolegend, London, United Kingdom). After 2 min of stasis, unbound label was removed by post-perfusion with label-free rinse buffer. Three representative fluorescence images per label and microspot were immediately captured during rinse. Materials were purchased from sources described before [17].

Brightfield and 3-color fluorescence images were taken with two equivalent EVOS-FL microscopes (Life Technologies, Beringen, Belgium), equipped with GFP, RFP, and Cy5 LEDs and dichroic cubes, an Olympus UPLSAPO 60× oil-immersion objective, and a sensitive CCD camera (1360 × 1024 pixels) [15]. Microscopes were used at standard settings of illumination and camera chip sensitivity. Duplicate flow runs were performed when possible. Test variability was 5-8%, depending on surface and parameter.

Standard image analysis and delineation of outcome microfluidic parameters

Semi-automated scripts, using a manual threshold setting, were used for standardized image analysis in the open-access program Fiji (based on ImageJ) [15]. In brief, for brightfield images and each fluorescent label, scripts included [18]: *(i)* optimized fast Fourier transformation to reduce background noise; *(ii)* morphological vertical and horizontal dilate and erode steps to remove noise pixels and enhance the relevant structures; *(iii)* automated threshold settings to generate binary mask images; *(iv)* overlay images to verify by eye the binary images; and *(v)* back loops to re-set thresholds if the analysis was incorrect. Images were evaluated by observers, blinded to the condition (genotypes, other subjects, and platelet characteristics). Per microspot, eight outcome parameters were obtained (Table S2). Brightfield images provided five outcome parameters: *P1*, platelet deposition (%SAC), obtained from thresholded, binary images, representing identified regions of all adhered platelet and thrombus structures; *P2*, platelet multilayers (%SAC), representing identified regions of multi-layered platelets; *P3*, thrombus multilayer score (scale 0-3); *P4*, thrombus contraction score (scale 0-3); *P5*, thrombus morphological score (scale 0-5). Scoring (half units) of the

auto-enhanced brightfield images was based on a predefined gallery of typical images across microspots [18]. Threshold, binary fluorescence images, indicative of platelet activation stages, gave %SAC per label: *P6*, integrin αIIbβ3 activation (FITC anti-fibrinogen mAb); *P7*, P-selectin expression (AF647 anti-CD62P mAb); *P8*, phosphatidylserine exposure (AF568-annexin A5). Scores were always compared to those of predefined reference images. The adequacy of the transfer of image analysis data into Excel spreadsheets for data processing was checked by an independent observer.

Statistics and bioinformatics

For heatmap construction in R, mean values of defined outcome parameters from the microfluidic measurements were linearly normalized to a range from 0-10 [15]. Subtraction heatmaps used a filter of 2× SD versus control runs. One-way unsupervised hierarchical clustering was performed using the R package version 4.2.1 (www.r-project.org). For the construction of correlation matrices, normality was assessed with a univariate Shapiro-Wilk's test for each of the variables; variables with a $p<0.05$ were considered to be non-normally distributed. In this case, the non-parametric Spearman correlation analysis was chosen. For clustering analyses, k-means and hierarchical clustering were calculated in R, and algorithms to determine the optimal number of clusters were used (k = 3). To impute missing values, we decided to use means. Euclidean distances were calculated, and clustering was performed by complete linkages.

Supplemental Tables

8

Table S1. Subject codes, characteristics and identified genetic variants. *Abbrev:* AR, autosomal recessive; CH, compound heterozygous.

Subject nr.	Publ.	Family	Code	Subject type	Diagnosis	Age	M/F	Phenotype	Genetic variant	Protein mutation	Disorder code
CCF	new	N/A	CCF1-5	day controls (n=5)	healthy controls	25-48	2/3	day controls	no pathogenic variant known	n/a	none
CCB	publ.	N/A	CCB1-97	reference control (n=97)	healthy controls, blood type O	25-79	38/59	reference controls	whole-genome sequenced, blood type O	n/a	none
Pat01*	new	Fam1	P1040	index patient	CalDAG-GEFI deficiency (AR)	4	m	severe bleeding	RASGRP2: c.240-1G>A, homozygous	splice defect	BDPLT18
Pat02	new	Fam1	P1041	unaffected father	carrier *RASGRP2* pathogenic variant	49	m	healthy family member	RASGRP2: c.240-1G>A, heterozygous	splice defect	carrier BDPLT18
Pat03	new	Fam1	P1042	unaffected mother	carrier *RASGRP2* pathogenic variant	44	f	healthy family member	RASGRP2: c.240-1G>A, heterozygous	splice defect	carrier BDPLT18
Pat04	new	Fam1	P1043	unaffected sister	carrier *RASGRP2* pathogenic variant	10	f	healthy family member	RASGRP2: c.240-1G>A, heterozygous	splice defect	carrier BDPLT18
Pat05*	new	Fam2	P1006	index twin patients	P2Y12 receptor defect (AR, CH)	9	m	severe bleeding	P2RY12: c.537del; c.571A>T, comp. heterozygous	Lys179Asnfs*6, Asn191Tyr	BDPLT8
Pat06*	new	Fam2	P1007	index twin patients	P2Y12 receptor defect (AR, CH)	9	m	severe bleeding	P2RY12: c.537del; c.571A>T, comp. heterozygous	Lys179Asnfs*6, Asn191Tyr	BDPLT8
Pat07	new	Fam2	P1008	unaffected mother	carrier *P2RY12* likely pathogenic variant	42	f	healthy family member	P2RY12: c.571A>T, heterozygous	Asn191Tyr	carrier BDPLT8
Pat08*	new	Fam3	P1028	index patient	P2Y12 receptor defect, variant	33	m	mild bleeding	P2RY12: c.853T>C, heterozygous	Trp285Arg	BDPLT8?
Pat09*	new	Fam4	P1000	index patient	SPD + thrombocytopenia	41	f	moderate bleeding	no relevant variant identified	not identified	not identified
Pat10*	new	Fam4	P1001	affected son	SPD + thrombocytopenia; VWD-1 pathogenic variant	20	m	moderate bleeding	VWF: c.7987C>T, heterozygous; other variant?	Arg2663Cys	VWD-1
Pat11*	new	Fam4	P1004	affected son	SPD + thrombocytopenia; VWD-1 pathogenic variant	18	m	moderate bleeding	VWF: c.7987C>T, heterozygous; other variant?	Arg2663Cys	VWD-1
Pat12	new	Fam4	P1005	unaffected father	no SPD, VWD-1 pathogenic variant	46	m	healthy family member	VWF: c.7987C>T, heterozygous	Arg2663Cys	carrier VWD-1
Pat13*	new	Fam5	P1021	index patient	δ-SPD, no variant identified	18	m	moderate bleeding	no relevant variant identified	not identified	not identified
Pat14*	new	Fam5	P1022	affected mother	δ-SPD, no variant identified	60	f	moderate bleeding	no relevant variant identified	not identified	not identified
Pat15	new	Fam5	P1023	unaffected father	unaffected family member	62	m	healthy family member	no relevant variant identified	not identified	none

Table S1. Subject codes, characteristics and identified genetic variants. *Abbrev:* AR, autosomal recessive; CH, compound heterozygous (Continued).

Subject nr.	Publ.	Family	Code	Subject type	Diagnosis	Age	M/F	Phenotype	Genetic variant	Protein mutation	Disorder code
Pat16*	publ.	Fam6	P1012	index patient	HPS-3 (AR), δ-SPD	17	m	oculocutaneous albinism	HPS3: c.2771del, homozygous + del 17q12q21.1	Ans924Ilefs*4	HPS-3
Pat17	publ.	Fam6	P1013	unaffected mother	carrier *HPS3* pathogenic variant	47	f	healthy family member	HPS3: c.2771del, heterozygous	Ans924Ilefs*4	carrier HPS-3
Pat18	publ.	Fam6	P1014	unaffected sister	carrier *HPS3* pathogenic variant	25	f	healthy family member	HPS3: c.2771del, heterozygous	Ans924Ilefs*4	carrier HPS-3
Pat19*	publ.	Fam7	P1019	index patient	δ-SPD, *HPS3* (CH) variants of uncertain significance	7	f	ocular albinism	HPS3 : c.65C>G; c.1193G>A, comp. heterozygous	Pro22Arg, Cys398Tyr	HPS-3?
Pat20	publ.	Fam7	P1020	mildly affected father	carrier variant *HPS3*	47	m	healthy family member	HPS3: c.65C>G, heterozygous	Pro22Arg	carrier HPS-3?
Pat21*	publ.	Fam8	P1035	index patient	HPS-1 (AR, CH), δ-SPD	16	m	oculocutaneous albinism	HPS1: c.97_100delTCAG; c.1189del, comp. heteroz.	Ser33Argfs*18, Gln397Serfs*2	HPS-1
Pat22	new	Fam8	P1033	unaffected sister	carrier *HPS1* pathogenic variant	7	f	healthy family member	HPS1: c.1189del, heterozygous	Gln397Serfs*2	carrier HPS-1
Pat23	publ.	Fam8	P1034	unaffected father	carrier *HPS1* pathogenic variant	50	m	healthy family member	HPS1: c.1189del, heterozygous	Gln397Serfs*2	carrier HPS-1
Pat24*	publ.	Fam9	P1029	index patient	HPS-1 (AR, CH), δ-SPD	11	m	oculocutaneous albinism	HPS1: c.355del, c.1189del	His119Thrfs*5, Gln397Serfs*2	HPS-1
Pat25	publ.	Fam9	P1030	unaffected mother	carrier *HPS1* pathogenic variant	49	f	healthy family member	HPS1: c.1189del, heterozygous	Gln397Serfs*2	carrier HPS-1
Pat26	publ.	Fam9	P1031	unaffected brother	wild type in family genotyping	19	m	healthy family member	wildtype	n/a	none
Pat27	publ.	Fam9	P1032	unaffected father	carrier *HPS1* pathogenic variant	53	m	healthy family member	HPS1: c.355del, heterozygous	His119Thrfs*5	carrier HPS-1
Pat28*	publ.	Fam10	P1036	index patient	HPS-1 (AR, CH), δ-SPD	9	m	oculocutaneous albinism	HPS1: c.987+1G>A, c.1189del, comp. heterozygous	splice defect, Gln397Serfs*2	HPS-1
Pat29*	publ.	Fam10	P1037	affected brother	HPS-1 (AR, CH), δ-SPD	5	m	oculocutaneous albinism	HPS1: c.987+1G>A, c.1189del, comp. heterozygous	splice defect, Gln397Serfs*2	HPS-1
Pat30	publ.	Fam10	P1038	unaffected mother	carrier *HPS1* pathogenic variant	33	f	healthy family member	HPS1: c.1189del, heterozygous	Gln397Serfs*2	carrier HPS-1
Pat31*	publ.	Fam11	P1039	index patient	HPS-1 (AR, CH), δ-SPD	30	m	oculocutaneous albinism	HPS1: c.355del, c.1189del, comp. heterozygous	His119Thrfs*5, Gln397Serfs*2	HPS-1

8

Table S2. Microspots and parameters coding of the microfluidic assay. Indicated are the employed microspotted surfaces (*M1-6*), involved platelet receptors per microspot, and analyzed parameters and platelet responses from brightfield and fluorescence microscopic images (*P1-8*). Relative involvement of platelet receptors GPIb-IX-V, GPVI, and integrin α2β1 per surface is indicated. See also Ref [15].

	Microspot surface	GPIb	GPVI	α2β1	Other receptors
M1	collagen type I (VWF)	+	++	+	o
M2	GFOGERGPO + VWF-BP	+	++	++	o
M3	collagen type III (VWF)	+	+	++	o
M4	rhodocytin + VWF-BP	+	o	o	CLEC2 +
M5	laminin + VWF	+	o	o	α6β1 +
M6	fibrinogen + VWF-BP	+	o	o	αIIbβ3 +

++ strongly involved; + involved, o not involved

Brightfield/fluorescence	Response		Range (0-)	Normalized
P1	platelet deposition (%SAC)	adhesion	89.25	0-10
P2	platelet multilayers (%SAC)	aggregate size	62.31	0-10
P3	thrombus multilayer score (0-3)	aggregate score	3.0	0-10
P4	thrombus contraction score (0-3)	contraction	3.0	0-10
P5	thrombus morphological score (0-5)	morphology type	5.0	0-10
P6	integrin αIIbβ3 activation (%SAC)	fibrinogen binding	49.45	0-10
P7	P-selectin expression (%SAC)	α-secretion	72.46	0-10
P8	annexin A5 fluorescence (%SAC)	PS exposure	42.22	0-10

Supplemental Figures
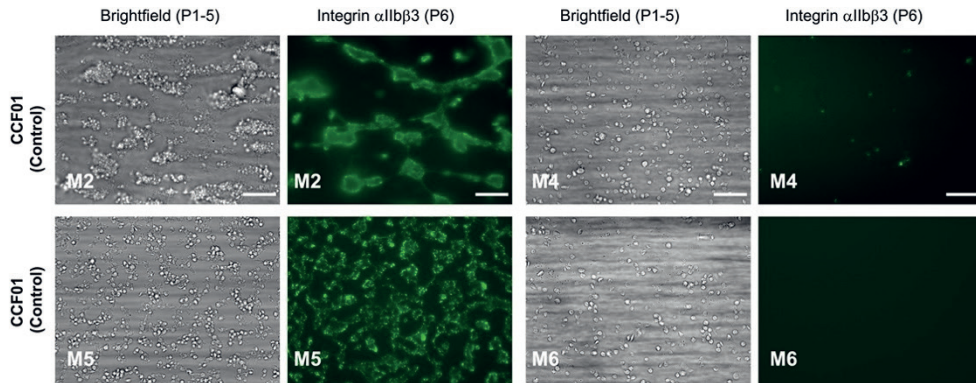
Figure S1. Reference images of thrombus formation. Altered thrombus formation with perfused in blood from patients with genetically proven platelet function disorders. Whole blood from patients and control subjects was perfused over microspots *M1-6* for 3.5 min at wall-shear rate of 1000 s^{-1}. Brightfield and fluorescence images were captured and analyzed for platelet phenotypes (see Figure 2). Shown are representative brightfield and fluorescence (FITC α-fibrinogen mAb) images at end stage (scale bar = 20 µm) for microspots *M2* (GFOGERGPO + VWF-BP), *M4* (rhodocytin + VWF-BP), *M5* (laminin + VWF) and M6 (fibrinogen + VWF-BP). Blood was obtained from a control subject.
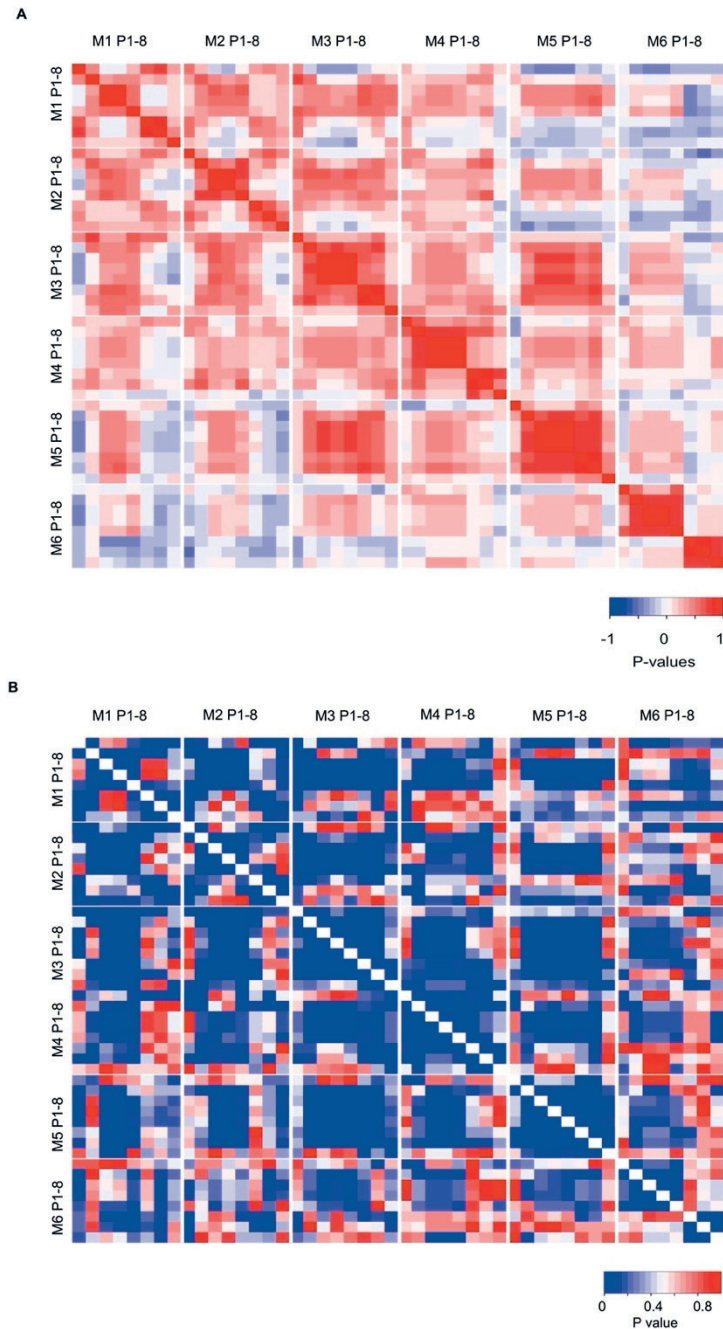
Figure S2. Cohesion matrix of scaled parameters across all size microspots. Whole blood from 31 patients (11 families) or 5 day control subjects were perfused over microspots *M1-6,* as described in Figure 2. Brightfield and tricolor fluorescence images were analyzed for parameters *P1-8* (Table S1), which were univariately scaled across all surfaces. (**A**) Spearman correlation matrix (R) for the complete dataset. Color bar indicates positive (red) and negative (blue) Spearman R values. (**B**) P-values of correlation analysis; $p<0.05$ indicated as dark blue. Raw data are provided in Datafile S1.

A CalDAG-GEFI deficiency (family 1)

B P2Y12 receptor defect (families 2-3)

C SPD and moderate thrombocytopenia (family 4)

D δSPD (family 5)

E δSPD and HSP-3 (family 6)

F δSPD and variants in HSP3 (family 7)

G δSPD and HSP-1 (family 8)

H δSPD and HSP-1 (family 9)

8
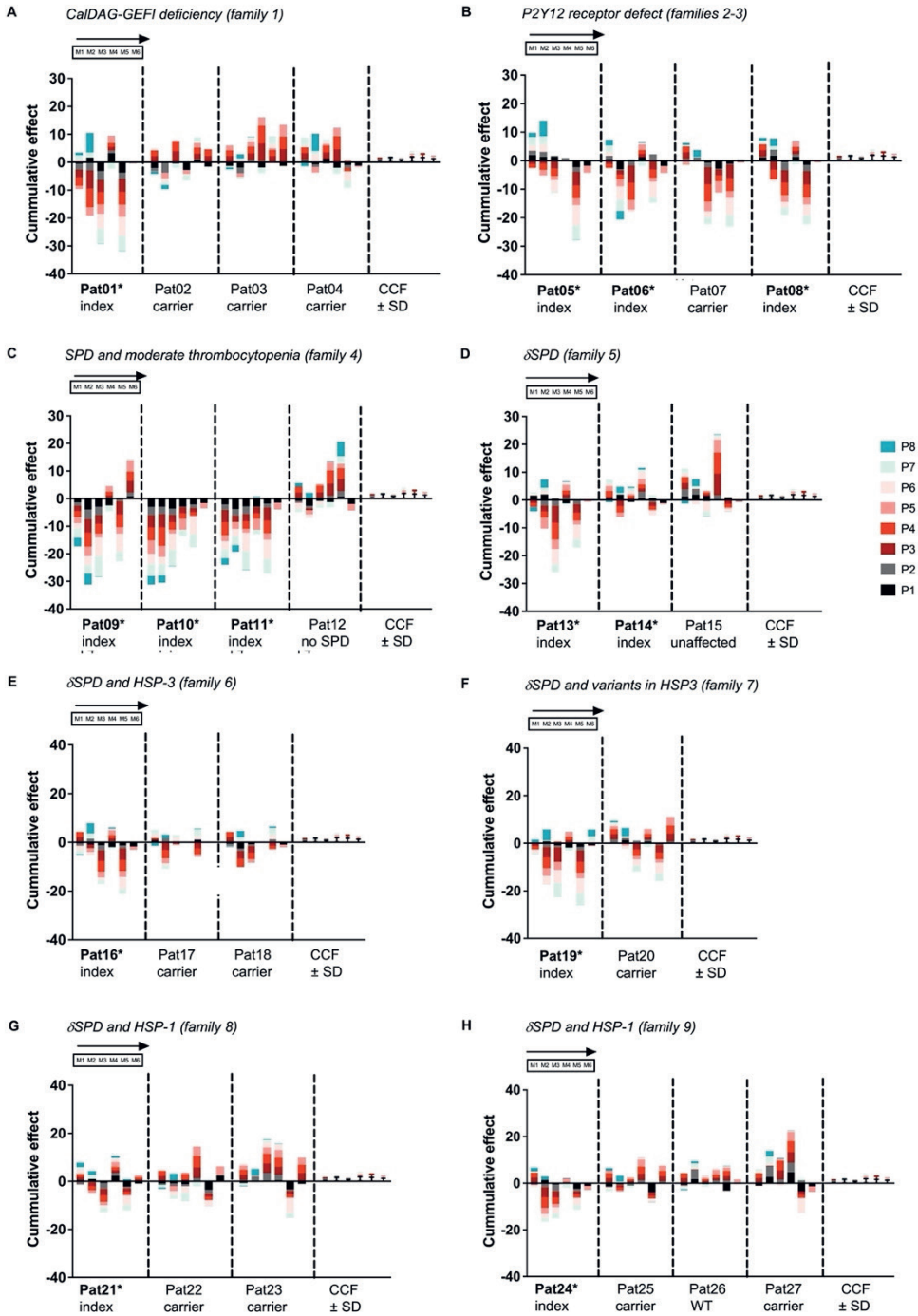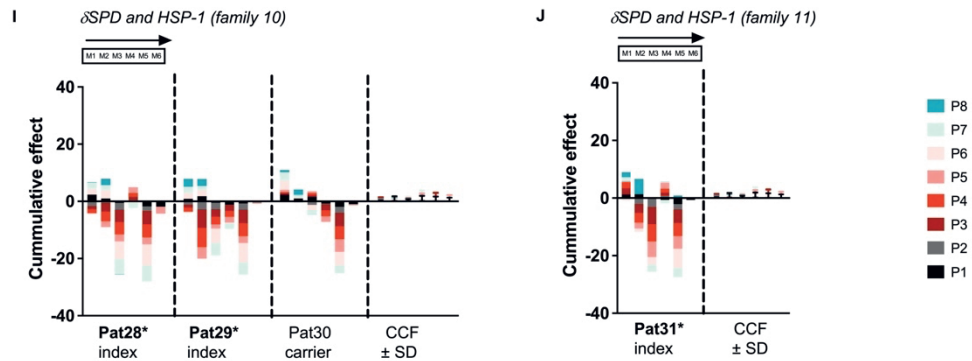
Figure S3. Cumulatively changed parameters of thrombus formation per surface of included patients. Univariate scaled parameters *P1-8* of thrombus formation on microspots *M1-6* were compared per family (panels **I-J**) of the index (bold*) and non-index patients versus mean values from control subjects (CCF01-05, mean ± SD). Subtracted scaled data were used, as described in Figure 3. Indicated are cumulative changes in parameters (*P1-8*) versus means of CCF controls (no statistical filtering) per family member; presentation in order of microspots *M1-6*. For patient description, see Supplementary Materials; for raw data, see Datafile S1.

Figure S4. Principal component analysis for all patients based on combinations of datasets. Clustering of scaled data from 31 patients and control cohorts, was performed using k-means analysis (k=3). (**A**) Clusters were obtained by comparing all parameters of thrombus formation plus hematology, LTA, and flow cytometry. For the individual parameters per component, see Figure S5. (**B**) Clusters were obtained by comparing only parameters of hematology, LTA, and flow cytometry. For the listed patients (index in bold), color bars correspond to the found clusters. Comparisons were also made to the initial PCA of Figure 5A (*i.e.,* thrombus formation and hematology parameters only). Missing values were imputed when needed (*e.g. M4*).
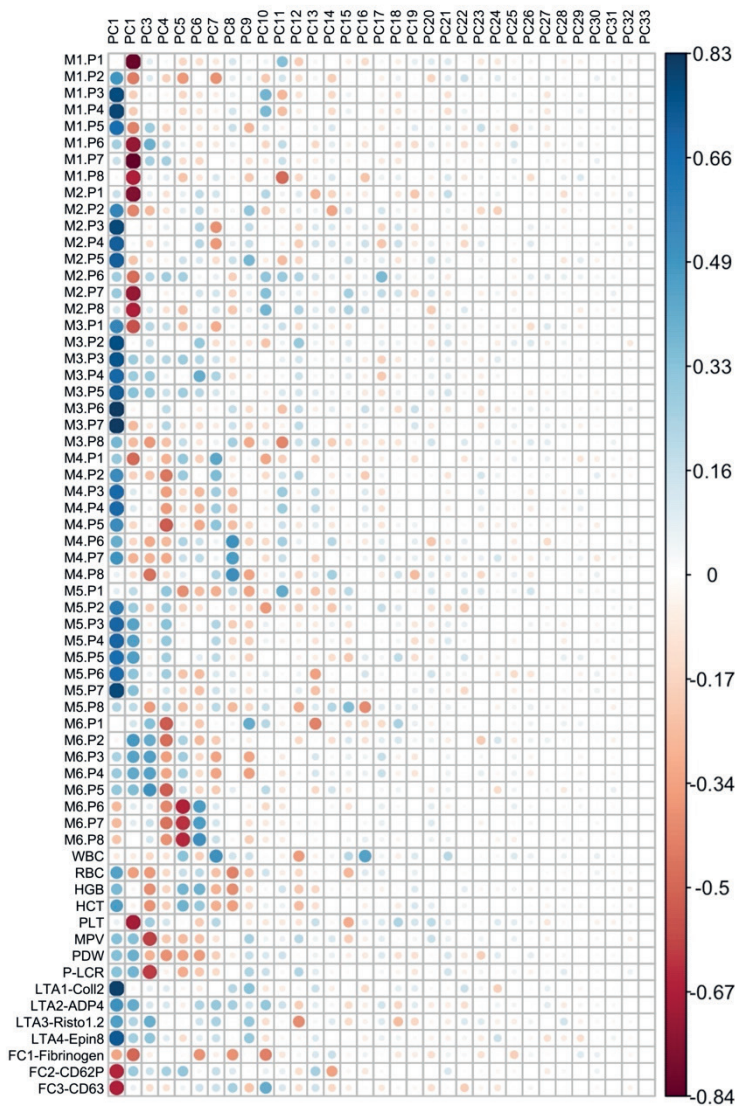
Figure S5. Matrix of principal components (PC) in cluster analysis for all patients and combined datasets. Clustering analysis was performed as in Figure S4A. Included were 31 patients and CCF and CCB control subjects. Compared were: microspot parameters (6 × 8 *MP*), hematology parameters (WBC, RBC, HGB, HCT, PLT, MPV, PDW, P-LCR), platelet aggregation by LTA (collagen 2 µg/mL, ADP 4 µM, ristocetin 1.2 mg/mL, epinephrine 8 µM), and flow cytometry (thrombin-induced fibrinogen binding, CD62P expression, CD63 expression). Visualized is per component (PC1-33) the relative contribution of each variable. The size and color of the dot indicate relative contribution (coding as in color bar). Positive correlations are shown in blue, and negative correlations are in red. Variables contributing to PC1 and PC2 account for 27.1% and 14.9% of the variation in the dataset.

Supplemental Datafile S1: Subject characteristics; raw microfluidic and hematology parameters; platelet aggregation and flow cytometry; principal component analysis; clustering k-means; legends for thrombus formation.

References

1. Boeckelmann D, Lenz A, Fels S, et al. Novel splice-site mutation in RASGRP2 leading to CalDAG-GEFI deficiency. *Blood*. 2020;136 (Suppl. 1):16-17.

2. Dupuis A, Boeckelmann D, Laeuffer P, et al. Two novel compound heterozygous pathogenic variants in P2YR12 gene. *Blood*. 2018;132 (Suppl. 1):1154.

3. Daly ME, Dawood BB, Lester WA, et al. Identification and characterization of a novel P2Y$_{12}$ variant in a patient diagnosed with type 1 von Willebrand disease in the European MCMDM-1VWD study. *Blood*. 2009;113:4110-4113.

4. Mundell SJ, Rabbolini D, Gabrielli S, et al. Receptor homodimerization plays a critical role in a novel dominant negative P2RY12 variant identified in a family with severe bleeding. *J Thromb Haemost*. 2018;16:44-53.

5. Castaman G, Giacomelli SH, Jacobi PM, et al. Reduced von Willebrand factor secretion is associated with loss of Weibel-Palade body formation. *J Thromb Haemost*. 2012;10:951-958.

6. Sandrock-Lang K, Bartsch I, Buechele N, et al. Novel mutation in two brothers with Hermansky Pudlak syndrome type 3. *Blood Cells Mol Dis*. 2017;67:75-80.

7. Boeckelmann D, Wolter M, Neubauer K, et al. Hermansky-Pudlak syndrome: identification of novel variants in the genes HPS3, HPS5, and DTNBP1 (HPS7). *Front Pharmacol*. 2021;12:786937.

8. Oh J, Ho L, Ala-Mello S, *et al*. Mutation analysis of patients with Hermansky-Pudlak syndrome: a frameshift hot spot in the HPS gene and apparent locus heterogeneity. *Am J Hum Genet*. 1998;62:593-598.

9. Huizing M, Malicdan MC, Wang JA, et al. Hermansky-Pudlak syndrome: mutation update. *Hum Mutat*. 2020;41:543-580.

10. Sandrock K, Bartsch I, Rombach N, et al. Compound heterozygous mutations in two siblings with Hermansky-Pudlak syndrome type 1 (HPS1). *Klin Pediatr*. 2010;222:168-174.

11. Boeckelmann D, Sobotta F, Andresen F, et al. Panel sequencing identified a novel splice site mutation in Hermansky-Pudlak syndrome type 1 patients. *Arch Clin Med Case Rep*. 2020;4:1172-1181.

12. Lahav J, Jurk K, Hess O, et al. Sustained integrin ligation involves extracellular free sulfhydryls and enzymatically catalyzed disulfide exchange. *Blood*. 2002;100:2472-2478.

13. Nakamura L, Sandrock-Lang K, Speckmann C, et al. Platelet secretion defect in a patient with stromal interaction molecule 1 deficiency. *Blood*. 2013;122:3696-3698.

14. Canault M, Ghalloussi D, Grosdidier C, et al. Human CalDAG-GEFI gene (RASGRP2) mutation affects platelet function and causes severe bleeding. *J Exp Med*. 2014;211:1349-1362.

15. Van Geffen JP, Brouns S, Batista J, et al. High-throughput elucidation of thrombus formation reveals sources of platelet function variability. *Haematologica*. 2019;104:1256-1267.

16. De Witt SM, Swieringa F, Cavill R, et al. Identification of platelet function defects by multi-parameter assessment of thrombus formation. *Nat Commun*. 2014;5:4257.

17. Gilio K, Harper MT, Cosemans JM, et al. Functional divergence of platelet protein kinase C (PKC) isoforms in thrombus formation on collagen. *J Biol Chem*. 2010;285:23410-23419.

18. Huang J, Jooss NJ, Fernandez DI, et al. Roles of focal adhesion kinase PTK2 and integrin αIIbβ3 signaling in collagen- and GPVI-dependent thrombus formation under shear. *Int J Mol Sci*. 2022;23:8688.

8

9
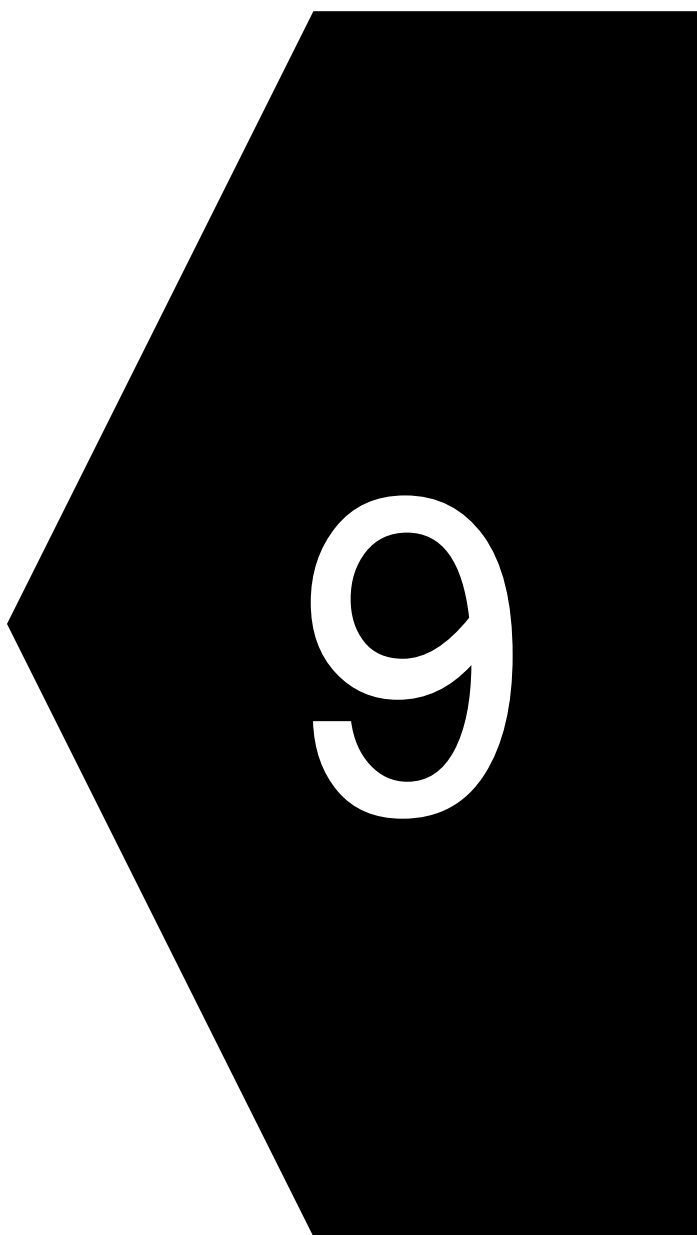
Chapter 9

General Discussion

Platelets are major contributors to the processes of hemostasis and arterial thrombosis. In physiological situations, upon vessel wall injury, the formation of a platelet plug or a thrombus initially stops the bleeding. On the other hand, in pathological situations such as after atherosclerotic plaque rupture, platelet activation and thrombus formation can result in acute occlusion of a cardiac or carotid artery, causing myocardial infarction or ischemic stroke [1]. Current treatment options to prevent new thrombotic events with antiplatelet drugs are accompanied by an increased risk of bleeding. Better knowledge of the mechanisms of platelet activation is essential to find safer and specific antithrombotic drugs.

The overall aim of this thesis is to develop and use high-throughput assays to better evaluate the major functions and signaling pathways of platelets, and to find novel ways of platelet inhibition in cardiovascular disease (**Chapter 1**). In most experimental chapters, I measure signaling via the second messenger Ca^{2+} as a proxy for platelet activation. In addition, I refer to *in silico* methods to find new platelet-inhibiting agents.

Integrative signals of platelet activation: the additive value of studying Ca^{2+} signaling

Controlled elevation of the cytosolic Ca^{2+} concentration is regarded as an essential event in the activation of many cell types [2]. In platelets, the Ca^{2+} elevation induces multiple functional responses, including shape change, aggregation, granule secretion, and switching to a procoagulant phenotype [3]. Investigated receptors in the thesis, triggering the release of Ca^{2+} from intracellular stores are either G-protein coupled receptors (GPCRs) or immunoreceptor tyrosine-based activation motif (ITAM)-linked receptors (ILRs) [2,4,5].

Chapter 2 provides an overview of the kinetics of Ca^{2+} rises in response to GPCRs for thrombin (PAR1, PAR4), ADP ($P2Y_1$), and thromboxane A_2 (TP), all acting via phospholipase Cβ (PLCβ) activation; and also in response to the ILRs for collagen (GPVI), podoplanin (CLEC2) and immunoglobulins (FcγRIIa), acting via PLCγ2 activation [1]. High-throughput screening is suggested as a potential way to find new small molecules that affect the agonist-induced Ca^{2+} rises, and thereby interfere in the thrombus formation. In the next **Chapters 3-5**, the different patterns of Ca^{2+} rises in response to GPCRs and ILRs are studied, and the results are compared with various platelet function assays. In general, the findings underline the great potential of Ca^{2+} signaling measurements for platelet research, as also recognized by other authors [6,7].

Although the focus of this thesis is on receptor- and PLC-induced Ca^{2+} rises, it is worth indicating that also several ion channels generate this second messenger [8,9]. Well-studied Ca^{2+} permeable ion channels involved in extracellular Ca^{2+} entry include Orai1 (a store-operated Ca^{2+} channel) and $P2X_1$ (an ATP-triggered Ca^{2+} channel). Several other ion channels and exchangers, not studied in this thesis, contribute to the platelet Ca^{2+} response, as well as Ca^{2+}-ATPases in the endoplasmic reticulum (SERCAs) and plasma membrane (PMCAs), which are responsible for the pumping of Ca^{2+} out of the cytosol. The specific contribution of each channel to the cytosolic Ca^{2+} rise upon stimulation by agonists is not

always clear.

In particular, the Orai1 and STIM1 proteins involved in store-operated Ca^{2+} entry have been shown to play an important role in platelet activation and in pathological thrombus formation *in vivo* [2,10]. Patients with mutations in Orai1 or STIM1 present with immune deficiencies and a variable platelet-based bleeding phenotype [11], and inhibiting drugs affect platelet functionality [12]. Whilst these proteins present promising targets for the pharmacological prevention of thrombotic disorders, we can learn from the patients' immune deficiency that drug development needs to consider off-target effects.

Glycoprotein VI (GPVI) is the major ILR studied in this thesis. It is activated by collagen types and fibrin, among other ligands. Vascular collagens, with their triple-helical structure and multimer fibril formation, provide an inherent complexity to study receptor-specific platelet activation. Hence, synthetic collagen-related peptide (CRP), which is also triple-helical and contains multiple GPO sequences, mimics essential features of the collagens in stimulating platelets via GPVI [13]. The same also holds for triple-helical peptides mimicking the platelet interaction with the other collagen receptor, integrin $\alpha2\beta1$ [14,15].

In **Chapter 3**, different collagen-like agonists are compared for their ability to support the GPVI-induced signaling pathway via the protein tyrosine kinase Syk and PLCγ2, by using two methods, *i.e.* a well-plate-based measurement of cytosolic Ca^{2+} rises and a microfluidic whole-blood assay of thrombus formation. The results can be read as looking at the suitability of either method to study GPVI-induced platelet signaling in the context of arterial thrombosis. As a readout of the GPVI activation pathway, we used the Syk inhibitor PRT-0630318 (Figure 1). Recording of the Ca^{2+} fluxes in 96-well plates shows that in particular the CRP-induced GPVI signal is highly suppressed by PRT-060318, whereas in the microfluidics setup, the inhibitor strongly blocked the collagen-induced thrombus formation, thus providing physiologically relevant information on the roles of GPVI and Syk.

The global advantages and disadvantages of the two methods are summarized in Figure 2. Importantly, the application of suspended fibrillar collagens results in only low Ca^{2+} rises, as the high molecular mass of the collagen fibers leads to a heterogeneous interaction with the receptors on a population of platelets. In contrast, CRP with a smaller mass, and thus higher density, provokes a larger Ca^{2+} signal, which is considered to be more evenly distributed across all platelets. On the other hand, the fibrillar collagens (collagen-I and -III) support the thrombus formation process at high-shear flow rate. One of the reasons for this high activity is the complex structure of fibrillar collagens containing multiple binding sites for GPVI, integrin $\alpha2\beta1$, and von Willebrand factor (VWF) on each fiber [13,16,17]. The immobilized collagens thereby enforce both platelet adhesion and activation. This is also supported by the observation that adjacent GPVI-binding sites on the collagens facilitate receptor clustering [18-20].

Another circumstance is that in well-plate-based Ca^{2+} flux assays the absence of shear or stirring limits the diffusion of added fibrillar collagens to the platelets (Figure 2).

This limitation becomes apparent by the monitoring of collagen-adhered single-platelet Ca^{2+} responses which are perfused in whole-blood through microfluidic chambers. Several authors performing these experiments have reported fast and steep, spiking rises in cytosolic $[Ca^{2+}]_i$ upon contact of platelets with collagen [21-23] or VWF [24,25]. Interestingly, these platelet Ca^{2+} responses are downregulated by the presence of endothelial cells (I. Provenzale, personal communication). However, a limitation of the microfluidic method is the difficulty of studying the contribution of specific receptors to the Ca^{2+} traces because multiple (autocrine) agonists contribute to the thrombus-forming process [5]. In addition, the method has a low throughput for studies using inhibitors.
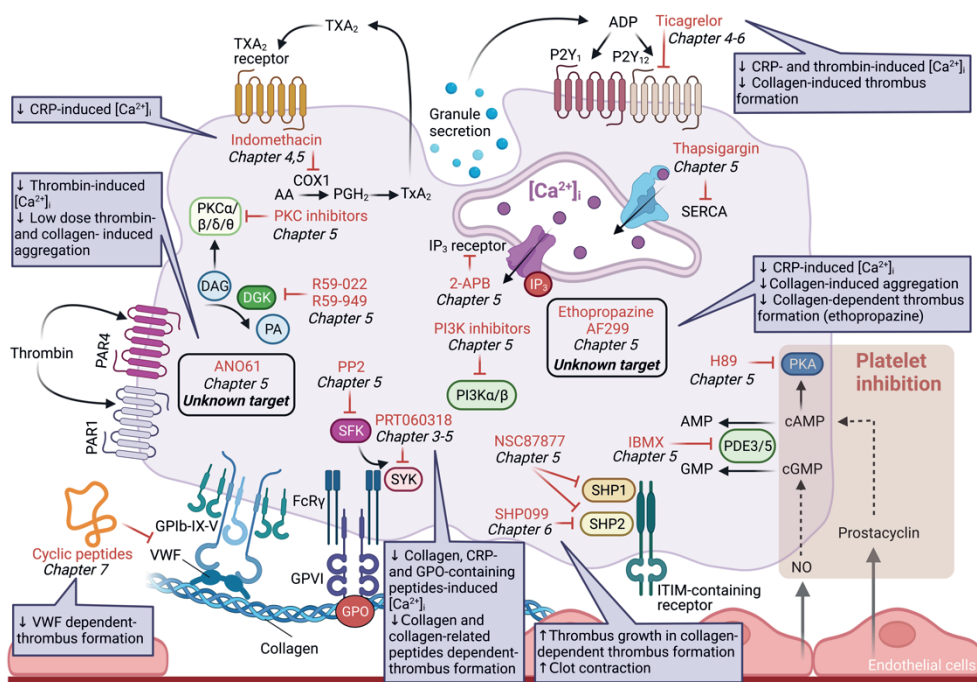
Figure 1. Pharmacological inhibitors and their protein targets in platelets used throughout this thesis. Shown is the chapter, where the concerning inhibitor is used. Main inhibitor effects are indicated in purple boxes. PKC inhibitors include GFX109203X (PKCα/β inhibitor), PKCβ inhibitor, Ro-318220 (pan-PKC inhibitor), rottlerin (PKCδ inhibitor), and PKCθ inhibitor; PI3K inhibitors are LY2940002 (pan-PI3K inhibitor), PIK75 (PI3Kα inhibitor) and TGX221 (PI3Kβ inhibitor). *Abbreviations*: PAR1/4, protease-activated receptor 1 and 4; PI3K, phosphatidylinositol 3-kinase; PKA, protein kinase A; PKC, protein kinase C; SERCA, sarco- and endoplasmic reticulum Ca^{2+} ATPase; SFK, Src family kinase; Syk, spleen tyrosine kinase; TxA$_2$, thromboxane A$_2$; IP$_3$, inositol 1,4,5-triphosphate. Figure created using BioRender.com.

The GPVI agonist CRP as well as the PAR1/4 agonist thrombin induce a high platelet activation in suspension assays. Based on this, in **Chapter 4**, a novel ultra-high throughput (UHT) Ca^{2+} flux assay is developed using CRP- or thrombin-stimulated platelets (loaded with fluorescent Ca^{2+} dye, Calcium 6) in 1536-well plates. This UHT assay reveals a long-term GPVI-induced Ca^{2+} signal and a more transient GPCR-induced activation effect; and, for that, it is used in the following chapter to compare the effects of a high number of

compounds on both ILR- and GPCR-induced platelet activation. In comparison to the more common 96- or 384-well-plate formats [6,26], the new downscaled method to 1536-well plates has several advantages. These include the small sample volume per well of both agonist and platelets. In addition, the used FLIPR robot system allows fully automatic addition of inhibitors and automated pipetting of agonists, while the sensitive camera system allows the simultaneous recording of fluorescent changes in all well-plates. As recognized before [27], this UHT format enables a high capability of testing with reduction of time and costs (reagents, consumables, and biological materials).
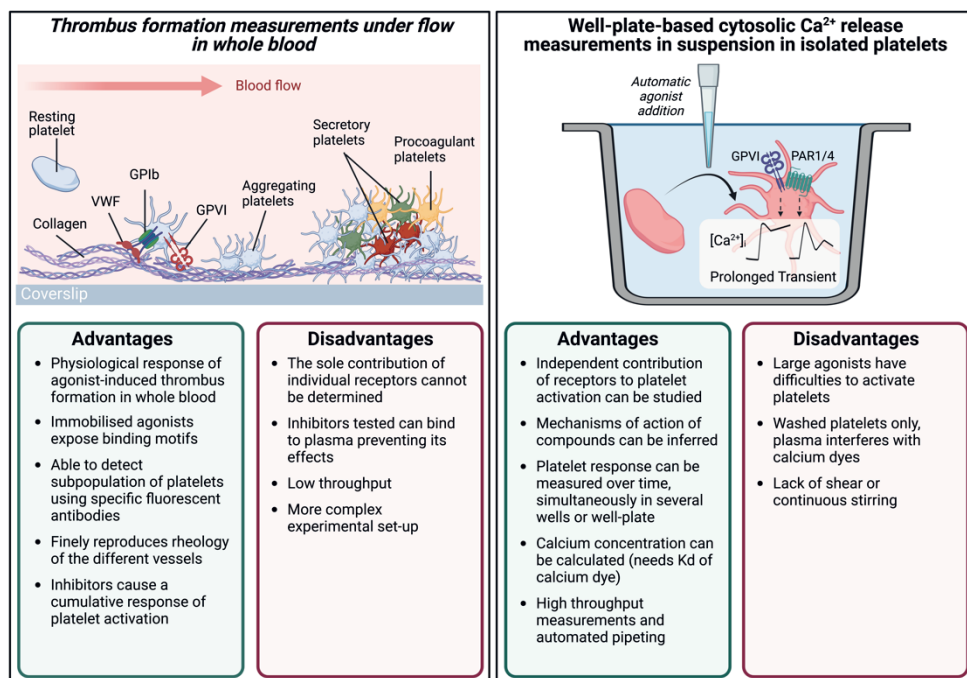
Figure 2. Schematic representation of advantages and disadvantages of whole-blood microfluidic assays in comparison to well-plate-based cytosolic Ca^{2+} assay. *Left:* microfluidic measurement of thrombus formation, using a coverslip coated with collagen over which blood is perfused at defined wall-shear rate. Depicted are stages with platelets adhered to collagen and VWF; then GPVI-induced activation, resulting in different platelet populations (aggregating, secretory and procoagulant platelets). *Right:* principle of [Ca^{2+}]$_i$ measurement of dye-loaded platelets in a well upon stimulation with a GPVI or PAR1/4 agonist (automatically added by robotic machines. *Bottom*: Listing of main advantages and disadvantages of either assay. Figure created using BioRender.com.

The UHT assay developed in **Chapter 4** has appeared to be a sensitive tool to assess drug effects in real-time on the activation of platelets, such as in parallel to platelet function responses measured by light transmission aggregometry. In addition, the pattern of effect on agonist-induced Ca^{2+} rises can discriminate between physiological and toxic effects. Testing of the suitability of the UHT assay by using a robustness compound library of 263 DMSO-soluble compounds revealed excellent performance with CRP as agonist, and a lower but still acceptable performance with thrombin as agonist. The latter can be explained by the

enzymatic nature of the large protein thrombin, which makes it sensitive to interference in its proteolytic activity required for PAR activation. Moreover, the early and late responses can be separated from the time-dependent $[Ca^{2+}]_i$ curves, which is useful for detecting the late effects of autocrine mediators such as ADP and TxA2.

Although our well plate-based fluorescent measurement presents with many advantages, kinetic measurements of Ca^{2+} signaling in platelets can also be done using flow cytometry techniques. Flow cytometry can assess Ca^{2+} dynamics in dye-loaded platelets and even separate platelet populations, but the method comes with considerable noise because every platelet is measured only once [3,28,29]. In addition, using flow cytometry, measurements can only be performed in a single sample simultaneously, and the agonist addition occurs manually, thus excluding its use in screening avenues.

Drug development: small molecule screening to suppress platelet activation

The time-dependent analyses of CRP- and thrombin-induced $[Ca^{2+}]_i$ curves are further developed in **Chapter 5**, by defining a set of profiling parameters for the early and late curve phases using an automated Matlab algorithm. The algorithm was tested using a panel of 22 known inhibitors of defined platelet signaling pathways. By linking the outcome to the Reactome pathway database, the signaling landscapes downstream of GPVI- (CRP-induced) or PAR1/4 (thrombin-induced) were defined. The relevance of this in our view is that these landscapes may help to define why PAR4 and GPVI seem to contribute more to arterial thrombosis than to hemostasis [1,30]. This is in particular supported by murine knockout studies, indicating a thrombosis-stimulating role of these platelet receptors with limited effects on tail bleeding times [31].

In **Chapter 5**, the UHT assay has also been used for large-scale screening of compounds in order to find novel antiplatelet agents. The screen involved $>10^4$ small molecules from a larger patent-free library with defined physical-chemical properties. Part of the screen was 1280 compounds of the so-called Prestwick Chemical Library, which are off-patented drugs approved by the Federal Drug Administration (FDA), also with high chemical and pharmacological diversity [32]. By its nature, the UHT platelet assay is not protein-targeted, and it is designed to identify serendipitous compounds affecting the GPVI and/or PAR1/4 pathway of $[Ca^{2+}]_i$ rises. After applying stringent selection criteria, as indicated in the chapter, three candidate compounds were found, consistently affecting the platelet Ca^{2+} signal with one agonist.

The first selected compound, present in the Prestwick library, is ethopropazine. In our assay, ethopropazine selectively suppresses the CRP-induced Ca^{2+} signal. In addition, at reasonable concentrations, it inhibits the platelet aggregation induced by CRP or collagen, when tested with washed platelets as well as platelet-rich plasma (PRP). As an FDA-approved compound, the phenothiazine ethopropazine has earlier been described as an antipsychotic drug for the treatment of Parkinson's disease, inhibiting the butyrylcholinesterase activity in plasma [33]. Thus, our finding points to a novel off-target

effect of ethopropazine to affect platelet functions. This may lead to application of a repurposing strategy, in which a drug approved for one indication is repurposed for the treatment of another disease. Such a strategy will reduce the time of investigation, the costs, and the associated risks in comparison to traditional drug discovery [34]. Examples of repurposing drugs from the FDA-approved drug library are compounds recently shown to also affect SARS coronavirus replication [35].

Interestingly, the drug losartan, an angiotensin II type I receptor antagonist, had been shown by structure-based repurposing to act as a GPVI antagonist [36,37]. However, later findings indicated that losartan interferes with the platelet signaling responses induced via the ILRs GPVI and CLEC2 [38].

Two other non-Prestwick compounds identified in the UHT screening are coded as AF299 and ANO61, which specifically affected CRP- or thrombin-induced Ca^{2+} fluxes. AF299 reduced specifically collagen-induced platelet aggregation in washed platelets, whereas ANO61 reduced both collagen and low thrombin-induced platelet aggregation in washed platelets. However, the presence of plasma reduced AF299's and ANO61's potency in platelet aggregation, indicating high plasma binding characteristics. These highly plasma-bound attributes may reduce drug efficiency and complicate diffusion through cell membranes. [39]. Other factors such as membrane penetration or even affinity to the target can be responsible for the reduced drug potency in plasma observed with AF299 and ANO61.

As we describe in **Chapter 5**, UHT screening of small molecules based on Ca^{2+} flux measurements provides a promising way to find new inhibitors interfering with platelet activation. For further assessment of the early hit compounds, secondary assays were performed, such as aggregation of washed platelets and PRP. The use of PRP was important to check for the effects of plasma protein binding [40]. For the three selected compounds in **Chapter 5**, the FAFDrugs4 algorithm was applied to predict small molecule effects on absorption, distribution, metabolism, excretion, and toxicity - the so-called ADME-Tox characteristics. This algorithm provides a way to eliminate molecules with unfavorable physiological or pharmacological properties or with predicted cellular toxicity [41]. It has been shown that the application of this or a similar algorithm improves the success rate to come to effective and safe drug candidates [42]. In addition, early ADME-Tox evaluation decreases the attrition of hit compounds in clinical trials, thus reducing the costs and increasing the chances of success [42]. Extensive further testing will be needed of early hit compounds, such as identified in this thesis, by pharmacokinetics studies in animal models and metabolism testing in human cell cultures.

Drug development: peptide-based *in silico* design

In **Chapter 7,** another approach is used to find platelet-directed inhibitors; this time to obtain peptides targeting a specific protein-protein interaction. By computational modeling, we designed cyclic peptides that were predicted to interfere with the binding of the A1 domain from VWF to platelet GPIbα. It is suggested that the VWF A1 domain is only accessible to

inhibitors after its conformational change induced by high shear stress [43]. Accordingly, agents blocking the interaction with GPIbα will only inhibit the adhesion of platelets at high, arterial shear rate, such as in thrombotic situations. Moreover, small peptides have low manufacturing costs, are easy to synthesize and modify, and have good biocompatibility [44,45]. Besides, we used cyclic peptides, since the cysteine-induced cyclization imposes a conformational restraint, leading to higher peptide stability, a more selective interaction with the target protein, and a longer predicted half-life in plasma and tissue [44-46].

After *in silico* design of a large set of peptides and molecular dynamic simulations, specific monocyclic and bicyclic peptides were selected, based on a predicted lowest-binding free energy to the relevant amino acids 221-246 of GPIbα. As a confirmation, in flow cytometry, these peptides showed reduced binding of ristocetin-activated VWF to platelet GPIb-V-IX. Furthermore, in high-shear blood perfusion over collagen-VWF, the peptides reduced the adhesion and aggregation of platelets. However, even at low doses, the anti-VWF A1 domain antibody RAg35 had a stronger inhibitory effect in both assays, likely related to its higher affinity to VWF. The small anti-thrombus effects prompted us to a second round of peptide design and synthesis, but still, their inhibitory potential was limited. These studies provide proof-of-principle evidence for the *in silico* design of peptides against VWF. However, further studies are needed to determine the optimal binding residues and affinities for the peptide-based antagonism of VWF, including an assessment of the peptides' stability in plasma and the clearance *in vivo*.

Several other agents have been designed against the VWF A1 domain and tested for interfering with the VWF-GPIbα binding. These include the nanobody caplacizumab, now approved for the treatment of acquired thrombotic thrombocytopenic purpura [47,48], the anti-VWF A1 domain aptamers ARC-1779 [49], TAGX-0004 [50], and BT200 [51], and a single domain antibody KB-VWF-006bi [52]. These biological compounds performed a strong inhibition effect in mice, monkeys, or human blood perfusion experiments and/or ristocetin- or botrocetin-platelet aggregation, similarly to the effect of RAg35 [50-53]. Thus, they are stronger inhibitory agents in comparison to the cyclic peptides from Chapter 7. An unexpected application of such VWF A1 domain inhibitors or antibodies targeting the binding domain in GPIbα might be the suppression of platelet-tumor cell interactions via the axis VWF-GPIbα in cancer metastasis [54-57]. Hence, there is good potential for better working modifications of the peptides developed in this thesis. Others have already listed the possibilities for improvement in the structure of peptides or peptidomimetics, while preserving optimal characteristics regarding bioavailability and pharmacokinetics [45].

Drug development: modulation of glycoprotein VI activity

For long it has been reasoned that the combination of experimental and virtual approaches helps to improve the outcome of screening avenues [58]. This integration aims to reduce the number of compounds to be physically tested for obtaining hits. In addition, molecular simulations and homology modeling result in libraries for the targeting of specific proteins, for instance in cell-based assays with a choice of inhibitor types (small molecule, peptide, or

antibody-like [57].

These approaches have been followed in the development of GPVI-directed drugs. Of these, two direct targeting drugs are at present tested in clinical trials, namely GPVI-Fc dimer construct Revacept and the GPVI-blocking antibody Glenzocimab, both of which with partly different blocking profiles of platelet-collagen interactions [1,60]. The compound ethopropazine, identified in **Chapter 5**, may prove to be a GPVI-signaling antagonist. The GPVI antagonists CDRI-S002-333 [61] and losartan [36,37] were also found via screening approaches, the latter of which now appears to be a more general ILR signaling antagonist [38]. Complementary screening methods using platelets have also led to the identification of katacine as a CLEC-2 agonist and 7,4'-dimethoxy-3-hydroxyflavone as a PAR4 antagonist[62,63].

Recently, also the successful generation of cameloid nanobodies against GPVI has been reported, some of which with an inhibitory profile [64]. This demonstrates the possibility to use the structure-activity relationship of GPVI and nanobody scaffolds to develop possible inhibitors [59]. Moreover, these nanobodies were also used as a tool to disclose the clustering of GPVI receptors along collagen fibers [20], highlighting their suitability for a variety of techniques in platelet research.

From a different perspective, in **Chapter 6**, the negative GPVI signaling regulator SHP099 is used, targeting the protein tyrosine phosphatase SHP2 (gene *PTPN11*) [65,66], which suppresses the platelet activation via GPVI. Derivatives of SHP099 are evaluated in clinical trials for the treatment of solid cancers [67]. In our study, we investigated if and how the inhibition of SHP2 by SHP099 was able to restore impairments in collagen- and GPVI-dependent activation in platelets from Noonan syndrome patients with a gain-of-function mutation in the *PTPN11* gene.

Microfluidic assays to assess anti-platelet compounds and genetic platelet function disorders

In various chapters of this thesis, the Maastricht flow chamber operating with whole blood flowing at high shear stress has been employed to either assess drug effects on platelet properties or to determine altered platelet function in patients with a bleeding disorder. Shear stress, exerted by laminar blood flow, is fundamental for platelet activation in hemostasis and thrombosis. Shear is essential, for example, in the early stages of platelet adhesion to a damaged vessel in order to unfold VWF and allow interaction with GPIb-V-IX, platelet rolling, and subsequent attachment to exposed collagen (Figure 2) [68,69]. In general, *in vitro* microfluidic models have provided more detailed insights into the processes of thrombus initiation, amplification, and stabilization and the signaling mechanisms involved [9,70,71].

Previous group members have used the Maastricht flow chamber to investigate the interplay of platelets, coagulation, and vascular components under physiological flow conditions [72-74]. Moreover, the device has been useful to evaluate platelet responses due to mutations in

9

humans or genetically modified mice or interventions in thrombus formation using signaling agents, antiplatelet or anticoagulant drugs administered *in vivo* or *in vitro* [72,75-77].

In this thesis, the effects have been examined of several novel antiplatelet agents on collagen-dependent thrombus formation under flow. Our findings include an inhibition seen with ethopropazine (**Chapter 5**), enhancing effects under certain conditions with the SHP2 inhibitor SHP099 (**Chapter 6**), and a shear-dependent suppression of the anti-VWF antibody RAg35 and to a limited degree of inhibitory GPIbα cyclic peptides (**Chapter 7**).

Regarding SHP099, an increased thrombus build-up and more contraction were observed when blood samples were perfused over type I collagen. In the presence of tissue factor, the drug SHP099 caused a faster platelet-dependent fibrin formation. In blood from the majority of Noonan patients with a gain-of-function mutation of SHP2 (*PTPN11*), the addition of SHP099 improved the extent of thrombus formation over collagen (**Chapter 6**). This result is a promising sign that the pharmacological inhibition of SHP2 can help to regulate the hemostatic process in these patients. Our *in vitro* microfluidic results are in agreement with findings in *Shp2* knockout mouse models which show negative regulation of platelet GPVI signaling pathway by SHP2 [78-80]. In the past decades, also other microfluidic devices have been developed for the assessment of bleeding risks or a prothrombotic potential [81,82]. It will be interesting to directly compare these tests with our model for the testing of drugs and the evaluation of patient blood samples, rather than to extrapolate from mouse thrombosis models, given the interspecies differences in biorheology. On the other hand, further standardization of microfluidic testing is needed, due to variability of the source, composition, and concentration of the thrombogenic substrates along with the variability of preanalytical blood samples [73,76,83].

In **Chapter 8**, a cohort of patients with congenital platelet-based disorders was studied, including the rare CalDAG-GEFI deficiency, $P2Y_{12}$ receptor deficiency, platelet storage pool disease, and Hermansky-Pudlak syndromes. Blood samples from the index patients and their affected or unaffected family members were analyzed in a multiparametric manner using the Maastricht flow chamber. Among the patients, a novel homozygous splice mutation of the *RASGRP2* gene (encoding for CalDAG-GEFI) and novel heterozygous mutations in the *P2RY12* gene (encoding for $P2Y_{12}$) were identified as (likely) pathogenic variants. On the other hand, in some of the patients with a familial bleeding defect, extensive genetic screening did not reveal variants of interest. This is in agreement with other studies, indicating that defined molecular associations are difficult to find in a substantial part of patients with mild bleeding defects [84,85].

We observed that the combination of the multiparameter microfluidic method, using four platelet-adhesive surfaces, with conventional platelet function assays provided a nearly complete separation between the values from affected patients and their unaffected family members. Several parameters and surfaces appeared to contribute most to this differentiation. Interestingly, also patients with Hermansky-Pudlak syndrome and only mild hemostatic defects could be distinguished from patients with a major bleeding disorder when

considering platelet aggregation parameters. However, there was variation between the included control subjects, in agreement with earlier larger-size studies of thrombus formation (using the same microfluidic setup) with blood from 96 healthy subjects [86]. In the latter case, only a small proportion of the inter-individual variation was explained by common single nucleotide variants of the *GP6* and *FCER1G* genes. Together, this points to the need of establishing reference ranges with attention to general subject characteristics such as sex and age. Additionally, larger cohorts of patients with genetically confirmed bleeding disorders need to be included as a way to advance the development of microfluidic testing into a reliable diagnostic tool. As it was shown in **Chapter 8**, combining the test outcomes with bioinformatic tools can help to develop an algorithm to identify patients.

Gene panel and sequencing tests are increasingly used for the diagnostics of inherited bleeding disorders, but their yield is still limited [85,87]. Improvements are expected from whole genome sequencing, revealing non-coding, deep intronic, and large structural variants, but this goes at the expense of finding many variants without functional meaning, when we consider that about 10% of the genome is variable [87,88]. Concerning the results of this thesis, the use of microfluidic flow chambers for establishing pathogenic or likely pathogenic gene variants can help clarify the link between (heterozygous) genotype and phenotype for platelet-related bleeding disorders.

In addition to the presently used Maastricht flow chamber, also other microfluidic and related devices have been developed to phenotype diverse aspects of blood function. Although none of these have made it to a clinical standard for hemostasis diagnostics [73,81]. Potential modifications to include in microfluidic devices are spatiotemporal changes in blood flow and pressure, geometry, bifurcation, and shear gradients, all of which can cause alterations in platelet function [89]. The incorporation of endothelial cells with or without adjacent smooth muscle cells, from patients or different vascular beds, are interesting developments [82,90,91]. However, so far these are more research methods than diagnostic tools. In sum, additional work is needed to come to devices with improved (patho)physiological conditions to better mimic the patient's circulation. One day, such methods could be predictive to assess thrombosis or bleeding tendencies and to detect the effects of anti-thrombotic interventions in a personalized manner.

Concluding remarks

Major findings reported in this thesis are: *(i)* the development and use of an ultra-high throughput platelet cytosolic Ca^{2+} assay, able to differentiate between activation or inhibition of specific signaling pathways in platelets; *(ii)* the identification of an off-patented FDA-approved compound specifically reducing GPVI-induced Ca^{2+} release, likely affecting signaling proteins downstream of GPVI; *(iii)* the potential use of SHP2 inhibitors to improve GPVI-induced platelet activation in Noonan patients; *(iv)* the application of *in silico* tools to design peptides interfering with the shear-induced binding of VWF to GPIbα; and *(v)* establishment of an added value of multiparameter microfluidic whole-blood testing to

phenotype patients with different platelet-related bleeding disorders. Thereby, this thesis aims to integrate several areas in platelet research from pharmacology, drug discovery (method development, screening, and early hit identification), platelet biology, and clinically relevant research.

References

1. Van der Meijden PE, Heemskerk JW. Platelet biology and functions: new concepts and clinical perspectives. *Nat Rev Cardiol.* 2019;16:166-179.

2. Mammadova-Bach E, Nagy M, Heemskerk JW, Nieswandt B, Braun A. Store-operated calcium entry in thrombosis and thrombo-inflammation. *Cell Calcium.* 2019;77:39-48.

3. Spiryova DV, Vorobev AY, Klimontov VV, Koroleva EA, Moskalensky AE. Optical uncaging of ADP reveals the early calcium dynamics in single, freely moving platelets. *Biomed Opt Express.* 2020;11:3319-3330.

4. Offermanns S. Activation of platelet function through G protein-coupled receptors. *Circ Res.* 2006;99:1293-1304.

5. Varga-Szabo D, Braun A, Nieswandt B. Calcium signaling in platelets. *J Thromb Haemost.* 2009;7:1057-1066.

6. Bye AP, Unsworth AJ, Gibbins JM. Screening and high-throughput platelet assays. *Methods Mol Biol.* 2018;1812:81-94.

7. Vilahur G, Gutierrez M, Arzanauskaite M, Mendieta G, Ben-Aicha S, Badimon L. Intracellular platelet signalling as a target for drug development. *Vascul Pharmacol.* 2018;111:22-25.

8. Mahaut-Smith MP. The unique contribution of ion channels to platelet and megakaryocyte function. *J Thromb Haemost.* 2012;10:1722-1732.

9. Ilkan Z, Wright JR, Goodall AH, Gibbins JM, Jones CI, Mahaut-Smith MP. Evidence for shear-mediated Ca^{2+} entry through mechanosensitive cation channels in human platelets and a megakaryocytic cell line. *J Biol Chem.* 2017;292:9204-9217.

10. Munzer P, Borst O. CRACking the molecular regulatory mechanism of SOCE during platelet activation in thrombo-occlusive diseases. *Cells.* 2022;11:619.

11. Nagy M, Mastenbroek TG, Mattheij NJ, et al. Variable impairment of platelet functions in patients with severe, genetically linked immune deficiencies. *Haematologica.* 2018;103:540-549.

12. Van Kruchten R, Braun A, Feijge MA, et al. Antithrombotic potential of blockers of store-operated calcium channels in platelets. *Arterioscler Thromb Vasc Biol.* 2012;32:1717-1723.

13. Farndale RW, Lisman T, Bihan D, et al. Cell-collagen interactions: the use of peptide toolkits to investigate collagen-receptor interactions. *Biochem Soc Trans.* 2008;36:241-250.

14. Munnix IC, Gilio K, Siljander PR, et al. Collagen-mimetic peptides mediate flow-dependent thrombus formation by high- or low-affinity binding of integrin α2β1 and glycoprotein VI. *J Thromb Haemost.* 2008;6:2132-2142.

15. Pugh N, Simpson AM, Smethurst PA, de Groot PG, Raynal N, Farndale RW. Synergism between platelet collagen receptors defined using receptor-specific collagen-mimetic peptide substrata in flowing blood. *Blood.* 2010;115:5069-5079.

16. Jung SM, Takemura Y, Imamura Y, Hayashi T, Adachi E, Moroi M. Collagen-type specificity of glycoprotein VI as a determinant of platelet adhesion. *Platelets.* 2008;19:32-42.

17. Herr AB, Farndale RW. Structural insights into the interactions between platelet receptors and fibrillar collagen. *J Biol Chem.* 2009;284:19781-19785.

18. Poulter NS, Pollitt AY, Owen DM, et al. Clustering of glycoprotein VI (GPVI) dimers upon adhesion to collagen as a mechanism to regulate GPVI signaling in platelets. *J Thromb Haemost.* 2017;15:549-564.

19. Pallini C, Pike JA, O'Shea C, et al. Immobilized collagen prevents shedding and induces sustained GPVI clustering and signaling in platelets. *Platelets.* 2021;32:59-73.

20. Jooss NJ, Smith CW, Slater A, et al. Anti-GPVI nanobody blocks collagen- and atherosclerotic plaque-induced GPVI clustering, signaling, and thrombus formation. *J Thromb Haemost.* 2023:in press.

21. Heemskerk JW, Vuist WM, Feijge MA, Reutelingsperger CP, Lindhout T. Collagen but not fibrinogen surfaces induce bleb formation, exposure of phosphatidylserine, and procoagulant activity of adherent platelets: evidence for regulation by protein tyrosine kinase-dependent Ca^{2+} responses. *Blood.* 1997;90:2615-2625.

22. Gilio K, Harper MT, Cosemans JM, et al. Functional divergence of platelet protein kinase C (PKC) isoforms in thrombus formation on collagen. *J Biol Chem.* 2010;285:23410-23419.

23. Nesbitt WS, Giuliano S, Kulkarni S, Dopheide SM, Harper IS, Jackson SP. Intercellular calcium communication regulates platelet aggregation and thrombus growth. *J Cell Biol.* 2003;160:1151-1161.

24. Yap CL, Hughan SC, Cranmer SL, et al. Synergistic adhesive interactions and signaling mechanisms operating between platelet glycoprotein Ib/IX and integrin αIIbβ3. Studies in human platelets and transfected Chinese hamster ovary cells. *J Biol Chem.* 2000;275:41377-41388.

25. Goncalves I, Nesbitt WS, Yuan Y, Jackson SP. Importance of temporal flow gradients and integrin αIIbβ3 mechanotransduction for shear activation of platelets. *J Biol Chem.* 2005;280:15430-15437.

26. Liu EC, Abell LM. Development and validation of a platelet calcium flux assay using a fluorescent imaging plate reader. *Anal Biochem.* 2006;357:216-224.

27. Entzeroth M, Flotow H, Condron P. Overview of high-throughput screening. *Curr Protoc Pharmacol.* 2009;Chapter 9:Unit 9 4.

28. Assinger A, Volf I, Schmid D. A novel, rapid method to quantify intraplatelet calcium dynamics by ratiometric flow cytometry. *PLoS One.* 2015;10:e0122527.

29. Aliotta A, Bertaggia Calderara D, Alberio L. Flow cytometric monitoring of dynamic cytosolic calcium, sodium, and potassium fluxes following platelet activation. *Cytometry A.* 2020;97:933-944.

30. Tscharre M, Michelson AD, Gremmel T. Novel antiplatelet agents in cardiovascular disease. *J Cardiovasc Pharmacol Ther.* 2020;25:191-200.

31. Baaten CC, Meacham S, de Witt SM, et al. A synthesis approach of mouse studies to identify genes and proteins in arterial thrombosis and bleeding. *Blood.* 2018;132:e35-e46.

32. Langer T, Hoffmann R, Bryant S, Lesur B. Hit finding: towards 'smarter' approaches. *Curr Opin Pharmacol.* 2009;9:589-593.

33. Brocks DR. Anticholinergic drugs used in Parkinson's disease: an overlooked class of drugs from a pharmacokinetic perspective. *J Pharm Pharm Sci.* 1999;2:39-46.

34. Parvathaneni V, Kulkarni NS, Muth A, Gupta V. Drug repurposing: a promising tool to accelerate the drug discovery process. *Drug Discov Today.* 2019;24:2076-2085.

35. Touret F, Gilles M, Barral K, et al. In vitro screening of a FDA approved chemical library reveals potential inhibitors of SARS-CoV-2 replication. *Sci Rep.* 2020;10:13093.

36. Taylor L, Vasudevan SR, Jones CI, et al. Discovery of novel GPVI receptor antagonists by structure-based repurposing. *PLoS One.* 2014;9:e101209.

37. Jiang P, Loyau S, Tchitchinadze M, Ropers J, Jondeau G, Jandrot-Perrus M. Inhibition of glycoprotein VI clustering by collagen as a mechanism of inhibiting collagen-induced platelet responses: the example of losartan. *PLoS One.* 2015;10:e0128744.

38. Onselaer MB, Nagy M, Pallini C, et al. Comparison of the GPVI inhibitors losartan and honokiol in platelet activation processes. *Platelets.* 2020;31:187-197.

39. Roberts JA, Pea F, Lipman J. The clinical relevance of plasma protein binding changes. *Clin Pharmacokinet.* 2013;52:1-8.
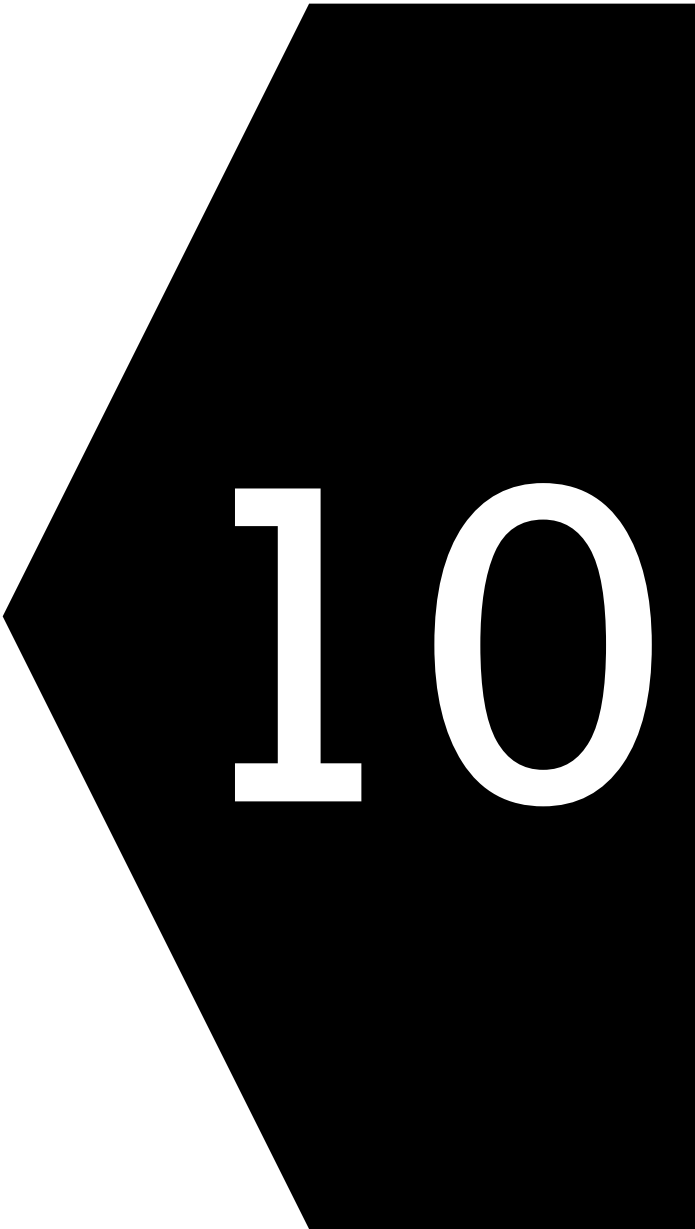
9

40. Di L. An update on the importance of plasma protein binding in drug discovery and development. *Expert Opin Drug Discov.* 2021;16:1453-1465.

41. Lagorce D, Sperandio O, Galons H, Miteva MA, Villoutreix BO. FAF-Drugs2: free ADME/tox filtering tool to assist drug discovery and chemical biology projects. *BMC Bioinformatics.* 2008;9:396.

42. Pantaleao SQ, Fernandes PO, Goncalves JE, Maltarollo VG, Honorio KM. Recent advances in the prediction of pharmacokinetics properties in drug design studies: a review. *Chem Med Chem.* 2022;17:e202100542.

43. Bartunek J, Barbato E, Heyndrickx G, Vanderheyden M, Wijns W, Holz JB. Novel antiplatelet agents: ALX-0081, a nanobody directed towards von Willebrand factor. *J Cardiovasc Transl Res.* 2013;6:355-363.

44. Lee AC, Harris JL, Khanna KK, Hong JH. A comprehensive review on current advances in peptide drug development and design. *Int J Mol Sci.* 2019;20:2383.

45. Wang X, Ni D, Liu Y, Lu S. Rational design of peptide-based inhibitors disrupting protein-protein interactions. *Front Chem.* 2021;9:682675.

46. Henninot A, Collins JC, Nuss JM. The current state of peptide drug discovery: back to the future? *J Med Chem.* 2018;61:1382-1414.

47. Plow EF, Wang Y, Simon DI. The search for new antithrombotic mechanisms and therapies that may spare hemostasis. *Blood.* 2018;131:1899-1902.

48. Poullin P, Bornet C, Veyradier A, Coppo P. Caplacizumab to treat immune-mediated thrombotic thrombocytopenic purpura. *Drugs Today (Barc).* 2019;55:367-376.

49. Gilbert JC, DeFeo-Fraulini T, Hutabarat RM, et al. First-in-human evaluation of anti von Willebrand factor therapeutic aptamer ARC1779 in healthy volunteers. *Circulation.* 2007;116:2678-2686.

50. Sakai K, Someya T, Harada K, Yagi H, Matsui T, Matsumoto M. Novel aptamer to von Willebrand factor A1 domain (TAGX-0004) shows total inhibition of thrombus formation superior to ARC1779 and comparable to caplacizumab. *Haematologica.* 2020;105:2631-2638.

51. Zhu S, Gilbert JC, Hatala P, et al. The development and characterization of a long acting anti-thrombotic von Willebrand factor (VWF) aptamer. *J Thromb Haemost.* 2020;18:1113-1123.

52. Ayme G, Adam F, Legendre P, et al. A novel single-domain antibody against von Willebrand factor A1 domain resolves leukocyte recruitment and vascular leakage during inflammation. *Arterioscler Thromb Vasc Biol.* 2017;37:1736-1740.

53. Stel HV, Sakariassen KS, Scholte BJ, et al. Characterization of 25 monoclonal antibodies to factor VIII-von Willebrand factor: relationship between ristocetin-induced platelet aggregation and platelet adherence to subendothelium. *Blood.* 1984;63:1408-1415.

54. Erpenbeck L, Nieswandt B, Schon M, Pozgajova M, Schon MP. Inhibition of platelet GPIba and promotion of melanoma metastasis. *J Invest Dermatol.* 2010;130:576-586.

55. Qi Y, Chen W, Liang X, et al. Novel antibodies against GPIba inhibit pulmonary metastasis by affecting vWF-GPIba interaction. *J Hematol Oncol.* 2018;11:117.

56. Wang Q, Liu W, Fan J, et al. von Willebrand factor promotes platelet-induced metastasis of osteosarcoma through activation of the VWF-GPIb axis.*J Bone Oncol*. 2020;25:100325

57. Yang AJ, Wang M, Wang Y, et al. Cancer cell-derived von Willebrands factor enhanced metastasis of gastric adenocarcinoma. *Oncogenesis*. 2018; 7:12

58. Mestres J. Virtual screening: a real screening complement to high-throughput screening. *Biochem Soc Trans.* 2002;30:797-799.

59. Damaskinaki FN, Moran LA, Garcia A, Kellam B, Watson SP. Overcoming challenges in developing small molecule inhibitors for GPVI and CLEC-2. *Platelets.* 2021;32:744-752.

60. Jooss NJ, Henskens YM, Watson SP, et al. Pharmacological inhibition of glycoprotein VI- and integrin α2β1-induced thrombus formation modulated by the collagen type. *Thromb Haemost.* 2023:in press.

61. Bhunia SS, Misra A, Khan IA, et al. Novel glycoprotein VI antagonists as antithrombotics: synthesis, biological evaluation, and molecular modeling studies on 2,3-disubstituted tetrahydropyrido(3,4-b)indoles. *J Med Chem.* 2017;60:322-337.

62. Moran LA, Di Y, Sowa MA, et al. Katacine Is a new ligand of CLEC-2 that acts as a platelet agonist. *Thromb Haemost.* 2022;122:1361-1368.

63. Lin YT, Li Y, Hsu HC, et al. Discovery of 7, 4'-dimethoxy-3-hydroxyflavone as a protease-activated receptor 4 antagonist with antithrombotic activity and less bleeding tendency in mice. *Biochem Pharmacol.* 2022;202:115152.

64. Slater A, Di Y, Clark JC, et al. Structural characterization of a novel GPVI-nanobody complex reveals a biologically active domain-swapped GPVI dimer. *Blood.* 2021;137:3443-3453.

65. Chen YN, LaMarche MJ, Chan HM, et al. Allosteric inhibition of SHP2 phosphatase inhibits cancers driven by receptor tyrosine kinases. *Nature.* 2016;535:148-152.

66. Garcia Fortanet J, Chen CH, Chen YN, et al. Allosteric inhibition of SHP2: identification of a potent, selective, and orally efficacious phosphatase inhibitor. *J Med Chem.* 2016;59:7773-7782.

67. Liu C, Lu H, Wang H, et al. Combinations with allosteric SHP2 inhibitor TNO155 to block receptor tyrosine kinase signaling. *Clin Cancer Res.* 2021;27:342-354.

68. Plow EF, McEver RP, Coller BS, Woods VL, Marguerie GA, Ginsberg MH. Related binding mechanisms for fibrinogen, fibronectin, von Willebrand factor, and thrombospondin on thrombin-stimulated human platelets. *Blood.* 1985;66:724-727.

69. Zwaginga JJ, Nash G, King MR, et al. Flow-based assays for global assessment of haemostasis. Part 1: biorheologic considerations. *J Thromb Haemost.* 2006;4:2486-2487.

70. Kulkarni S, Nesbitt WS, Dopheide SM, Hughan SC, Harper IS, Jackson SP. Techniques to examine platelet adhesive interactions under flow. *Methods Mol Biol.* 2004;272:165-186.

71. Versteeg HH, Heemskerk JW, Levi M, Reitsma PS. New fundamentals in hemostasis. *Physiol Rev.* 2013;93:327-358.

72. Nagy M, Heemskerk JW, Swieringa F. Use of microfluidics to assess the platelet-based control of coagulation. *Platelets.* 2017;28:441-448.

73. Provenzale I, Brouns SLN, van der Meijden PE, Swieringa F, Heemskerk JW. Whole blood based multiparameter assessment of thrombus formation in standard microfluidic devices to proxy in vivo haemostasis and thrombosis. *Micromachines (Basel).* 2019;10:787.

74. Brouns SL, van Geffen JP, Campello E, et al. Platelet-primed interactions of coagulation and anticoagulation pathways in flow-dependent thrombus formation. *Sci Rep.* 2020;10:11910.

75. Li R, Grosser T, Diamond SL. Microfluidic whole blood testing of platelet response to pharmacological agents. *Platelets.* 2017;28:457-462.

76. Brouns SL, van Geffen JP, Heemskerk JW. High-throughput measurement of human platelet aggregation under flow: application in hemostasis and beyond. *Platelets.* 2018;29:662-669.

77. Heubel-Moenen FC, Brouns SL, Herfs L, et al. Multiparameter platelet function analysis of bleeding patients with a prolonged platelet function analyser closure time. *Br J Haematol.* 2022;196:1388-1400.

78. Mazharian A, Mori J, Wang YJ, et al. Megakaryocyte-specific deletion of the protein-tyrosine phosphatases Shp1 and Shp2 causes abnormal megakaryocyte development, platelet production, and function. *Blood.* 2013;121:4205-4220.

79. Hu M, Liu P, Liu Y, et al. Platelet SHP2 negatively regulates thrombus stability under high shear stress. *J Thromb Haemost.* 2019;17:220-231.

80. Bellio M, Garcia C, Edouard T, et al. Catalytic dysregulation of SHP2 leading to Noonan syndromes affects platelet signaling and functions. *Blood.* 2019;134:2304-2317.

81. Diamond SL, Rossi JM. Point of care whole blood microfluidics for detecting and managing thrombotic and bleeding risks. *Lab Chip.* 2021;21:3667-3674.

9

82. Berry J, Peaudecerf FJ, Masters NA, Neeves KB, Goldstein RE, Harper MT. An "occlusive thrombosis-on-a-chip" microfluidic device for investigating the effect of anti-thrombotic drugs. *Lab Chip.* 2021;21:4104-4117.

83. Heemskerk JW, Sakariassen KS, Zwaginga JJ, et al. Collagen surfaces to measure thrombus formation under flow: possibilities for standardization. *J Thromb Haemost.* 2011;9:856-858.

84. Vries MJ, van der Meijden PE, Kuiper GJ, et al. Preoperative screening for bleeding disorders: a comprehensive laboratory assessment of clinical practice. *Res Pract Thromb Haemost.* 2018;2:767-777.

85. Bourguignon A, Tasneem S, Hayward CP. Screening and diagnosis of inherited platelet disorders. *Crit Rev Clin Lab Sci.* 2022;59:1-40.

86. Van Geffen JP, Brouns SL, Batista J, et al. High-throughput elucidation of thrombus formation reveals sources of platelet function variability. *Haematologica.* 2019;104:1256-1267.

87. Perez Botero J, Di Paola J. Diagnostic approach to the patient with a suspected inherited platelet disorder: who and how to test. *J Thromb Haemost.* 2021;19:2127-2136.

88. Ver Donck F, Labarque V, Freson K. Hemostatic phenotypes and genetic disorders. *Res Pract Thromb Haemost.* 2021;5:e12637.

89. Mangin PH, Neeves KB, Lam WA, et al. In vitro flow-based assay: from simple toward more sophisticated models for mimicking hemostasis and thrombosis. *J Thromb Haemost.* 2021;19:582-587.

90. Westein E, van der Meer AD, Kuijpers MJ, Frimat JP, van den Berg A, Heemskerk JW. Atherosclerotic geometries exacerbate pathological thrombus formation poststenosis in a von Willebrand factor-dependent manner. *Proc Natl Acad Sci USA.* 2013;110:1357-1362.

91. Brouns SL, Provenzale I, van Geffen JP, van der Meijden PE, Heemskerk JW. Localized endothelial-based control of platelet aggregation and coagulation under flow: a proof-of-principle vessel-on-a-chip study. *J Thromb Haemost.* 2020;18:931-941.

9

10

Chapter 10

Samenvatting

Summary

Resumen

Impact

Curriculum vitae

Publications

Samenvatting

Bloedplaatjes spelen een belangrijke rol in de ontwikkeling van een arteriële trombose. Daardoor vormen medicijnen die bloedplaatjes remmen de belangrijkste therapie tegen een nieuwe trombose. Echter, de huidige medicijnen beschermen niet volledig, en daarnaast krijgt een aanzienlijk aantal van de behandelde patiënten te maken met (sub)klinische bloedingen. Daarom zijn er nieuwe middelen nodig voor antitrombotische therapie, die meer volledig werken en toch de hemostase in stand houden. Aan de andere kant kunnen kwantitatieve of kwalitatieve defecten in de functie van bloedplaatjes aanleiding geven tot bloedingen van variabele omvang. De diagnose van deze ziektes is nog steeds niet eenvoudig vanwege beperkingen van de huidige plaatjesfunctietesten. Dit proefschrift heeft als doel om recente *high-throughput* plaatjesfunctietesten toe te passen voor het screenen van nieuwe remmers van bloedplaatjesfunctie, en voor een mogelijke verbetering van de diagnose van patiënten met een hemostatisch defect.

Hoofdstuk 1 geeft achtergrondinformatie over de mechanismen van plaatjesactivering en trombusvorming, waarbij benadrukt wordt hoe huidige geneesmiddelen deze processen beïnvloeden. Daarnaast beschrijft dit hoofdstuk hoe flowkamers kunnen worden gebruikt om een klinische fenotypering en diagnose van plaatjesfunctiestoornissen te verbeteren. Verder geef ik algemene informatie over ultra high-throughput (UHT) screeningsmethoden, die ingezet worden voor de ontwikkeling van medicijnen. In **Hoofdstuk 2** is een gedetailleerd literatuuroverzicht opgenomen, waarin de mechanismen van Ca^{2+}-signalering worden beschreven, zoals opgewekt door G-eiwit-gekoppelde receptoren (GPCR) zoals de receptor voor trombine (via fosfolipase Cβ, PLCβ) en door ITAM-gekoppelde receptoren zoals de receptor voor collageen (via PLCγ2). Bovendien wordt uitgelegd dat de synergie van beide typen receptoren leidt tot supramaximale intracellulaire Ca^{2+}-niveaus. Dit resulteert in de activering van het fosfolipide-scramblase anoctamine-6, wat vervolgens zorgt voor een fenotypische *switch* van aggregaatvormende naar stollingsbevorderende plaatjes. Gezien de verschillen tussen GPCR- en ITAM-gekoppelde receptoren, concluderen wij dat intracellulaire Ca^{2+}-responsmetingen met plaatjes kunnen helpen bij het zoeken naar nieuwe plaatjesremmers met een selectief werkingsmechanisme.

Het tyrosine kinase Syk is cruciaal in de collageen- and glycoproteïne VI (GPVI)-geïnduceerde signaalroute in bloedplaatjes, en diens activering leidt tot een verhoging van intracellulair Ca^{2+} in plaatjes. In **Hoofdstuk 3** zijn we nagegaan, hoe diverse collagenen uit de bloedvatwand, alsmede collageen-gerelateerde peptiden (CRP), in staat zijn deze signaalroute te stimuleren, door gebruik te maken van de Syk-remmer PRT-060318. We vonden dat vooral CRP-typen met een GPO-motief leidden tot een sterke, Syk-afhankelijke stimulering, voor wat betreft de Ca^{2+}-respons en de plaatjesaggregatie in een trombus onder stromingscondities. Echter ook zwakkere CRP-typen met een GPP-motief bewerkstelligden (een geringe) trombusvorming via nog steeds een Syk-afhankelijke route. In beide soorten assays bleken verder fibrillaire collagenen zwakke plaatjesactivatoren op een Syk-afhankelijke manier, met uitzondering van de sterkere agonist (fibrillair) Horm-type

collageen, die als standaard collageen in het diagnostisch laboratorium gebruikt wordt bij plaatjesfunctieonderzoek. Tezamen geven deze resultaten het belang aan van een fibrillaire structuur van collageen voor de GPVI- and Syk-afhankelijke plaatjesactivering. Ons werk laat tevens zien dat geïmmobiliseerde collagenen meer effectief zijn in plaatjesactivering dan collagenen in oplossing.

Signalering via calcium neemt een centrale plaats in bij de activering van bloedplaatjes, en een automatische meting van dit proces kan plaatjesdefecten aan het licht brengen. In **Hoofdstuk 4** hebben we een UHT-test opgezet met Calcium-6-geladen plaatjes, om daarmee de Ca^{2+}-stijgingen onder invloed van CRP (GPVI agonist) en trombine (GPCR agonist) te kunnen meten in 96, 384 en 1536 well-platen. Daarnaast werd een algoritme ontwikkeld voor de automatische karakterisering van Ca^{2+}-responscurven middels gefitte parameters. Zelfs bij de kleine 1536 well-platen liet deze procedure een verschil zien tussen CRP (vertraagde en langdurige respons) en trombine (snelle en transiënte respons). Validatie van de assay kon worden uitgevoerd met behulp van stoffen die deel uitmaken van een *robustness* set en enige klinisch relevante plaatjesremmers. Deze bevindingen samen vormen het principebewijs dat de plaatjes Ca^{2+}-responsen te gebruiken zijn voor de screening van nieuwe remmers in een UHT test.

In **Hoofdstuk 5** is de UHT-assay gebruikt om een screening voor antiplaatjes-verbindingen uit te voeren op 16.635 kleine organische moleculen. De set omvatte 1280 verbindingen van de klinisch goedgekeurde stoffen van de Prestwick Chemicals bibliotheek en een in eigen beheer gemaakte SPCA-bibliotheek met 15.355 verbindingen met drug-compatibele fysisch-chemische eigenschappen. Middels een aangepast algoritme voor Ca^{2+}-curve profilering werden de effecten van alle verbindingen op de Ca^{2+}-responsen van CRP- of trombine-gestimuleerde plaatjes automatisch in kaart gebracht. Door een filterprocedure middels Z-scores, mogelijke toxiciteit, verwachte ongunstige farmacokinetiek en selectiviteit, verkregen we 13 moleculen met een remmend effect op de CRP-geïnduceerde respons en 9 moleculen die de trombine-geïnduceerde respons beïnvloedden. Verder proeven bevestigden uiteindelijk de werking van drie hit-moleculen, te weten AF299 en ethopropazine (beide CRP-effecten) en ANO61 (trombine-effecten). Deze drie verbindingen bleken ook selectief remmend te werken op de plaatjesaggregatie. Uit dosis-respons curves kwam naar voren dat ethopropazine het meest effectief remmend was in de aanwezigheid van bloedplasma. Ethopropazine verminderde ook de collageen-geïnduceerde trombusgroei onder stromingscondities. De plaatjesremmende werking van deze hit-moleculen kan worden verbeterd door nader onderzoek naar structuur-activiteit relaties.

Een deel van de patiënten met het Noonan-syndroom vertoont bloedingssymptomen, die gekoppeld zijn aan een mutatie in het *PTPN11*-gen, dat codeert voor het tyrosine fosfatase SHP2. De middel SHP099 is een allosterische remmer van SHP2, waarvan derivaten in klinisch onderzoek worden getest op de behandeling van solide tumoren. In bloedplaatjes wordt SHP2 beschouwd als een negatieve regulator van de GPVI-signalering. In **Hoofdstuk 6** hebben we onderzocht in welke mate remming van SHP2 met

SHP099 de plaatjesfuncties kan verbeteren, zoals in de collageen-geïnduceerde trombusvorming onder stromingscondities. We vonden dat behandeling met SHP099 resulteerde in een verhoogde activering van integrine αIIbβ3 en een versterkte trombusopbouw. Deze effecten werden ook gezien onder omstandigheden waarin de bloedstolling geactiveerd werd. Bij onderzoek naar de trombusvorming met bloed van zes Noonan-patiënten (met *PTPN11*-mutaties) bleek dat de collageen-geïnduceerde trombusvorming relatief laag was. Behandeling met SHP099 verhoogde de trombusopbouw, hetgeen wijst op de mogelijkheid dat een op SHP2 gericht middel stoornissen van de plaatjesrespons, zoals bij Noonan-patiënten, kan herstellen.

De binding van von Willebrand-factor (VWF) aan glycoproteïne Ibα (GPIbα) op plaatjes initieert de trombusvorming onder stromingscondities, en blokkering van deze binding zal naar verwachting gunstig zijn voor patiënten met immuun gemedieerde trombotische trombocytopenie purpura (iTTP). In **Hoofdstuk 7** hebben we gebruik gemaakt van *in silico* ontworpen en gesynthetiseerde peptiden, om de interactie van het VWF A1-domein met GPIbα te verminderen. Moleculair-dynamische simulaties gaven na selectie twee cyclische peptiden, namelijk mono-ORbIT (26 aminozuren) en bi-ORbIT (36 aminozuren). Beide peptiden interfereerden met de door ristocetine of botrocetine geïnduceerde binding van VWF aan plaatjes, alhoewel de remming zwakker was vergeleken met een antilichaam gericht tegen het VWF A1-domein. Middels een tweede ontwerpronde werd een verbeterd peptide opt-mono-ORbIT (28 aminozuren) getest, dat beter presteerde in het verminderen van de trombusvorming, maar nog steeds niet zo goed als het antilichaam. We concludeerden dat het goed mogelijk is om de VWF-afhankelijke plaatjesaggregatie te beïnvloeden door middel van een op structuur gebaseerd ontwerp van peptiden.

De diagnose van patiënten met een bloedplaatjes gerelateerde bloedingsaandoening is moeilijk, gezien de beperkingen van de standaard plaatjesfunctietesten. In **Hoofdstuk 8** hebben we de multiparameter *microfluidic* test gebruikt om te helpen bij de fenotypering van verschillende patiënten en familieleden met genetische aandoeningen, d.w.z. CalDAG-GEFI-deficiëntie, SPD (*storage pool disease*), Hermansky-Pudlak-syndroom of P2Y$_{12}$-receptor-deficiëntie. Moleculair genetische analyse gaf nieuwe pathologische mutaties van de genen *RASGRP2* (coderend voor CalDAG-GEFI) en *P2RY12* (P2Y$_{12}$-receptor), en bevestigde mutaties van de Hermansky-Pudlak-genen *HPS1* en *HPS3*. Met behulp van de multiparameter test, die 48 parameters opleverde, vonden wij dat voor de meeste symptomatische patiënten, maar niet voor hun gezonde familieleden, het algemene patroon van trombusvorming in stromend bloed verstoord was. Deze informatie werd gecombineerd met diagnostische gegevens van plaatjesfunctie (lichttransmissie-aggregometrie, flow-cytometrie) en hematologische variabelen met behulp van een k-means clusteranalyse. Dit resulteerde in separate clusters van gezonde proefpersonen plus de (heterozygote) niet-aangedane familieleden en van de meeste symptomatische patiënten. Al met al blijkt dat de multiparameterbepaling van trombusvorming een belangrijke rol kan spelen bij de herkenning van genetisch gekoppelde trombocytenstoornissen.

Het afsluitende **Hoofdstuk 9** beschouwt de belangrijkste bevindingen van mijn proefschrift in relatie tot de literatuur van nu. Voor- en nadelen van de toegepaste UHT-methoden - in well-platen en middels *microfluidic* assays - worden besproken, evenals mogelijkheden van de bio-informatica voor analyse van complexe resultaten om de disfunctie van bloedplaatjes in te schatten ten behoeve van de kliniek.

Summary

Platelets are major contributors in the development of an arterial thrombotic event, and accordingly, antiplatelet drugs form the main therapy against secondary thrombosis. However, current therapies are not fully protective, and a significant number of treated patients develop sub-clinically or clinically relevant bleeding. Therefore, new agents for antithrombotic therapy are needed to target thrombosis whilst preserving hemostasis more effectively. Alternatively, quantitative or qualitative platelet disorders can also result in bleeding episodes of variable severity. Diagnosis of these defects is still difficult due to the limitations of the current platelet function tests. This thesis aimed to use recent high-throughput platelet function assays for the screening and testing of novel antiplatelet compounds and to provide possibilities for improvements in the diagnosis of patients with a hemostatic defect.

Chapter 1 provides background information on the mechanisms of platelet activation and thrombus formation, emphasizing how current clinically used drugs target these processes. In addition, this chapter describes how microfluidic chambers can be employed to improve the clinical phenotyping and diagnosis of platelet function disorders. Moreover, general information on the use of ultrahigh throughput (UHT) screening methods for drug development is provided. In **Chapter 2**, a detailed literature-based review is given, describing the mechanisms of platelet Ca^{2+} signaling induced by G-protein coupled receptors (GPCR) such as for thrombin (via phospholipase Cβ, PLCβ) and by ITAM-linked receptors such as for collagen (via PLCγ2). Moreover, it features the synergy when both types of receptors are stimulated in terms of supramaximal cytosolic Ca^{2+} levels. This condition triggers the phospholipid scramblase anoctamin-6, thus causing a phenotypic switch from aggregatory to procoagulant platelets. Given the different kinetics of Ca^{2+} rises in response to GPCR or ITAM receptors, we conclude that a platelet Ca^{2+} flux assay can help to find new platelet inhibitors with a discriminative mode of action.

Protein tyrosine kinase Syk is crucial in the collagen- and glycoprotein (GPVI)-induced signaling pathway, and its activation through phosphorylation, leads to the elevation of cytosolic Ca^{2+} in platelets. In **Chapter 3**, we studied how several vascular-derived collagens and collagen-related peptides (CPR) were able to trigger this pathway using the Syk inhibitor PRT-060318. We found that especially CRP forms with a GPO motif were strong, Syk-dependent stimuli for platelet responses, such as elevated cytosolic Ca^{2+} and accumulation of platelets in a thrombus under flow conditions. However, also weaker CRP forms with a GPP-motif led to (low) thrombus formation through Syk activation. In both assay types, fibrillar collagens were weak activators of platelets in a Syk-dependent way, with the exception of the stronger activating (fibrillar) Horm-type collagen, used as a standard in the diagnostic laboratory in platelet function tests. Together, our results underline the importance of a fibrillar structure of collagens for GPVI- and Syk-dependent platelet activation. This work also shows that immobilized collagens are more effective in the activation of platelets than suspended collagens.

Calcium signaling is a node in platelet responses, and the automated measurement

of this process can reveal drug-induced platelet defects. In **Chapter 4**, we used Calcium-6 loaded platelets for the development of a UHT assay based on the Ca^{2+} rises in response to CRP (GPVI agonist) or thrombin (GPCR agonist), which could be performed in 96-, 384- and 1536-well plates. The method showed a different curve shape with CRP (delayed and prolonged) or thrombin (fast and transient), even in the miniature, 1536-well plate. A set of quantitative parameters described the Ca^{2+} response in depth. Validation of the assay was done using a robustness compound library and by a small panel of clinically relevant platelet inhibitors. The findings of this chapter presented proof-of-principle evidence that the platelet Ca^{2+} responses can be used for the screening to find new inhibitors in a UHT manner.

In **Chapter 5**, the UHT assay was subsequently used to conduct a screening for antiplatelet compounds with 16,635 small molecules. This included 1280 small organic compounds from the clinically approved Prestwick chemical library, and further a diversity-based (SPCA) compound library of 15,355 small molecules with drug-compatible physicochemical characteristics. Using an adapted algorithm of $[Ca^{2+}]_i$ curve profiling, we automatically examined the effects of all compounds on the Ca^{2+} responses of CRP- or thrombin-activated platelets loaded with Calcium-6. By filtering for Z-score effects, potential toxicity, expected unfavorable pharmacokinetics, and specific agonist inhibition, we obtained 13 compounds negatively affecting the CRP-induced Ca^{2+}-response and 9 compounds interfering with the thrombin-induced Ca^{2+}-response. After additional confirmation measurements, we obtained three hits, *i.e.* AF299 and ethopropazine (specifically inhibitory with CRP) and ANO61 (inhibitory with thrombin). All three hit compounds also selectively inhibited platelet aggregation. Dose-response studies indicated that the phenothiazine compound, ethopropazine, was most effective in the presence of plasma and suppressed collagen-induced thrombus growth under flow conditions. The inhibitory characteristics of these hits need to be improved by structure-activity relationship studies.

Part of the patients with Noonan syndrome present with bleeding symptoms, which are linked to mutations in the *PTPN11* gene, encoding for the tyrosine phosphatase SHP2. The drug SHP099 is an allosteric inhibitor of SHP2, derivatives of which are being tested in clinical trials to treat solid tumors. In platelets, SHP2 is considered as a negative regulator of GPVI signaling. In **Chapter 6**, we studied to which extent SHP2 inhibition by SHP099 can improve platelet functions, such as in collagen-dependent thrombus formation under flow. We found that the treatment with SHP099 resulted in an increased integrin $\alpha IIb\beta 3$ activation and thrombus buildup. These effects were also observed under coagulating conditions. When examining the thrombus formation process with blood from six Noonan patients (with confirmed *PTPN11* mutations), we found that the collagen-induced thrombus formation was moderately impaired. Treatment with SHP099 increased the thrombus size, pointing to the ability of an SHP2-directed drug to restore Noonan-linked impairments of platelet responsiveness.

The binding of von Willebrand factor (VWF) to platelet glycoprotein Ibα (GPIbα)

is one of the initial stages of thrombus formation under shear, and interference with this binding is expected to be beneficial for patients with immune-mediated thrombotic thrombocytopenic purpura (iTTP). In **Chapter 7**, we used *in silico* designed and chemically synthesized peptides, which were constructed to interfere with the interaction of the VWF A1 domain with GPIbα. Molecular dynamic simulations resulted after selection into two cyclic peptides, *i.e.* mono-ORbIT (26 amino acids) and bi-ORbIT (36 amino acids). Both peptides interfered with the ristocetin- or botrocetin-induced VWF binding to platelets, although the inhibition was weaker than with an antibody directed against the VWF A1 domain. After a second design round, an improved *opt*-mono-ORbIT (28 amino acids) was tested, which performed better in suppressing thrombus formation, but still not to the extent seen with the antibody. Thus, we concluded that the structure-based design of peptides has good potential in affecting VWF-dependent platelet aggregation.

Diagnosis of patients with platelet-related bleeding symptoms is difficult, given the limitations of standard platelet function tests. In **Chapter 8** we used a multiparameter microfluidic assay to aid in the phenotyping of several patients and family members with genetically linked disorders, *i.e.* CalDAG-GEFI deficiency, storage pool disease, Hermansky-Pudlak syndrome or $P2Y_{12}$ receptor deficiency. Molecular genetic analysis identified novel pathogenetic mutations of the genes *RASGRP2* (encoding for CalDAG-GEFI) and *P2RY12* ($P2Y_{12}$ receptor), and confirmed mutations of the Hermansky-Pudlak genes *HPS1* and *HPS3*. Using the multiparameter assay, providing 48 parameters, the overall pattern of whole-blood thrombus formation was different for the majority of symptomatic patients, but not for their unaffected family members. These findings were combined with diagnostic platelet phenotyping data (light transmission aggregometry and flow cytometry) and hematological values by using k-means cluster analysis. This separated the healthy control subjects plus the (heterozygous) non-affected relatives from the large majority of symptomatic patients. All in all, this indicated that the multiparameter assessment of whole-blood thrombus formation can have an important role in the recognition of genetically linked platelet function disorders.

The conclusive **Chapter 9** discusses the most important findings of my thesis in relation to the current literature. The advantages and disadvantages of the applied UHT methods - well plates and microfluidic assays - are discussed, as well as the possibility of using bioinformatic tools to assess platelet inhibition or dysfunction in the clinic.

Resumen

Las plaquetas contribuyen en gran medida al desarrollo de trombos arteriales. Por ello, los antiagregantes plaquetarios constituyen el principal tratamiento para prevenir un nuevo evento trombótico. Sin embargo, como el uso de los antiagregantes plaquetarios está condicionado por el riesgo de sangrado y hay un número significativo de pacientes que desarrolla hemorragias subclínicas o clínicamente relevantes, se necesitan fármacos antitrombóticos más eficaces que no desregulen los procesos hemostáticos. Por otra parte, los trastornos plaquetarios tanto cuantitativos como cualitativos también pueden dar lugar a episodios hemorrágicos de gravedad variable, aunque de difícil diagnóstico por las limitaciones de las pruebas de función plaquetaria. El objetivo de esta tesis fue utilizar ensayos recientes de alto rendimiento de la función plaquetaria para el cribado y ensayo de nuevos compuestos antiplaquetarios, y ofrecer posibilidades de mejora del diagnóstico de pacientes con un defecto hemostático.

El **Capítulo 1** aporta información sobre los mecanismos de activación plaquetaria y formación de trombos, haciendo hincapié en cómo los fármacos de uso clínico actual se dirigen a estos procesos. Este capítulo también describe como pueden emplearse las cámaras de microfluídica para mejorar el fenotipado clínico y el diagnóstico de los trastornos de la función plaquetaria. Además, se ofrece información general sobre el uso de métodos de cribado de ultra alto rendimiento (UHT, del inglés, *ultra high throughput*) para el descubrimiento de fármacos. En el **Capítulo 2**, se ofrece una revisión detallada basada en la literatura, donde se describen los mecanismos de señalización plaquetaria mediados por calcio citosólico (Ca^{2+}), que pueden estar inducidos por receptores acoplados a proteínas G (GPCR) como por la trombina (vía fosfolipasa Cβ, PLCβ) y por receptores vinculados a ITAM como por el colágeno (vía PLCγ2). Al mismo tiempo se destaca la sinergia cuando tanto los receptores GPCRs y los ITAM son estimulados y causan niveles supra-máximos de Ca^{2+}. Esta condición desencadena la actividad fosfolipídica de la anoctamina-6, provocando así un cambio fenotípico de plaquetas con función agregante a plaquetas procoagulantes. Dada la diferente cinética de las elevaciones de Ca^{2+} en respuesta a receptores GPCR o ITAM, concluimos que un ensayo de flujo de Ca^{2+} plaquetario puede ayudar a encontrar nuevos inhibidores plaquetarios con un modo de acción distintivo.

La proteína tirosina quinasa Syk es crucial en la vía de señalización inducida por el colágeno y su receptor la glicoproteína VI (GPVI). La activación de esta vía mediante una cascada de fosforilación conduce a la elevación del Ca^{2+} en las plaquetas. En el **Capítulo 3**, estudiamos como varios tipos de colágenos y péptidos relacionados con el colágeno (CRP, del inglés *collagen-related peptide*) de origen vascular eran capaces de desencadenar esta vía utilizando el inhibidor de Syk, PRT-060318. Descubrimos que principalmente las formas de CRP con un motivo GPO proporcionaron estímulos fuertes dependientes de Syk para las respuestas plaquetarias, como la elevación del Ca^{2+} y la acumulación de plaquetas en un trombo en condiciones de flujo. Sin embargo, también formas más débiles de CRP con un motivo GPP condujeron a la formación reducida de trombos a través de la activación de Syk. En ambos tipos de ensayo, los colágenos fibrilares fueron activadores débiles de las plaquetas

de forma dependiente de Syk, con la excepción de la mayor activación por el colágeno (fibrilar) tipo Horm, utilizado como agonista estándar en las pruebas de diagnóstico de función plaquetaria. En conjunto, estos resultados recalcan la importancia de la estructura fibrilar de los colágenos para la activación plaquetaria dependiente de GPVI y Syk. Este trabajo también demuestra que los diferentes tipos de colágenos inmovilizados son más eficaces en la activación de las plaquetas que cuando se usan en suspensión.

La señalización del calcio es central en la respuesta plaquetaria y la medición automatizada de este proceso tiene la capacidad de revelar defectos plaquetarios inducidos por fármacos. En el **Capítulo 4**, se utilizaron plaquetas cargadas con el marcador fluorescente, Calcium-6, para el desarrollo de un ensayo de alto rendimiento basado en las subidas de Ca^{2+} en respuesta a CRP (agonista del receptor GPVI) o a la trombina (agonista de receptores GPCR), en placas de 96, 384 y 1536 pocillos. El método mostró un tipo de curva diferente con CRP (retardada y prolongada) que con trombina (rápida y transitoria), incluso en la placa miniaturizada de 1536 pocillos. Usando un conjunto de parámetros cuantitativos se pudo describir la respuesta del Ca^{2+} en detalle. La validación del ensayo se realizó mediante una biblioteca de compuestos robustos y mediante un panel pequeño de inhibidores plaquetarios clínicamente relevantes. Los hallazgos de este capítulo indican que las respuestas de Ca^{2+} de las plaquetas pueden utilizarse para el cribado de compuestos de alto rendimiento con el fin de encontrar nuevos inhibidores plaquetarios.

En el **Capítulo 5**, el ensayo de medición de calcio de alto rendimiento se utilizó para realizar un cribado de compuestos antiplaquetarios con 16635 pequeñas moléculas. Esto incluyó 1280 compuestos orgánicos pequeños de la biblioteca química Prestwick, clínicamente aprobada junto con una biblioteca con diversidad de estructuras químicas (SPCA) que contiene 15355 moléculas pequeñas con características fisicoquímicas compatibles con la generación de fármacos. Utilizando un algoritmo para caracterizar las curvas de $[Ca^{2+}]_i$, se examinaron automáticamente los efectos de todos los compuestos sobre las respuestas de Ca^{2+} de plaquetas cargadas con Calcium-6 y posteriormente activadas con CRP o trombina. Al filtrar por el efecto del Z-score, la toxicidad y farmacocinética potencialmente desfavorable y la inhibición específica de un agonista, obtuvimos 13 compuestos que afectaban negativamente a la respuesta de Ca^{2+} inducida por CRP y 9 compuestos que interferían con la respuesta de Ca^{2+} inducida por trombina. Tras realizar ensayos de confirmación adicionales, se obtuvieron tres compuestos, esto es, AF299 y etopropazina (inhibidores específicos de la vía activada por CRP) y ANO61 (inhibidor de la vía activada con trombina). Los tres compuestos también inhibieron selectivamente la agregación plaquetaria. Los estudios dosis-respuesta indicaron que la fenotiazina, etopropazina, era la más eficaz en presencia de plasma y suprimía el crecimiento del trombo inducido por colágeno en condiciones de flujo. Sin embargo, las características inhibitorias de estos compuestos deben mejorarse mediante estudios de relación estructura-función.

Parte de los pacientes con síndrome de Noonan presentan síntomas hemorrágicos,

vinculados a mutaciones en el gen *PTPN11*, que codifica la tirosina fosfatasa SHP2. El fármaco SHP099 es un inhibidor alostérico de la SHP2, cuyos derivados se están probando en ensayos clínicos para tratar tumores sólidos. En las plaquetas, SHP2 se considera un regulador negativo de la señalización de GPVI. En el **Capítulo 6**, se estudió hasta qué punto la inhibición de SHP2 mediante SHP099 puede mejorar las funciones plaquetarias, usando, entre otros, ensayos microfluídicos de formación de trombos dependientes de colágeno. Descubrimos que el tratamiento con SHP099 producía un aumento de la activación de la integrina αIIbβ3 y del volumen del trombo. Resultados similares se observaron en condiciones de coagulación. Al examinar el proceso de formación de trombos con sangre de seis pacientes con síndrome de Noonan (con mutaciones confirmadas en el gen *PTPN11*), descubrimos que la formación de trombos inducida por colágeno estaba moderadamente alterada. El tratamiento con SHP099 aumentó el tamaño del trombo, lo que indica que fármacos dirigidos a SHP2 podrían utilizarse para restaurar las alteraciones de la capacidad de respuesta plaquetaria vinculadas a pacientes con síndrome de Noonan.

La unión del factor von Willebrand (VWF) a la glicoproteína Ibα (GPIbα) es una de las etapas iniciales de la formación de trombos en condiciones de flujo y se presume que interferir con esta unión es beneficioso para los pacientes que sufren de púrpura trombocitopénica inmunitaria (iTTP, del inglés *immune thrombocitopenic purpura*). En el **Capítulo 7**, se diseñaron péptidos cíclicos *in silico* para interferir con la interacción del dominio A1 de VWF con la GPIbα. Las simulaciones de dinámica molecular resultaron en la selección de dos péptidos, mono-ORbIT (26 aminoácidos) y bi-ORbIT (36 aminoácidos). Ambos péptidos interfirieron en la unión de VWF a las plaquetas inducida por la ristocetina o la botrocetina, aunque la inhibición fue más débil que con un anticuerpo dirigido contra el dominio A1 del VWF. Tras una segunda ronda de diseño, se evaluó un péptido mejorado denominado *opt-mono-ORbIT* (28 aminoácidos), que funcionó mejor en la supresión de la formación de trombos, pero aún no alcanzó la inhibición observada con el anticuerpo. Por todo lo anterior, el diseño de péptidos basado en la estructura de proteínas tiene un buen potencial para afectar a la agregación plaquetaria dependiente de VWF.

El diagnóstico en pacientes con síntomas hemorrágicos relacionados con las plaquetas es difícil, dadas las limitaciones de las pruebas estándar de función plaquetaria. En el **Capítulo 8**, utilizamos un ensayo de microfluídica de forma multiparamétrica para ayudar en el fenotipado de varios pacientes y familiares con trastornos relacionados genéticamente, es decir*,* deficiencia de CalDAG-GEFI, enfermedad de deficiencia de almacenamiento del pool plaquetario, síndrome de Hermansky-Pudlak o deficiencia del receptor $P2Y_{12}$. El análisis genético molecular identificó nuevas mutaciones patogénicas de los genes *RASGRP2,* que codifica para CalDAG-GEFI, y *P2RY12,* que codifica para el receptor $P2Y_{12}$, y confirmó mutaciones de los genes Hermansky-Pudlak *HPS1* y *HPS3*. Mediante el ensayo multiparamétrico de 48 parámetros, el patrón general de formación de trombos en sangre total fue deficiente en la mayoría de los pacientes sintomáticos, pero no en sus familiares asintomáticos. Estos resultados en combinación con datos de fenotipado plaquetario

10

(agregación plaquetaria y citometría de flujo) y valores hematológicos, se estudiaron usando un análisis de conglomerados *k-means*, que separaron los sujetos control y los familiares (heterocigotos) no afectados de la gran mayoría de pacientes sintomáticos. En conjunto, esto indica que la evaluación multiparamétrica de la formación de trombos en sangre total puede desempeñar un papel importante en el reconocimiento de los trastornos de la función plaquetaria relacionados genéticamente.

El **Capítulo 9** analiza los hallazgos más importantes de esta tesis en relación con la bibliografía actual. Se discuten las ventajas e inconvenientes de los métodos de alto rendimiento aplicados en esta tesis, tales como las placas de pocillos y ensayos microfluídicos, así como el posible uso de herramientas bioinformáticas para evaluar la inhibición o disfunción plaquetaria en la clínica.

Impact

Platelet activation is considered a cornerstone in the pathogenesis of cardiovascular diseases [1]. Under physiological conditions, such as upon injury, excessive blood loss is prevented by the activation of hemostatic mechanisms, including the formation of a platelet aggregate (thrombus). The coagulation cascade is also triggered, which causes the formation of fibrin (blood clot) as a vital protective role. On the other hand, undesired platelet activation due to atherosclerotic plaque damage or blood stasis can lead to intravascular thrombosis and impacts major health issues such as heart attack, stroke, cancer, and infection. Cardiovascular diseases are still the major causes of death worldwide, estimated to take almost 18 million lives each year [2]. Antiplatelet drugs are essential in the treatment of cardiovascular diseases. One of the main questions in the treatment of thrombosis is how to balance the anti-thrombotic benefits of antiplatelet drugs against the negative side effects, in particular an increased bleeding risk [3]. In addition, malfunction of the hemostasis system can lead to a bleeding disorder, which is often difficult to diagnose due to the high heterogeneity among affected patients and the lack of molecular information on the exact cause of the disease [4]. Current diagnostic tests often lack sensitivity for an accurate bleeding or thrombotic risk prediction, because these do not integrate the various processes involved in thrombus formation, especially lacking blood flow. Therefore, additional research is needed to measure platelet functions in physiological and pathological conditions, as well as to develop advanced methods to find novel antiplatelet drugs. Such efforts can improve the current cardiovascular medicine and result in a more optimal diagnosis and treatment of patients.

The Horizon 2020 TAPAS consortium is a European Joint Doctorate program (No. 76118), which stands for Targeting Platelet Adhesion Receptors in Thrombosis. TAPAS aims to develop new expertise to identify, understand and test new molecular targets on blood platelets for the selective prevention and treatment of thrombotic diseases. TAPAS focuses on the research of two receptors on platelets, glycoprotein (GP)VI and CLEC-2, both of which play a major role in platelet-related thrombotic disorders and a lesser role in hemostasis. As an early-stage researcher of this consortium, my thesis focuses on the platelet collagen receptor GPVI, defining in particular how its activation mechanism differs from the stimulation of platelets by the coagulation protein thrombin, acting via protease-activated receptors (PARs) (**Chapter 2**). During this research, I focused on these two receptor signaling pathways to develop new high throughput methods that can be used for small molecule screening purposes, aiming to find novel inhibitors (**Chapters 3-5**).

Collagen as one of the major components of the extracellular matrix is a potent activator of platelets acting through interaction with the immunoglobulin-type receptor GPVI. GPVI is considered to be a promising antithrombotic drug target due to its restricted expression pattern in platelets and megakaryocytes and its relatively minor role in hemostasis. Yet, it is important to better understand the basic biology behind GPVI signaling and platelet activation in order to develop novel approaches to modulate GPVI receptor function. Another platelet receptor, GPIb, promotes platelet adhesion to collagen under shear conditions via collagen-bound von Willebrand factor (VWF). In addition, G-protein coupled receptors (GPCRs) for soluble platelet agonists are major contributors to platelet activation.

10

Currently, the majority of anti-platelet drugs target the latter receptors. This concerns the clinically used $P2Y_{12}$ receptor antagonists (clopidogrel, prasugrel, ticagrelor), the cyclooxygenase inhibitor aspirin preventing thromboxane receptor TP activation, and thrombin receptor PAR1 antagonists (vorapaxar). All these drugs have limitations such as an increased risk of bleeding, despite a clear reduction of secondary thrombotic events. In addition, there are partly genetically determined different interpatient responses linked to an incomplete mode of action. Here, I intended to find new small molecules (**Chapter 5**) or peptides (**Chapter 7**) that interfere with the platelet activation pathways and receptors mentioned above for the development of improved candidate drugs.

The diagnosis of patients with a (mild) bleeding phenotype remains a difficult issue. Bleeding symptoms can have various underlying causes, which in most cases remain unclear even when extensive genetic sequencing has been performed [5]. Current platelet function tests appear not to always pick up a likely platelet-related bleeding disorder. Therefore, in order to gain more insight into the phenotype of patients with a familial history of bleeding, we used a high-throughput whole blood microfluidic assay (**Chapter 8**). This microfluidic assay is performed under conditions of shear stress mimicking the physiology of arteries or veins and promises to be of added value to assess platelet responsiveness and functions in a clinical setting. Moreover, the use of multiple thrombogenic surfaces, mimicking the components present in the vessel wall, allows us to distinguish several processes of platelet activation and thrombus formation, to better characterize platelet defects in patients. Further research is still needed and modifications should be implemented. These include the use of physiological temperature, studying bigger cohorts of patients, establishing reference ranges of healthy controls, and the generation of prediction models to simplify the diagnostic approach. Nevertheless, the results of this thesis emphasize that whole blood flow measurements are valuable in clinical settings with patients with a familial history of bleeding and assumed abnormal platelet functions. The microfluidic assays are also relevant for basic research as a proxy measurement of thrombotic or hemostatic disturbances, when studying specific signaling proteins or molecular inhibitors to further understand their effects. I have studied all this in the context of thrombosis (**Chapters 3, 5**), when evaluating the blood from patients with mutations associated with a bleeding disorder (**Chapter 6**), or aiming to develop agents against thrombotic thrombocytopenia (**Chapter 7**). Taken together, the results obtained during this thesis have provided additional knowledge on method development in thrombosis and hemostasis, drug identification using platelet function testing, and the unraveling of defective platelet functions in patients with a bleeding disorder.

References

1.   Koupenova M, Kehrel BE, Corkrey HA, Freedman JE. Thrombosis and platelets: an update. *Eur Heart J.* 2017;38:785-791.

2.   World Health Organisation. Cardiovascular disease (CVDs). https://www.who.int/en/news-room/fact-sheets/detail/cardiovascular-diseases-(cvds). Published 11 June, 2021. Accessed 10 November, 2022.

3.   Michelson AD. Antiplatelet therapies for the treatment of cardiovascular disease. *Nat Rev Drug Discov.* 2010;9:154-169.

4. Bourguignon A, Tasneem S, Hayward CP. Screening and diagnosis of inherited platelet disorders. Crit Rev Clin Lab Sci. 2022:1-40.

5. Ver Donck F, Labarque V, Freson K. Hemostatic phenotypes and genetic disorders. Res Pract Thromb Haemost. 2021;5:e12637.

10

Curriculum Vitae

Delia Irene Fernández de la Fuente was born on the 29th of April 1995 in Madrid, Spain. In 2007 she started her secondary education at the Maria Zambrano High School in El Espinar (Segovia, Spain), where she obtained her diploma with a specialization in Science and Technology. In 2013, she started a bachelor's study in Biochemistry at the Autonomous University of Madrid, with a research project on adiponectin and tumor growth with Dr. Guadalupe Sabio at the National Centre of Cardiovascular Diseases Carlos III (CNIC). After graduating in 2017, she started her master's study in Molecular Biotechnology at the University of Birmingham (United Kingdom), where she completed the thesis on tetraspanins and *Staphylococcus aureus* with Dr. Michael Tomlinson at the School of Biosciences. In 2018, she joined the platelet group at the Cardiovascular Research Institute Maastricht (CARIM) at the Department of Biochemistry (Maastricht University). She was an early-stage researcher in the innovative training network TAPAS of the Marie-Slodowska Curie program of the European Union Horizon 2020 scheme. During her PhD study, she performed research on platelet biology, thrombosis, and drug development. In the Pivot Park Screening Centre (Oss, The Netherlands) she performed a small molecule screening study. From January 2021-2022, she worked in the Platelet Proteomics Group at the Center for Research in Molecule Medicine and Chronic Diseases (CiMUS) of the University of Santiago de Compostela (Spain). She performed the PhD research under the supervision of Prof. Dr. Johan Heemskerk, Dr. Marijke Kuijpers, and Dr. Ángel García. As a PhD student, she also collaborated with the groups of Prof. Dr. Barbara Zieger (Freiburg, Germany) and Dr. Kerstin Jurk (Mainz, Germany). She presented her research at multiple international scientific conferences.

Publications

Publications

1. Jooss NJ*, De Simone I*, Provenzale I*, **Fernández DI***, Brouns SL, Farndale RW, Henskens YMC, Kuijpers MJE, ten Cate H, van der Meijden PEJ, Cavill R, Heemskerk JWM. Role of platelet glycoprotein VI and tyrosine kinase Syk in thrombus formation on collagen-like surfaces. *Int. J. Mol. Sci.* 2019; 20(11) e2788.

2. D'Alessandro E, Becker C, Bergmeier W, Bode C, Bourne JH, Brown H, Buller, HR, ten Cate-Hoek AJ, ten Cate, V, van Cauteren YJM, Cheung YF, Cleuren A, Coenen D, Crijns HJGM, de Simone I, Dolleman SC, Espinola Klein C, **Fernández DI**, Granneman, L, van 't Hof A, Henke P, Henskens YMC, Huang J, Jennings LK, Jooss N, Karel M, van de Kerhof D, Klok FA, Kremers B, Lämmle B, Leader A, Lundstrom A, Mackman N, Mannucci PM, Maqsood Z, van der Meijden PEJ, van Moorsel M, Moran LA, Morser J, van Mourik M, Navarro S, Neagoe RAI, Olie RH, van Paridon P, Posma J, Provenzale I, Reitsma PH, Scaf B, Schurgers L, Seelig J, Siegbahn A, Siegerink B, Soehnlein O, Soriano EM, Sowa MA, Spronk HMH, Storey RF, Tantiwong C, Veninga A, Wang X, Watson SP, Weitz J, Zeerleder SS, ten Cate H. Thrombo-inflammation in cardiovascular disease: an expert consensus document from the third Maastricht Consensus Conference on Thrombosis. *Thromb. Haemost.* 2020; 120:538-564.

3. **Fernández DI**, Kuijpers MJE, Heemskerk JWM. Platelet calcium signalling by G-protein coupled and ITAM-linked receptors regulating anoctamin-6 and procoagulant activity. *Platelets.* 2021; 32: 863-871.

4. Tullemans BME, Veninga A, **Fernández DI**, Aarts MJ, Eble JA, van der Meijden PEJ, Heemskerk JWM, Kuijpers MJE. Multiparameter evaluation of the platelet-inhibitory effects of tyrosine kinase inhibitors used for cancer treatment. *Int. J. Mol. Sci.* 2021; 22: 11199.

5. **Fernández DI**, Provenzale I, Cheung HYF, van Groningen J, Tullemans BME, Veninga A, Dunster JL, Honarnejad S, van den Hurk H, Kuijpers MJE, Heemskerk JWM. Ultra-high throughput Ca^{2+} assay in platelets to distinguish between ITAM-linked and G- protein coupled receptor activation. *iScience.* 2022; 25: 103718.

6. Hrdinova J, **Fernández DI**, Ercig B, Tullemans BME, Suylen DP, Agten SM, Jurk K, Hackeng TM, Vanhoorelbeke K, Voorberg J, Reutelingsperger CPM, Wichapong K, Heemskerk JWM, Nicolaes GA. Structure-based cyclic glycoprotein Ibα-derived peptides interfering with von Willebrand factor binding affecting platelet aggregation under shear. *Int. J. Mol. Sci.* 2022; 23: 2046.

10

7. Tullemans BME, **Fernández DI**, Veninga A, Baaten CCFMJ, Peters LJF, Aarts MJB, Eble JA, Campello E, Spiezia L, Simioni P, van der Vorst EPC, van der Meijden PEJ, Heemskerk JWM, Kuijpers MJE. Tyrosine kinase inhibitor sunitinib delays platelet-induced coagulation: additive effects of aspirin. *Thromb Haemost.* 2022; 122: 92-104.

8. Huang J, Jooss NJ, **Fernández DI**, Sickmann A, Garcia A, Wichapong K, Dijkgraaf I, Heemskerk JWM. Roles of focal adhesion kinase PTK2 and integrin αIIbβ3 signalling in collagen- and GPVI-dependent thrombus formation under shear. *Int. J. Mol. Sci.* 2022; 23:8688

Submitted papers

1. Huang J, **Fernández DI**, Zou J, Wang X, Heemskerk JW, García A. Restrained glycoprotein VI-induced platelet signalling by tyrosine protein phosphatases independent of phospholipase Cγ2. 2023 (submitted).

2. Jooss NJ, Diender MG, **Fernández DI**, Huang J, Heubel-Moenen FC, van der Veer A, Kuijpers MJE, Poulter NS, Henskens YMC, te Loo M, Heemskerk JWM. Modulating roles of platelet PECAM1 in glycoprotein VI and integrin α2β1-mediated thrombus formation. 2023 (submitted).

3. **Fernández DI,** Sobota V, Tullemans BME, van Groningen J, Zou J, Trotiño S, van den Hurk H, García A, Hornanejad S, Kuijpers MJE, Heemskerk JWM. Ultra-high throughput screening to identify antiplatelet drugs with discriminative receptor-dependent action mechanism. 2023 (submitted).

4. **Fernández DI**, Diender MG, Kuijpers MJE., Hermida-Nogueira L, Huang J, Veiras S, Henskens YMC, te Loo M, Heemskerk JWM, Kuijpers MJE, García A. Role of SHP2 (PTPN11) in glycoprotein VI-dependent thrombus formation: restored platelet response in Noonan patients by the allosteric drug SHP099. 2023 (revision).

5. **Fernández DI**, Provenzale I, Canault M, Fels S, Lenz A, Andresen F, Krümpel A, Dupuis A, Heemskerk JWM, Boeckelmann D, Zieger, B. High-throughput microfluidic blood testing to phenotype patients with genetically linked platelet disorders: an aid to diagnosis. 2023 (submitted).

6. Provenzale I, Solari FA, Schönichen C, Brouns SL, **Fernández DI**, Kuijpers MJE, van der Meijden PEJ, Gibbins JM, Sickmann A, Jones C, Heemskerk JWM. Endothelial regulation of platelet activation and signaling: endothelial effects on platelet phosphoproteome. 2023 (submitted).

7. Cheung HYF, Zou J, Tantiwong C, **Fernández DI**, Huang J, Ahrends R, Roest M, Cavill R, Gibbins J, Watson SP, Heemskerk JWM. High-throughput assessment identifying major platelet Ca^{2+} entry pathways via tyrosine kinase-linked and G protein-coupled receptors. 2023 (accepted).

Abstracts

1. **Fernández DI,** I Provenzale I, van Groningen J, Reutelingsperger CPM, van den Hurk H, Heemskerk JWM, Kuijpers MJE. Ultra-high throughput assays for calcium flux measurements to profile platelet signaling through ITAM-linked or G- protein coupled receptors. The Platelet Society Meeting, Cambridge, United Kingdom, September 2019.

2. Tullemans BME, Veninga A, **Fernández DI**, Aarts MJ, van der Meijden PEJ, Heemskerk JWM, Kuijpers MJE. Multiparameter screening for platelet-inhibitory effects of tyrosine kinase inhibitors used for cancer treatment. The Platelet Society Meeting, Cambridge, United Kingdom, 2019.

3. **Fernández DI**, Provenzale I, Tullemans BME, van Groningen J, Heemskerk JWM, van den Hurk H, Kuijpers MJE. Ultrahigh-throughput screening assay to identify new antiplatelet drugs with discriminative mode of receptor-dependent action. Virtual congress of the International Society on Thrombosis and Haemostasis (ISTH), Milan, Italy, 2020.

4. Tullemans BME, **Fernández DI**, Veninga A, Aarts MJB, van der Meijden PEJ, Heemskerk JWM, Kuijpers MJE. Tyrosine kinase inhibitor sunitinib delays platelet-induced coagulation: additive effects of aspirin. Virtual congress of the International Society on Thrombosis and Haemostasis (ISTH), Milan, Italy, 2020.

5. **Fernández DI**, Provenzale I, Tullemans BME, van Groningen J, Heemskerk JWM, van den Hurk H, Kuijpers MJE. Ultrahigh-throughput screening assay to identify new antiplatelet drugs with discriminative mode of receptor-dependent action. CARIM symposium, Online, Maastricht 2020.

6. Hrdinova J, **Fernández DI**, Ercig B, Tullemans BME, Suylen DP, Aagten SM, Jurk K, Hackeng TM, Vanhoorelbeke K, Voorberg J, Reutelingsperger CPM, Wichapong K, Heemskerk JWM, Nicolaes GA. Structure-based design of cyclic glycoprotein Ia-derived peptides affecting platelet interaction with von Willebrand factor under shear conditions. Virtual Congress of the International Society on Thrombosis and Haemostasis (ISTH), Philadelphia, PA, USA, 2021.

7. Provenzale I, Brouns SLN, Schönichen C, **Fernández DI**, Gibins JM, van der Meijden PEJ, Jones, C, Heemskerk JWM. Vessel-on-a-chip model reveals rapid on and off mechanisms of collagen- and thrombin-induced platelet activation. The Platelet Society Meeting, Keele, Online, 2021

8. Huang J, Jooss NJ, **Fernández DI**, García A, Heemskerk JWM. Role of novel shear-dependent receptor GPR56 and integrin-linked CIB in GPVI-dependent thrombus formation and signalling. CiMUS Workshop, Santiago de Compostela, Spain, 2021

9. **Fernández DI**, Huang J, Kuijpers MJE, Heemskerk JWM, García A. Intracellular suppressive pathways of collagen-induced GPVI activation: effects on thrombus formation. CiMUS workshop, Santiago de Compostela, Spain, 2021

10. **Fernández DI,** Hermida-Nogueira L, Huang, J, Veiras S, Kuijpers MJE, Heemskerk JWM, García A. Characterization of thrombogenic effects of platelet tyrosine phosphatase SHP2 inhibition using the allosteric inhibitor SHP099. Congress of the International Society of Thrombosis and Haemostasis (ISTH), London, UK, July 2022.

11. Provenzale I, Solari FA, Schönichen C, **Fernández DI**, Brouns SLN, Kuijpers MJE, van der Meijden PEJ, Gibbins JM, Sickmann A, Jones C, Heemskerk JWM. Endothelial-induced regulation of platelet signalling under flow: establishing the endothelial-controlled platelet phosphoproteome. Congress of the International Society of Thrombosis and Haemostasis (ISTH), London, UK, July 2022.

12. Troitiño S, **Fernández DI,** Hermida-Nogueira L, Bulán-Garmendia S, López-Fernández D, Sueiro AM, García A. Obese patients show enhanced ex vivo collagen-induced thrombus formation in flowing human blood. Congress of the International Society of Thrombosis and Haemostasis (ISTH), London, UK, July 2022.

13. **Fernández DI,** Zou J, Sobota V, Tullemans BME, van Groningen J, van den Hurk H, García A, Hornanejad S, Kuijpers MJE, Heemskerk JWM. Ultra-high throughput screening identifies novel calcium-dependent antiplatelet drugs with discriminative mode of receptor-dependent action. EUPLAN meeting, Milan, September 2022.

14. Troitiño S, **Fernández DI,** Hermida-Nogueira L, Bulán-Garmendia S, López-Fernández D, Sueiro AM, García A. Obese patients show enhanced ex vivo collagen-induced thrombus formation in flowing human blood. EUPLAN meeting, Milan, September 2022.

Oral and poster presentations

1. **Fernández DI,** I Provenzale I, van Groningen J, Reutelingsperger CPM, van den Hurk H, Heemskerk JWM, Kuijpers MJE. Ultra-high throughput assays for calcium flux measurements to profile platelet signaling through ITAM-linked or G- protein coupled receptors. The Platelet Society Meeting, Cambridge, United Kingdom, September 2019 (Poster presentation).

2. **Fernández DI**, Provenzale I, Tullemans BME, van Groningen J, Heemskerk JWM, van den Hurk H, Kuijpers MJE. Ultrahigh-throughput screening assay to identify new antiplatelet drugs with discriminative mode of receptor-dependent

action. Congress of the International Society on Thrombosis and Haemostasis (ISTH), Milan, Italy, 2020. Online (Oral communication).

3. **Fernández DI**, Provenzale I, Tullemans BME, van Groningen J, Heemskerk JWM, van den Hurk H, Kuijpers MJE. Ultrahigh-throughput screening assay to identify new antiplatelet drugs with discriminative mode of receptor-dependent action. CARIM symposium, Online, Maastricht 2020 (Poster presentation).

4. Hrdinova J, **Fernández DI**, Ercig B, Tullemans BME, Suylen DP, Aagten SM, Jurk K, Hackeng TM, Vanhoorelbeke K, Voorberg J, Reutelingsperger CPM, Wichapong K, Heemskerk JWM, Nicolaes GA. Structure-based design of cyclic glycoprotein Iα-derived peptides affecting platelet interaction with von Willebrand factor under shear conditions. Congress of the International Society on Thrombosis and Haemostasis (ISTH), Philadelphia, USA, 2021. Online (Poster presentation).

5. **Fernández DI**, Huang J, Kuijpers MJE Heemskerk JWM, García A. Intracellular suppressive pathways of collagen-induced GPVI activation: effects on thrombus formation. CiMUS workshop, Santiago de Compostela, Spain, 2021 (Poster presentation).

6. **Fernández DI,** Hermida-Nogueira L, Huang, J, Veiras S, Kuijpers MJE, Heemskerk JWM, García A. Characterization of thrombogenic effects of platelet tyrosine phosphatase SHP2 inhibition using the allosteric inhibitor SHP099. Congress of the International Society of Thrombosis and Haemostasis (ISTH), London, UK, July 2022 (Poster presentation).

7. **Fernández DI,** Zou J, Sobota V, Tullemans BME, van Groningen J, van den Hurk H, García A, Hornanejad S, Kuijpers MJE, Heemskerk JWM. Ultra-high throughput screening identifies novel calcium-dependent antiplatelet drugs with discriminative mode of receptor-dependent action. EUPLAN meeting, Milan, September 2022 (Oral communication)

Acknowledgements

"I was taught that the way of progress was neither swift nor easy"(Marie Curie)

I can indeed relate to this quote. Progress towards achievements is not easy, but it is at least better when you are supported by many incredible human beings.

I would like to begin with those who gave me the opportunity to start this journey, my promoter**, Prof. Johan Heemskerk, Dr. Marijke Kuijpers and Dr. Ángel Garcia**. I know it has been hard for everybody but thanks for trusting me. Dear Johan, thank you for providing me with your knowledge, creativity, innovative ideas, and support. I really appreciate the open meetings with space to discuss my own ideas, which really made me grow as a scientist. Thanks for the giving me the opportunity to go to a "Flow Chamber" trip to amazing Freiburg, which was a great experience. Dear Marijke, I really appreciate your kindness, your support mentally and scientifically. You were always a person to go to ask for help. Thanks for your patience and continuous effort in reading some of my not-so-good thesis drafts. Dear Ángel, thank you for welcoming me in Santiago and giving me independenceand including me in some of your projects there. I know it was a complicated time, but I appreciate all the time that I had there and everything I learned.

Dear members of the assessment committee thank you very much for reading and reviewing my thesis.

I could not continue this part of the thesis without expressing my gratitude to all the collaborators of the different chapter of this thesis. Many thanks to **Prof. Barbara Zieger** and **Dr. Doris Böckelmann**, for the great week in Freiburg, your kindness, and all you taught us about bleeding disorders. I'm very thankful of the interesting data we generated. Thanks to the people at Pivot Park Screening Centre, **Jan**, **Hans**, **Dr. Helma van den Hurk** and **Dr. Saman Hornanejad** for all the help I got during my time there and with all the data from the screening. Many thanks to **Dr. Kerstin Jurk** and **Dr. Gerry Nicolaes** for helping with suggestions and experiments for the GPIb project. Me gustaría también agradecer a las **enfermeras del Servicio de Salud de la Universidad de Santiago de Compostela** por su paciencia, alegría y tiempo en sacar sangre a mis los tan apreciados donantes. Por último, me gustaría agradecer a la **Dra. Sonia Veiras** por su gran interés en investigación y enseñarme todo sobre el ROTEM y al **departamento de anestesiología del CHUS** por enseñarme su trabajo en cirugía y hacerme sentir muy cómoda y acogida cuando tuve que trabajar allí.

I could not have finished this thesis without my companion in crime. Dear **Isabella**, thank you for all the support, all the laughs, trips, and amazing help in the lab. We will create another PhD book with all the adventures surrounding this professional one, but for now I am thankful we crossed our paths.

Next comes my office roomates. Dear **Gina**, I am extremely happy you arrived in Maastricht some months after me and happen to be in my office!! We had the best, international, and most chatty office! Thank you for all your scientific and mature advice, and support with blood drawing, for being a great friend, and for taking care of me with all your tasty meals. Dear **Ilaria**, my first roommate and TAPAS colleague, thanks for supporting and be a go-to

10

person for experiments and chats, all the fun trips and moments. Dear **Claudia**, thanks for the calming and useful advice in the moments of stress. Dear **Gaukhar**, one of the most curious and chattiest people I have ever met. I am happy you made me question life and the European culture. Dear **Jinmi**, I have learnt a lot about the Chinese culture from you, thanks for all the help and fun moments. Dear **Giorgia**, our lunch conversations were always insightful. I am very happy for all the laughs and nice moments at work and outside. Dear **Simone**, I am your fan! Thanks for bringing happiness and laugh at work, I really appreciate ALL your help. Dear **Nerea**, thank you for joining me and creating a Spanish office in the department ☺.

I would also like to thank all the current and past members of the Maastricht Platelet group for all the teaching and helping in the lab, and for your contribution in some chapters of this thesis. Dear **Natalie**, thanks for being a great and funny colleage, I have learnt a lot from you and I am very grateful for all your help. Dear **Bibian**, **Sanne**, and **Daniëlle** thanks for being the platelet teachers, for all the support looking for reagents, listening when I was panicking or helping during the screening. **Daniëlle,** you are a kind crazy soul, I am happy we went to the PhD events together. Dear **Alicia**, thanks for the boat parties, the fun chats and the PhD Friday drinks mingling around Maastricht. Dear **Frauke** and **Titus,** thanks for all the help in the lab and the fun outside of it. Dear **Magdi** and **Constance**, thanks so much for all your advice experimental and personal, for offering it without doubt and finding time in your busy schedule agendas. I appreciate you kindly. Dear **Judith** and **Paola**, thanks for all the meaningful chats and advise I have received from you.

Dear **Trees** and **Lidewig**, thank you for the nice chats and help with all types of documents, I am very happy we were office neighbors for most of my PhD. Dear **people of the Biochemistry Department** thank you for all the good moments around Maastricht. Dear **Johana**, it was a pleasure working and learning the flow assay with you, I always appreciated your kind and caring character.

Thank you to all the people involved in **TAPAS,** especially the **15 ESRs** for making the PhD much more enjoyable, especially during all the TAPAS conferences and extra trips we organized. Especially thanks to Natalie, Ilaria, Isabella, **Jingnan** and **Xueqing**, for all the help in the lab, all the support, the lovely chats, laughs, fun gatherings and the trips around. I am very happy we happen to share labs.

To those that kept me sane all this year, thank you! Dear **Toni**, thanks for all the crazy but memorable stories that we created together, for your amazing support, and friendship. Dear **Vladi**, thanks for caring about me, for being a wonderful friend and for saving the most difficult chapter of my thesis using your coding skills. I am very happy we got the best climbing master teacher ever and especially a true friend. Dear **Nico**, thank you for your warm and cheerful character, for caring, and for always opening your place for gatherings. Dear **Marco**, **Robin, Anxhela**, **Alex**, **Cristian**, **Timo**, **Anne**, **Jana**, **Daniele, Celia, Minke, Ryan**, I am extremely happy that over the years we have created a small international family. Dear **Elisa** and **Tate**, my first two years in Maastricht were fun also because of you. Thanks

for all the spinning classes we got together to sweat all the stress and the nice and fun gatherings we enjoyed together. Dear **Pilar**, querida amiga, gracias por tener ese carácter atrayente y alegre y esas ganas de querer hacer planes juntas, gracias por todo tu apoyo durante estos años. Dear **Giulia**, thanks for all the hugs, amazing chats, and moments we always have together.

I would like to thank all the friendly faces of the **Toxicogenomics Department**, Nikki, Nicolaj, Jelmer, Daniela, and a big appreciation goes to Nhan for all her help with the layout and Juan, your uniqueness and authenticity are especial.

Durante mi tesis doctoral también tuve el placer de hacer una estancia en Santiago de Compostela. Allí conocí a mi amiga y compañera **Lidia,** que es una persona excepcional. Mil gracias por tu ayuda, pero también por acompañarme en mi estancia en Santiago con unos vinitos de vez en cuando y las divertidas clases de zumba. Gracias a mi amiga **Marina** por hacerme sentir en casa en esas tierras gallegas. Gracias al piso internacional y, por ende, a mis amigos **Alex**, **Axel**, **Oude**, **Sandra** y **Víctor**, por todos esos momentos y la sangre de alguno de vosotros ;) También me gustaría agradecer a **Sara**, por toda su ayuda en el lab, enseñarme a manejarme en el CiMUS y en las sesiones de comunicación científica, a **Antonia**, **Clara**, **Fran** y **Gema** por toda la ayuda en el lab. Gracias **Alberto**, **Sonia** y **Nuria** por los paseos al café y las agradables conversaciones. Gracias a toda la gente que me ayudó en el CIMUS y que tuve el placer ce conocer en mi estancia en Santiago.

Gracias a mis amigos que, aunque mayormente desde la distancia, siempre me han apoyado a seguir y a confiar en mí, **Claus**, **Jacobo**, **Richi** y **Carreras**. Mis amigos **Irene**, **Juan**, **María**, **Gloria** y **Rocío** porque parece que fue ayer cuando empezamos Bioquímica y aquí seguimos apoyándonos en nuestras aventuras doctorales y en la vida en general, gracias por formar parte de esto con vuestra amistad.

Querido **Toni**, GRACIAS, gracias por dejarme acabar la tesis ;) y acompañarme en el proceso haciéndomelo un poco más suave y ameno. Gracias por ofrecerme tu tiempo, tu apoyo, tu cariño y por seguir a mi lado. Gracias por enseñarme mucho más de lo que conocía de R y ayudarme con todos los plots, ajuste de ejes, colorines y análisis de datos, y siempre con todo lo que necesito.

Finalmente, me gustaría agradecer a mis padres, **Javier** y **Carmen**, y mis hermanos **Marina** y **Miguel**. No tengo palabras para agradeceros todo lo que significa vuestro apoyo en esta tesis y siempre. Por todos los momentos en los que no he sabido como seguir y habéis estado apoyándome y animándome a continuar. Siempre me sentiré muy afortunada por teneros, gracias por ser hogar aun desde la distancia. Esta tesis os la dedico a vosotros ya que es gracias a vosotros que he llegado hasta aquí.

Con cariño,

Delia